DYNAMIC RESPONSE OF COMPOSITE PLATES WITH CUT-OUTS AND HOLES

By
A. RAJAMANI

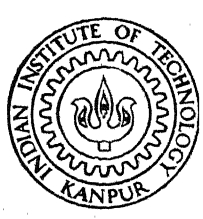

DEPARTMENT OF MECHANICAL ENGINEERING
INDIAN INSTITUTE OF TECHNOLOGY, KANPUR
MARCH, 1978

DYNAMIC RESPONSE OF COMPOSITE PLATES WITH CUT-OUTS AND HOLES

A Thesis Submitted
In Partial Fulfilment of the Requirements
for the Degree of
DOCTOR OF PHILOSOPHY

By
A. RAJAMANI

to the
DEPARTMENT OF MECHANICAL ENGINEERING
INDIAN INSTITUTE OF TECHNOLOGY, KANPUR
MARCH, 1978

ME-1978-D-RAJ-DYN

CERTIFICATE

This is to certify that the thesis entitled, "Dynamic Response of Composite Plates with Cut-Outs and Holes", by A. Rajamani, has been carried out under my supervision and has not been submitted elsewhere for a degree.

R. Prabhakaran

(R. Prabhakaran)
Assistant Professor
Department of Mechanical Engineering
Indian Institute of Technology, Kanpur
INDIA

March, 1978

ACKNOWLEDGEMENTS

I wish to express my gratitude to Dr. R. Prabhakaran for his guidance and inspiration throughout the course of this work.

I am thankful to Prof. V. Sundararajan for his assistance in the early stages of this work.

Thanks are also due to Prof. V. Rajaraman and Mrs. Rajaraman for their affection and encouragement.

I wish to express my thanks to Dr. K.K. Dwivedy, Sri N.P. Roberts, Sri P.K. Sinha and all other friends for their help whenever needed.

I am also thankful to Sri M.M. Singh, Sri S.L. Srivastava, Sri Munna Singh, Sri Rajeshwari and others for their help. Thanks are also due to Sri J.K. Misra for excellent typing of the manuscript, Sri B.L. Arora, Sri Kushwaha and Sri Panesar for tracing the figures.

I am thankful to Aeronautical Research and Development Board (Ministry of Defence) for supporting the work and financial assistance.

Finally, I am indebted to my wife Lakshmi who took extra pains and helped me in my computational and experimental work.

A. RAJAMANI

CONTENTS

LIST OF TABLES

LIST OF FIGURES

NOMENCLATURE

a	dimension of plate in x-direction,
a_{eff}	effective length of the plate
A_c	area of the cut-out
A_H	area of the hole
A_m, A_{ij}	modal coefficients
$\{\bar{A}\}_i$	eigenvector corresponding to frequency $\bar{\omega}_i$
b	dimension of plate in y-direction
c	length of cut-out in x-direction
c/a	cut-out parameter
C_{mn}^{ij}	stiffness coefficients
$C_{mn} C_{ij}$	stiffness coefficients
d	length of the cut-out in y direction; diameter of the hole in the plate
d/a	hole parameter
D	flexural rigidity for an isotropic plate $= Eh^3/12(1-\nu^2)$
D_{ij}	elements of the plate bending stiffness matrix
D_{22}^o	$E_{22}h^3/12(1 - \nu_{12}\,\nu_{21})$
E	Young's modulus for an isotropic plate
E_{11}	Young's modulus in 1 direction
E_{22}	Young's modulus in 2 direction

$F(x,y,t)$	dynamic external load
g	gravitational constant
$[G]$	modal transformation matrix
G_{12}	shear modulus in 1-2 plane
h	depth of the beam; thickness of the plate
k_n	characteristic mode constant for a beam
$\overline{K}_{pl}$	modified stiffness matrix coefficients
K	shape factor constant
l	free length of the beam
m	mode number in x-direction
M_{mn}^{ij}	mass coefficients
$\overline{M}_{ij}$	modified mass matrix coefficients
n	mode number in y-direction
n'	constant for a particular clamping
N_c	number of cut-outs
$N(t)$	modal generalized force
P_{Fij}	generalized force
$\overline{P}_p$	P_{Fij} as defined in equation (5.2)
q_{mn}	generalized displacement coordinate in the mn mode
$\overline{q}_l$	q_{mn} as defined in equation (5.2)
Q_{ij}	reduced bending stiffness coefficients
$\overline{Q}_{ij}$	transformed reduced bending stiffness coefficients
r	radius of gyration
R	a/b ; number of modes taken in x-direction

S	clamped length of the plate; number of terms taken in y-direction
S_{mn} S_{ij}	integration constants
S_{mn} C_{ij}	integration constants
t	time variable
t_1, t_2	time parameters defining the blast load
T	kinetic energy of the plate
U	invariants necessary for the transformation of bending stiffness coefficients
V	potential energy of the plate
w	transverse deflection of the plate
x_A, x_B	distances of the cut-out edges from x = 0
y_A, y_B	distances of the cut-out edges from y = 0
X_A	x_A/a
X_B	x_B/b
X_m, Y_n	beam characteristic functions
Y_A	y_A/a
Y_B	y_B/b
α_{mn}^{ij}, β_{mn}^{ij}	stiffness and mass coefficients due to a cut-out or a hole
α_m, α_n	frequency parameters for a clamped-clamped beam
ϕ_{mn}	admissible functions
ν_{12}	major Poisson's ratio

ρ	mass density
γ	specific weight of the beam
ω_n	measured natural frequency
ω_{nc}	corrected natural frequency
ω_1, ω_2	half-power point frequencies
ω_{mn}	natural frequency of the plate in mn mode
$\bar{\omega}_{mn}$	non-dimensional frequency ($\bar{\omega}_{mn} = \omega_{mn} / \sqrt{D_{22}^{\circ} / \rho h a^4}$)

SYNOPSIS

DYNAMIC RESPONSE OF COMPOSITE PLATES WITH CUT-OUTS AND HOLES

A Thesis Submitted

In Partial Fulfilment of the Requirements

For the Degree of

DOCTOR OF PHILOSOPHY

by

A. RAJAMANI

to the

Department of Mechanical Engineering
Indian Institute of Technology, Kanpur
March, 1978

The study of the dynamic behaviour of structural elements made of composite materials has attracted considerable attention in recent years. In spite of the many recent investigations in the area of vibration of composite plates, not much attention has been focussed on the dynamic response of composite plates with discontinuities. The thesis first reviews, in Chapter 1, the literature on the study of dynamic response of composite plates. The principal objective of the present work is to develop a general computation technique based on Lagrange's equations of motion and to study the effect of discontinuities on the free vibration and blast response of isotropic and composite plates. The work can be broadly divided into three sections:

1) theoretical study on the free vibration characteristics of a composite plate with discontinuities,

2) experimental verification of these characteristics on a

3) investigation into the effect of blast loading on the response of composite plates.

The free vibration characteristics of a composite plate with central cut-outs and circular holes is studied respectively in Chapters 2 and 3. The effect of discontinuity is assumed to be similar to a displacement-dependent loading. Lagrange's equations of motion have been employed and these lead to an infinite system of frequency equations in the case of free vibrations. A suitable size of the frequency equations is chosen, striking a compromise between the accuracy and the computation time involved. The convergence of the results has been studied. Square and rectangular plates are considered as examples. Two edge conditions, namely simply-supported and clamped-clamped, are taken for detailed investigation.

The analysis of composite plates with cut-outs is simpler. The integrals necessary in the development of frequency equations have been derived in closed form for both simple-support and clamped-clamped edge conditions. For clamped-clamped plates, these integrals are given in an Appendix. However, in the analysis of plates with holes a numerical integration scheme has been employed to evaluate these integrals. The results are first compared with available results on isotropic solid plates and it is found that the results obtained are sufficiently accurate. A good agreement is also found with the available results on isotropic plates with cut-outs and holes. The cause of discrepancy, if any, has been explained. Numerical results have been computed for

square, simply-supported and clamped-clamped composite plates for different fibre-orientations. Ratios of principal Young's moduli of 1 (balanced bidirectionally reinforced glass-epoxy), 3(unidirectionally reinforced glass-epoxy), 10(unidirectionally reinforced boron-epoxy) and 40 (unidirectionally reinforced graphite-epoxy) have been used in the computation. The behaviour of frequencies in the case of balanced bidirectional plates with cut-outs is found very similar to isotropic plates and hence no results have been computed for these plates with holes. The effect of various parameters such as the ratio of the cut-out dimension (or hole dimension) to plate length, fibre-orientation angle and modulus ratio is considered on the natural frequencies and mode shapes of the composite plate. Some interesting observations have been made on the behaviour of natural frequencies and mode shapes.

The second part of the work is concerned with the experimental verification of theoretical results obtained earlier. Chapter 4 describes the experimental set-up and procedure. Only square plates with centrally located circular holes are considered in the present experimental study. A test fixture was designed and fabricated to conduct experiments on the free vibration studies of composite plates with holes. The simple-support and clamped-clamped boundary conditions were simulated by first conducting experiments an isotropic solid plates and verifying the results with available theoretical results. A fairly good agreement showed that these edge conditions have been approximated. The effect of clamping arrangement has also been taken into account.

The unidirectionally reinforced glass-epoxy composite plates were made by a hand lay-up technique. The material was characterized to determine its static and dynamic properties. The dynamic properties have been used in the computation of numerical results. Experiments were conducted on simply-supported and clamped-clamped square plates with central circular holes. The frequencies and mode shapes have been determined as the hole size was enlarged in steps in the aluminium plate as well as in the unidirectionally reinforced fibre-glass epoxy plates with fibre-orientations 0°, 15°, 30° and 45°. The influence of the holes on the natural frequencies and mode shapes have been shown. There is a good agreement between the theoretical results and experimental results. A comparison of theoretical results for the hole and the cut-out is also made and it is found that small cut-outs and holes influence the frequencies in a similar way. The mode shapes are found to be influenced due to the presence of cut-outs and holes.

Chapter 5 deals with the last phase of the work - the transient response of composite plates with and without holes. The modal approach has been used in the computation of numerical results. The results have been obtained for isotropic and unidirectionally reinforced E-glass-epoxy plates and are given for two cases: 1) when there is no hole in the plate and 2) when there is a centrally located hole in the plate. Results have been obtained for both simply-supported and clamped-clamped boundary conditions but are given only for clamped-clamped plates. In order to

verify the theoretical results, experiments have been conducted on isotropic and unidirectional E-glass-epoxy rectangular plates using a shock tube as the loading device. The experimental peak dynamic strains have been normalized with respect to the pressure and compared with theoretical peak strains. The strain-time history is also shown for a particular gauge location in the unidirectional reinforced glass-epoxy plate. Finally, a comparison of dynamic amplification factors (theoretical) has been made between an isotropic and a unidirectional glass-epoxy plate.

In Chapter 6, some general conclusions of the present work are summarized and possible extensions of the present work are discussed.

CHAPTER 1

INTRODUCTION

1.1 General

The potential use of fibre-reinforced composite materials for various design applications in aerospace, marine and terresterial structures is well known. An improvement in the performance of these structures requires a study of the dynamic response characteristics of the structural elements, the most common being plates and shells, made of composite materials. Structural and architectural requirements may necessitate the presence of discontinuities either geometrical or material in these structural elements. Geometrical discontinuities such as cut-outs or holes may lighten the structure, alter the resonant frequency and are needed for venting purposes. The present investigation is concerned with the dynamic response of unidirectionally reinforced composite plates with the geometrical discontinuities.

In the last two decades considerable amount of work has been done on the dynamic response of composite plates. The work done on the dynamic behaviour of these plates can be placed into four groups.

In the first, the plate is studied using an approximate theory based on Kirchoff hypotheses specifying the behaviour of the plate through its thickness with shear deformation neglected. The theories based on Kirchoff hypotheses have been developed by Pister and Dong [1], Reissner and

Stavsky [2], Dong, Pister and Taylor [3], Stavsky [4] and are summarized in [5].

In the case of high degree of orthotropy in the plate, an extension of Mindlin's theory for homogeneous isotropic plates [6] has been proposed by Yang, Norris and Stavsky [7] and by Whilney and Pagano [8]. In these theories linear displacements are again assumed across the plate thickness. Transverse shear deformation, however, is not neglected. Whitney [9] obtained closed form solution for bending deflection, flexural vibration frequencies and buckling loads of simply-supported rectangular plates of special construction and showed the significance of shear deformation on the response of highly anisotropic laminated plates. Sun and Whitney [10] also showed the effect of heterogeneous shear deformation over the thickness of the plate on the dynamical behaviour of general laminates. These theories are classified in the second group.

The third category may be characterized as approximate elasticity solutions [11,12,13] in which attempts were made to bridge the gap between the approximate plate theories and the general theory of elasticity formulation by smoothing and averaging procedures. These approaches lead to 'Effective Modulus' and 'Effective Stiffness' theories which are again approximate.

In the final group, vibrations of an (infinite) laminated plate are based on the complete three-dimensional theory of elasticity where the solutions for all layers are combined in accordance with the interface traction and displacement conditions to give a frequency equation.

However, for all but the simplest case of two layer construction [14-17] the algebra involved in both the generation and solution of frequency equations become intractable.

1.2 Review of Previous Work

A fairly exhaustive review of the literature on the mechanics and dynamics of structures made of composite materials can be found in three servey papers by Bert and Francis [18] and Bert [19,20].

Huffington and Hoppmann [21] investigated the free transverse vibration of thin rectangular orthotropic and isotropic plates for a variety of boundary conditions all of which have the characteristics that two opposite boundaries were simply-supported. Levi's method [22] has been used to obtain frequency equations and mode shapes. Hearmon [23] applied Rayleigh's method to derive closed formulas for the vibration of specially orthotropic plates using beam characteristic functions appropriate to the boundary conditions. Dickinson [24] extended a sine series solution developed by Dill and Pister [25] to the vibration of orthotropic plates. Plates with two opposite edges simply-supported, clamped along all four edges, and clamped along two opposite edges and free along the other edges were taken as examples. Swarup and Sundararajan [26] obtained natural frequencies and buckling loads of generally orthotropic rectangular plates with different combinations of simply-supported, clamped and free edges using Rayleigh-Ritz procedure.

Ashton and Waddoups [27] presented a Rayleigh-Ritz solution for the buckling and free vibration of plane anisotropic rectangular plates with various boundary conditions. They obtained natural frequencies and mode shapes for free-free and contilever plates and these compared well with their experimental results. Whitney and Leissa [28,29] obtained closed form solutions for the case of arbitrarily laminated orthotropic plates with simple support boundary conditions. Their results showed a strong effect of bending-streching coupling in lowering the frequencies.

An analytical and experimental study of transverse vibrations of laminated orthotropic plates was carried out by Hikami [30] involving combinations of simply-supported and free edge conditions. He considered 1) all edges simply-supported, 2) three edges simply-supported, fourth free, 3) two opposite edges simply-supported, other two free and 4) two adjacent edges simply-supported, other two free. The solution of the vibration problem for the first three edge conditions was obtained by the method of Levy [22] and for the fourth-edge condition was obtained by the Rayleigh-Ritz method using product of beam characteristic functions. A good agreement was obtained between the theoretical and experimental results for symmetric modes.

Ashton and Anderson [31] studied the natural frequencies and mode shapes of clamped-clamped boron-epoxy plates using Ritz method. They obtained excellent agreement between analytical and experimental results. Bert and Mayberry [32] presented an analysis based on Rayleigh-Ritz method

to determine the natural frequencies of vibration of laminated cross-ply rectangular plates. They gave results for fully clamped boundary conditions and compared them with experimental results also. Ashton [33] also studied the natural frequencies and characteristic mode shapes of free-free plates and illustrated the effect of 1) the orientation of the constituent plies, 2) the stacking sequence, and 3) the degree of orthotropy.

Mohan and Kingsbury [34] made an analytical study of the natural frequencies and mode shapes of anisotropic thin plates by use of Galerkin's method. They investigated the change in natural frequencies and mode shapes as the material elastic axes of the plate were rotated with respect to the geometrical edges.

Whitney [35,36] showed that use of energy methods in conjunction with classical beam characteristic function yields very slow convergence of the vibration frequencies for highly anisotropic materials when the natural boundary conditions are not satisfied. He obtained improved results by using a classical double Fourier Series [37] analysis in which both geometric and natural boundary conditions are satisfied. Decapua and Sun [38] obtained frequencies and mode shapes of a class of orthotropic plates with either clamped or simply-supported boundaries using Rayleigh-Ritz method. Maurizi and Laura [39] determined the frequencies of vibration of clamped rectangular plates by using a simple polynomial expression and applying Galerkin method.

Clary and Cooper [40] used a finite element analysis to study the vibration characteristics of cantilever wing like flat trapezoidal aluminium plates reinforced with boron-epoxy (placed symmetrically about the middle surface). The analytical results were in qualitative agreement with experimental trends for nodal patterns and frequency variations with filament orientation. Thornton and Clary [41] made correlation study of finite-element modelling for vibrations of composite material panels. They obtained excellent agreement of their results with those given by Ashton and Anderson [31]. Rosettos and Tong [42] used hybrid stress finite element method to study the effect of fibre-orientation angle and orthotropy parameter (ratio of Principal Young's moduli) on the vibration and flutter characteristics of cantilevered anisotropic plates.

Jones [43] presented an exact solution and numerical results for simply-supported plates that are laminated unsymmetrically about their middle surface. Elishakoff [44] gave frequencies of clamped plates in a form analogous to the corresponding frequencies of a simply-supported plate. In the case of a simply-supported plate, the wave numbers are equal to $m\pi/a$ and $n\pi/a$ respectively and m and n are positive integers which determine the mode shape. For a clamped plate the wave numbers were presented in the form $p\pi/a$ and $q\pi/a$ where the pair of real quantities p and q could be found from the solution of two supplementary eigenvalue problems. Recently Lin and King [45] extended the work of Whitney and Leissa [28] to the more general case of two opposite edges simply supported and two with arbitrary edge conditions.

Thus a study of the vibrations of composite plates has been made earlier using double Fourier series method, Rayleigh-Ritz method, Galerkin method and the finite element method. No work seems to have been done on the vibrations of composite plates with cut-outs or holes. Earlier work done include vibrations of isotropic plates and shells with cut-outs and/or holes. Kumai [46] found three natural frequencies of vibrations of square plates with circular holes analytically as well experimentally. He computed the natural frequencies for a given mode by means of superposition of solutions of circular ring plates satisfying the boundary conditions at several points along the edges of the square plate. His approximation allowed small residual deflections at some portion of the outer boundary of the square plate. Takahashi [47] analyzed the problem of rectangular plates with circular holes and all ends clamped using Rayleigh-Ritz method. Joga Rao and Pickett [48] also used the Rayleigh-Ritz method to find the fundamental frequency of vibrations of square plates with circular holes and square cut-outs. They modified the deflection functions for the mode shapes of solid plates to account for the appropriate singularity due to the presence of the circular hole. Brogan et.al. [49] did a systematic analytical and experimental investigation of the dynamic behaviour of a cylinder with a rectangular cut-out. They approximated the potential and kinetic energies of a thin shell by two-dimensional finite difference methods. They obtained excellent agreement between experimental and theoretical results. Anderson, Irons and Zienkieuicz [50] computed natural frequencies of vibrations of clamped square plates with central circular holes using finite element method. They used triangular elements

and the mesh size was finer near the hole boundary. Results were given for the first and fourth mode frequencies only. Kristiansen and Soedel [51] found fundamental frequencies of clamped, square plates with various types of cut-outs using Rayleigh Method. Paramsivam [52] described a method of determining the effects of openings on the natural frequencies with different types of boundary conditions using a grid frame work model. Basdekas and Chi [53] found the natural frequencies of a simply-supported isotropic plate with square cut-outs assuming the effect of cut-out to be equivalent to a displacement-dependent loading. In the methodology used by them, a knowledge of the normal modes is necessary. They extended this approach to investigate the dynamic response of oddly reinforced shells [54] and the non-linear forced vibrations of a non-prismatic beam [55] . Aksu and Ali [56] predicted the dynamic characteristics of orthotropic plates by a finite difference unequal interval formulation and extended this formulation to determine the dynamic characteristics of rectangular plates with cut-outs [57] . Further studies have been made on the vibrations of cylinders with cut-outs recently [58, 59, 60] .

The study of the transient response of structures is quite complex. Earlier studies were made on the elastic and plastic response of structural elements subjected to impact and shock loading. Elastic response studies have been made by Baker et.al. [61], Cheng and Beneveniste [62, 63] , Banerjee [64] , Crocker [65], Crocker and Hudson [66], and Rajamani and Sundararajan [67] on elastic beams and plates. A good review of the work done on the dynamic plastic behaviour of plates and shells can be found

in [68, 69, 70]. A few studies have also been made on the dynamic response of composite plates. These include the works done by Moon [71], Chow [72], Sun and Whitney [73, 74, 75], Sieu and Bert [76], Sun and Chattopadhyay [77] and Kubo and Nelson [78].

1.3 Present Work

The principal objective of the present work is to develop a general computation technique based on Lagrange's equations of motion and to study the effect of geometrical discontinuities on the free vibration and blast response of isotropic and composite plates with cut-outs and holes. The work can be broadly divided into three categories:

1) theoretical study on the free vibration characteristics of a composite plate with discontinuities,

2) experimental verification of these characteristics on a unidirectionally reinforced glass-epoxy plate with holes,

3) investigation into the blast response of composite plates with and without holes.

The free vibration characteristics of a composite plate with central cut-outs and circular holes is studied respectively in Chapters 2 and 3. The effect of discontinuity is assumed to be equivalent to a displacement dependent loading. Lagrange's equations of motion have been employed and these lead to an infinite system of frequency equations in the case of free vibrations. A suitable size of the frequency equations is chosen, striking a compromise between the accuracy and the computation time involved.

Square plates with two edge conditions, simply-supported and clamped-clamped, are taken for detailed investigation.

The analysis of composite plates with cut-outs is simpler. The integrals necessary in the development of frequency equations have been derived in closed form for both simple-support and clamped-clamped boundary conditions. For clamped-clamped plates, these integrals are given in Appendix A. In the analysis of plates with holes, the integrals cannot be evaluated in closed form and therefore, a numerical integration scheme has been employed to evaluate these integrals. The results are first compared with available results and it is found that the results obtained are sufficiently accurate. A good agreement is also found with the available results on isotropic plates with cut-outs and holes. The cause of discrepancy, if any, has been explained. Numerical results have been computed for square, simply-supported and clamped-clamped composite plates for different fibre-orientation angles. Ratios of principal Young's moduli of 1 (balanced bidirectionally reinforced glass-epoxy), 3 (unidirectionally reinforced glass-epoxy), 10 (unidirectionally reinforced boron-epoxy) and 40 (unidirectionally reinforced graphite-epoxy) have been used in the computation. The behaviour of frequencies in the case of balanced bidirectional plates is found very similar to isotropic plates and hence no results have been computed for these plates with holes. The effect of various parameters such as the ratio of the cut-out dimension (or hole dimension) to plate length, fibre-orientation angle and modulus ratio is considered on the natural frequencies and mode shapes of the composite plate. Some interesting

observations have been made on the behaviour of natural frequencies and mode shapes.

The second part of the work is concerned with the experimental verification of theoretical results obtained earlier. Chapter 4 describes the experimental set-up and procedure. Only square plates with centrally located circular holes are considered in the present experimental study. A test fixture was designed and fabricated to conduct experiments on the free vibration studies of composite plates with holes. The simple-support and clamped-clamped boundary conditions were simulated by first conducting experiments on isotropic solid plates and verifying the results with available theoretical results. A fairly good agreement showed that these edge conditions have been approximated. The effect of clamping arrangement has also been taken into account.

The unidirectionally reinforced glass-epoxy composite plates were made by a hand lay-up technique. The material was characterized to determine its static and dynamic properties. The dynamic properties have been used in the computation of numerical results. Experiments were conducted on simply-supported and clamped-clamped square plates with central circular holes. The frequencies and mode shapes have been determined as the hole size was enlarged in steps in the aluminium plate as well as in the unidirectionally reinforced fibre-glass epoxy plates with fibre-orientations 0°, 15°, 30° and 45°. The influence of the holes on the natural frequencies and mode shapes have been shown. There is a good agreement between the theoretical results and experimental results.

A comparison of theoretical results for the hole and the cut-out is also made and it is found that small cut-outs and holes influence the frequencies in a similar way. The mode shapes are found to be influenced due to the presence of cut-outs and holes.

Chapter 5 deals with the last phase of the work - the transient response of composite plates with and without holes. The modal approach has been used in the computation of numerical results. The results have been obtained for isotropic and unidirectionally reinforced E-glass-epoxy plates and are given for two cases: 1) when there is no hole in the plate and 2) when there is a centrally located hole in the plate. Results have been obtained for both simply-supported and clamped-clamped boundary conditions but are given only for clamped-clamped plates. In order to verify the theoretical results, experiments have been conducted on isotropic and unidirectional E-glass-epoxy rectangular plates using a shock tube as the loading device. The experimental peak dynamic strains have been normalized with respect to the pressure and compared with theoretical peak strains. The strain-time history is also shown for a particular gauge location in the unidirectional reinforced glass-epoxy plate. Finally, a comparison of dynamic amplification factors (theoretical) has been made between an isotropic and a unidirectional glass-epoxy plate.

In Chapter 6, some general conclusions of the present work are summarized and possible extensions of the present work are discussed.

CHAPTER 2

VIBRATIONS OF COMPOSITE PLATES WITH CUT-OUTS

2.1 Introduction

One of the problems in structural dynamics is the vibrations of plates or shells with discontinuities. Several approximate methods, such as Rayleigh-Ritz [48], finite difference [49,57] and grid frame work analogy [52] have been previously used to study the dynamic behaviour of plates or shells with cut-outs. In the present chapter, natural frequencies of generally orthotropic plates with cut-outs are determined by using Lagrange's equations of motion. The potential and kinetic energies based on Kirchoff's plate theory are used to determine the motion of the plate. The effect of the cut-out is expressed as a displacement-dependent loading similar to the treatment of Basdekas and Chi [53]. The present approach, however, is more general and the mode shapes of the"reference plate" need not be eigenfunctions as in reference [53]. In the methodology used by Basdekas and Chi a knowledge of the normal modes is necessary. The analysis employs an assumed space-mode approach with multimode expansions by taking characteristic beam functions and finally an infinite system of second order differential equations is obtained in generalized co-ordinates. A suitable size of the frequency equations is chosen based on the accuracy and convergence of results. The mode of convergence has been discussed. Results are given for square, simply-supported and clamped-clamped

composite plates with square cut-outs for different composite materials. A comparison is made with available results on isotropic plates. Certain interesting observations have been made and discussed in this chapter.*

2.2 Equations of Motion

The Lagrange's equations of motion in the presence of nonconservative forces have the form

$$\frac{d}{dt}\left(\frac{\partial T}{\partial \dot{q}_r}\right) - \frac{\partial T}{\partial q_r} + \frac{\partial V}{\partial q_r} = P_r \quad ; \quad r = 1,2,\ldots \tag{2.1}$$

where T is the kinetic energy, V is the potential energy, q_r are the time-dependent generalized displacement co-ordinates and P_r are time-dependent generalized forces.

In case of plates with cut-outs, the generalized forces $P_r(t)$ will include the effect of cut-outs.

The potential energy for a solid uniform plate, shown in Figure 2.1a due to bending is

$$V = \frac{1}{2}\int_0^a \int_0^b \left[D_{11} w_{,xx}^2 + 2D_{12} w_{,xx} w_{,yy} + D_{22} w_{,yy}^2 + 4D_{66} w_{,xy}^2 + 4D_{16} w_{,xx} w_{,xy} + 4D_{26} w_{,yy} w_{,xy}\right] dA \tag{2.2}$$

where w is the normal deflection of the plate and a comma denotes partial differentiation.

---

* A part of Chapter 2 is reported in [79,80].

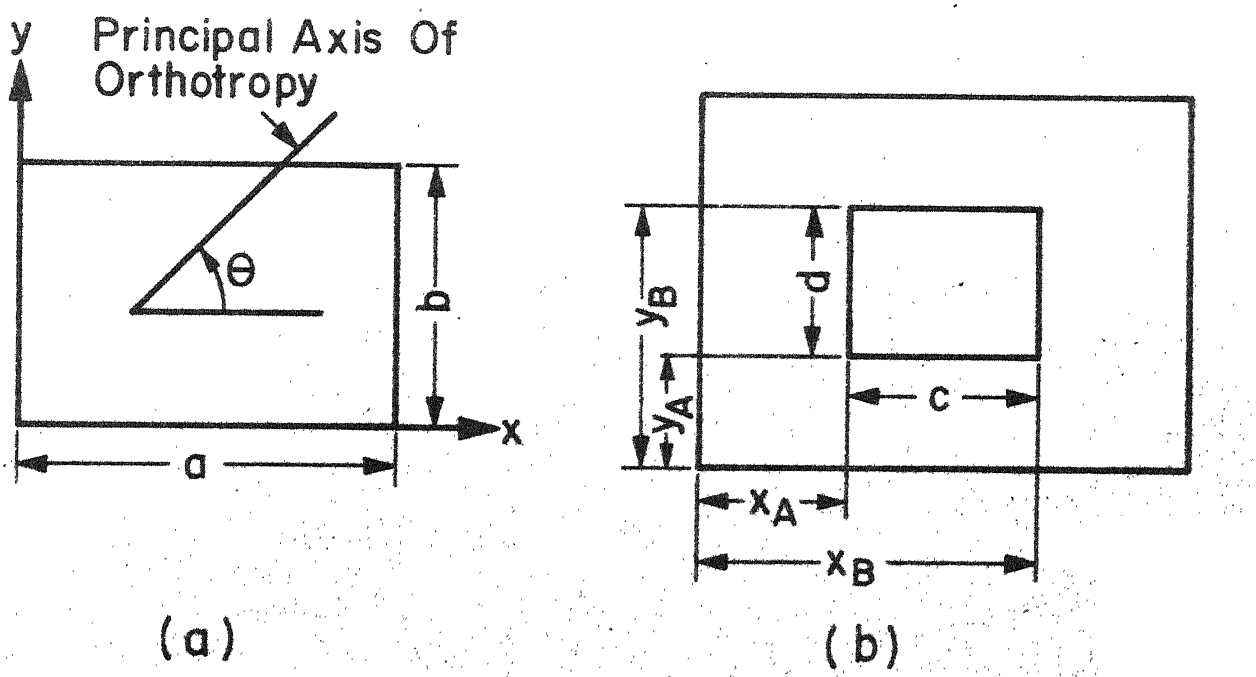

Fig.2.1 Plate Geometry

D_{ij}'s can be written as [81]

$$D_{ij} = \frac{1}{3} \sum_{k=1}^{N} (\overline{Q}_{ij})_k \, (h_k^3 - h_{k-1}^3)$$

$\overline{Q}_{ij}$ for each layer are given below in terms of the invariants [81] and the fibre-orientation angle for the layer with respect to the geometrical axes of the plate.

$$\overline{Q}_{11} = U_1 + U_2 \cos 2\theta + U_3 \cos 4\theta$$

$$\overline{Q}_{22} = U_1 - U_2 \cos 2\theta + U_3 \cos 4\theta$$

$$\overline{Q}_{12} = U_4 - U_3 \cos 4\theta$$

$$\overline{Q}_{66} = U_5 - U_3 \cos 4\theta$$

$$\overline{Q}_{16} = -\frac{1}{2} U_2 \sin 2\theta - U_3 \sin 4\theta$$

$$\overline{Q}_{26} = -\frac{1}{2} U_2 \sin 2\theta + U_3 \sin 4\theta \qquad (2.3)$$

in which,

$$U_1 = (3Q_{11} + 3Q_{22} + 2Q_{12} + 4Q_{66})/8$$

$$U_2 = (Q_{11} - Q_{22})/2$$

$$U_3 = (Q_{11} + Q_{22} - 2Q_{12} - 4Q_{66})/8$$

$$U_4 = (Q_{11} + Q_{22} + 6Q_{12} - 4Q_{66})/8$$

$$U_5 = (Q_{11} + Q_{22} - 2Q_{12} + 4Q_{66})/8$$

$$Q_{11} = \frac{E_{11}}{1-\nu_{12}\,\nu_{21}} \quad , \quad Q_{22} = \frac{E_{22}}{1-\nu_{12}\,\nu_{21}} \quad , \quad Q_{66} = G_{12}$$

$$Q_{12} = \frac{\nu_{12}\,E_{22}}{1-\nu_{12}\,\nu_{21}} = \frac{\nu_{21}\,E_{11}}{1-\nu_{12}\,\nu_{21}}$$

The kinetic energy of the solid plate is given by,

$$T = \frac{1}{2} \int_o^a \int_o^b \rho h \dot{w}\dot{w}\, dA \qquad (2.5)$$

where ρ is the mass density

and h is the thickness of the plate.

The effect of size, shape and location of the cut-out can be considered as a displacement-dependent external loading and, therefore, it is expedient to express w as

$$w(x,y,t) = \sum_{m=1}^{R} \sum_{n=1}^{S} q_{mn}(t)\ \phi_{mn}(x,y) \qquad (2.6)$$

where $q_{mn}(t)$ is the generalized co-ordinate in the mn mode,

$\phi_{mn}(x,y)$ are admissible functions in the mn mode.

Substituting for $w(x,y,t)$ in the expressions for T and V in equation (2.1) and simplifying,

$$\sum_{m=1}^{R} \sum_{n=1}^{S} \left(\int_o^a \int_o^b \rho h\, \phi_{ij}\, \phi_{mn}\, dA \right) \ddot{q}_{mn} - \sum_{m=1}^{R} \sum_{n=1}^{S} \left(\sum_{N_c} \iint_{A_c} \rho h\, \phi_{ij}\, \phi_{mn}\, dA \right) \ddot{q}_{mn}$$

$$+ \sum_{m=1}^{R} \sum_{n=1}^{S} \left(\int_o^a \int_o^b \Big[D_{11}\ \phi_{ij,xx}\, \phi_{mn,xx} + D_{12} (\phi_{ij,xx}\, \phi_{mn,yy} + \phi_{ij,yy}\, \phi_{mn,xx} \right.$$

$$\left. + D_{22}\, \phi_{ij,yy}\, \phi_{mn,yy} + 4D_{66}\, \phi_{mn,xy}\, \phi_{ij,xy} + 2D_{16} (\phi_{mn,xx}\, \phi_{ij,xy} \right.$$

$$+ \phi_{ij,xx}\,\phi_{mn,xy}) + 2D_{26}\,(\phi_{mn,yy}\,\phi_{ij,xy} + \phi_{mn,xy}\,\phi_{ij,yy})\big]dA)\,q_{mn}$$

$$- \sum_{m=1}^{R}\sum_{n=1}^{S}\Big(\sum_{N_c}\iint_{A_c}\big[D_{11}\,\phi_{ij,xx}\,\phi_{mn,xx} + D_{12}\,(\phi_{ij,xx}\,\phi_{mn,yy}$$

$$+ \phi_{ij,yy}\,\phi_{mn,xx}) + D_{22}\,\phi_{ij,yy}\,\phi_{mn,yy} + 4D_{66}\,\phi_{mn,xy}\,\phi_{ij,xy}$$

$$+ 2D_{16}\,(\phi_{mn,xx}\,\phi_{ij,xy} + \phi_{ij,xx}\,\phi_{mn,xy}) + 2D_{26}\,(\phi_{mn,yy}\,\phi_{ij,xy}$$

$$+ \phi_{mn,xy}\,\phi_{ij,yy})\big]dA)\,q_{mn}$$

$$= \iint_{A} F(x,y,t)\,\phi_{ij}(x,y)\,dA\;;\quad \begin{matrix} i = 1,2,\ldots R, \\ j = 1,2,\ldots S \end{matrix}\quad , \qquad (2.7)$$

where N_c is the number of cut-outs.

Defining M_{mn}^{ij}, β_{mn}^{ij}, C_{mn}^{ij}, α_{mn}^{ij} and P_{Fij}, the above equation can be written as,

$$\sum_{m=1}^{R}\sum_{n=1}^{S} M_{mn}^{ij}\,\ddot{q}_{mn} - \sum_{m=1}^{R}\sum_{n=1}^{S}\beta_{mn}^{ij}\,q_{mn} + \sum_{m=1}^{R}\sum_{n=1}^{S} C_{mn}^{ij}\,q_{mn}$$

$$- \sum_{m=1}^{R}\sum_{n=1}^{S}\alpha_{mn}^{ij}\,q_{mn} = P_{Fij}\;;\quad \begin{matrix} i = 1,2,\ldots, R \\ j = 1,2,\ldots, S \end{matrix}\quad , \qquad (2.$$

where,

$$M_{mn}^{ij} = \int_{0}^{a}\int_{0}^{b} \rho h\,\phi_{ij}\,\phi_{mn}\,dA \qquad (2.9)$$

$$\beta_{mn}^{ij} = \sum_{N_c}\iint_{A_c} \rho h\,\phi_{ij}\,\phi_{mn}\,dA \qquad (2.10)$$

$$C_{mn}^{ij} = \int_0^a \int_0^b \Big[D_{11}\,\phi_{ij,xx}\,\phi_{mn,xx} + D_{12}\,(\phi_{ij,xx}\,\phi_{mn,yy} + \phi_{ij,yy}\,\phi_{mn,xx}) + D_{22}\,\phi_{ij,yy}\,\phi_{mn,yy} + 4D_{66}\,\phi_{mn,xy}\,\phi_{ij,xy} + 2D_{16}\,(\phi_{mn,xx}\,\phi_{ij,xy} + \phi_{ij,xx}\,\phi_{mn,xy}) + 2D_{26}\,(\phi_{mn,yy}\,\phi_{ij,xy} + \phi_{mn,xy}\,\phi_{ij,yy}) \Big] dA \tag{2.11}$$

$$\alpha_{mn}^{ij} = \sum_{N_c} \iint_{A_c} \Big[D_{11}\,\phi_{ij,xx}\,\phi_{mn,xx} + D_{12}\,(\phi_{ij,xx}\,\phi_{mn,yy} + \phi_{ij,yy}\,\phi_{mn,xx}) + D_{22}\,\phi_{ij,yy}\,\phi_{mn,yy} + 4D_{66}\,\phi_{mn,xy}\,\phi_{ij,xy} + 2D_{16}\,(\phi_{mn,xx}\,\phi_{ij,xy} + \phi_{ij,xx}\,\phi_{mn,xy}) + 2D_{26}\,(\phi_{mn,yy}\,\phi_{ij,xy} + \phi_{mn,xy}\,\phi_{ij,yy}) \Big] dA \tag{2.12}$$

$$P_{Fij} = \iint_{\Lambda} F(x,y,t)\,\phi_{ij}\,dA \tag{2.13}$$

The terms with negative sign in equation (2.8) can be thought of as an external loading on the plate and these terms are present because of the cut-outs in the plate. The equation of motion can be written as,

$$\sum_{m=1}^{R}\sum_{n=1}^{S} (M_{mn}^{ij} - \beta_{mn}^{ij})\,\ddot{q}_{mn} + \sum_{m=1}^{R}\sum_{n=1}^{S} (C_{mn}^{ij} - \alpha_{mn}^{ij})\,q_{mn} = P_{Fij}\,, \qquad i = 1,2,\ldots, R \quad j = 1,2,\ldots, S \tag{2.14}$$

For free vibrations, equation (2.14) reduces to

$$\sum_{m=1}^{R}\sum_{n=1}^{S} (M_{mn}^{ij} - \beta_{mn}^{ij})\,\ddot{q}_{mn} + \sum_{m=1}^{R}\sum_{n=1}^{S} (C_{mn}^{ij} - \alpha_{mn}^{ij})\,q_{mn} = 0\,; \qquad i = 1,2,\ldots, R \tag{2.15}$$

Equation (2.15) defines an eigenvalue problem and its solution gives the natural frequencies and corresponding eigenvectors. The eigenvalue problem has been solved for two boundary conditions: 1) simply-supported edge conditions, 2) clamped-clamped edge conditions.

2.2.1 Simply-Supported Plates

The simply-supported edge boundary conditions are,

$$x = o,a : \quad w = o \;, \quad M_x = -D_{11} w_{,xx} - D_{12} w_{,yy} - 2D_{16} w_{,xy} = 0$$

$$y = o,b : \quad w = o \;, \quad M_y = -D_{12} w_{,xx} - D_{22} w_{,yy} - 2D_{26} w_{,xy} = 0 \qquad (2.16)$$

It is not possible to give an exact solution for the eigenvalue problem. However, a good approximate solution can be obtained by assuming that the function $\phi_{mn}(x,y)$ can be given as a product of beam characteristic functions in x and y directions.

For a simply-supported plate,

$$w(x,y,t) = \sum_{m=1}^{R} \sum_{n=1}^{S} q_{mn}(t) \sin \frac{m\pi x}{a} \sin \frac{n\pi y}{b} \qquad (2.17)$$

$$\phi_{mn}(x,y) = \sin \frac{m\pi x}{a} \sin \frac{n\pi y}{b} \qquad (2.18)$$

The function $\phi_{mn}(x,y)$ in equation (2.18) satisfies the geometric boundary conditions but not the natural boundary conditions of equation (2.16) except in the case of an isotropic plate.

Substituting ϕ_{mn} in the expressions for M_{mn}^{ij}, β_{mn}^{ij}, C_{mn}^{ij} and α_{mn}^{ij}

$$M_{mn}^{ij} = \rho h \frac{ab}{4} \delta_{mn}^{ij} \tag{2.19}$$

where $\delta_{mn}^{ij} = 1$ for $mn = ij$

$= 0$ for $mn \neq ij$

$$\beta_{mn}^{ij} = \rho h S_{mn} S_{ij} \tag{2.20}$$

$$C_{mn}^{mn} = \frac{D_{22}\pi^4}{a^4} \frac{ab}{4} \left[\frac{D_{11}}{D_{22}} m^4 + \frac{2(D_{12} + 2D_{66})}{D_{22}} m^2 n^2 R^2 + n^4 R^4 \right]$$

$$C_{mn}^{ij} = \frac{D_{22}\pi^4}{a^4} \frac{ab}{4} \left[-\frac{2D_{16}}{D_{22}} R(m^2 + i^2) - \frac{2D_{26}}{D_{22}} R^3 (n^2 + j^2) \right]$$

$$\times \frac{16mnij}{\pi^2 (m^2 - i^2)(n^2 - j^2)}$$

$$= 0 \quad \begin{array}{l} \text{for } m \pm i \text{ odd} \\ \text{and } n \pm j \text{ odd} \\ \text{for } m \pm i \text{ even} \\ \text{or } n \pm j \text{ even} \end{array}, \tag{2.21}$$

$$\alpha_{mn}^{ij} = \frac{D_{22}\pi}{a^4} \left[\left\{ \frac{D_{11}}{D_{22}} (m^2 i^2) + \frac{D_{12}}{D_{22}} R^2 (i^2 n^2 + j^2 m^2) + j^2 n^2 R^4 \right\} S_{mn} S_{ij} + \left\{ 4 \frac{D_{66}}{D_{22}} (imnj) R^2 \right\} C_{mn} C_{ij} \right.$$

$$- \left\{ 2 \frac{D_{16}}{D_{22}} R (m^2 ij S_{mn} C_{ij} + i^2 mn S_{ij} C_{mn}) \right\}$$

$$\left. - \left\{ 2 \frac{D_{26}}{D_{22}} R^3 (n^2 ij S_{mn} C_{ij} + j^2 mn S_{ij} C_{mn}) \right\} \right] \tag{2.22}$$

here,

$$S_{mn}\,S_{ij} = \sum_{N_c} \iint_{A_c} \left(\sin\frac{m\pi x}{a} \sin\frac{i\pi x}{a}\right)\left(\sin\frac{n\pi y}{b} \sin\frac{j\pi y}{b}\right) dA$$

$$S_{mn}\,C_{ij} = \sum_{N_c} \iint_{A_c} \left(\sin\frac{m\pi x}{a} \cos\frac{i\pi x}{a}\right)\left(\sin\frac{n\pi y}{b} \cos\frac{j\pi y}{b}\right) dA$$

$$C_{mn}\,C_{ij} = \sum_{N_c} \iint_{A_c} \left(\cos\frac{m\pi x}{a} \cos\frac{i\pi x}{a}\right)\left(\cos\frac{n\pi y}{b} \cos\frac{j\pi y}{b}\right) dA$$

(2.23)

Considering only one cut-out (i.e. $N_c = 1$),

$$S_{mn}\,S_{ij} = \frac{ab}{4}\left[\frac{\sin\{(m-i)\pi X_B\}}{(m-i)\pi} - \frac{\sin\{(m-i)\pi X_A\}}{(m-i)\pi} - \frac{\sin\{(m+i)\pi X_B\}}{(m+i)\pi} + \frac{\sin\{(m+i)\pi X_A\}}{(m+i)\pi}\right]$$

$$\times\left[\frac{\sin\{(n-j)\pi Y_B\}}{(n-j)\pi} - \frac{\sin\{(n-j)\pi Y_A\}}{(n-j)\pi} - \frac{\sin\{(n+j)\pi Y_B\}}{(n+j)\pi} + \frac{\sin\{(n+j)\pi Y_A\}}{(n+j)\pi}\right] \quad (a)$$

$$S_{mn}\,S_{mn} = \frac{ab}{4}\left[X_B - X_A - \frac{1}{2}\left\{\frac{\sin(2m\pi X_B)}{m} - \frac{\sin(2m\pi X_A)}{m}\right\}\right]$$

$$\times\left[Y_B - Y_A - \frac{1}{2}\left\{\frac{\sin(2n\pi Y_B)}{n\pi} - \frac{\sin(2n\pi Y_A)}{n\pi}\right\}\right] \quad (b)$$

$$C_{mn}\,C_{ij} = \frac{ab}{4}\left[\frac{\sin\{(m-i)\pi X_B\}}{(m-i)\pi} - \frac{\sin\{(m-i)\pi X_A\}}{(m-i)\pi}\right.$$

$$\left. + \frac{\sin\{(m+i)\pi X_B\}}{(m+i)\pi} - \frac{\sin\{(m+i)\pi X_A\}}{(m+i)\pi}\right] x$$

$$x\left[\frac{\sin\{(n-j)\pi Y_B\}}{(n-j)\pi} - \frac{\sin\{(n-j)\pi Y_A\}}{(n-j)\pi}\right.$$

$$\left. + \frac{\sin\{(n+j)\pi Y_B\}}{(n+j)\pi} - \frac{\sin\{(n+j)\pi Y_A\}}{(n+j)\pi}\right] \qquad (c)$$

$$C_{mn}\,C_{mn} = \frac{ab}{4}\left[X_B - X_A + \frac{1}{2}\left\{\frac{\sin(2m\pi X_B)}{m\pi} - \frac{\sin(2m\pi X_A)}{m\pi}\right\}\right]$$

$$x\left[Y_B - Y_A + \frac{1}{2}\left\{\frac{\sin(2n\pi Y_B)}{n\pi} - \frac{\sin(2n\pi Y_A)}{n\pi}\right\}\right] \qquad (d)$$

$$S_{mn}\,C_{ij} = \frac{ab}{4}\left[\frac{\cos\{(m-i)\pi X_B\}}{(m-i)\pi} - \frac{\cos\{(m-i)\pi X_A\}}{(m-i)\pi}\right.$$

$$\left. + \frac{\cos\{(m+i)\pi X_B\}}{(m+i)\pi} - \frac{\cos\{(m+i)\pi X_A\}}{(m+i)\pi}\right]$$

$$x\left[\frac{\cos\{(n-j)\pi Y_B\}}{(n-j)\pi} - \frac{\cos\{(n-j)\pi Y_A\}}{(n-j)\pi}\right.$$

$$\left. + \frac{\cos\{(n+j)\pi Y_B\}}{(n+j)\pi} - \frac{\cos\{(n+j)\pi Y_A\}}{(n+j)\pi}\right] \qquad (e)$$

$$S_{mn}\,C_{mn} = \frac{ab}{4}\left[\frac{\cos(2m\pi X_B)}{2m\pi} - \frac{\cos(2m\pi X_A)}{2m\pi}\right]$$

$$x\left[\frac{\cos(2n\pi Y_B)}{2n\pi} - \frac{\cos(2n\pi Y_A)}{2n\pi}\right] \qquad (f)$$

(2.24)

In the case of an isotropic plate, the equation of motion (2.15) reduces to a simple form which is also given by Basdekas and Chi [53] as

$$\ddot{q}_{ij} + \omega_{ij}^2 q_{ij} = \frac{1}{M_{ij}} \left[P_{Fij} - \sum_{m=1}^{R} \sum_{n=1}^{S} \beta_{mn}^{ij} \ddot{q}_{mn} - \sum_{m=1}^{R} \sum_{n=1}^{S} \alpha_{mn}^{ij} q_{mn} \right] \tag{2.25}$$

This simplification is possible only when $\phi_{mn}(x,y)$ are eigen-functions in the mn mode.

2.2.2 Clamped-Clamped Plates

The boundary conditions for a clamped-clamped plate are given as

$$\begin{aligned} x = 0, a: \quad & w = 0 , \quad w_{,x} = 0 \\ y = 0, b: \quad & w = 0 , \quad w_{,y} = 0 \end{aligned} \tag{2.26}$$

A good approximation to the mode shape of the plate can be obtained by assuming the function $\phi_{mn}(x,y)$ to be a product of beam characteristics functions in x and y directions.

$$\phi_{mn}(x,y) = X_m(x)\, Y_n(y)$$

where,

$$X_m(x) = \cosh \frac{\alpha_m x}{a} - \cos \frac{\alpha_m x}{a} - A_m \left(\sinh \frac{\alpha_m x}{a} - \sin \frac{\alpha_m x}{a} \right) \tag{2.27}$$

$Y_n(y)$ is also given by a similar expression. The calculated values of α_m and A_m are given in Table 2.1.

Considering only one cut-out, the expressions for M_{mn}^{ij}, β_{mn}^{ij}, C_{mn}^{ij} and α_{mn}^{ij} given by equations (2.9 - 2.12) can be obtained by defining the following integrals,

$$F_1(m,n) = \int_0^1 X_m X_n \, dX$$

$$F_2(m,n) = \int_0^1 X_{m,X} X_{n,X} \, dX$$

$$F_3(m,n) = \int_0^1 X_{m,XX} X_{n,XX} \, dX$$

$$F_4(m,n) = \int_0^1 X_{m,X} X_n \, dX$$

$$F_5(m,n) = \int_0^1 X_{m,XX} X_n \, dX$$

$$F_6(m,n) = \int_0^1 X_{m,XX} X_{n,X} \, dX \qquad (2.28)$$

$$F_{1C}(m,n) = \int_{X_A}^{X_B} X_m X_n \, dX$$

$$F_{2C}(m,n) = \int_{X_A}^{X_B} X_{m,X} X_{n,X} \, dX$$

$$F_{3C}(m,n) = \int_{X_A}^{X_B} X_{m,XX} X_{n,XX} \, dX$$

$$F_{4C}(m,n) = \int_{X_A}^{X_B} X_{m,X} X_n \, dX$$

$$F_{5C}(m,n) = \int_{X_A}^{X_B} X_{m,XX} X_n \, dX$$

$$F_{6C}(m,n) = \int_{X_A}^{X_B} X_{m,XX} X_{n,X} \, dX \qquad (2.29)$$

where a comma denotes partial differentiation.

$$X_A = x_A/a \quad , \quad X_B = x_B/a \quad ;$$

x_A and x_B are the distances of the cut-out edges from the origin and are shown in Figure 2.1b . The integrals in equations (2.28) and (2.29) are given in Appendix A.

The expressions for M_{mn}^{ij}, β_{mn}^{ij}, C_{mn}^{ij} and α_{mn}^{ij} are

$$M_{mn}^{ij} = \rho \text{ hab } F_1(m, i)\, F_1(n, j) \tag{2.30}$$

$$\beta_{mn}^{ij} = \rho \text{ hab } F_{1C}(m,i)\, F_{1C}(n, j) \tag{2.31}$$

$$\begin{aligned} C_{mn}^{ij} = \frac{D_{22}\,ab}{a^4} \Bigg[& \frac{D_{11}}{D_{22}} F_3(m, i)\, F_1(n, j) + \frac{D_{12}}{D_{22}} R^2 \{F_5(m, i) \\ & F_5(j,n) + F_5(i, m)\, F_5(n, j)\} + R^4 F_1(m, i)\, F_3(n, j) \\ & + 4R^2 \frac{D_{66}}{D_{22}} F_2(m, i)\, F_2(n, j) + \frac{2D_{16}}{D_{22}} R \{F_6(m,i)\, F_4(j,n) \\ & + F_6(i,m)\, F_4(n, j)\} + \frac{2D_{26}}{D_{22}} R^3 \{F_4(i, m)\, F_6(n, j) \\ & + F_4(m,i)\, F_6(j, n)\} \Bigg] \end{aligned} \tag{2.32}$$

$$\begin{aligned} \alpha_{mn}^{ij} = \frac{D_{22}\,ab}{a^4} \Bigg[& \frac{D_{11}}{D_{22}} F_{3C}(m,i)\, F_{1C}(n,j) + \frac{D_{12}}{D_{22}} R^2 \{F_{5C}(m,i)\, F_{5C}(j,n) \\ & + F_{5C}(i,m)\, F_{5C}(n,j)\} + R^4 F_{1C}(m,i)\, F_{3C}(n,j) \\ & + 4R^2 \frac{D_{66}}{D_{22}} F_{2C}(m,i)\, F_{2C}(n,j) + \frac{2D_{16}}{D_{22}} R \{F_{6C}(m,i)\, F_{4C}(j,n) \\ & + F_{6C}(i,m)\, F_{4C}(n,j)\} + \frac{2D_{26}}{D_{22}} R^3 \{F_{4C}(i,m)\, F_{6C}(n,j) \\ & + F_{4C}(m,i)\, F_{6C}(j,n)\} \Bigg] \end{aligned} \tag{2.33}$$

Table 2.1

Parameters for a clamped-clamped beam

m or n	Frequency parameter α_m or α_n	Modal coefficient A_m or A_n
1	4.730040744862703	0.9825022145762379
2	7.853204624095836	1.000777311907269
3	10.99560783800167	0.9999664501254087
4	14.13716549125746	1.000001449897656
5	17.27875965739948	0.9999999373443833
6	20.42035224562606	1.000000002707595
7	23.56194490204045	0.9999999998829942
8	26.70353755550818	1.00000000005056
9	29.84513020910325	0.9999999999997815
10	32.98672286269281	1.000000000000009
11	36.12831551628262	0.9999999999999996

Unlike in the case of an isotropic simply-supported plate, the equation of motion (2.15) can not be reduced to a simple form for a clamped-clamped plate as $\phi_{mn}(x,y)$ are not eigenfunctions. Therefore, one cannot start with a differential equation of motion as given in references [53, 54]

2.3 Computation Technique

The method of solution in deriving equations of motion assumed the presence of discontinuities in plates as displacement-dependent external loading. An effective use of this method involves evaluation of numerous definite integrals necessary in the expressions for M_{mn}^{ij}, β_{mn}^{ij}, C_{mn}^{ij} and α_{mn}^{ij}. The computational technique employed product of beam characteristic functions for the admissible functions as tables of integrals [82] are available and the definite integrals in equation (2.29) can be evaluated in closed form without much difficulty. Once these integrals are evaluated, they can be stored in the computer memory and are accessible whenever needed. The natural frequencies and corresponding normalized eigenvectors have been determined using the power method. This is an iterative method with orthogonalization. The method has been found to give very accurate results for certain known cases.

2.4 Results and Discussion

The analysis presented in Section 2.2 has been applied to square, simply-supported and clamped-clamped plates with centrally located square cut-outs. Natural frequencies and corresponding eigenvectors were obtained

employing power method with orthogonalization for different fibre orientations in steps of 15^{o}. Four groups of symmetric, antisymmetric and a combination of symmetric and antisymmetric modes are considered. Ratios of principal Young's moduli of 1,3,10 and 40 have been used in the computation. In the case of unidirectionally reinforced composite plates results are given for fibre orientation angles 0^{o} and 45^{o} only in terms of non-dimensional frequency, $\bar{\omega}$.

The material properties of the plates for obtaining the numerical results are given in Table 2.2.

2.4.1 Mode of Convergence

The Lagrange's equations of motion, for free vibrations, lead to an infinite system of second order differential equations in generalized co-ordinates. It is essential to choose a proper size of the system of equations and to check the accuracy and convergence of frequency values so obtained. For this purpose, two cases are considered. For an isotropic simply-supported plate, a comparison is made between the frequency values obtained by taking 16, 25 and 36 equations for a combination of symmetric modes. It is found that the convergence of the frequency values is very good. The frequency values and the number of iterations required to get them for the same size of the system are given in Table 2.3. The frequency values do not differ upto seven significant digits for $c/a = 0.0$. Twenty five equations are taken for all the cases considered. Once the size of the system is fixed, a comparison in the frequency values is made again by taking symmetric, antisymmetric and a combination of

Table 2.2

Material properties used in the computation.

Material	Property		
	E_1/E_2	G_{12}/E_2	ν_{12}
Isotropic	1	0.385	0.30
Balanced Bidirectional glass-epoxy	1	0.200	0.10
Unidirectional glass-epoxy	3	0.5	0.25
Unidirectional boron-epoxy	10	0.333	0.30
Unidirectional graphite-epoxy	40	0.500	0.25

Table 2.3

Comparison of frequencies for different combinations of modes and size of the frequency equation system (N x N) for an isotropic simply-supported plate.

c/a	Mode	mnij (N x N) 1,3,5,7 (16x16)	1,3,5,7,9 (25x25)	1,3,5,7,9,11 (36x36)	1,3,5,7,9, 2,4,6,8,10 (25x25)	2,4,6,8,10 1,3,5,7,9 (25x25)	2,4,6,8,10 (25x25)	1,2,3,4,5 (25x25)
0.0	1st	19.739	19.739(6)[a]	19.739	-	-	-	19.739(9)
	2nd	-	-	-	49.348(8)	49.348(8)	-	49.348(14)
	3rd	-	-	-	-	-	78.956(8)	78.956(25)
	4th	98.696	98.696(11)	98.696	-	-	-	98.696(21)
	5th	-	-	-	128.30 (20)	128.30 (20)	-	128.30 (20)
	6th	-	-	-	167.78 (15)	167.78 (15)	-	167.78 (19)
	7th	177.65	177.65 (16)	177.65	-	-	-	177.65 (44)
	8th	-	-	-	-	-	197.39 (12)	197.39 (23)
0.3	1st	19.728	19.644(9)	20.666	-	-	-	19.997(9)
	2nd	-	-	-	45.913(13)	45.913(13)	-	49.310(21)
	3rd	-	-	-	-	-	74.445(13)	75.941(15)
	4th	118.58 (94.346)	118.45 (20) (93.975)	127.43 (97.901)	-	-	-	118.91 (65) (94.644)*
	5th	-	-	-	124.51 (35)	124.51 (35)	-	126.50 (30)
	6th	-	-	-	161.86 (23)	161.86 (23)	-	171.21 (34)
	7th	194.21	193.97 (27)	201.609	-	-	-	-
	8th	-	-	-	-	-	190.22 (19)	-

a. The numbers in the paranthesis show the number of iterations required in the eigenvalue evaluation.

* The numbers in the paranthesis correspond to frequency values for the new mode.

symmetric and antisymmetric modes. Two values of c/a (0.0 and 0.3) are considered. It is observed that the frequency values for a particular mode do not differ by taking any combination of modes for a solid isotropic plate (c/a = 0.0). This is found to be true for an orthotropic solid plate and also for clamped boundary conditions. The above observation, however, is not found true for a plate with a cut-out. When a comparison between the frequency values obtained by taking all modes and other combination of modes is made, the values are found to differ (see Table 2.3). The maximum error is found in the second mode for an isotropic simply-supported plate (the results for other cases are not given) and is approximately 7.5 percent. The error, however, is considerably less in symmetric modes. (for example, first, fourth and seventh in Table 2.3). A relative comparison in the frequency values led to the decision to compute natural frequencies by taking 25 equations and different combination of modes for all the cases considered. The different combination of modes is preferred as it is easier to keep track of the modes and the number of iterations required to compute the natural frequencies in the solution of eigenvalue problem is reduced.

It is worthwhile to mention here that the accuracy of the results depends to an appreciable extent on the capability of the employed admissible functions to approximate the true shape of the deflected surface to the required degree. An increase in the number of terms tends to improve the accuracy of the results in general, but the resulting increase in the size of the matrices leads to increased computation costs and the possible

round-off errors may limit the accuracy of the results.

2.4.2 Simply-Supported Plates

a) Effect of cut-out on the natural frequency

Table 2.4 gives a comparison of the non-dimensional frequencies for cut-out parameters equal to 0.0 and 0.5 in the case of an isotropic plate. The fundamental frequency obtained by Paramsivam [52] is lower than the exact value whereas the present method yields exact values. This may be due to the fact that a coarse mesh size has been taken in Ref. [52]. Even the value of the fundamental frequency obtained by Aksu and Ali [56] for a solid isotropic plate using finite difference scheme with optimum unequal intervals is lower than the exact value. A comparison of first four modes is also made with the available results of Paramsivam [52] and Basdekas [53] for a plate with c/a equal to 0.5. The results obtained by Basdekas [53] for the fundamental frequency is approximate as the influence of other modes has not been considered. When the influence of other modes is taken into consideration an extremely good agreement is obtained between the frequency values for two cases considered. The results are given in Table 2.5 for two values of c/a. This agreement is due to the reason that the equations of motion in the present method and in the approach used by Basdekas and Chi [53] are same.

The variation of frequencies with cut-out parameter, c/a, for an isotropic plate is shown in Figure 2.2. The frequencies have been subscripted (11, 12, 21, etc.) on the basis of largest amplitude coefficient

Table 2.4

Comparison of non-dimensional frequency for a simply-supported isotropic plate for c/a = 0.0 and c/a = 0.5.

c/a	0.0	0.5			
Mode	1	1	2	3	4
Source					
Paramsivam [52]	19.630	25.450	42.110	70.500	78.650
Basdekas [53]	19.739	25.082	-	-	-
Present	19.739	23.627	41.634	72.134	80.229
Exact	19.739	-	-	-	-
Aksu and Ali [56]	19.719	-	-	-	-

Table 2.5

Comparison of symmetric and all modes in terms of frequency ratio $(= 4\bar{\omega}/\bar{\omega}^{\circ}_{11})$ for a simply-supported isotropic plate, c/a = 0.2 and c/a = 0.6

Mode	Symmetric Modes		All Modes	
	c/a = 0.2	c/a = 0.6	c/a = 0.2	c/a = 0.6
1	3.8605	8.3811	4.0551	8.5042
	(3.86)[a]	(8.35)	(4.05)	(8.50)
2	94.197	57.629	25.051	23.214
	(94.2)	(57.5)	-	-
3	111.59	231.51	61.059	64.631
	(111)	(231)	(61.0)	(64.5)
4	346.89	1153.0	94.551	79.135
	(347)	(835)	(94.5)	(78.5)
5	-	-	114.56	159.49
			(114)	-
6	-	-	167.82	246.44
				(246)

a. The results in parentheses are from Reference [53]

in the corresponding normalized eigenvectors. A fairly good agreement is obtained for the fundamental frequency with the results obtained in [52] and in [53]. There is a slight decrease in the fundamental frequency for small cut-outs but the frequency increases as the cut-out size is increased. The behaviour of frequencies $\bar{\omega}_{12}$ (= $\bar{\omega}_{21}$), $\bar{\omega}_{22}$, $\bar{\omega}_{23}$ (= $\bar{\omega}_{32}$), $\bar{\omega}_{14}$ is found to be similar. They first decrease with the increase in cut-out size but increase as the cut-out size is increased. The frequency, $\bar{\omega}_{31}$, increases with the increase in c/a but at larger c/a ratios, it decreases abruptly. Two interesting features have been observed: (1) the existence of a new mode due to the presence of a cut-out and (2) the cross-over of frequencies. It is seen that the fourth mode is identical with the fifth mode for a solid isotropic plate. The presence of a cut-out gives rise to the fourth mode. This is observed for frequencies corresponding to both symmetric and antisymmetric modes ($\bar{\omega}_{15}$, $\bar{\omega}_{17}$, $\bar{\omega}_{24}$, $\bar{\omega}_{26}$ etc.) but not for frequencies corresponding to a combination of symmetric and antisymmetric modes ($\bar{\omega}_{12}$, $\bar{\omega}_{23}$, $\bar{\omega}_{14}$ etc.). The new mode, for example the fourth mode, has largest equal amplitude coefficients A_{13} and A_{31} with opposite signs whereas the fifth mode has largest equal amplitude coefficients A_{13} and A_{31} with same sign. The introduction of a small discontinuity seems to perturb the system for which an exact solution is known and gives rise to a new mode.

The other interesting feature observed is the cross-over of modes. Modes corresponding to $\bar{\omega}_{22}$ and $\bar{\omega}_{13}$ and these corresponding to $\bar{\omega}_{31}$ and $\bar{\omega}_{23}$ interchange. The mode shapes at the cross-over and nearby points have been obtained and shown later for an orthotropic plate. It is observed that the

mode shape for a particular mode at the cross-over and nearby points does not change. Moreover, at the cross-over frequencies the plate has the mode shape corresponding to either of the modes which cross over.

In Figures 2.3 and 2.4, the variation of $\bar{\omega}$ with c/a is shown for $\theta = 0°$ and $\theta = 45°$ respectively, for balanced bidirectionally reinforced plates. It is seen that $\bar{\omega}_{11}$ decreases with c/a for $\theta = 0°$ and then increases for larger cut-out sizes. However, there is no decrease in the value of the fundamental frequency with increasing c/a values for $\theta = 45°$. A similarity between the balanced-bidirectional plate and the isotropic plate is observed. In the case of balanced bidirectional plates also the modes corresponding to $\bar{\omega}_{13}$ and $\bar{\omega}_{31}$ are the same for a solid plate and the presence of a cut-out gives rise to a new mode corresponding to frequency $\bar{\omega}_{13}$.

It is seen in Figure 2.3 that the mode corresponding to $\bar{\omega}_{22}$ interchanges twice with that corresponding to $\bar{\omega}_{13}$. For $\theta = 45°$, the mode corresponding to $\bar{\omega}_{22}$ interchanges first with that corresponding to $\bar{\omega}_{13}$ and then with that corresponding to $\bar{\omega}_{31}$. There is a tendency for the modes corresponding to $\bar{\omega}_{22}$ and $\bar{\omega}_{31}$ to interchange and for the modes corresponding to $\bar{\omega}_{22}$ and $\bar{\omega}_{13}$ to separate from each other (after interchanging once) at higher c/a values as θ is increased. The frequencies $\bar{\omega}_{12}$ and $\bar{\omega}_{21}$ coincide for all fibre orientation angles in the balanced bidirectional case.

The variation of $\bar{\omega}$ with c/a is shown in Figures 2.5 and 2.6 for unidirectionally reinforced glass fibre-epoxy plates for $\theta = 0°$ and

$\theta = 45°$, respectively. For $\theta = 0°$, $\bar{\omega}_{11}$ decreases very little with increasing c/a values and then increases as the cut-out size is increased. There is no decrease in $\bar{\omega}_{11}$ with c/a for $\theta = 45°$ just as in the case of balanced bidirectional plates. It is seen that as the fibre orientation angle is increased, curves for $\bar{\omega}_{12}$ and $\bar{\omega}_{21}$ come closer together and when $\theta = 45°$, they coincide. This is also true for $\bar{\omega}_{13}$ and $\bar{\omega}_{31}$ for small c/a ratios. In this case also some of the modes interchange: the mode corresponding to $\bar{\omega}_{13}$ interchanges with that corresponding to $\bar{\omega}_{22}$ when $\theta = 0°$; mode corresponding to $\bar{\omega}_{22}$ interchanges with those corresponding to $\bar{\omega}_{13}$ and $\bar{\omega}_{31}$ when $\theta = 45°$. However, modes corresponding to $\bar{\omega}_{23}$ and $\bar{\omega}_{31}$ interchange with each other once and twice for fibre orientations 0° and 45° respectively. To study the behaviour of mode shapes at the cross-over and near by points, these have been obtained for $\bar{\omega}_{13}$ and $\bar{\omega}_{22}$ and shown in Figure 2.7 for fibre-orientation angle equal to 0°. It is observed that the mode shape for a particular mode at the cross-over and nearby points does not change, the plate can have either of the mode shapes at the cross-over point. As in the case of balanced bidirectional plates, when θ is increased, there is a tendency for the modes corresponding to $\bar{\omega}_{22}$ and $\bar{\omega}_{31}$ to interchange and for the modes corresponding to $\bar{\omega}_{22}$ and $\bar{\omega}_{13}$ separate from each other after interchanging once at higher c/a values.

In Figures 2.8 and 2.9, the variation of $\bar{\omega}$ with c/a is shown for unidirectional boron-epoxy plates. It is seen (Figure 2.8) that all frequencies except $\bar{\omega}_{13}$ decrease with increase in c/a values and at higher cut-outs they increase for $\theta = 0°$; the rate of decrease being maximum for

$\bar{\omega}_{21}$. However, for $\theta = 45°$, there is no decrease in $\bar{\omega}_{11}$ (Figure 2.9). Unlike isotropic, balanced bidirectional and unidirectional glass-epoxy plates, there is no interchange of modes corresponding to $\bar{\omega}_{22}$ and $\bar{\omega}_{13}$ for $\theta = 0°$ but in the case of $\theta = 45°$, these modes separate from each other after interchanging once at higher c/a ratio as in the previous cases considered.

For unidirectionally reinforced graphite-epoxy plates, Figures 2.10 and 2.11 show the variation of $\bar{\omega}$ with c/a for $\theta = 0°$ and $\theta = 45°$. When $\theta = 0°$, $\bar{\omega}_{11}$ and $\bar{\omega}_{21}$ decrease with increasing cut-out sizes and the rate of decrease is more as compared to isotropic, bidirectional glass-epoxy, unidirectional glass-epoxy and unidirectional boron-epoxy plates. However, for $\theta = 45°$, $\bar{\omega}_{11}$ increases with increase in cut-out size. It is interesting to note in Figure 2.10 that even the modes corresponding to $\bar{\omega}_{21}$ and $\bar{\omega}_{22}$ interchange for small (c/a = 0.3) cut-out sizes, but they exhibit normal behaviour for c/a greater than about 0.5. Moreover, for $\theta = 0°$, the mode corresponding to $\bar{\omega}_{22}$ does not interchange with that corresponding to $\bar{\omega}_{13}$ whereas they are found to interchange for balanced bidirectional and unidirectional glass-epoxy plates.

At this stage it is necessary to comment on the behaviour of frequencies. It is generally found that frequencies corresponding to different modes behave in different ways, However, some similarity is observed in this behaviour. The fundamental frequency for an orthotropic plate ($\theta = 0°$) is found to decrease for medium cut-out parameters (c/a = 0.2 - 0.5) unlike in the case of isotropic plates. This indicates

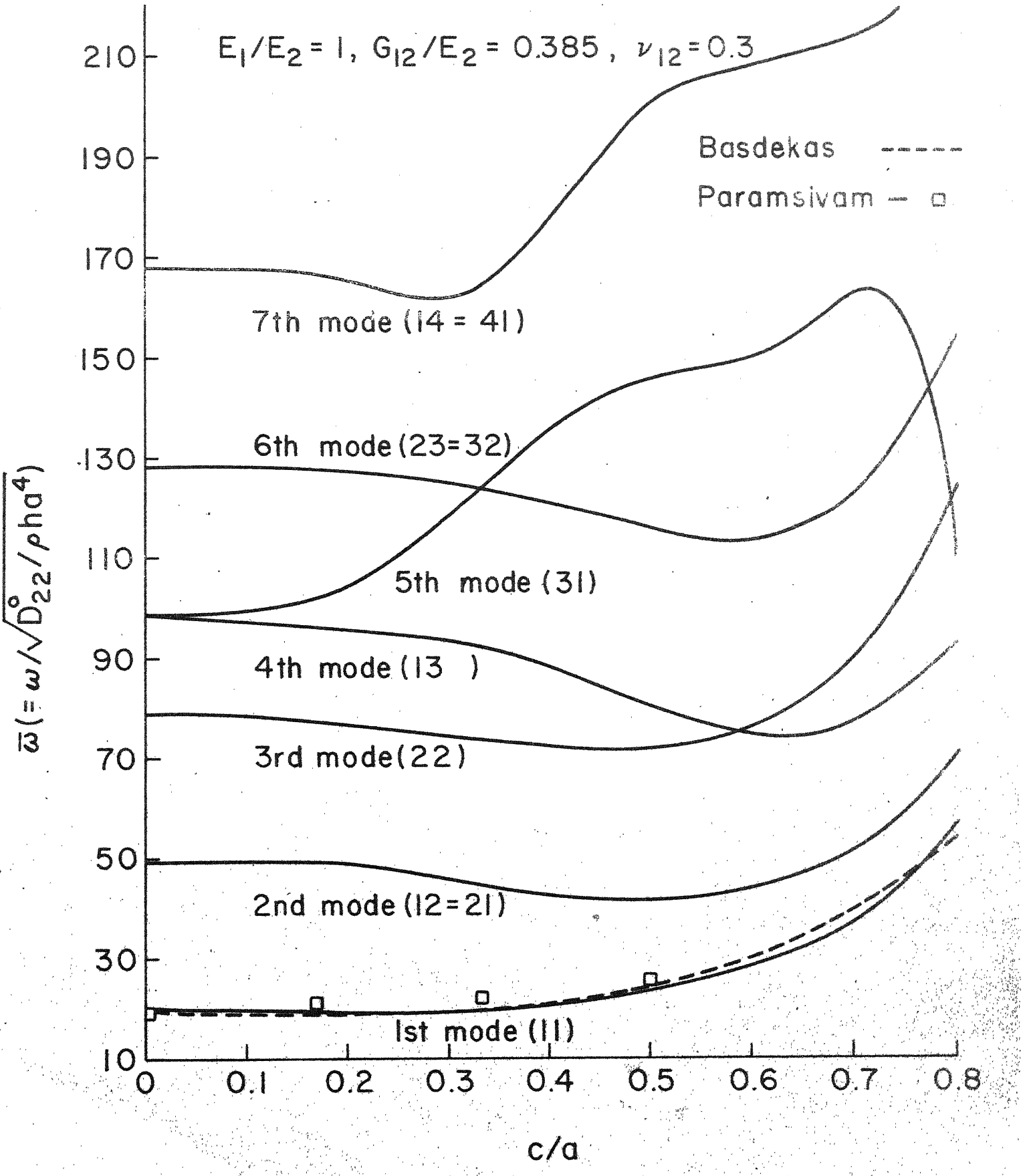

Fig.2.2 $\bar{\omega}$ vs c/a for a simply-supported isotropic plate; R = 1.0

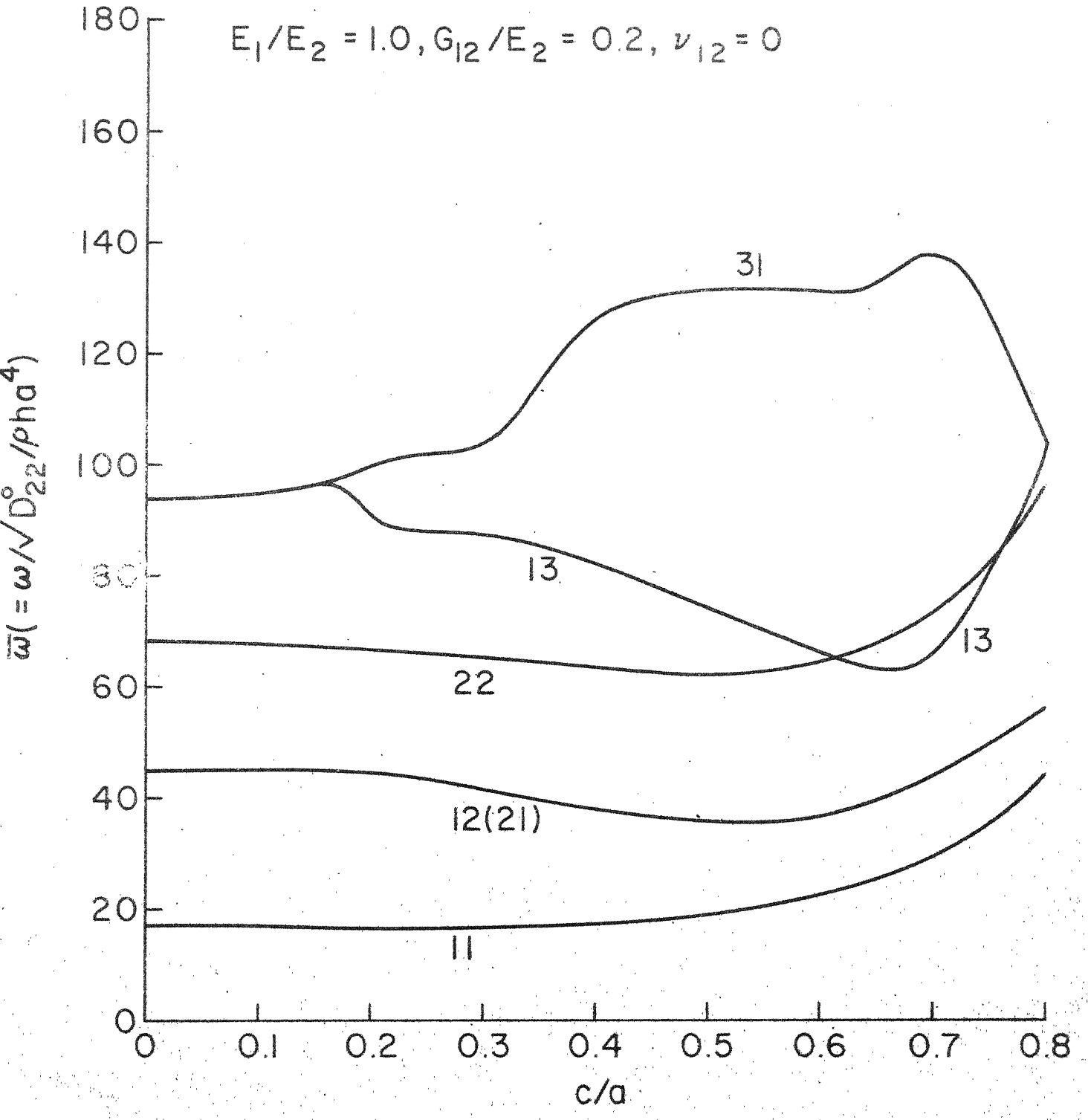

Fig.2.3 $\bar{\omega}$ vs c/a for a simply-supported plate; $\theta = 0°$, $R = 1.0$

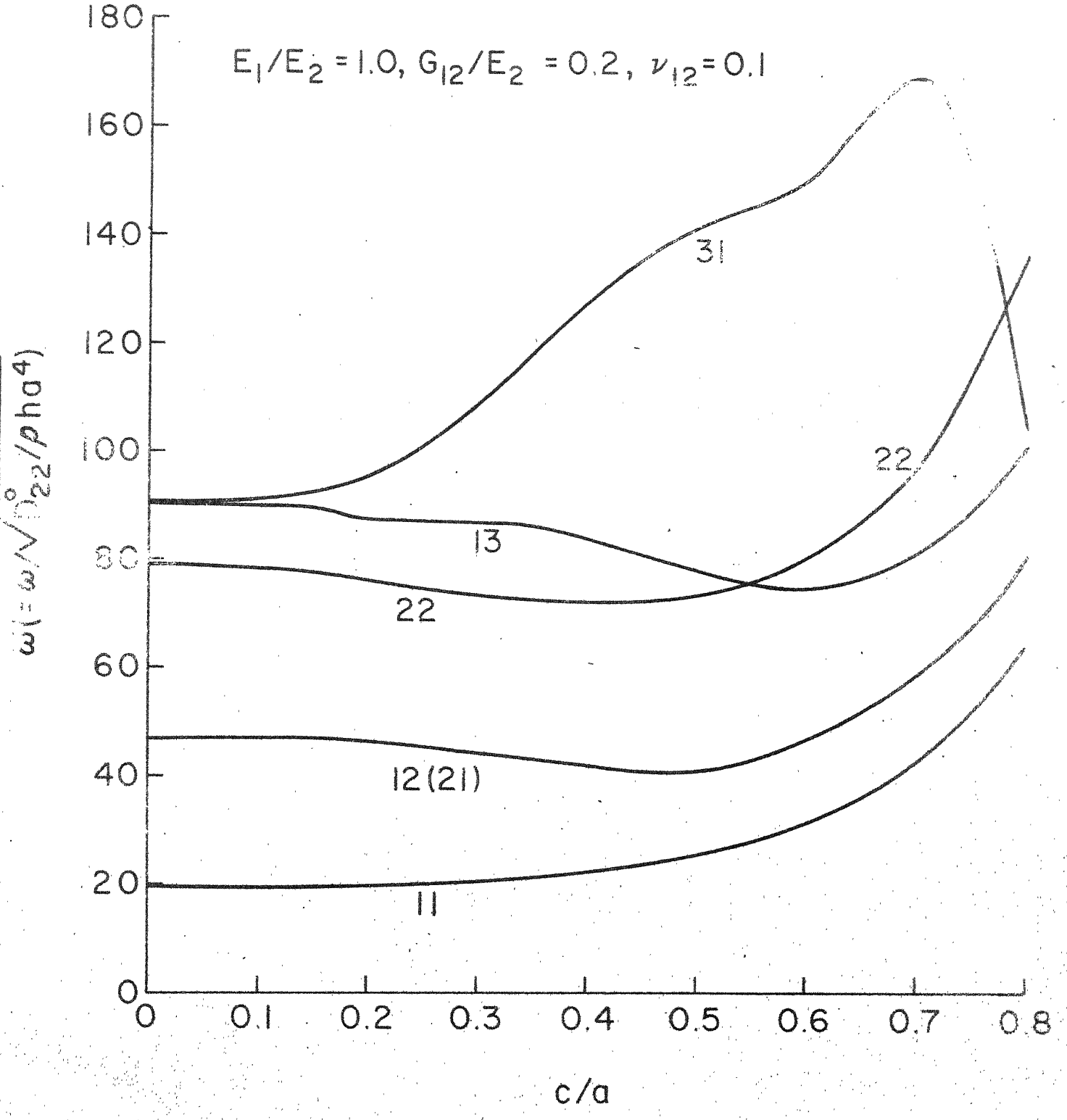

Fig.2.4 $\bar{\omega}$ vs c/a for a simply-supported plate; $\theta = 45°$, R = 1.0

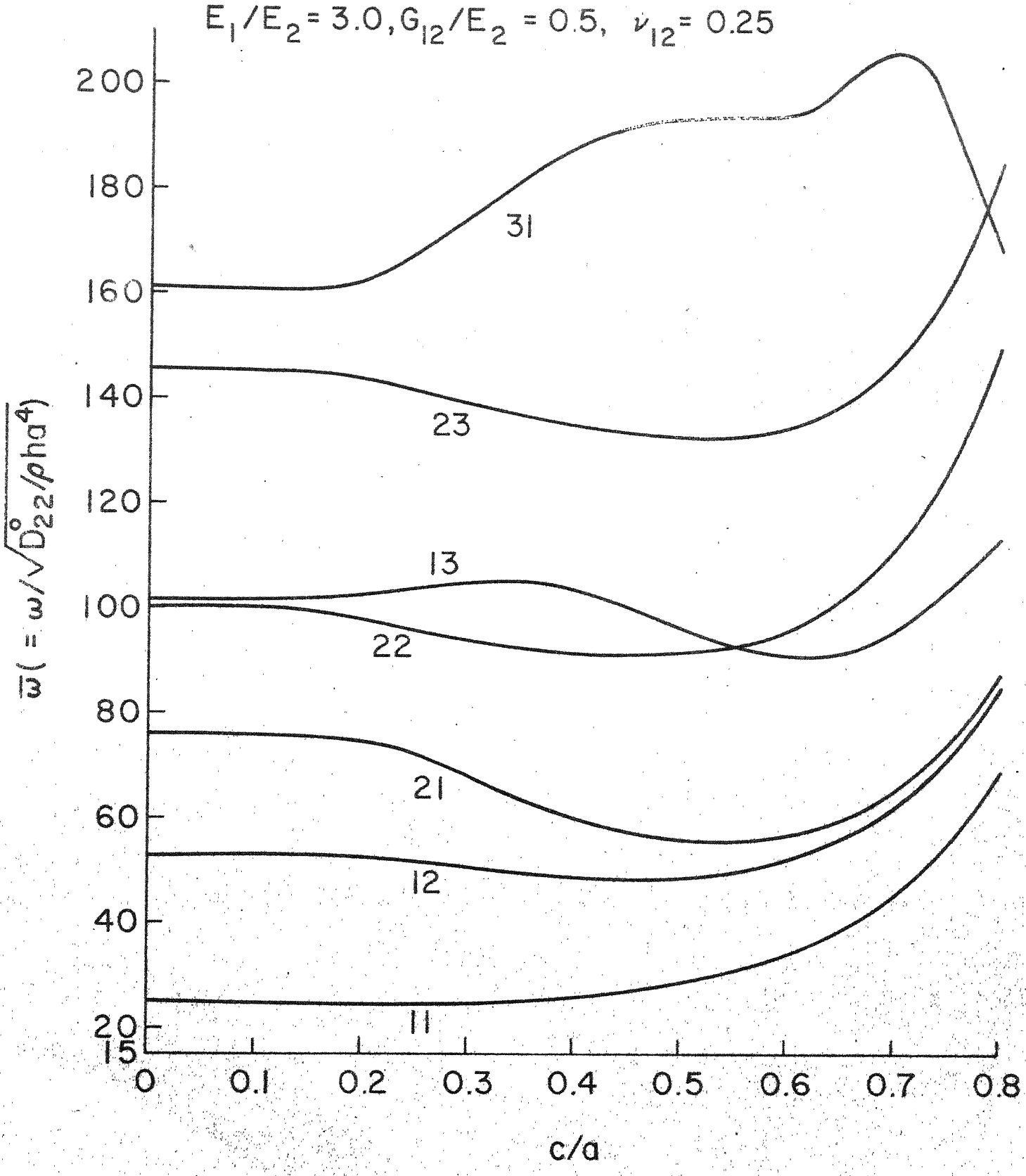

Fig.2.5 $\bar{\omega}$ vs c/a for a simply-supported plate; $\Theta = 0°$, $R = 1.0$

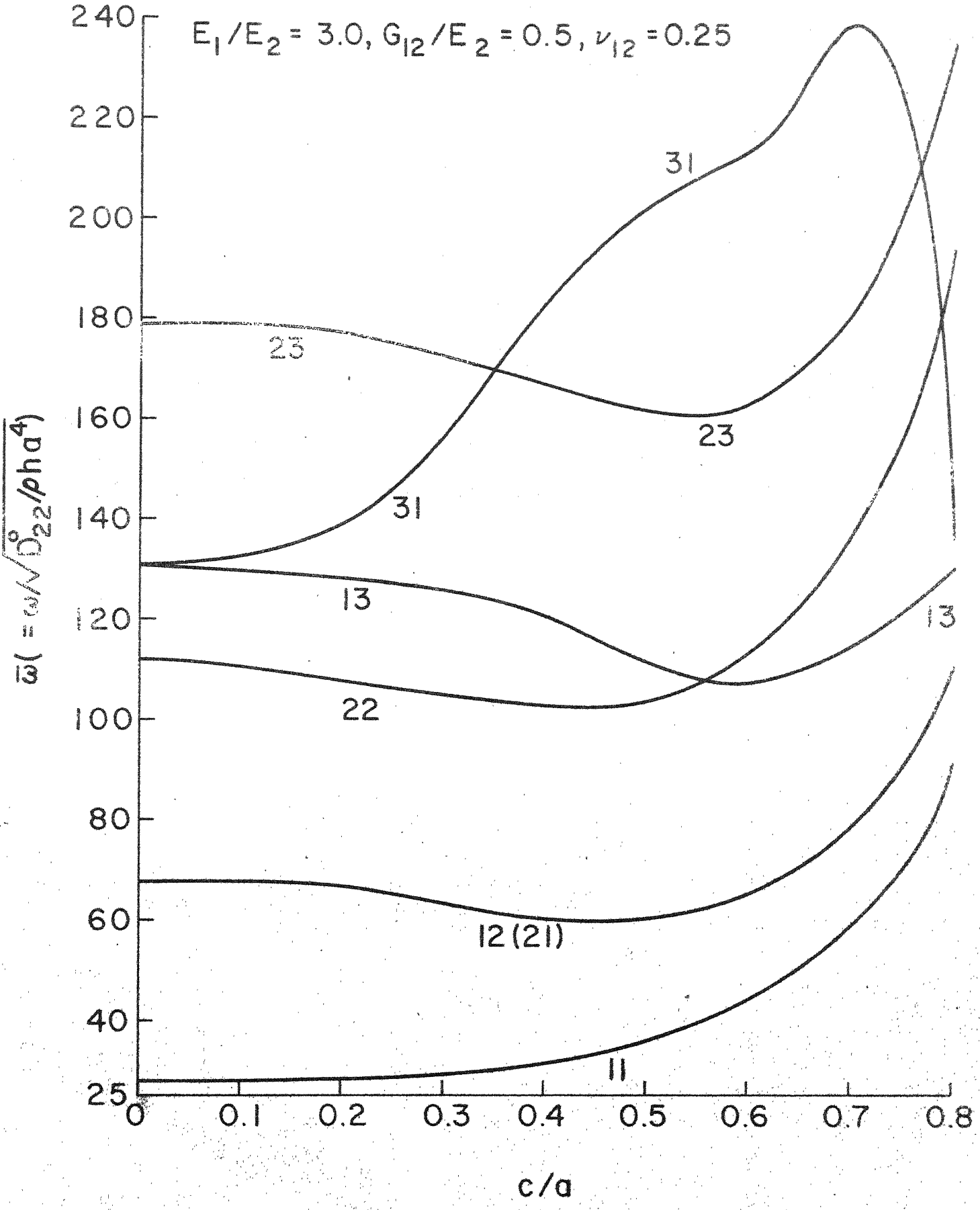

Fig.2.6 $\bar{\omega}$ vs c/a for a simply-supported plate; $\theta = 45^\circ$, R = 1.0

$E_1/E_2 = 3, G_{12} = 0.5, \nu_{12} = 0.25$

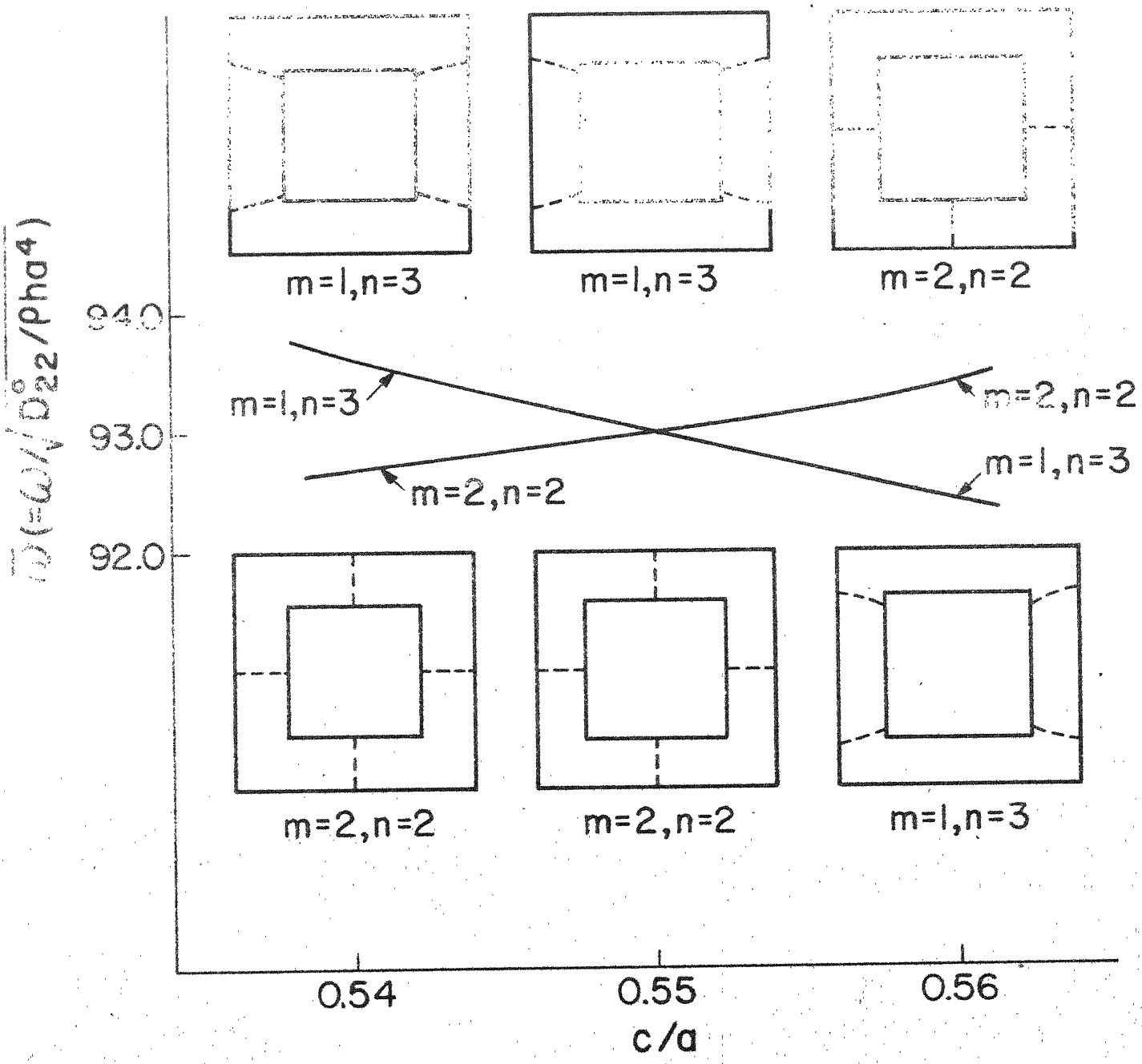

Fig 2.7 Mode shapes for a simply supported plate; $\Theta = 0°$, $R = 1.0$

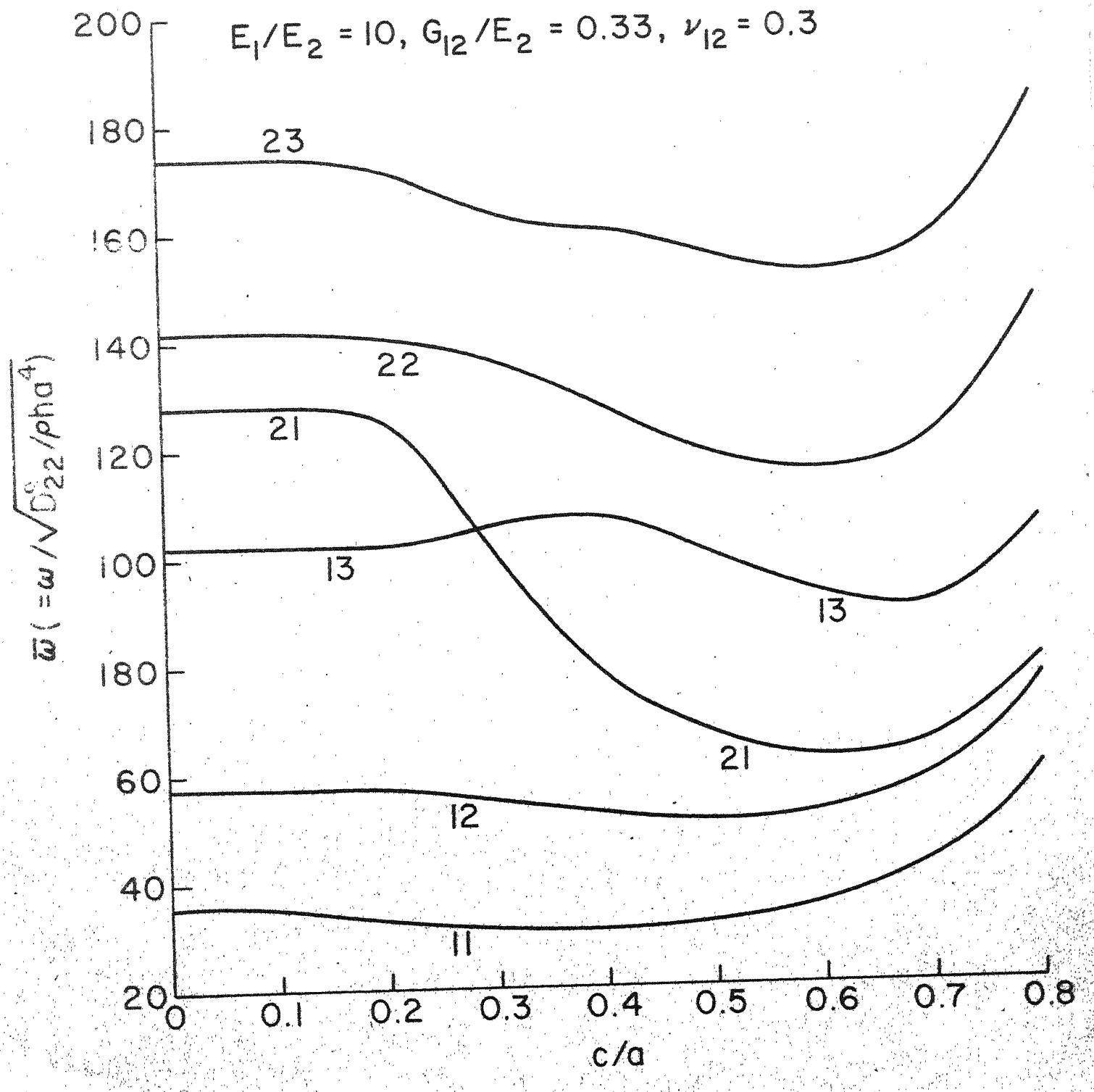

Fig.2.8 $\bar{\omega}$ vs c/a for a simply-supported plate; $\theta = 0^{\circ}$, R = 1.0

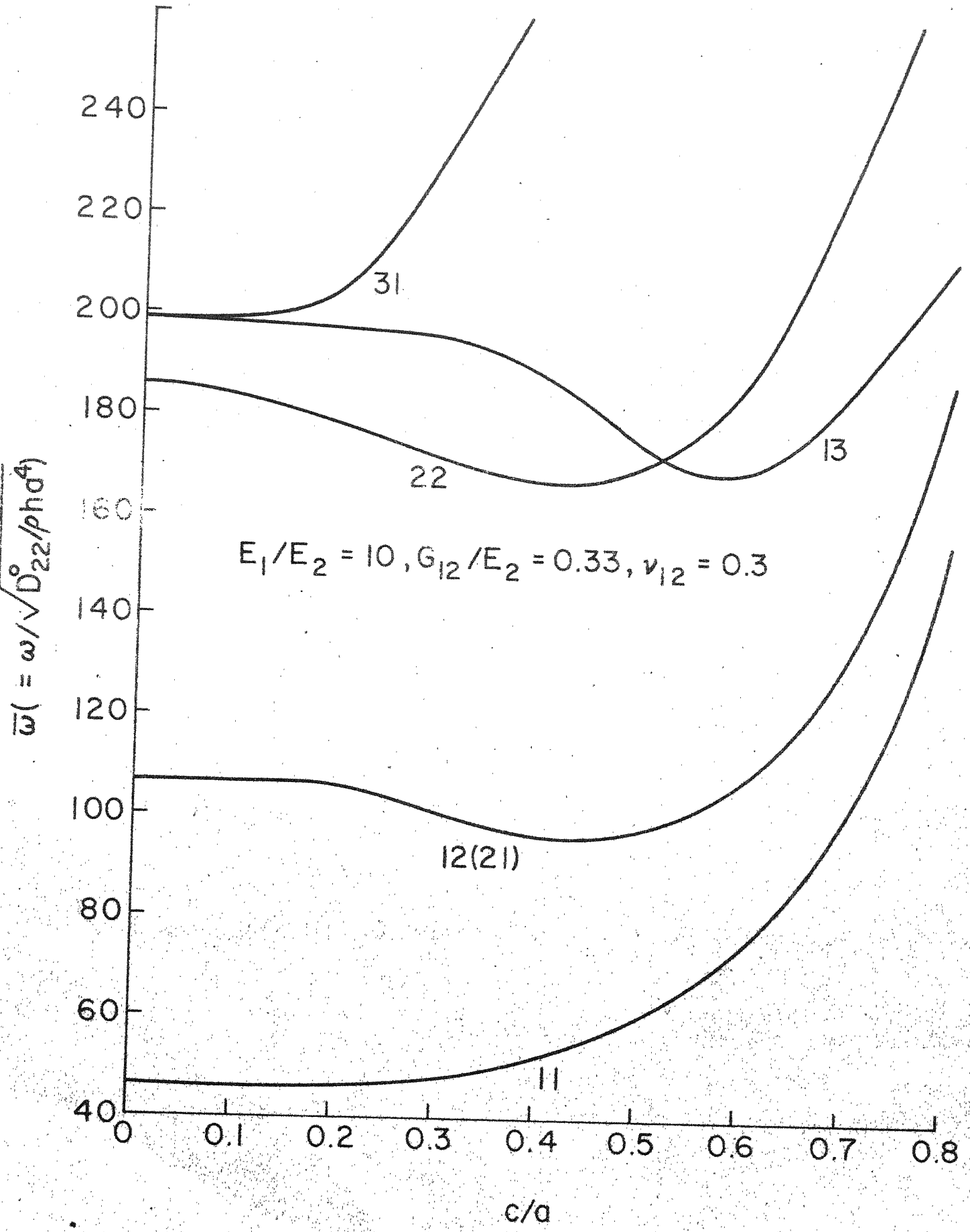

Fig.2.9 $\bar{\omega}$ vs c/a for a simply-supported plate; $\theta = 45°$ R = 1.0

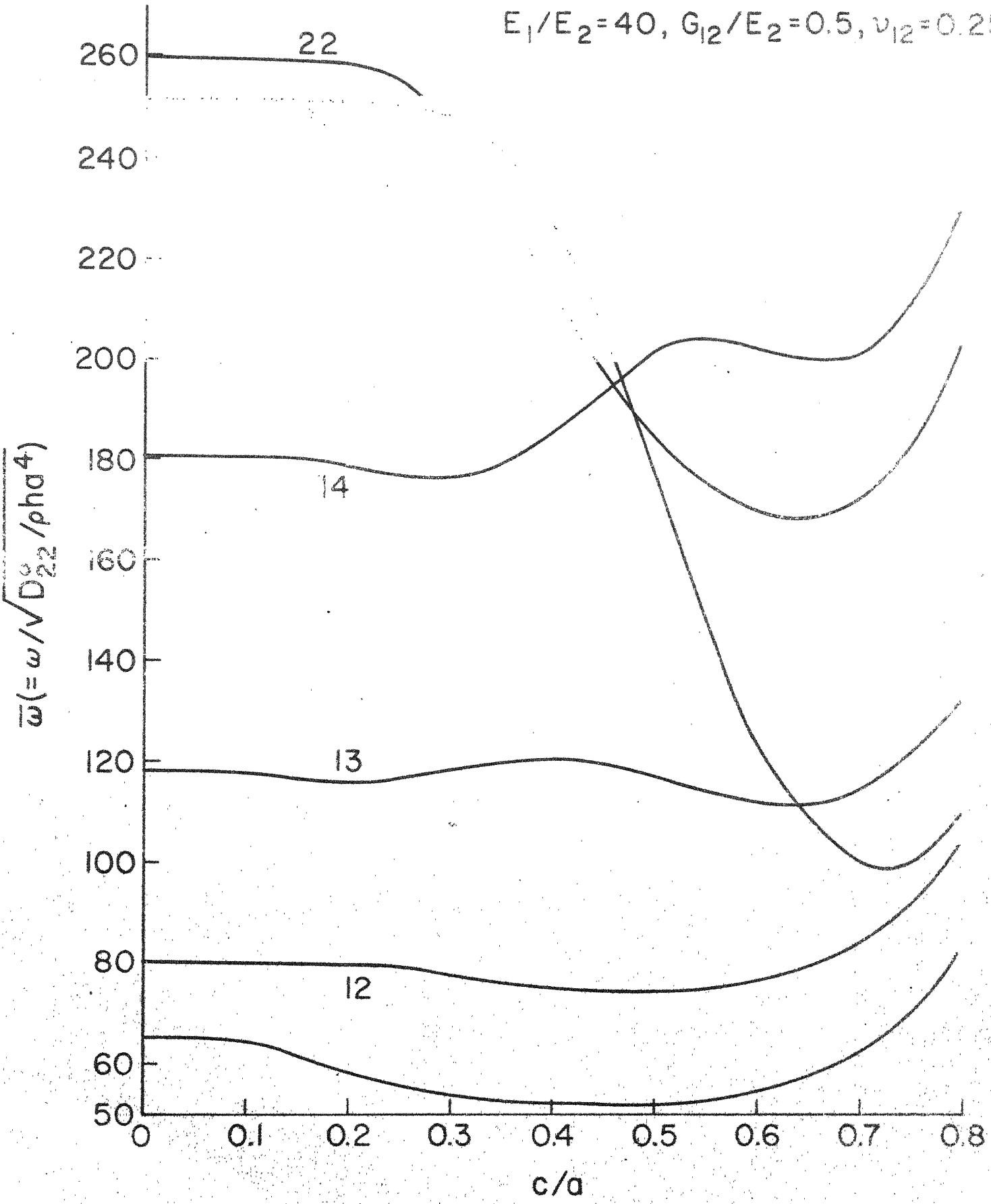

Fig.2.10 $\bar{\omega}$ vs c/a for a simply-supported plate; $\theta=0°$, $R=1.0$

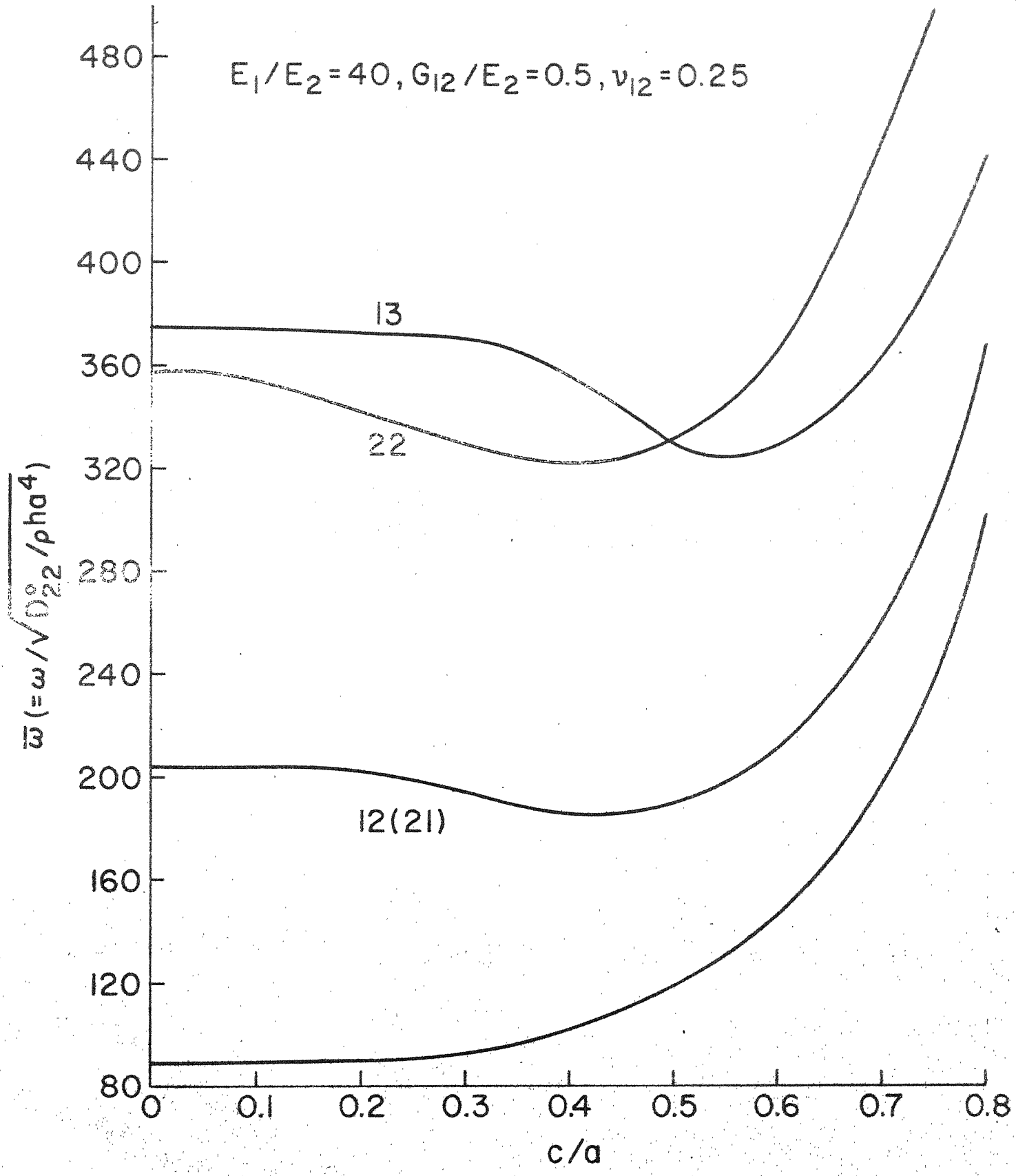

Fig.2.11 $\bar{\omega}$ vs. c/a for a simply-supported plate; $\Theta=45°, R=1.0$

$E_1/E_2=3, G_{12}/E_2=0.5, \nu_{12}=0.25$

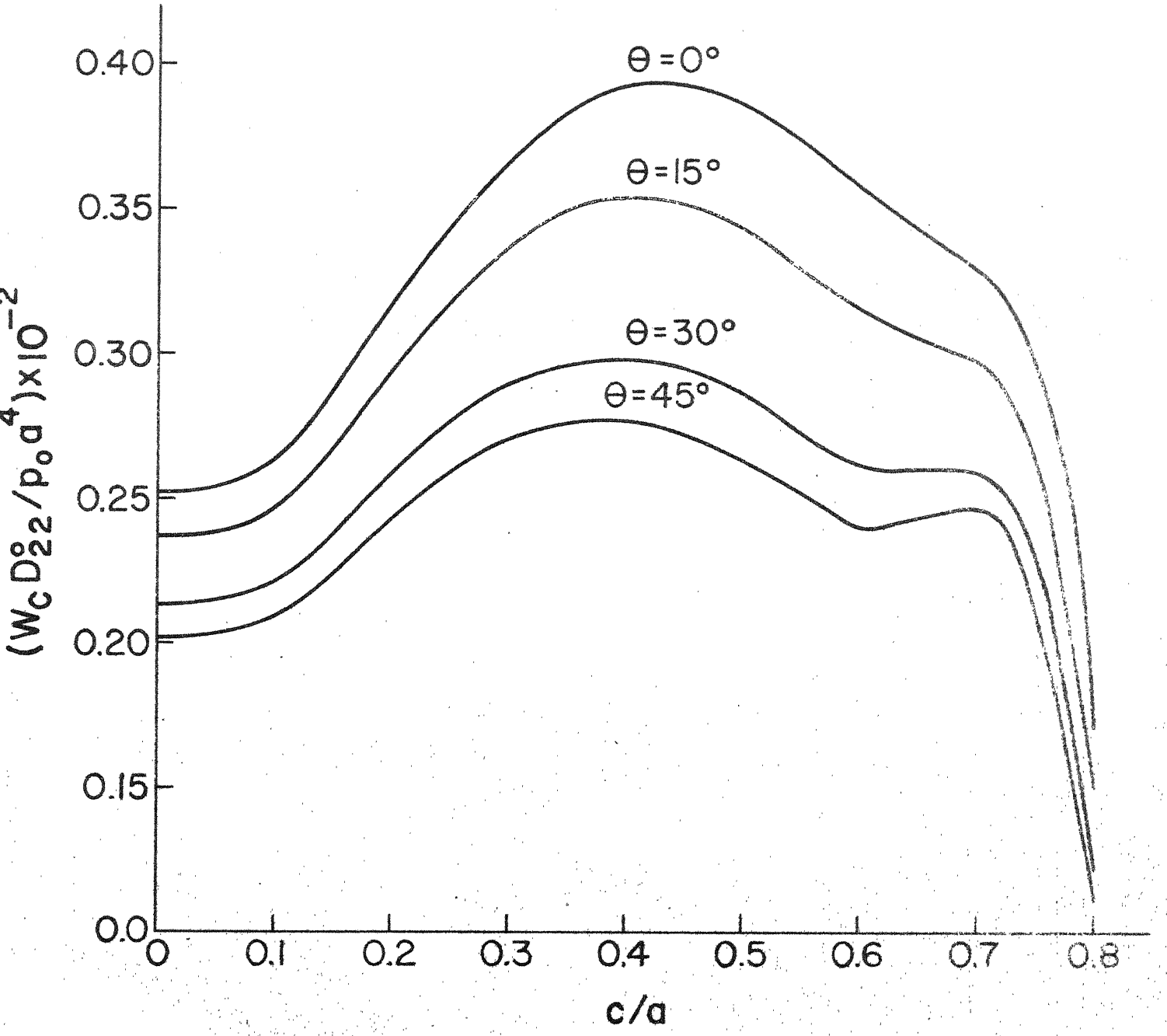

Fig.2.12 Deflection vs. c/a for a simply-supported plate; R=1.0

that cut-outs make orthotropic plates less stiff for medium cut-out sizes in all modulus ratios considered. Frequencies $\bar{\omega}_{12}$, $\bar{\omega}_{21}$, $\bar{\omega}_{22}$, $\bar{\omega}_{23}$ and $\bar{\omega}_{14}$ are found to decrease with increase in cut-out size for all fibre orientation angles and modulus ratios. They increase with larger cut-out ratios. The behaviour of frequency $\bar{\omega}_{13}$ is, however, unpredictable.

An attempt has been made to study the behaviour of frequencies. For this, the deflection at the centre is found in the case of a unidirectionally reinforced glass-epoxy, simply-supported plate which gives an idea about the variation in stiffness (and hence the fundamental frequency) with the cut-out ratio. In Figure 2.12 which shows the variation of the deflection with cut-out ratio for a unidirectionally reinforced glass-epoxy plate and for fibre orientation angles equal to 0°, 15°, 30° and 45°, the stiffness is found to decrease initially with c/a; the rate of decrease being maximum for $\theta = 0°$. As c/a is increased (c/a >0.4), stiffness starts increasing for all the fibre orientation angles. This explains the decrease in the fundamental frequency at medium cut-outs and the increase for larger cut-outs. The explanation of the behaviour of higher modes is, however, difficult.

b) The effect of fibre-orientation angle on the natural frequency

The effect of fibre-orientation angle on the frequencies $\bar{\omega}_{11}$ and $\bar{\omega}_{12}$ has been shown for different values of cut-out ratios. In Figures 2.13 to 2.16, the variation of $\bar{\omega}_{11}$ with θ for different c/a values is shown for balanced bidirectional, unidirectional glass-epoxy, unidirectional boron-epoxy and unidirectional graphite-epoxy plates. It is seen that in all the cases $\bar{\omega}_{11}$ increases with θ for all cut-out parameters. As the cut-out size is

increased, the rate of increase of $\bar{\omega}_{11}$ increases. For balanced bidirectional plates (Figure 2.13), $\bar{\omega}_{11}$ corresponding to c/a = 0.2 is lower than that corresponding to c/a = 0.0 at $\theta = 0°$ and the curves for $\bar{\omega}_{11}$ corresponding to these two values of c/a intersect as θ is increased. In Figures 2.14a and 2.14b, $\bar{\omega}_{11}$, for a unidirectional glass-epoxy plate, is shown to vary with θ for different cut-out parameters, the variation of $\bar{\omega}_{11}$ with θ for smaller cut-outs being shown in Figure 2.14a. It is observed in Figure 2.14a that $\bar{\omega}_{11}$ is minimum for c/a = 0.2 at $\theta = 0°$. The frequency, however, increases with θ . In Figure 2.14b, it is found that the frequency curves for c/a = 0.0 and 0.2 intersect just as in the case of balanced bidirectional plates. For unidirectional boron-epoxy and unidirectional graphite-epoxy plates (Figures 2.15 and 2.16 respectively), the frequency curves for c/a = 0.0 and c/a = 0.2 do not intersect and the frequency values become almost equal at $\theta = 45°$. However, in Figures 2.15 and 2.16 it is seen that the curve for c/a = 0.0 intersects with curves for c/a = 0.3, 0.4, 0.5 and 0.6 in case of unidirectional boron-epoxy plates whereas it is found to intersect with these for c/a = 0.3, 0.4, 0.5, 0.6 and 0.7 in case of unidirectional graphite-epoxy plates. Thus, there is a decrease in the fundamental frequency with increase in c/a in the case of simply-supported plates with higher modulus ratios for small values of γ . However, there is no trend in this decrease.

The variation of $\bar{\omega}_{12}$ with θ for different c/a values is shown in Figures 2.17 to 2.20 where it is found to increase with θ for all cut-out parameters similar to $\bar{\omega}_{11}$. It is also observed that for a given value of θ,

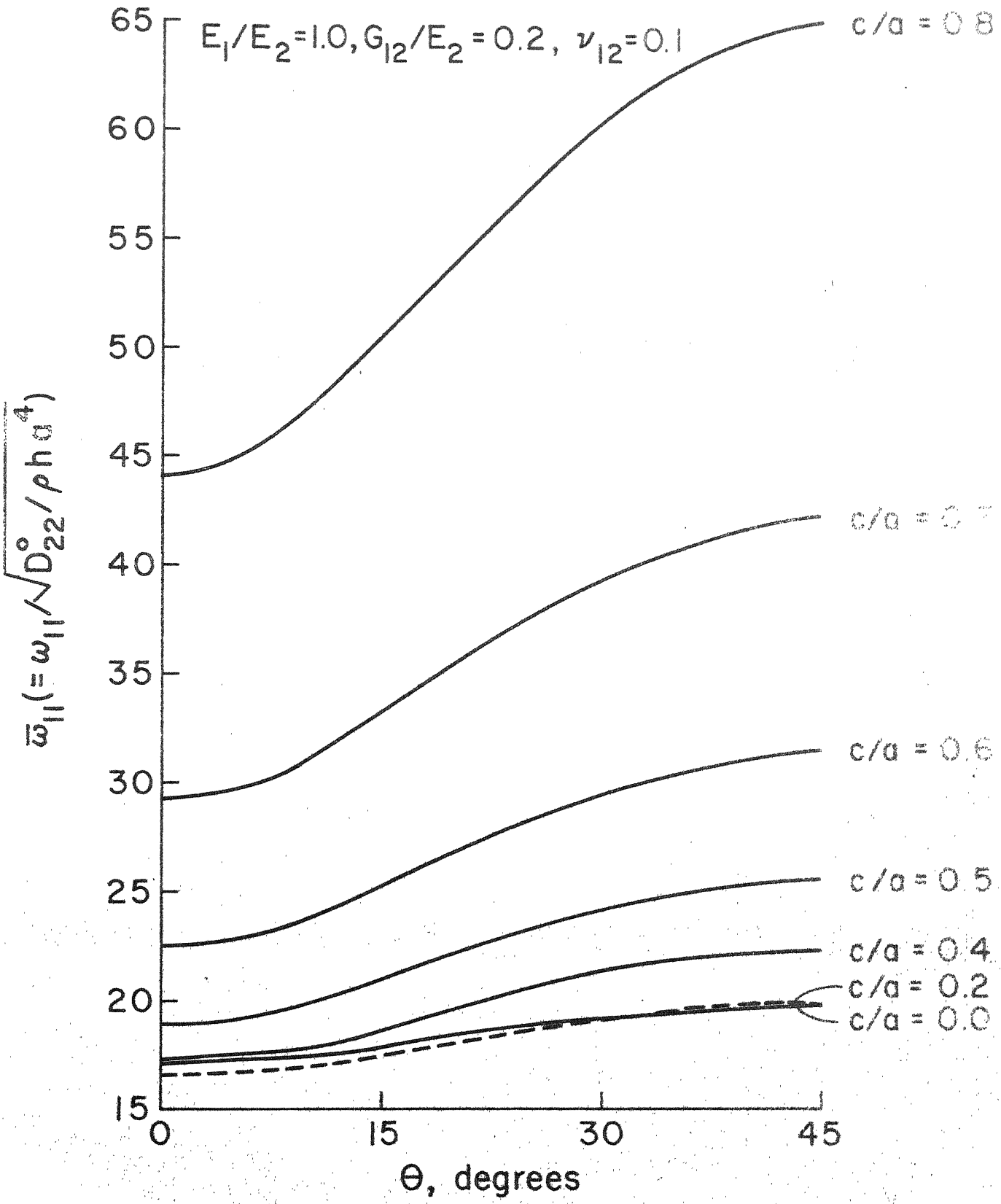

Fig.2.13 $\bar{\omega}_{11}$ vs Θ for different cut-out parameters for a simply-supported plate; R = 1.0

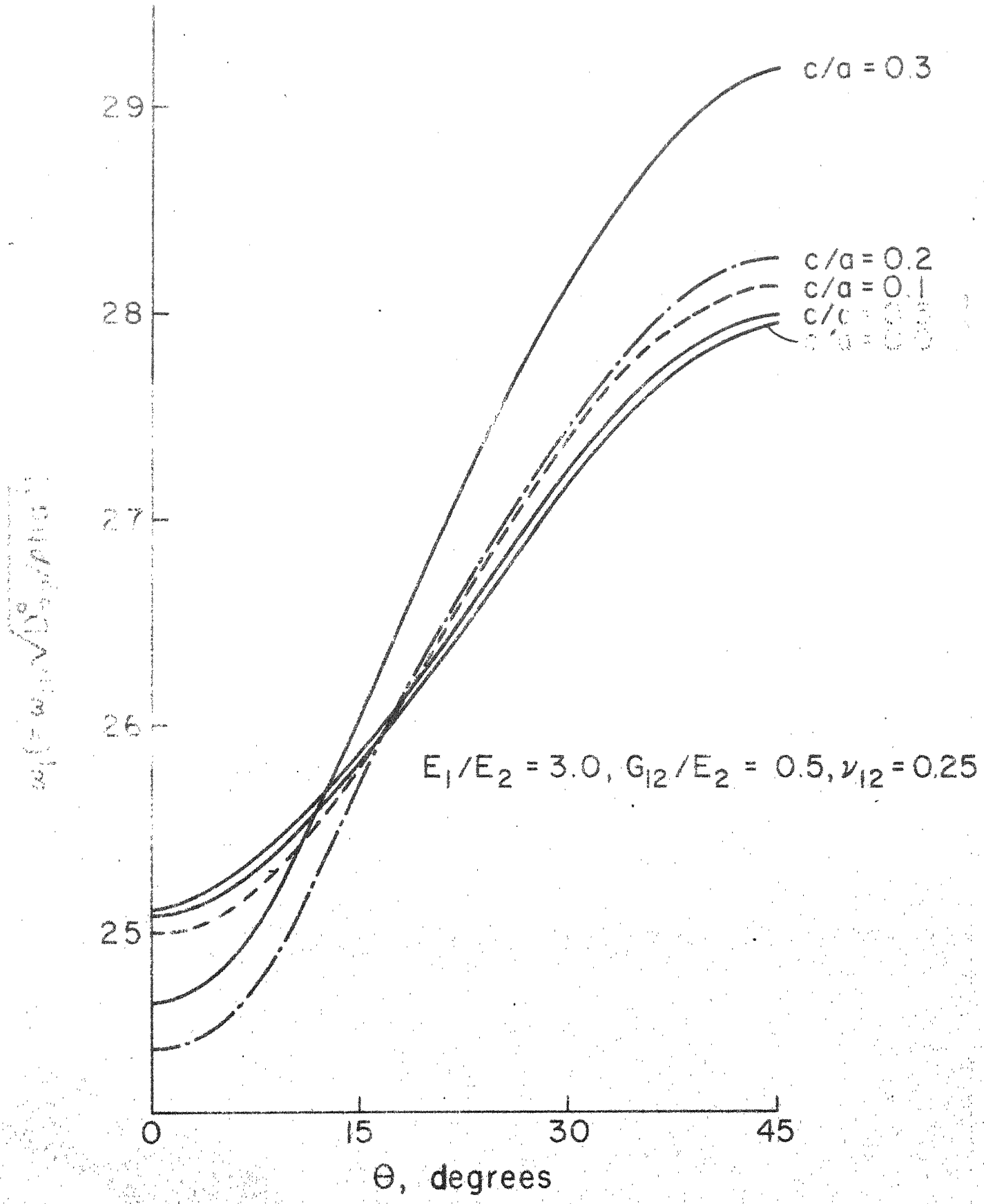

Fig.2.14a $\bar{\omega}_{11}$ vs Θ for different cut-out parameters for a simply-supported plate ; R = 1.0

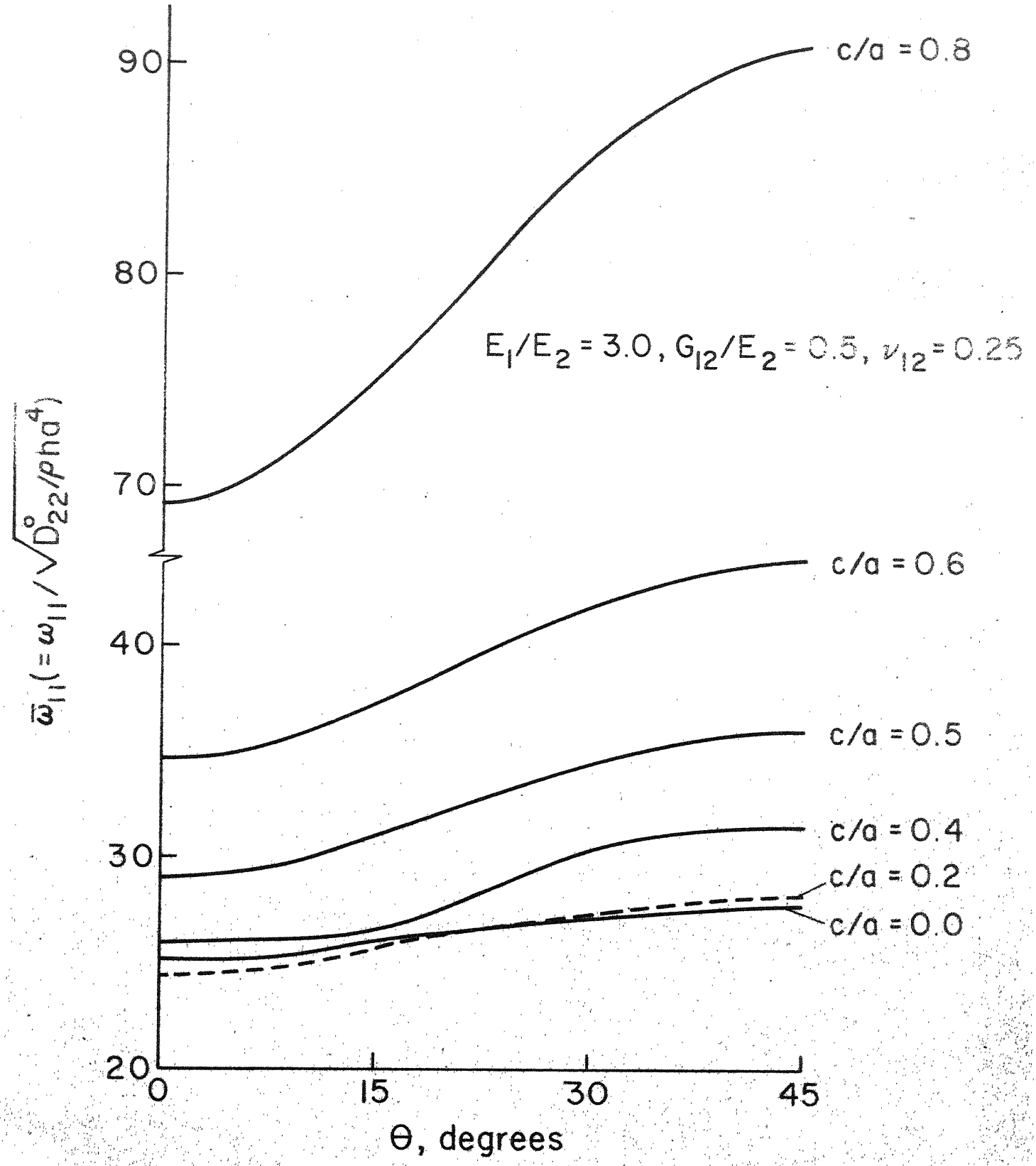

Fig. 2.14b $\bar{\omega}_{11}$ vs Θ for different cut-out parameters for a simply-supported plate; R = 1.0

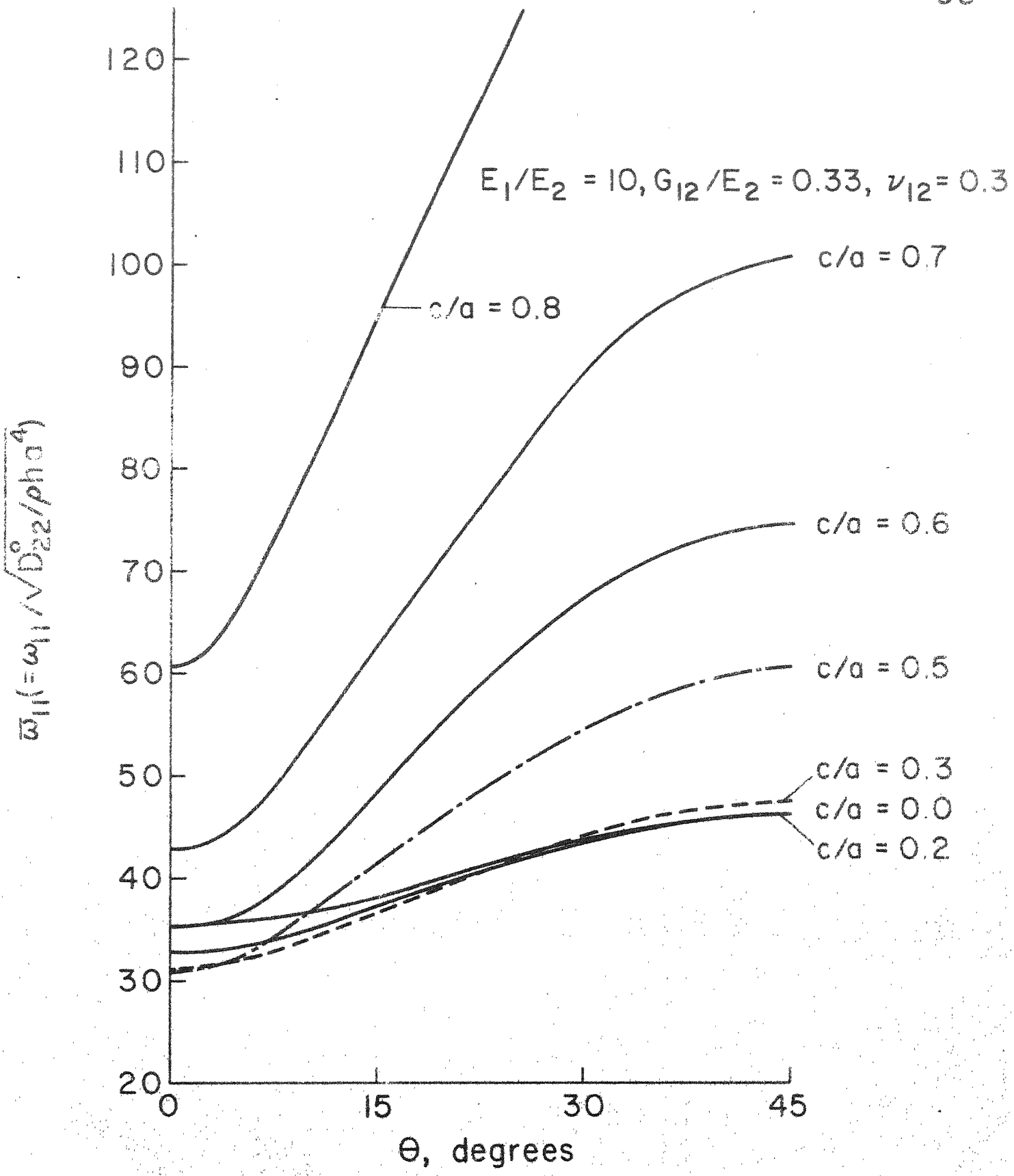

Fig.2.15 $\bar{\omega}_{11}$ vs θ for different cut-out parameters for a simply-supported plate ; R = 1.0

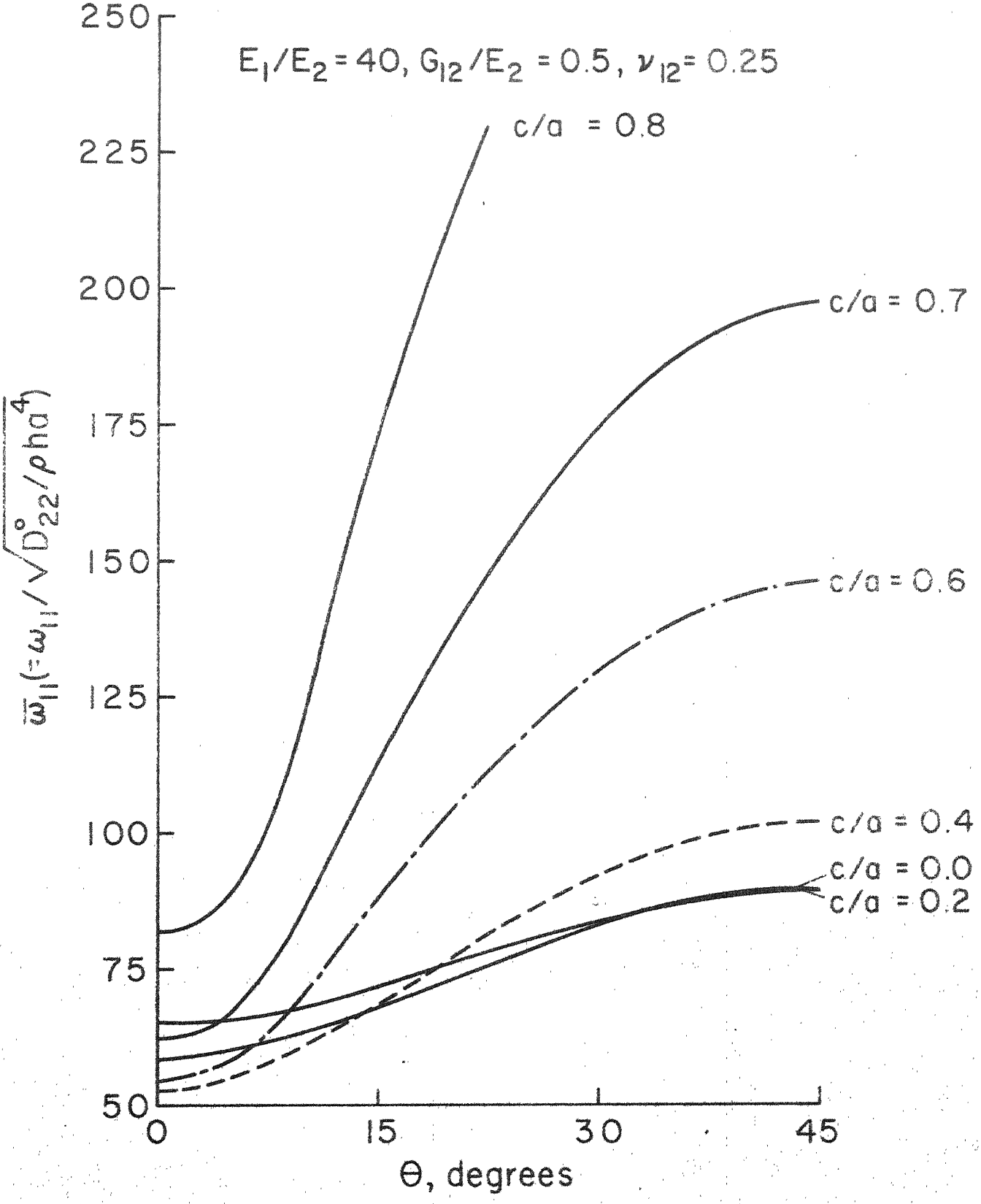

Fig.2.16 $\bar{\omega}_{11}$ vs Θ for different cut-out parameters for a simply-supported plate; R = 1.0

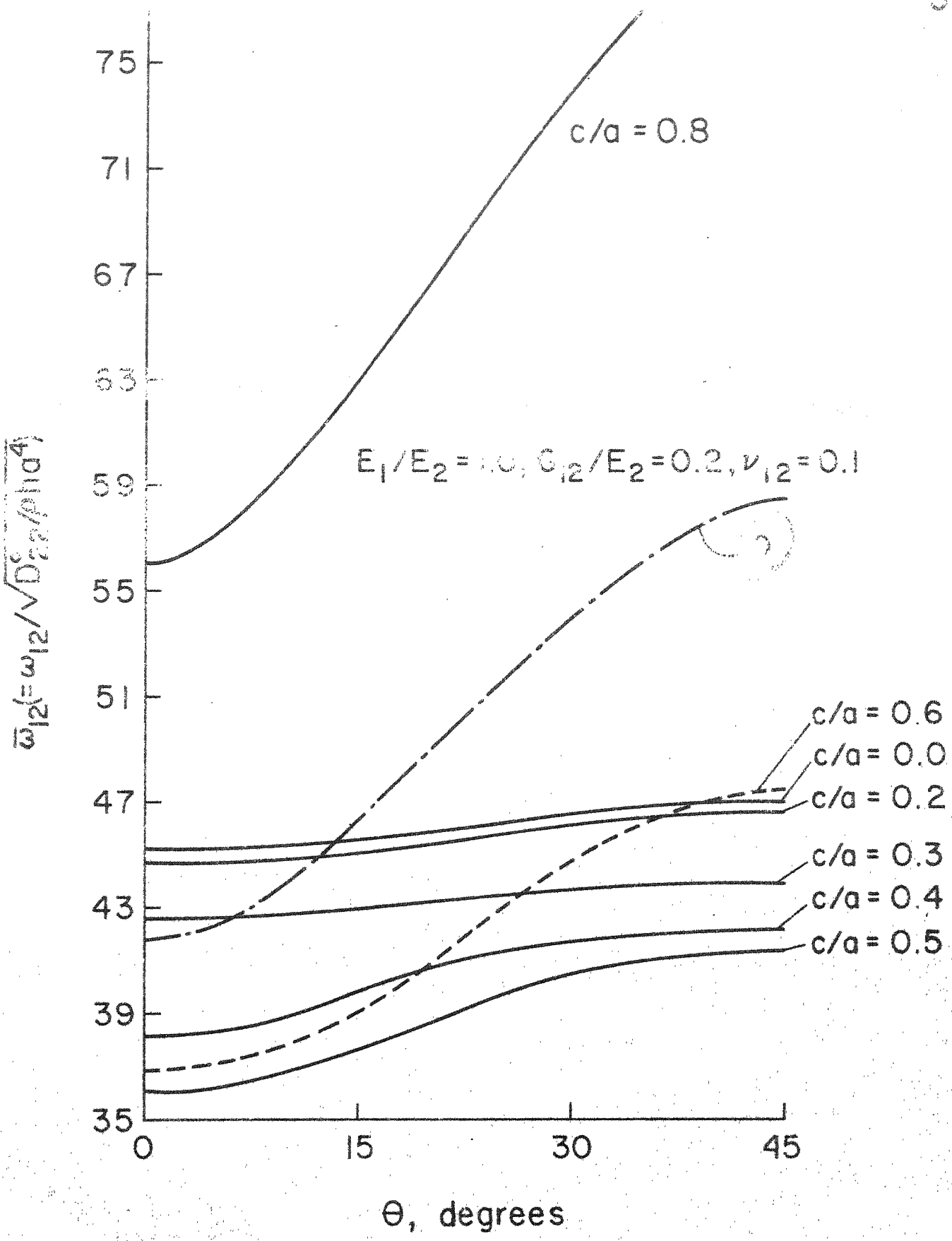

Fig.2.17 $\bar{\omega}_{12}$ vs Θ for different cut-out parameters for a simply-supported plate; R = 1.0

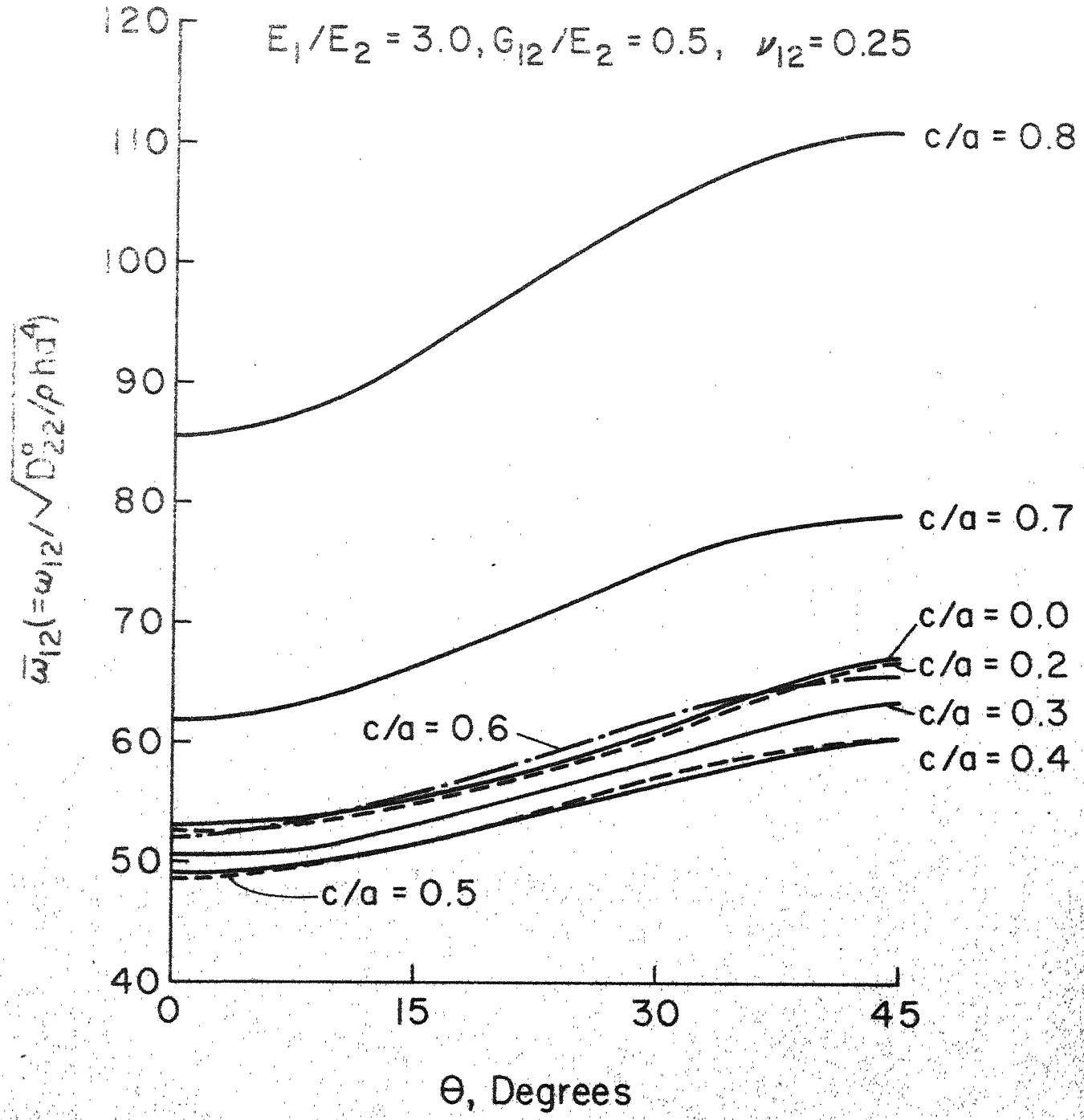

Fig.2.18 $\bar{\omega}_{12}$ vs Θ for different cut-out parameters for a simply-supported plate; R = 1.0

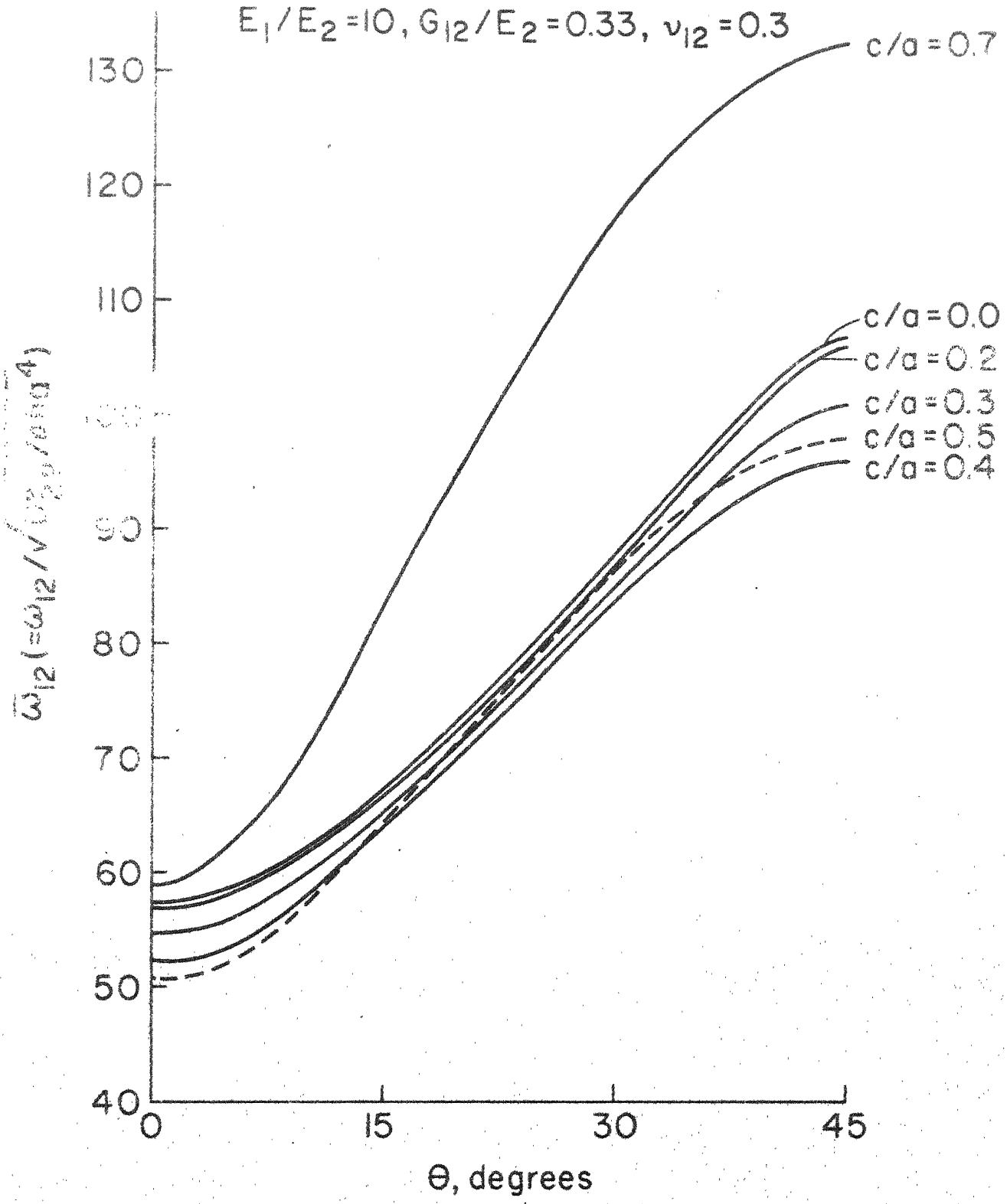

Fig.2.19 $\bar{\omega}_{12}$ vs. θ for diferent cut-out parameters for a simply-supported plate; R = 1.0

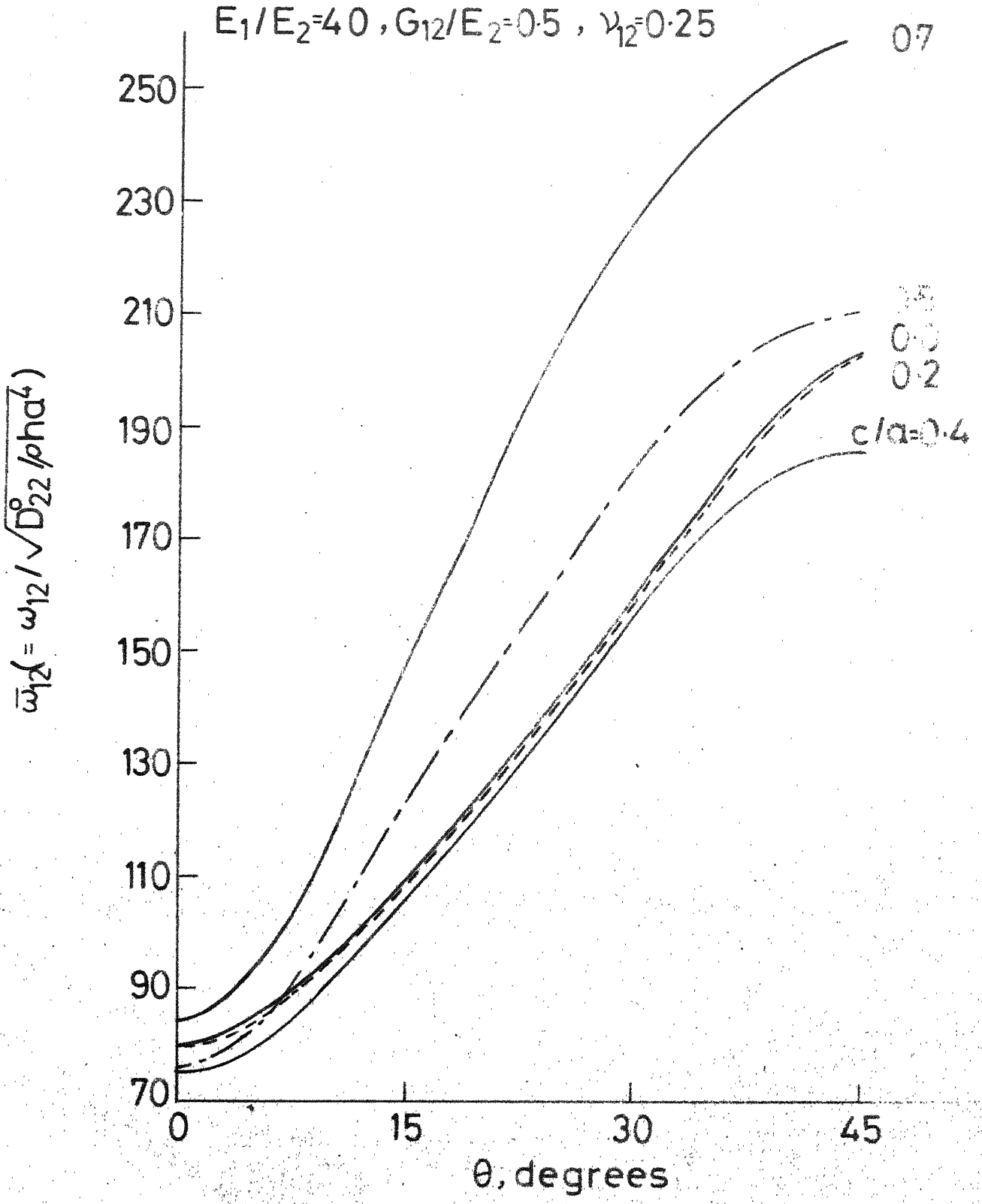

Fig.2·20 $\bar{\omega}_{12}$ Vs θ for different cut-out parameters for a Simply-supported plate, R=1·0

the frequency $\bar{\omega}_{12}$ decreases with increase in c/a values whereas this behaviour was observed in case of $\bar{\omega}_{11}$ only for smaller values of . The behaviour of other frequencies, for example $\bar{\omega}_{21}$, $\bar{\omega}_{22}$ etc., have not been shown. Mohan and Kingsbury [34] also observed the increase in $\bar{\omega}_{11}$, $\bar{\omega}_{12}$ and $\bar{\omega}_{21}$ with fibre-orientation angle for a square, simply-supported boron-epoxy plate with no cut-outs. This trend is also found here for all the modulus ratios considered.

c) The effect of modulus ratio on the natural frequency

In order to understand the effect of modulus ratio on the natural frequency of plates with cut-outs, the behaviour of $\bar{\omega}_{11}$ for different modulus ratios is shown with c/a in Figure 2.21 in the case of fibre orientation angles 0° and 45°. It is observed that for isotropic plates, $\bar{\omega}_{11}$ decreases for small cut-out ratios whereas for an orthotropic plate ($\theta = 0°$), the decrease in $\bar{\omega}_{11}$ occurs upto larger values of c/a. The rate of initial decrease is found to increase with increase in modulus ratios. For $\theta = 0°$, the curves for the fundamental frequency in the case of $E_1/E_2 = 3$ and $E_1/E_2 = 10$ are found to intersect at a value of c/a = 0.638 approximately. This suggests that the increase in orthotropy may not be useful for plates with higher cut-out ratios when the fibre-orientation angle is 0° as stiffness is considerably reduced. It is also seen that the fundamental frequency for a balanced bidirectional orthotropic glass-epoxy plate is always smaller than that for an isotropic plate for all cut-out parameters. The variation of $\bar{\omega}_{11}$ with c/a for different modulus ratios in the case of $\theta = 45°$ is shown by dotted lines. The fundamental

frequency is found to increase for all modulus ratios with c/a. Also, the fundamental frequency for a balanced bidirectional glass-epoxy plate is greater than that for an isotropic plate. Also, the frequency curves for different modulus ratios do not intersect. The frequency values for fibre-orientation angles 15° and 30° lie in between the solid line and the dotted line for a particular modulus ratio, but are not shown.

The variation of $\bar{\omega}_{11}$ and $\bar{\omega}_{21}$ with modulus ratio for c/a = 0.0 is shown in Figure 2.22 for a square, simply-supported plate. For all fibre-orientations $\bar{\omega}_{11}$ and $\bar{\omega}_{21}$ increase with modulus ratio. However, $\bar{\omega}_{11}$ and $\bar{\omega}_{21}$ behave in exactly opposite manner; for any modulus ratio, $\bar{\omega}_{11}$ increases with increase in fibre-orientation angle whereas $\bar{\omega}_{21}$ decreases. This trend is found to be true for all c/a values.

d) The effect of cut-out on the mode shape;

The eigenvectors, normalized with respect to the mass matrix have been obtained in all the cases. It is found that symmetric modes are more influenced due to the presence of a cut-out. The coupling between modes for a symmetric mode is found to be more pronounced at higher a cut-out ratios. This seems logical as the cut-outs considered are symmetrically, located. The antisymmetric modes and a combination of symmetric and antisymmetric modes are not influenced much. Table 2.6 gives a comparison of frequency values (for a symmetric mode) and the normalized eigenvectors for all modulus ratios in the case of $\theta = 0°$. The influence of cut-out can be seen on the eigenvectors.

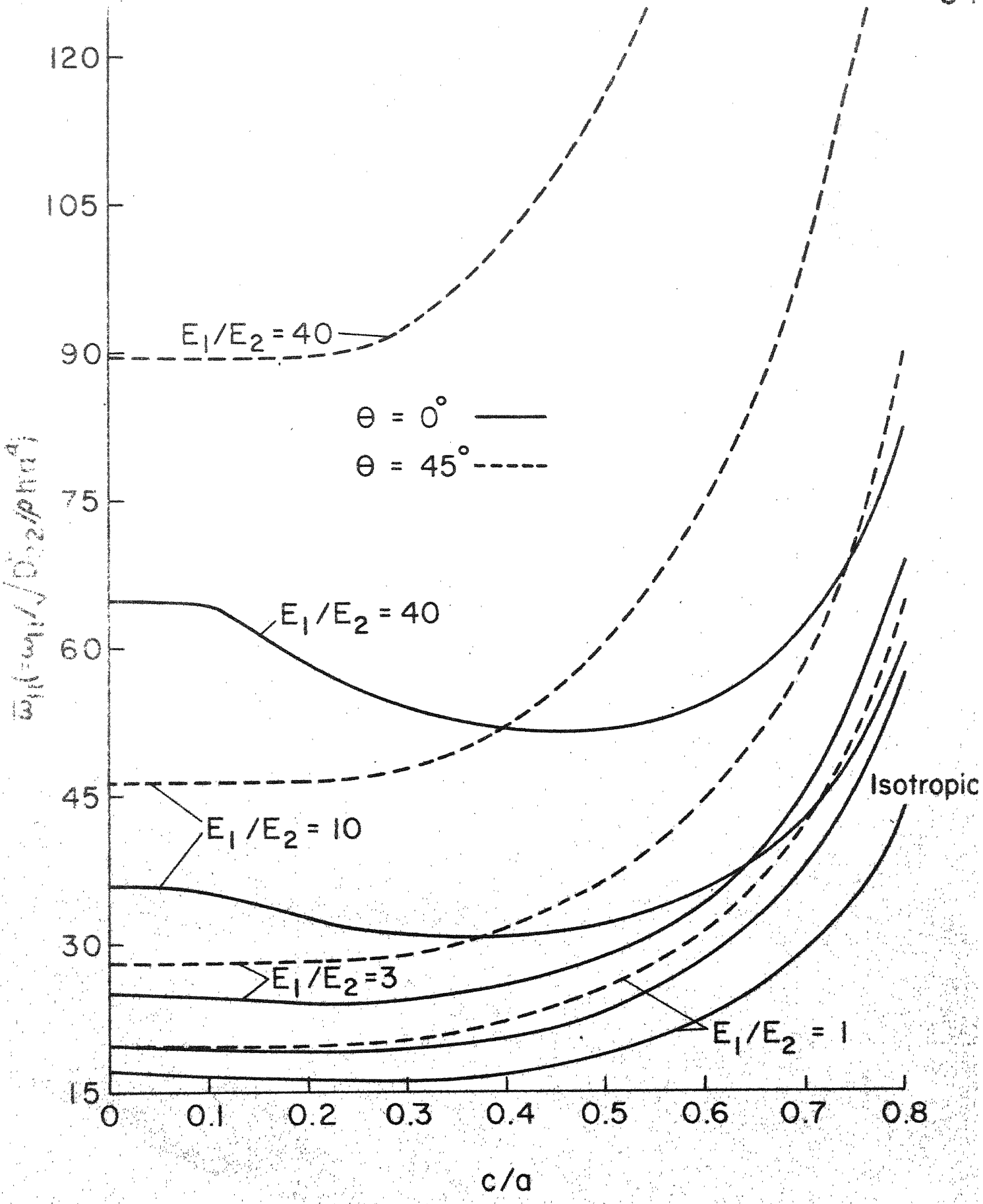

Fig.2.21 $\bar{\omega}_{11}$ vs c/a for different modulus ratios for a simply-supported plate; R = 1.0

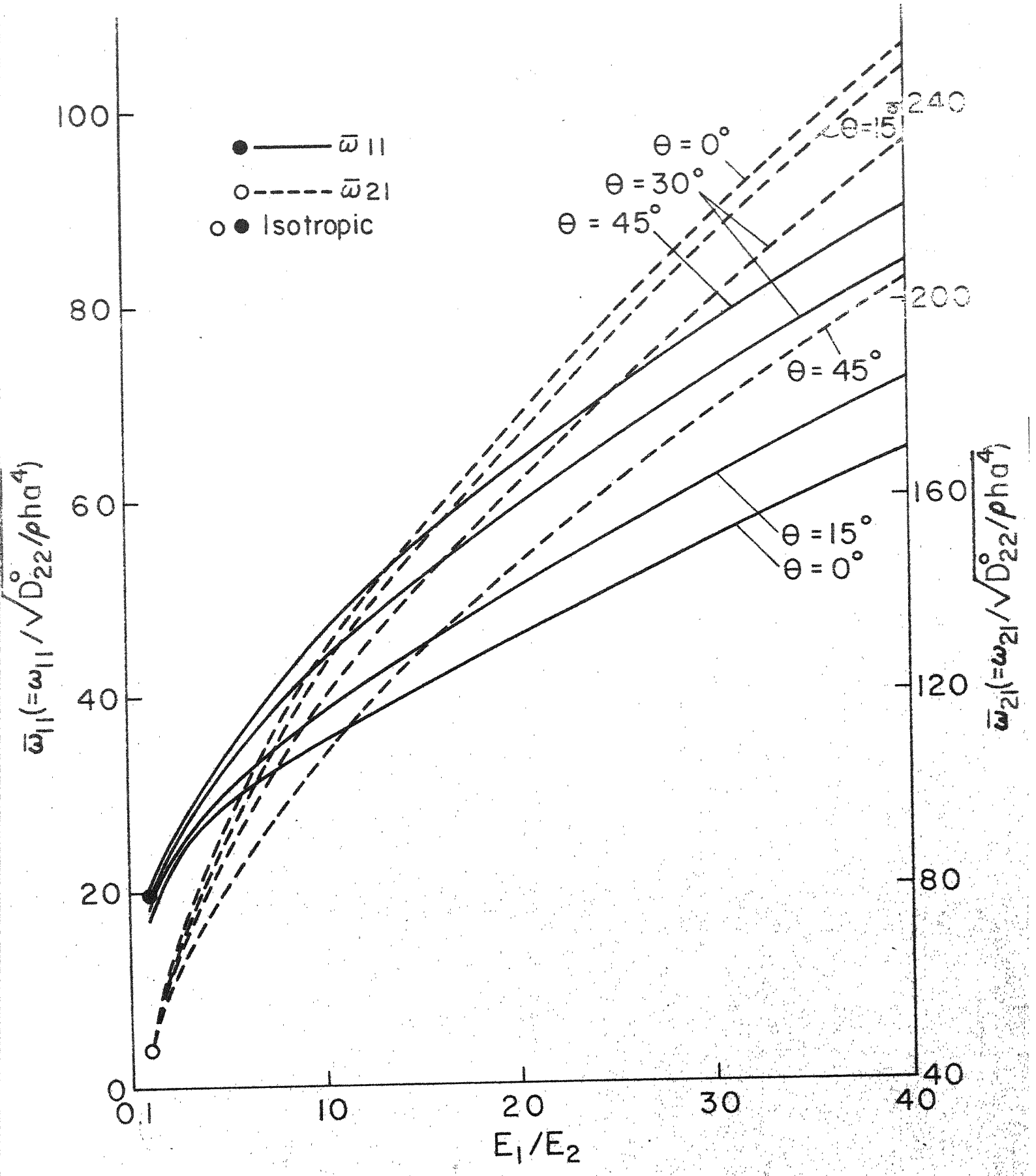

Fig.2.22 Frequency vs modulus ratio for a simply-supported plate; c/a = 0.0, R = 1.0

Table 2.6

Comparison of frequency values and normalized eigenvectors for a simply-supported plate; $\theta = 0°$ $\bar{\omega}_{13}$.

E_1/E_2	1(Isotropic)		1 (Balanced Bidirectional)		3		10		40	
c/a	0.0	0.5	0.0	0.5	0.0	0.5	0.0	0.5	0.0	0.5
$\bar{\omega}_{13}$	98.696	146.24	94.112	131.37	101.67	98.197	102.70	100.07	118.21	117.04
A_{ij}										
A_{11}	0.0	-1.3171	0.0	-0.9790	0.0	-0.6458	0.0	-0.9512	0.0	-0.9111
A_{13}	0.7071	1.0459	0.7071	0.8248	1.0	1.3996	1.0	1.6365	1.0	1.6653
A_{15}	0.0	-0.2263	0.0	-0.1617	0.0	-0.4435	0.0	-0.5291	0.0	-0.4732
A_{17}	0.0	0.0913	0.0	0.0633	0.0	0.1812	0.0	0.2100	0.0	0.1815
A_{31}	0.7071	1.0459	0.7071	0.8248	0.0	-0.4667	0.0	-0.1513	0.0	-0.2099
A_{33}	0.0	0.5021	0.0	0.6518	0.0	-0.0650	0.0	0.0959	0.0	-0.0963
A_{35}	0.0	0.0153	0.0	-0.0229	0.0	0.2066	0.0	0.2357	0.0	0.1785
A_{37}	0.0	-0.0118	0.0	0.0005	0.0	-0.1249	0.0	-0.1471	0.0	-0.1243
A_{51}	0.0	-0.2263	0.0	-0.1617	0.0	0.1945	0.0	0.1024	0.0	0.0466
A_{53}	0.0	0.0153	0.0	-0.0229	0.0	-0.0504	0.0	-0.0001	0.0	0.0180
A_{55}	0.0	0.0654	0.0	0.0913	0.0	-0.0564	0.0	-0.0855	0.0	-0.0740
A_{57}	0.0	-0.0430	0.0	-0.0482	0.0	0.0620	0.0	0.0805	0.0	0.0694
A_{71}	0.0	0.0913	0.0	0.0633	0.0	-0.0838	0.0	-0.0476	0.0	-0.0248
A_{73}	0.0	-0.0118	0.0	0.0005	0.0	0.0398	0.0	0.0089	0.0	-0.0021
A_{75}	0.0	-0.0430	0.0	-0.0482	0.0	0.0048	0.0	0.0276	0.0	0.0274
A_{77}	0.0	0.0390	0.0	0.0393	0.0	-0.0199	0.0	-0.0323	0.0	-0.0288

It has also been pointed out by Mahabaliraja et.al. [58] that the cut-out has an effect of coupling the different waveforms in an otherwise solid shell. This has been observed to be true in the present case of plates with cut-outs also and therefore, the identification of eigenvalues from the largest amplitude coefficient in the eigenvector becomes difficult. However, it is possible to identify the eigenvalues from a comparison of corresponding eigenvectors and finding the relative values of amplitude co-efficients in these eigenvectors.

2.4.3 Clamped-Clamped Plates

a) Effect of cut-out on the natural frequency

The frequencies and corresponding eigenvectors have been obtained in all the cases considered. A verification of results with available results is made for an isotropic solid plate. Table 2.7 gives a comparison of the frequencies and corresponding eigenvectors for a clamped-clamped isotropic solid plate. It is seen that the results obtained in the present investigation compare very well with Young's [83] results.

Table 2.8 gives a comparison of the non-dimensionalized frequencies of an isotropic plate for cut-out parameters equal to 0.0 and 0.5. It is observed that the value of the fundamental frequency for a plate without cut-out obtained in the present study is the same as obtained in [84]. However, the value obtained in [52] is even less than the lower bound reported in [84]. This indicates the improved accuracy of the present method over other methods. It is also seen that the values of frequencies for c/a = 0.5 reported in [52] are lower than the values obtained in the

Table 2.7

Comparison of frequencies and modes of vibration of an isotropic clamped-clamped square plate; c/a = 0.0.

	1st Mode			2nd Mode			3rd Mode			4th Mode			5th Mode	
	Present	Young		Present	Young		Present	Young		Present	Young		Present	Young
	35.985	35.94		73.397	73.41		108.22	108.27		131.58	131.64		132.21	132.25
	A_{11} 1.0000	1.0000	A_{12}	1.0000	1.0000	A_{22}	1.0000	1.0000	A_{11}	0.0000	0.0000	A_{11}	-0.0280	-0.0280
	A_{13} 0.0142	0.0142	A_{14}	0.0101	0.0101	A_{24}	0.0327	0.0326	A_{13}	1.0000	1.0000	A_{13}	1.0000	1.0000
	A_{15} 0.0020	0.0020	A_{16}	0.0020	0.0020	A_{26}	0.0073	0.0073	A_{15}	0.0085	0.0085	A_{15}	0.0054	0.0055
	A_{17} 0.0005		A_{18}	0.0006		A_{28}	0.0023		A_{17}	0.0021		A_{17}	0.0013	
	A_{31} 0.0142	0.0142	A_{32}	0.0408	0.0406	A_{42}	0.0327	0.0326	A_{31}	-1.0000	-1.0000	A_{31}	1.0000	1.0000
A_{ij}'s	A_{33} -0.0031	-0.0031	A_{34}	-0.0023	-0.0022	A_{44}	-0.0020	-0.0019	A_{33}	0.0000	0.0000	A_{33}	0.1281	0.1267
	A_{35} -0.0009	-0.0009	A_{36}	-0.0007	-0.0007	A_{46}	-0.0011	-0.0010	A_{35}	-0.0144	-0.0141	A_{35}	0.0119	0.0118
	A_{37} -0.0003		A_{38}	-0.0003		A_{48}	-0.0005		A_{37}	0.0044		A_{37}	0.0034	
	A_{51} 0.0020	0.0020	A_{52}	0.0070	0.0070	A_{62}	0.0073	0.0073	A_{51}	-0.0085	-0.0085	A_{51}	0.0054	0.0055
	A_{53} -0.0009	-0.0009	A_{54}	-0.0011	-0.0011	A_{64}	-0.0011	-0.0010	A_{53}	0.0144	0.0141	A_{53}	0.0119	0.0118
	A_{55} -0.0004	-0.0004	A_{56}	-0.0006	-0.0005	A_{66}	-0.0007	-0.0006	A_{55}	0.0000	0.0000	A_{55}	-0.0020	-0.0018
	A_{57} -0.0002		A_{58}	-0.0002		A_{68}	-0.0003		A_{57}	0.0000		A_{57}	-0.0010	

Table 2.8

Comparison of non-dimensionalized frequency for a clamped-clamped, square isotropic plate; c/a = 0.0 and c/a = 0.5

Source	Cut-out parameter					
	0.0	0.5				
	Mode 1	Mode 1	Mode 2	Mode 3	Mode 4	Mode 5
Kristiansen [51]	-	60.80	-	-	-	-
Paramsivam [52]	34.85	62.40	68.55	98.52	143.95	-
Agarwal [85]	35.7	69.10	77.20	105.0	-	-
Leissa [84]	35.985 (Lower bound-35.976)	-	-	-	-	-
Present	35.985	65.581	79.619	108.91	117.95	190.83

present study; this may be due to the fact that a coarse mesh size has been taken by Paramsivam. A comparison is also made with the available experimental results [85] and good agreement is found.

The variation of non-dimensional frequencies with c/a for a clamped-clamped isotropic plate is shown in Figure 2.23. It is interesting to note that the third and fourth modes as well as the fifth and sixth modes interchange. This has also been observed in [86] for a rectangular isotropic plate with a central square cut-out. Results obtained in [52] are lower than those obtained in the present study. The values given by Kristiansen and Soedel [51] compare well for smaller values of c/a but are low for higher values of c/a. This may be because of the reason that they have used Rayleigh's method. The experimental values given in [85] are also compared for the first three natural frequencies.

The fundamental frequency, unlike in the case of a simply-supported isotropic plate, does not decrease for small cut-outs but increases continuously as the cut-out size is increased. The behaviour of frequencies $\bar{\omega}_{12}$ ($= \bar{\omega}_{21}$), $\bar{\omega}_{22}$ and $\bar{\omega}_{23}$ ($= \bar{\omega}_{32}$) is found to be similar. They first decrease with the increase in cut-out size but again increase as the cut-out size is increased. This has also been observed for a simply-supported plate. It was also seen that the fourth mode and the fifth mode are identical for a simply-supported solid isotropic plate. This is not found to be true for a clamped-clamped plate. The reason is that a closed form solution for a clamped-clamped isotropic plate is not known and the approximation can be assumed to give rise to the fourth mode even when there is no cut-out in the plate.

In Figures 2.24 and 2.25, the variation of $\bar{\omega}$ with c/a is shown for balanced bidirectional composite plates in the case of $\theta = 0°$ and $\theta = 45°$ respectively. It is found that $\bar{\omega}_{11}$ and $\bar{\omega}_{31}$ increase with c/a for $= 0°$ and $\theta = 45°$ as well. For $\theta = 0°$ and $\theta = 45°$, $\bar{\omega}_{12}$, $\bar{\omega}_{22}$, $\bar{\omega}_{13}$ and $\bar{\omega}_{23}$ decrease with increasing values of c/a and then increase again for higher values of c/a. It is interesting to note that modes corresponding to $\bar{\omega}_{22}$ and $\bar{\omega}_{13}$ and those corresponding to $\bar{\omega}_{23}$ and $\bar{\omega}_{31}$ interchange for all fibre-orientation angles. The behaviour of balanced bidirectional composite plates is very similar to that of an isotropic plate.

The variation of $\bar{\omega}$ with c/a for unidirectional glass-epoxy plates is shown in Figures 2.26 and 2.27 for $\theta = 0°$ and $\theta = 45°$ respectively. Here also, like balanced bidirectional plates, $\bar{\omega}_{11}$ and $\bar{\omega}_{31}$ increase with increasing values of c/a. For $\theta = 0°$, modes corresponding to $\bar{\omega}_{22}$ and $\bar{\omega}_{13}$ interchange at a smaller value of c/a. As the fibre-orientation angle is increased they separate from each other at smaller values of c/a and interchange at a higher value of c/a (Figure 2.27). The modes corresponding to $\bar{\omega}_{23}$ and $\bar{\omega}_{31}$ do not interchange when $\theta = 0°$ (Figure 2.26) but as the fibre-orientation angle is increased they come closer and separate from each other after interchanging once with the increase in c/a ratios (Figure 2.27). As the fibre-orientation angle is increased, the frequency curves for $\bar{\omega}_{12}$ and $\bar{\omega}_{21}$ and those for $\bar{\omega}_{23}$ and $\bar{\omega}_{32}$ come closer and coincide for $\theta = 45°$.

The variation of frequencies with cut-out ratio is shown for a unidirectionally reinforced boron-epoxy plate in Figures 2.28 and 2.29 for

$\theta = 0°$ and $\theta = 45°$, respectively. The frequencies $\bar{\omega}_{11}$, $\bar{\omega}_{31}$ and $\bar{\omega}_{15}$ increase with c/a ratios for both $\theta = 0°$ and $\theta = 45°$. The behaviour of frequency $\bar{\omega}_{13}$ is, however, different; it increases with c/a ratios when $\theta = 0°$ (Figure 2.28) whereas it is found to decrease with increasing values of c/a and then to increase at higher values of c/a when $\theta = 45°$ (Figure 2.29). The behaviour of frequencies $\bar{\omega}_{12}$, $\bar{\omega}_{21}$, $\bar{\omega}_{22}$, $\bar{\omega}_{14}$ and $\bar{\omega}_{23}$ are found similar both for $\theta = 0°$ and $\theta = 45°$. The mode corresponding to $\bar{\omega}_{13}$ is found to interchange with those corresponding to $\bar{\omega}_{21}$, $\bar{\omega}_{22}$ and $\bar{\omega}_{23}$ when $\theta = 0°$. However, there is no interchange of modes except for those corresponding to $\bar{\omega}_{23}$ and $\bar{\omega}_{31}$ in the case of $\theta = 45°$. The frequency curves for $\bar{\omega}_{12}$ and $\bar{\omega}_{21}$ and those for $\bar{\omega}_{23}$ and $\bar{\omega}_{32}$ come closer with the increase in fibre-orientation angle and they coincide for $\theta = 45°$.

For unidirectional graphite-epoxy plates, the variation of $\bar{\omega}$ with c/a for $\theta = 0°$ is shown in Figure 2.30. The frequencies $\bar{\omega}_{11}$, $\bar{\omega}_{13}$ and $\bar{\omega}_{15}$ (corresponding to symmetric modes) increase with c/a. The behaviour of frequencies $\bar{\omega}_{12}$, $\bar{\omega}_{14}$, $\bar{\omega}_{21}$ and $\bar{\omega}_{22}$ is similar to that found for balanced-bidirectional, unidirectional glass-epoxy and unidirectional boron-epoxy plates. The mode corresponding to $\bar{\omega}_{22}$ first interchanges with that corresponding to $\bar{\omega}_{15}$ and then with modes corresponding to $\bar{\omega}_{21}$, $\bar{\omega}_{14}$ and $\bar{\omega}_{13}$. For $\theta = 45°$, the variation of $\bar{\omega}$ with c/a for unidirectional graphite-epoxy plates is shown in Figure 2.31. Here also, as for $\theta = 0°$, $\bar{\omega}_{11}$ increases with c/a. The frequencies $\bar{\omega}_{12}$, $\bar{\omega}_{22}$ and $\bar{\omega}_{13}$ are found to decrease with increase in c/a values; the decrease is significant in $\bar{\omega}_{22}$ compared to that in case of $\theta = 0°$. These frequencies, however, increase with higher

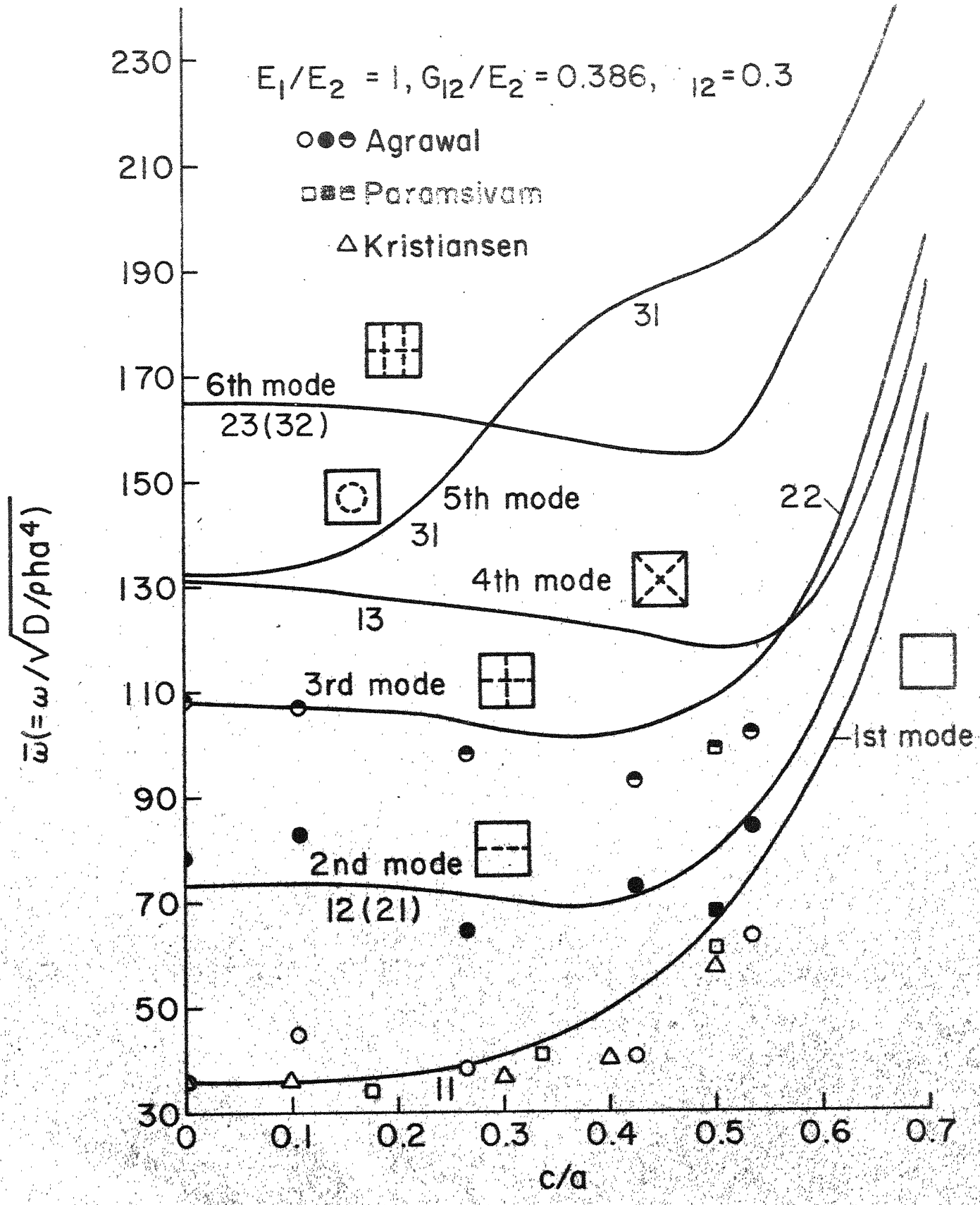

Fig.2.23 $\bar{\omega}$ vs c/a for a clamped-clamped isotropic plate; R = 1.0
○□△ 1st mode, ●■ 2nd mode, ⊖⊟ 3rd mode

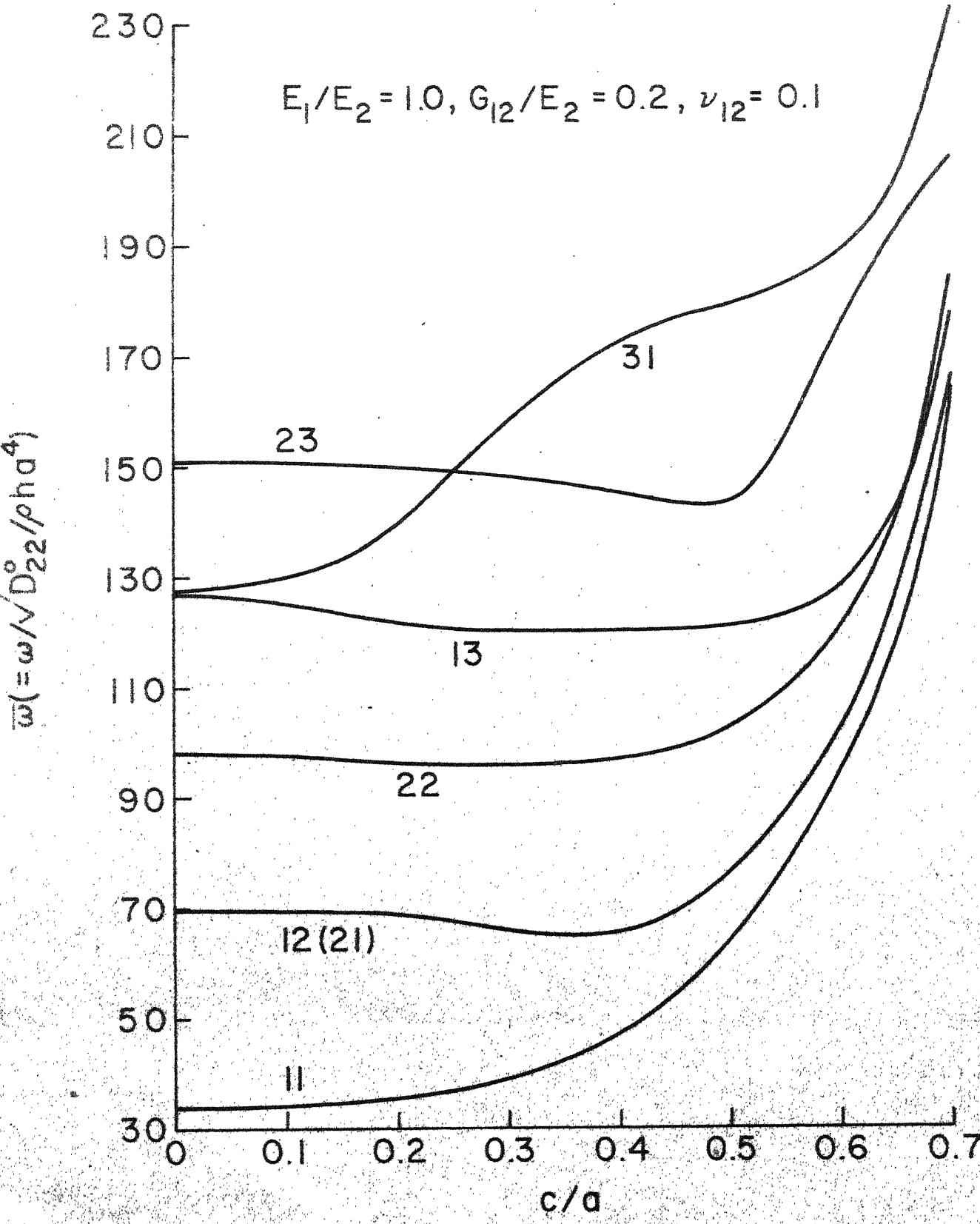

Fig.2.24 $\bar{\omega}$ vs for a clamped-clamped plate; $\Theta = 0°$, $R = 1.0$

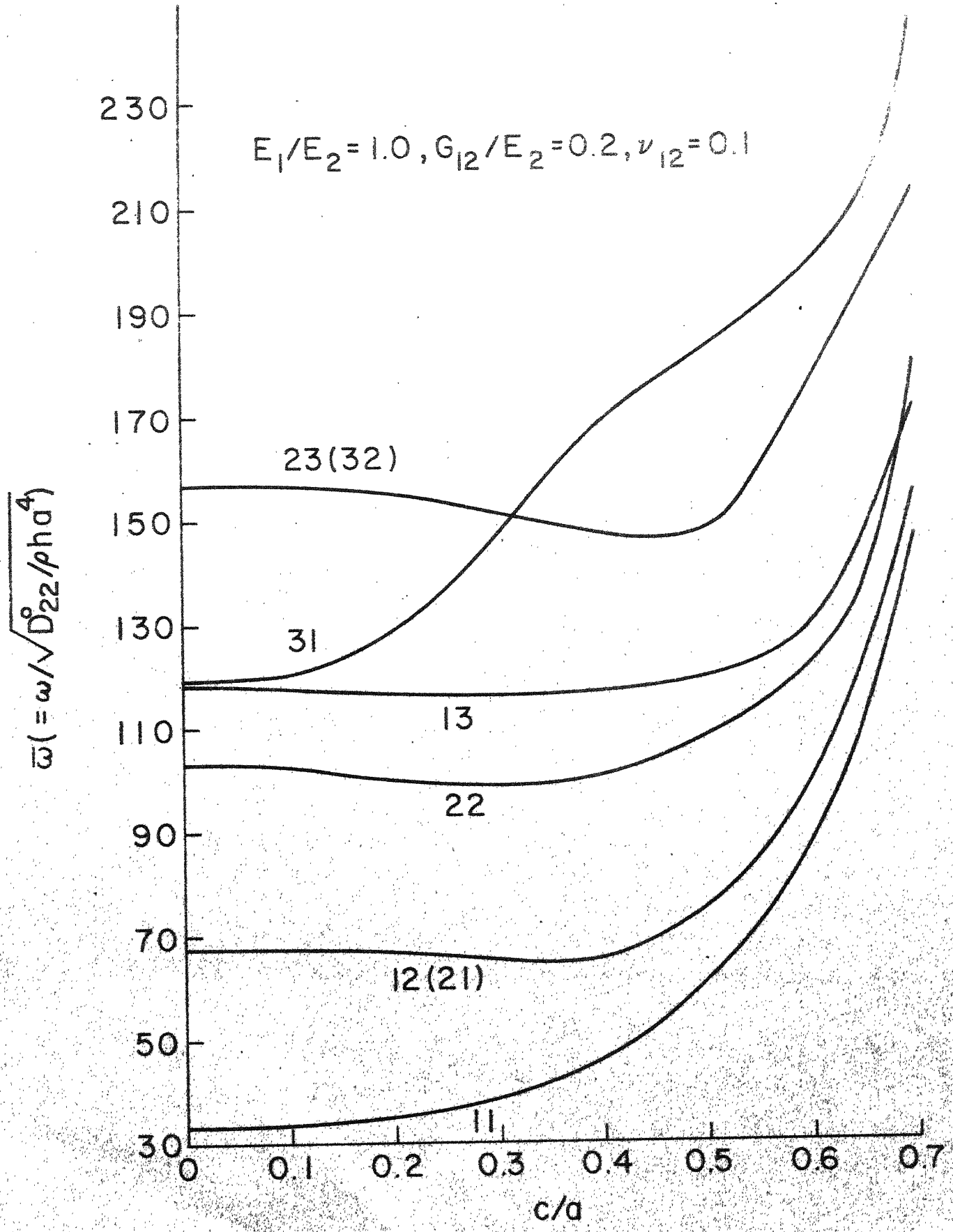

Fig.2.25 $\bar{\omega}$ vs c/a for a clamped-clamped plate; $\theta = 45^\circ$, R = 1.0.

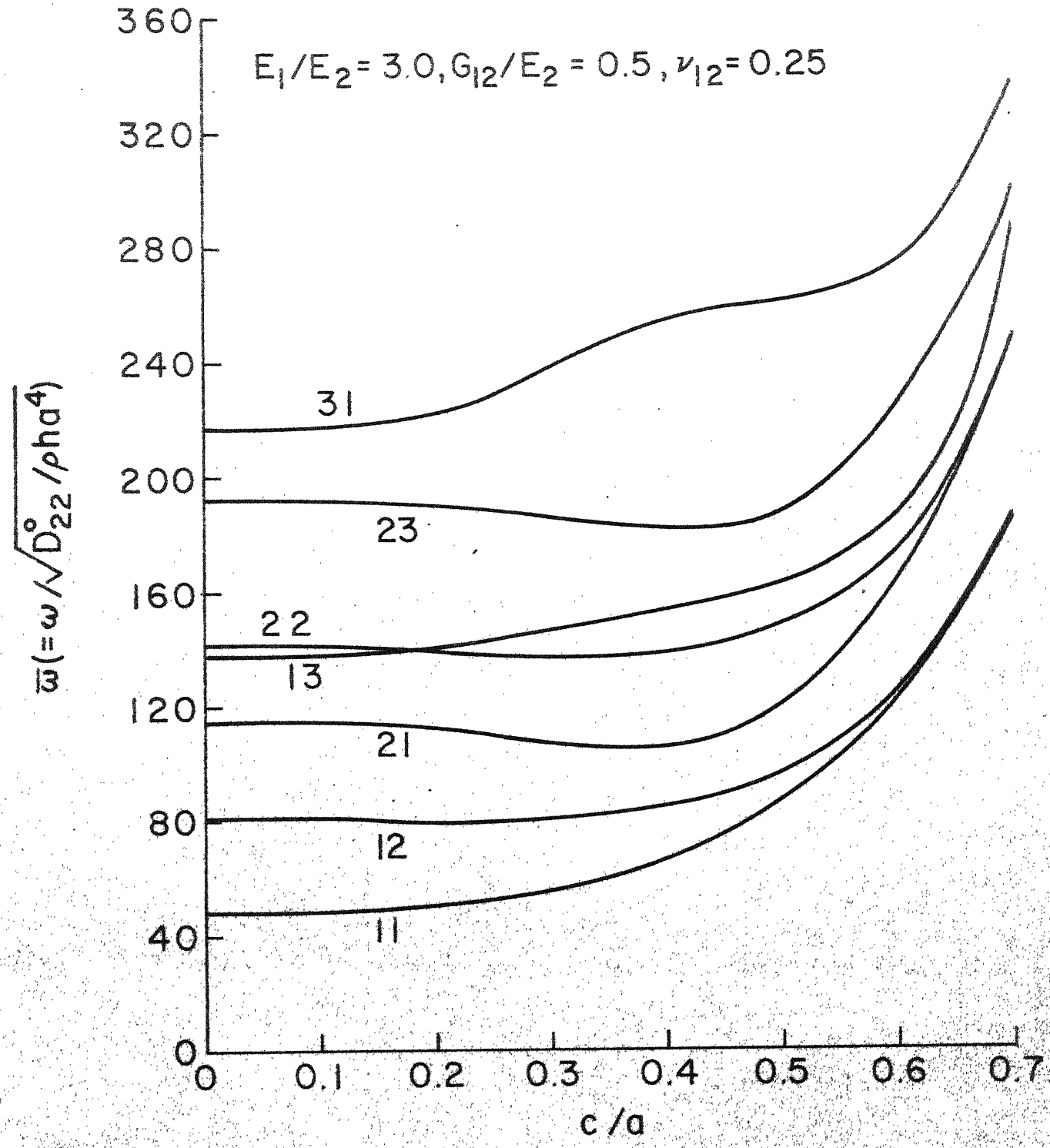

Fig.2.26 $\bar{\omega}$ vs c/a for a clamped-clamped plate; $\theta = 0°$, R = 1.0

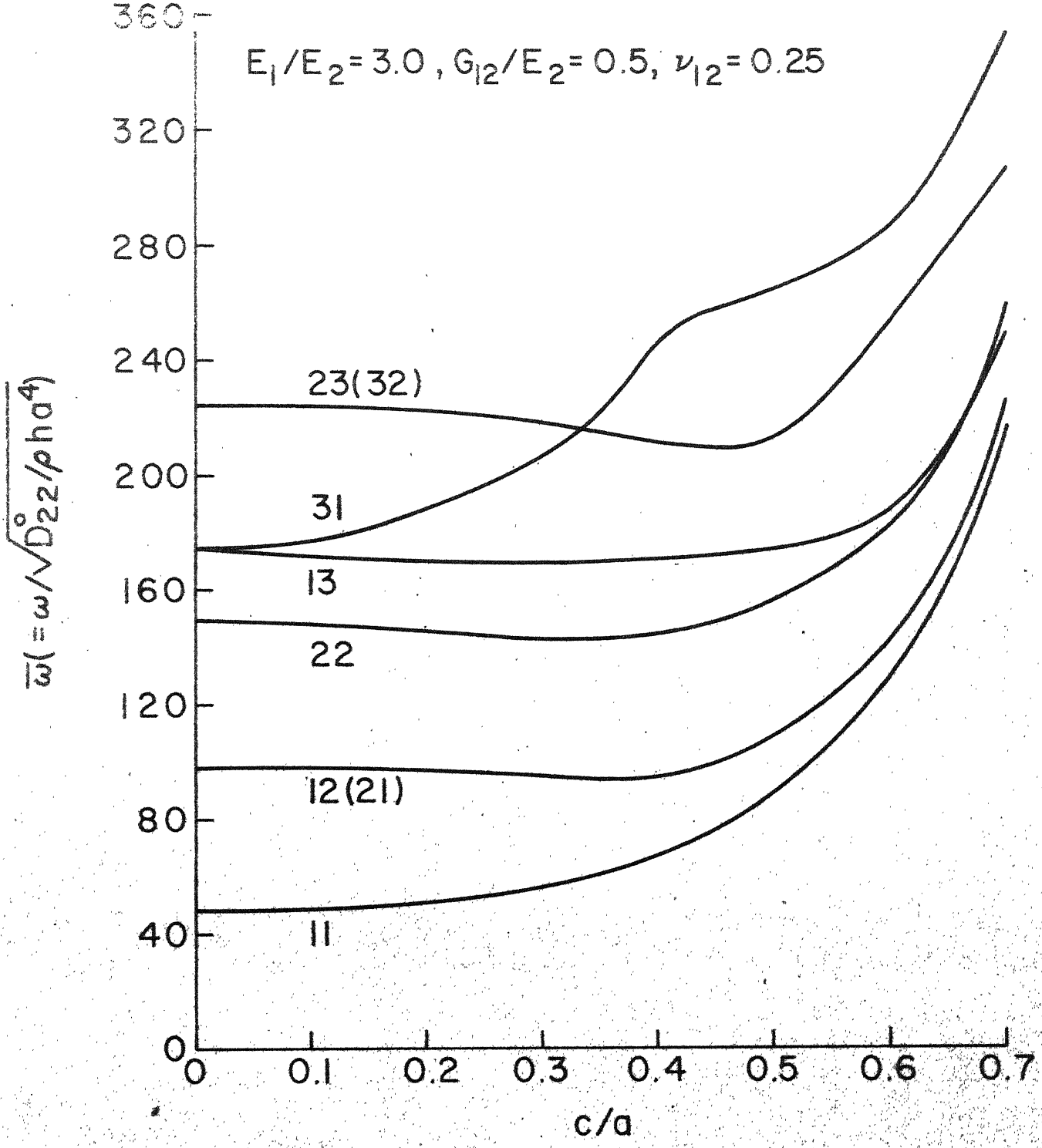

Fig.2.27 $\bar{\omega}$ vs c/a for a clamped-clamped plate; $\theta = 45^\circ$, R = 1.0

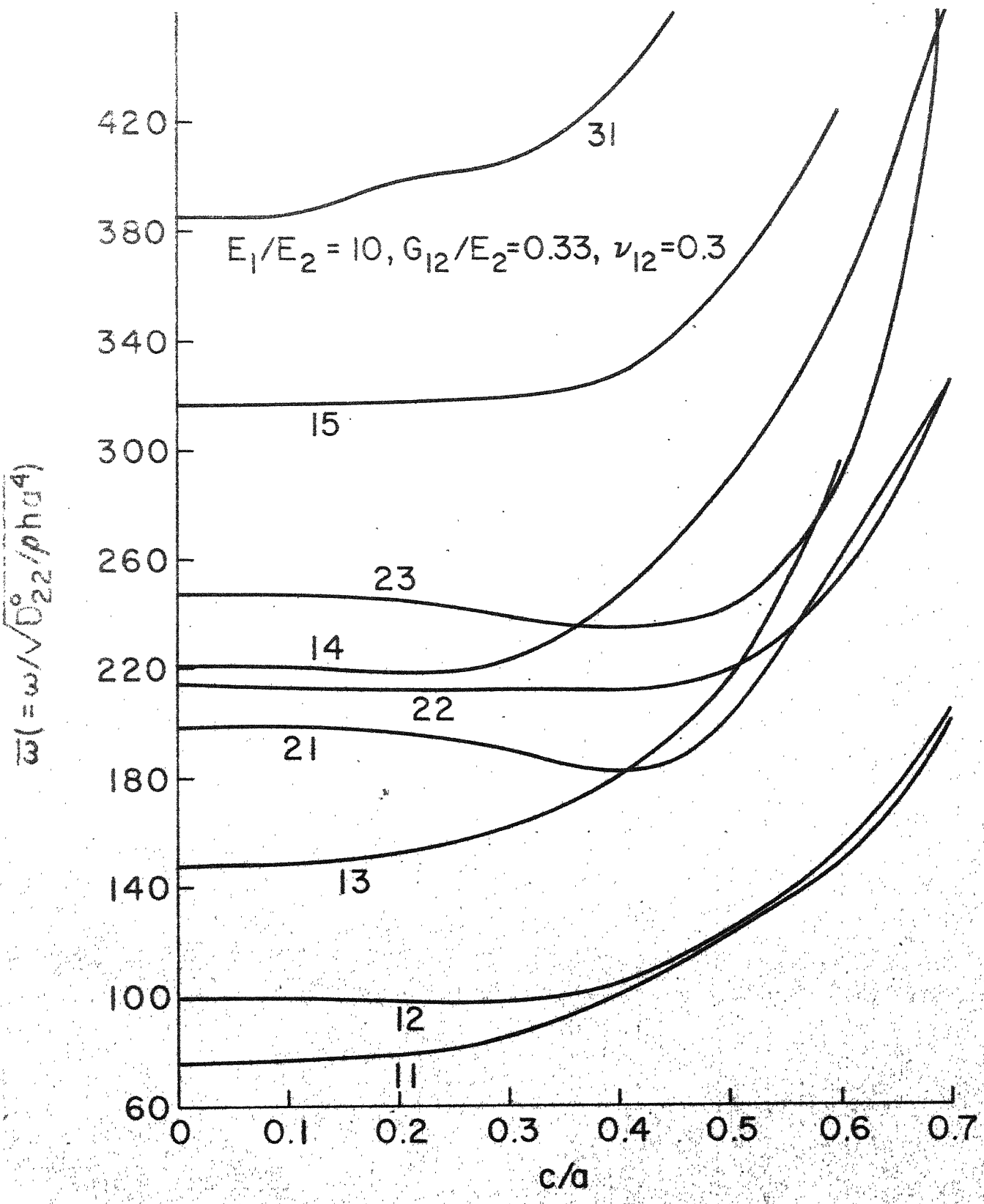

Fig.2.28 $\bar{\omega}$ vs c/a for a clamped-clamped plate; $\Theta = 0°$, R = 1.0

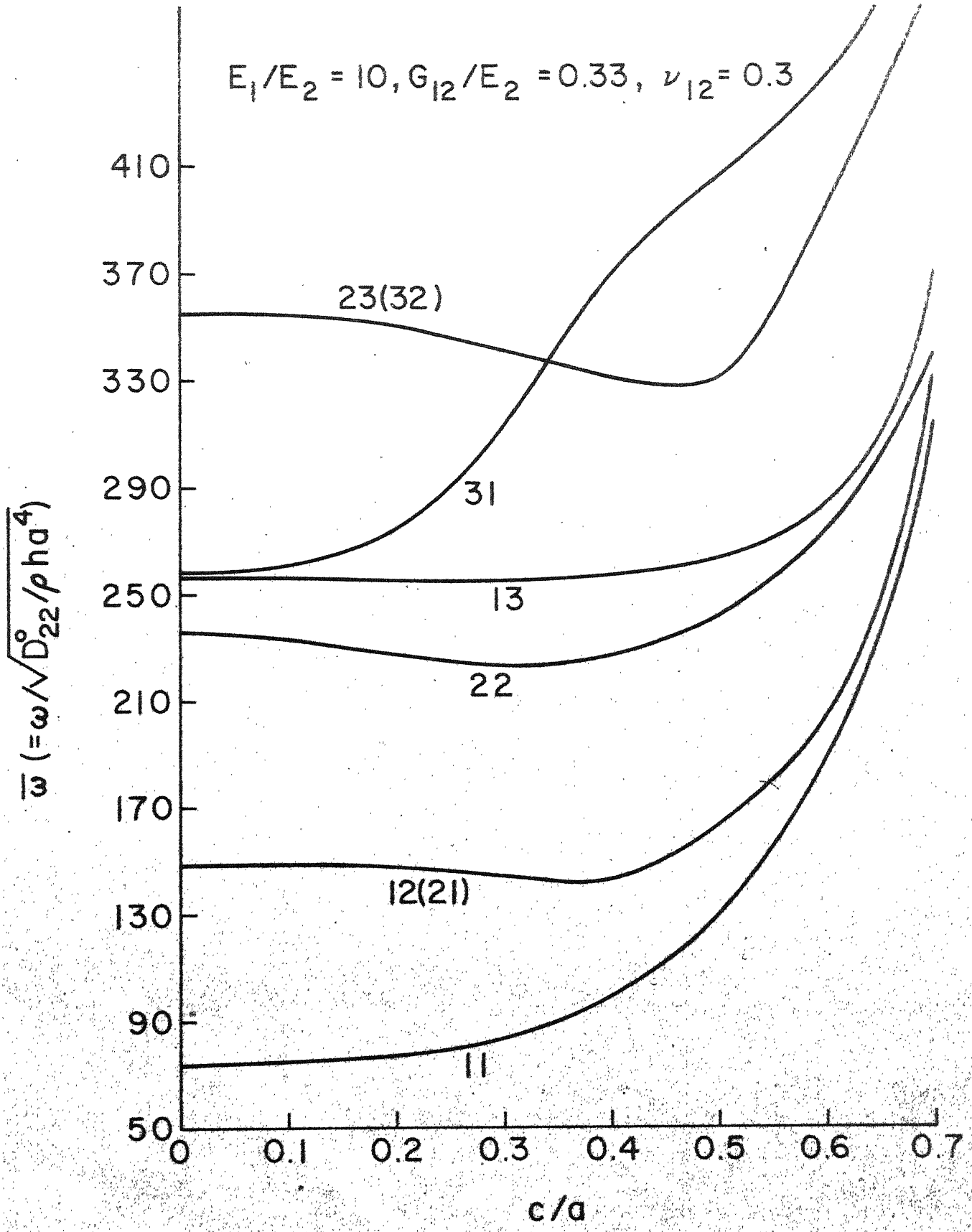

Fig.2.29 $\bar{\omega}$ vs c/a for a clamped-clamped plate; $\Theta = 45^\circ$, R = 1.0

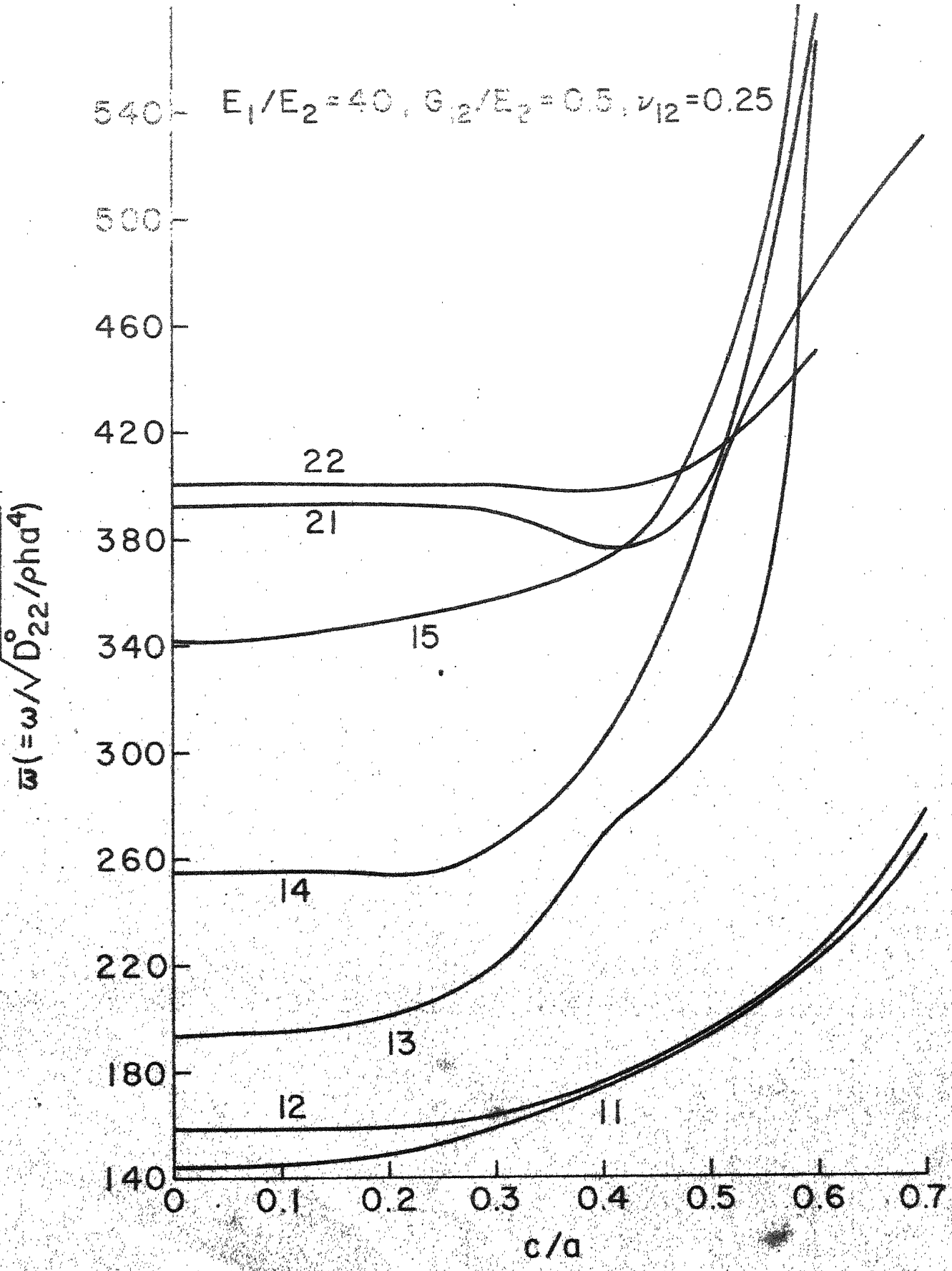

Fig. 2.30 $\bar{\omega}$ vs c/a for a clamped-clamped plate; $\theta = 0°$, R = 1.0

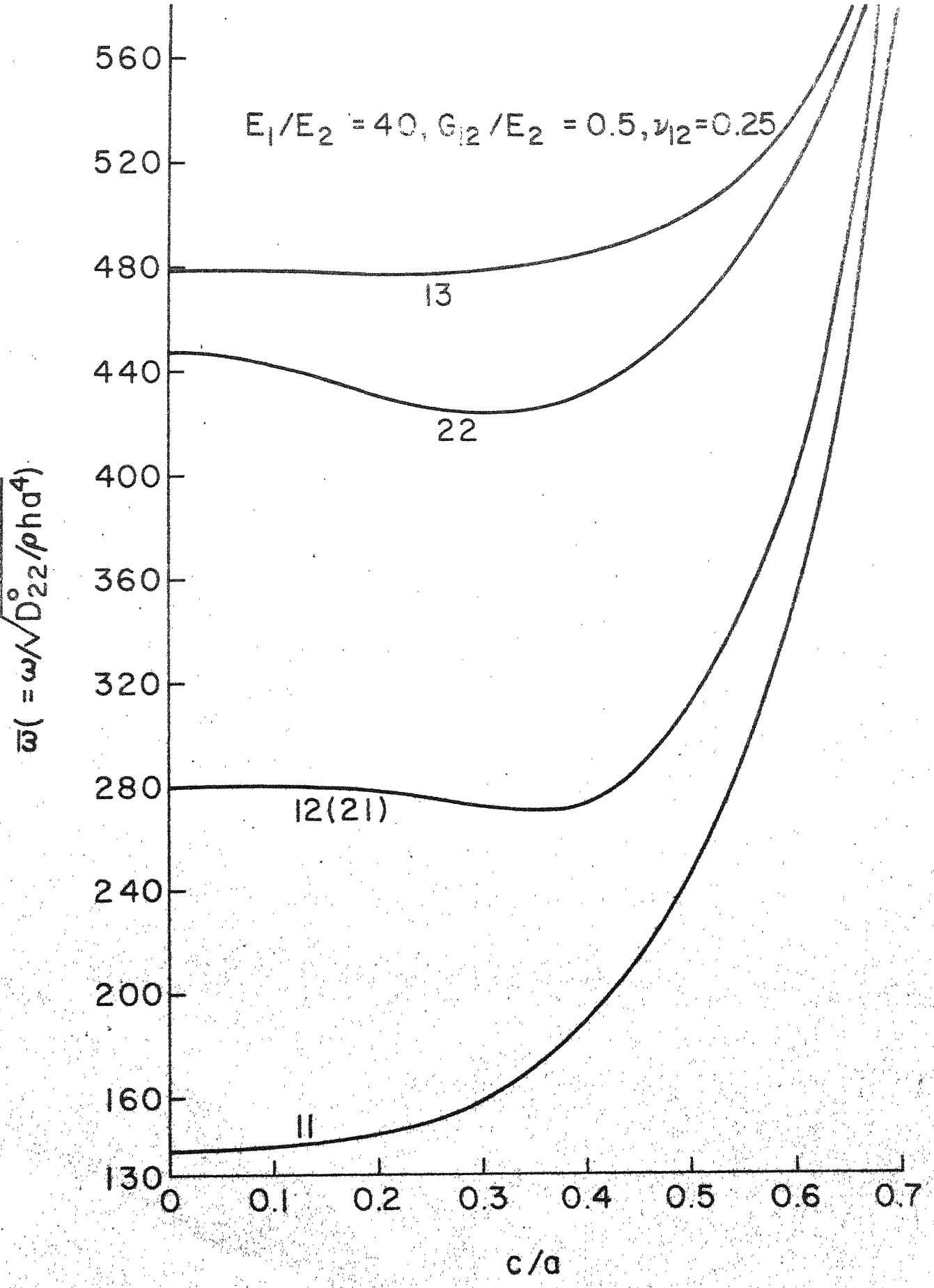

Fig.2.31 $\bar{\omega}$ vs c/a for a clamped-clamped plate; $\theta = 45°$, R = 1.0

values of c/a. It is interesting to note that there is no interchange of first four modes when $\theta = 45°$. It is observed that for clamped-clamped plates with central square cut-outs, the frequencies for each mode except the first vary with cut-out size in different ways and do not uniformly increase or decrease. However, as in the case of simply-supported plates some similarity is observed in their behaviour. The fundamental frequency in all the cases considered is found to increase with increasing c/a values. This suggests that cut-outs make plates stiffer for clamped-clamped edge conditions. Frequencies $\bar{\omega}_{12}$, $\bar{\omega}_{21}$, $\bar{\omega}_{22}$ and $\bar{\omega}_{23}$ are found to first decrease with increase in cut-out size for all fibre-orientation angles and modulus ratios. They, however, increase for larger cut-out ratios. The frequency curves for $\bar{\omega}_{12}$ and $\bar{\omega}_{21}$ and those for $\bar{\omega}_{23}$ and $\bar{\omega}_{32}$ are found to come closer as the fibre-orientation angle is increased and these coincide when $\theta = 45°$ for all the modulus ratios (this behaviour is found in an isotropic plate). The modes corresponding to $\bar{\omega}_{13}$ and $\bar{\omega}_{31}$ are not identical in this case as was seen in a simply-supported solid plate for fibre-orientation angle equal to 45°.

b) The Effect of Fibre-Orientation Angle on the Natural Frequency

The influence of fibre-orientation angle has been shown only for $\bar{\omega}_{11}$ for different values of c/a ratios. The variation of $\bar{\omega}_{11}$ with θ for different c/a values is shown in Figures 2.32 to 2.35 for various composite plates. In Figure 2.32, which shows the variation of $\bar{\omega}_{11}$ with θ for balanced bidirectional plates, it is observed that the rate of decrease of frequency increases with cut-out parameters. This suggests that the larger cut-outs in this case tend to make the plate less stiff

when θ is increased. In the case of unidirectional glass-epoxy plates (Figure 2.33), $\bar{\omega}_{11}$ decreases with increasing θ for medium cut-out sizes. As c/a increases, $\bar{\omega}_{11}$ increases continuously with increasing values of θ (c/a = 0.6, c/a = 0.7). The behaviour of $\bar{\omega}_{11}$ with θ for a unidirectional boron-epoxy plate is found similar to a unidirectional glass-epoxy plate and is shown in Figure 2.34. In Figure 2.35, which is a plot of $\bar{\omega}_{11}$ vs. θ for unidirectional graphite-epoxy plates, it is seen that for small values of c/a (upto 0.2), $\bar{\omega}_{11}$ decreases with increasing θ. For values of c/a lying between 0.3 and 0.4, it first increases upto a value of θ equal to 22.5° and then decreases. As c/a is further increased, $\bar{\omega}_{11}$ is found to increase with θ.

It is seen that the variation of the fundamental frequency with θ for small values of c/a (upto 0.2) is similar for all composite plates; it is found to decrease with increase in the fibre-orientation angle. Thus increase in the fibre-orientation angle makes clamped-clamped plates with small cut-outs less stiff. At higher c/a values, the fundamental frequency except in the case of balanced bidirectional plates increases with the fibre-orientation angle. Maurizi and Laura [39] also observed the decrease in the fundamental frequency with fibre-orientation angle for a square, clamped-clamped boron-epoxy plate with no cut-out.

c) The effect of modulus ratio on the natural frequency

The influence of modulus ratio on the fundamental frequency of a plate with a cut-out is shown for two fibre-orientation angles - 0° and 45°. For different modulus ratios, the variation of $\bar{\omega}_{11}$ with c/a is shown in

Figure 2.36 in the case of $\theta = 0°$ and $\theta = 45°$. It is found that $\bar{\omega}_{11}$ increases with c/a for all modulus ratios. The frequency curves for $\theta = 0°$ and $\theta = 45°$ for a given modulus ratio, except in the case of balanced-bidirectional plates, are found to intersect with each other. This indicates the increase in stiffness, at higher c/a values as the fibre-orientation angle is increased, for plates with ratios of principal Young's modulus equal to 3, 10 and 40. It is also observed that the frequency values for an isotropic plate are higher as compared to those for a balanced-bidirectional plate in the case of $\theta = 0°$ and $\theta = 45°$.

The variation of $\bar{\omega}_{11}$ and $\bar{\omega}_{12}$ with modulus ratio for c/a = 0.0 is shown in Figure 2.37. For all fibre-orientation angles, $\bar{\omega}_{11}$ and $\bar{\omega}_{12}$ increase with modulus ratio. But for a given modulus ratio, $\bar{\omega}_{11}$ and $\bar{\omega}_{12}$ behave in exactly opposite manner.: $\bar{\omega}_{11}$ is found to decrease with increase in fibre-orientation angle whereas $\bar{\omega}_{12}$ is found to increase with increase in fibre-orientation angle.

d) The effect of cut-out on the mode shape

The eigenvectors normalized with respect to the mass matrix have been obtained in all the cases considered. It is found that symmetric modes are more influenced due to the presence of a cut-out. This is because of the symmetric location of the cut-out. Table 2.9 gives a comparison of frequency values for a symmetric mode and the normalized eigenvectors for all modulus ratios in case of $\theta = 0°$.

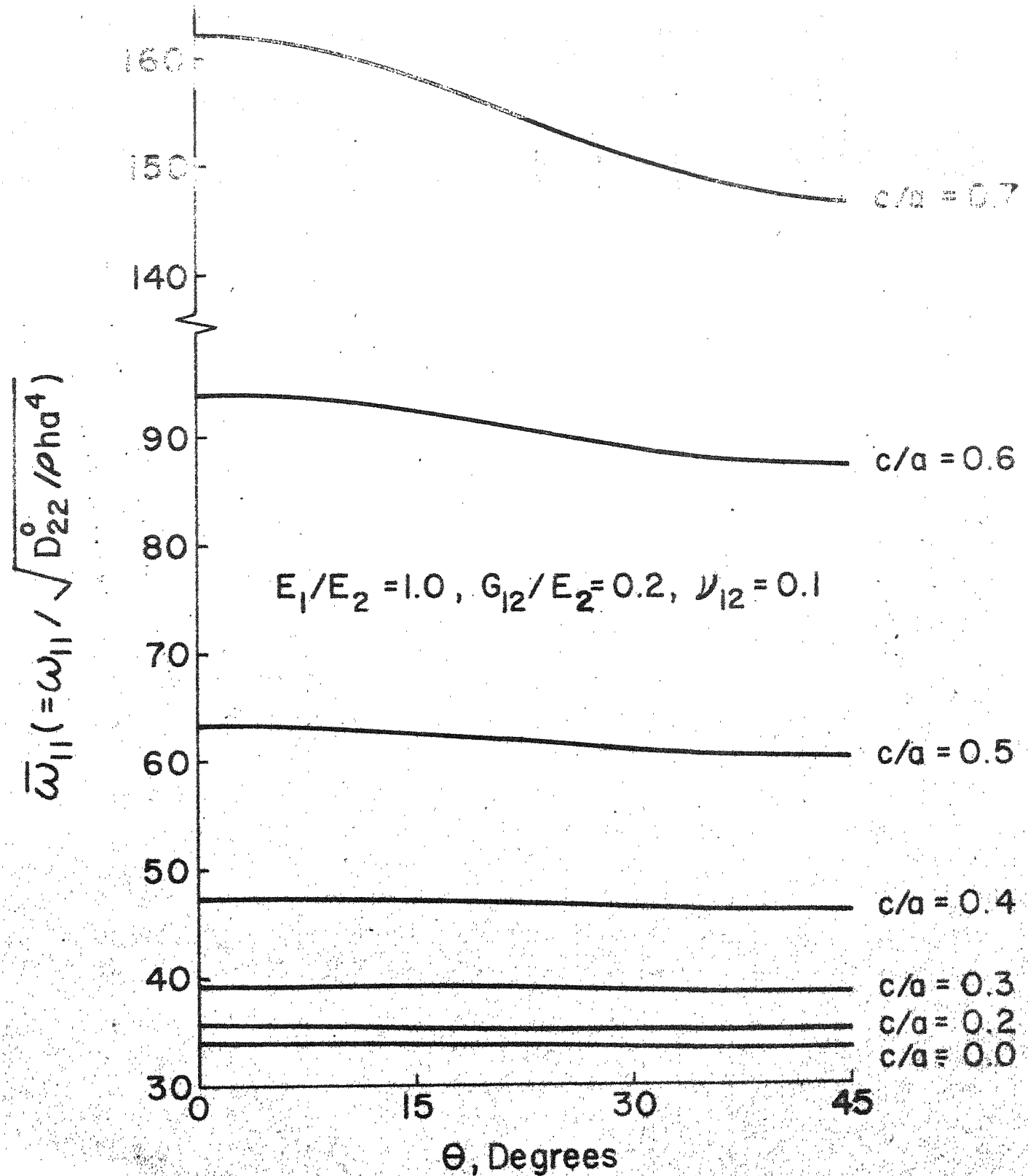

Fig.2.32 $\bar{\omega}_{11}$ vs. Θ For Different Cut-out Parameters For a Clamped-Clamped Plate; R = 1.0

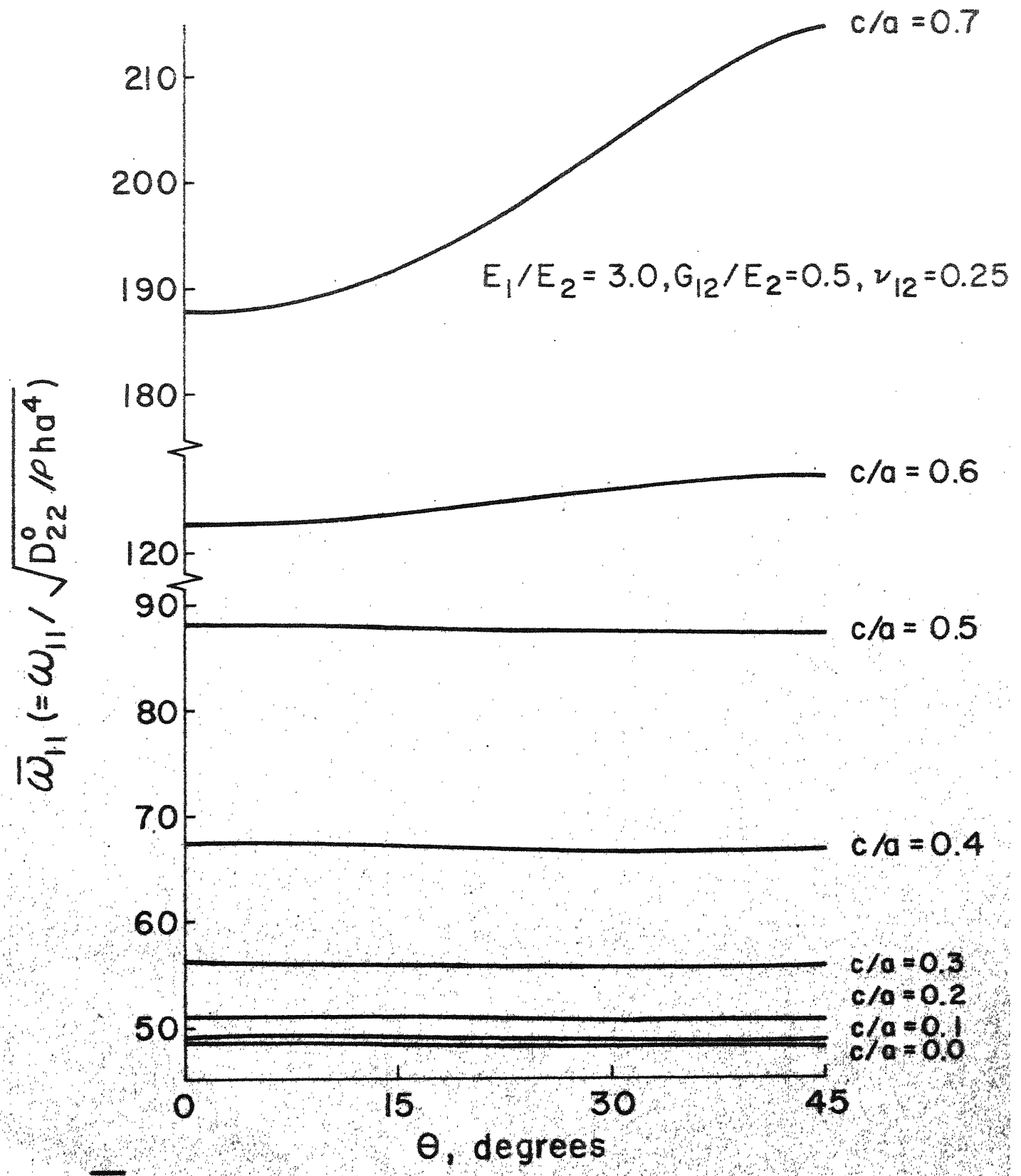

Fig.2.33 $\bar{\omega}_{11}$ vs. Θ For Different Cut-out Parameters For a Clamped-Clamped Plate; R=1.0

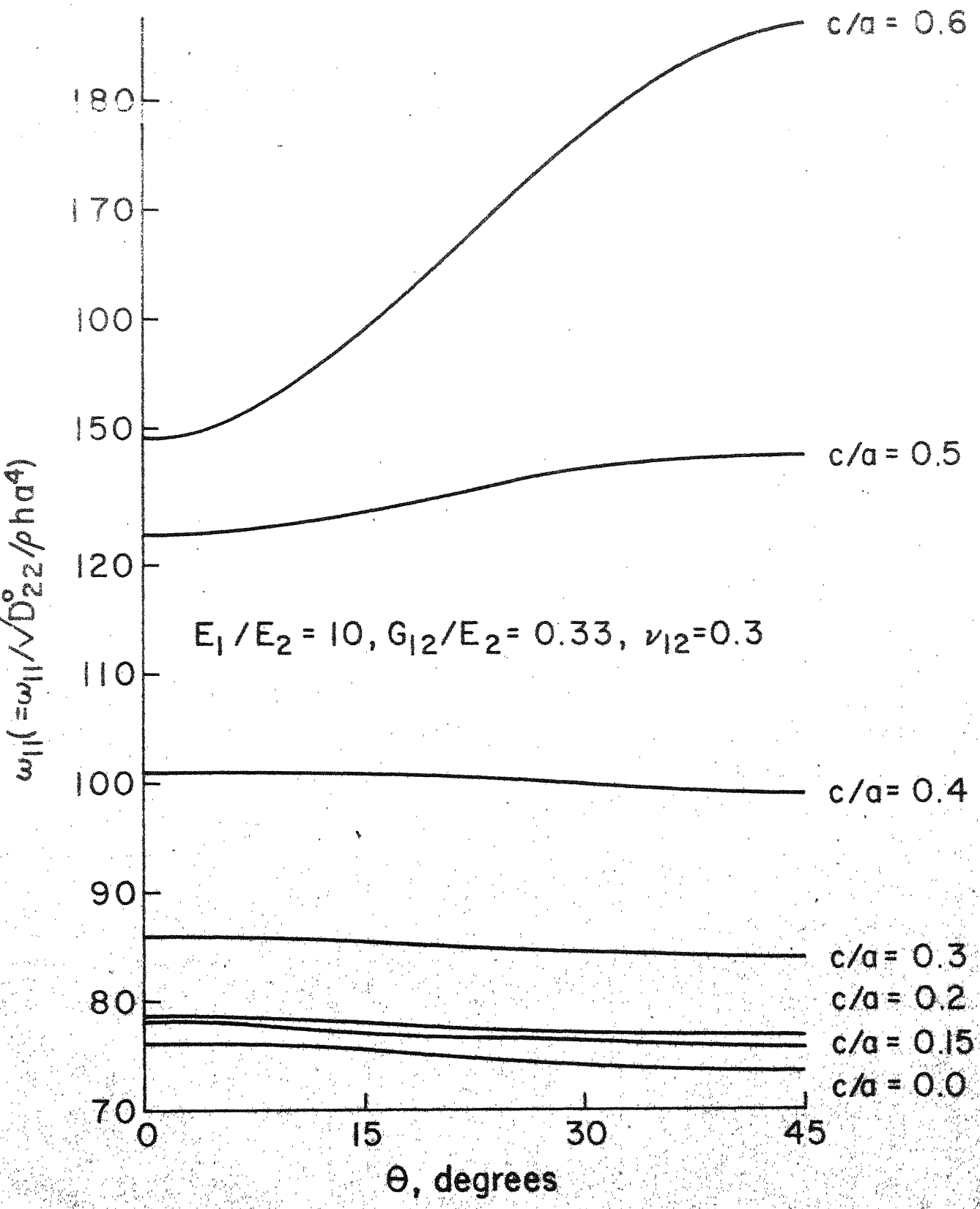

Fig. 2.34 $\bar{\omega}_{11}$ vs θ for different cut-out parameters for a clamped-clamped plate; R = 1.0

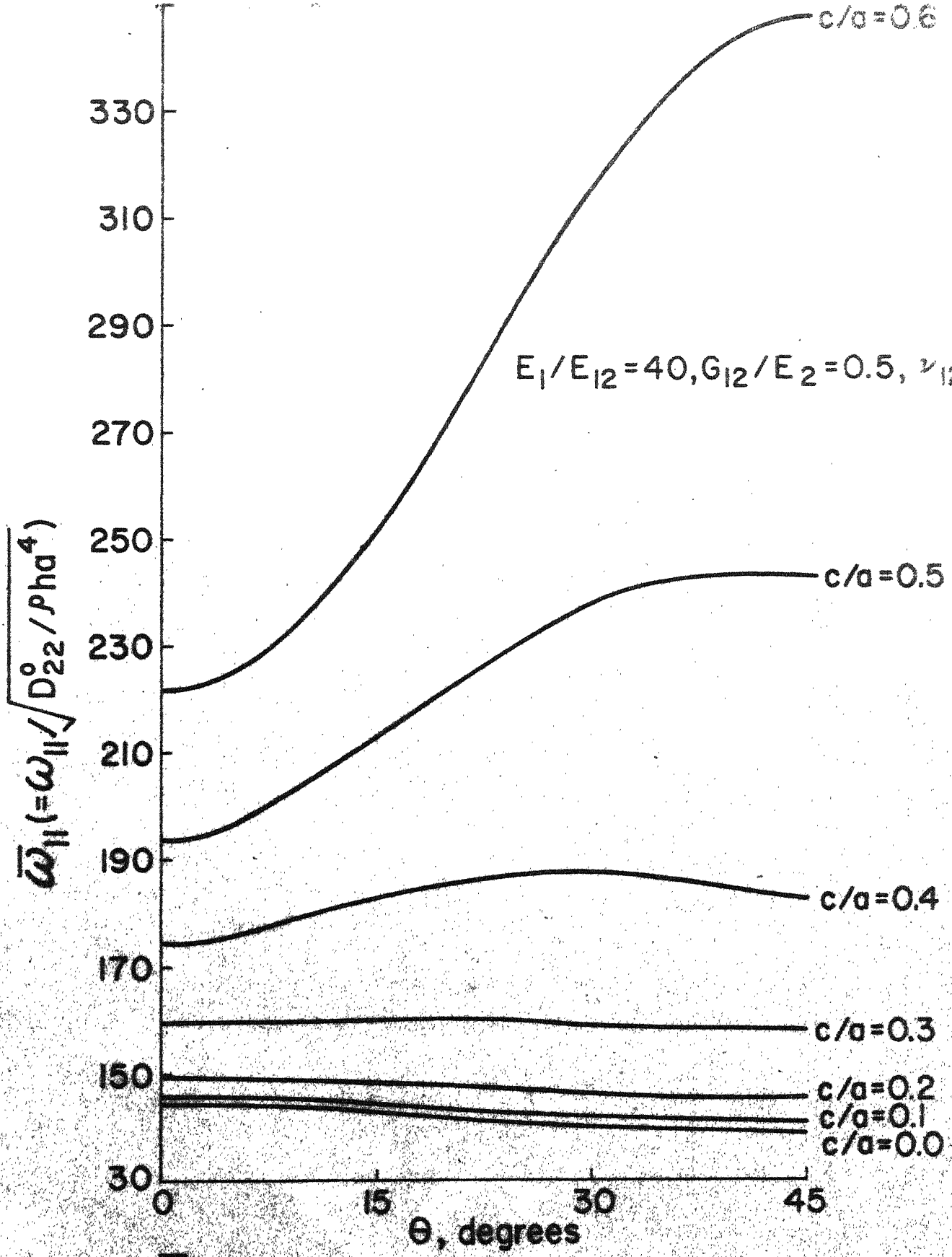

Fig.2.35 $\bar{\omega}_{11}$ vs. θ For Different Cut-out Parameters For A Clamped-Clamped Plate; R=1.0

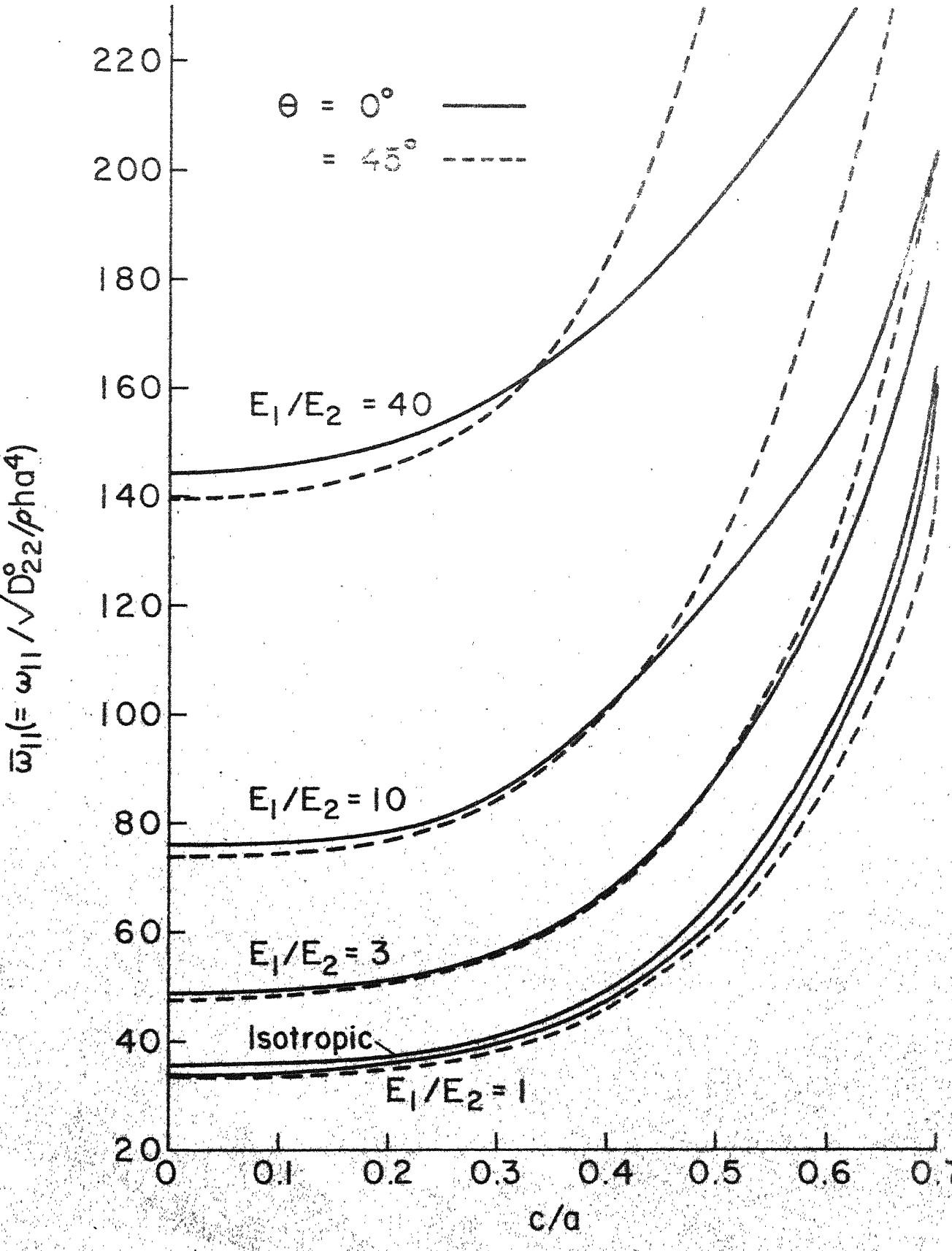

Fig. 2.36 $\bar{\omega}_{11}$ vs c/a for different modulus ratios for a clamped-clamped plate; R = 1.0

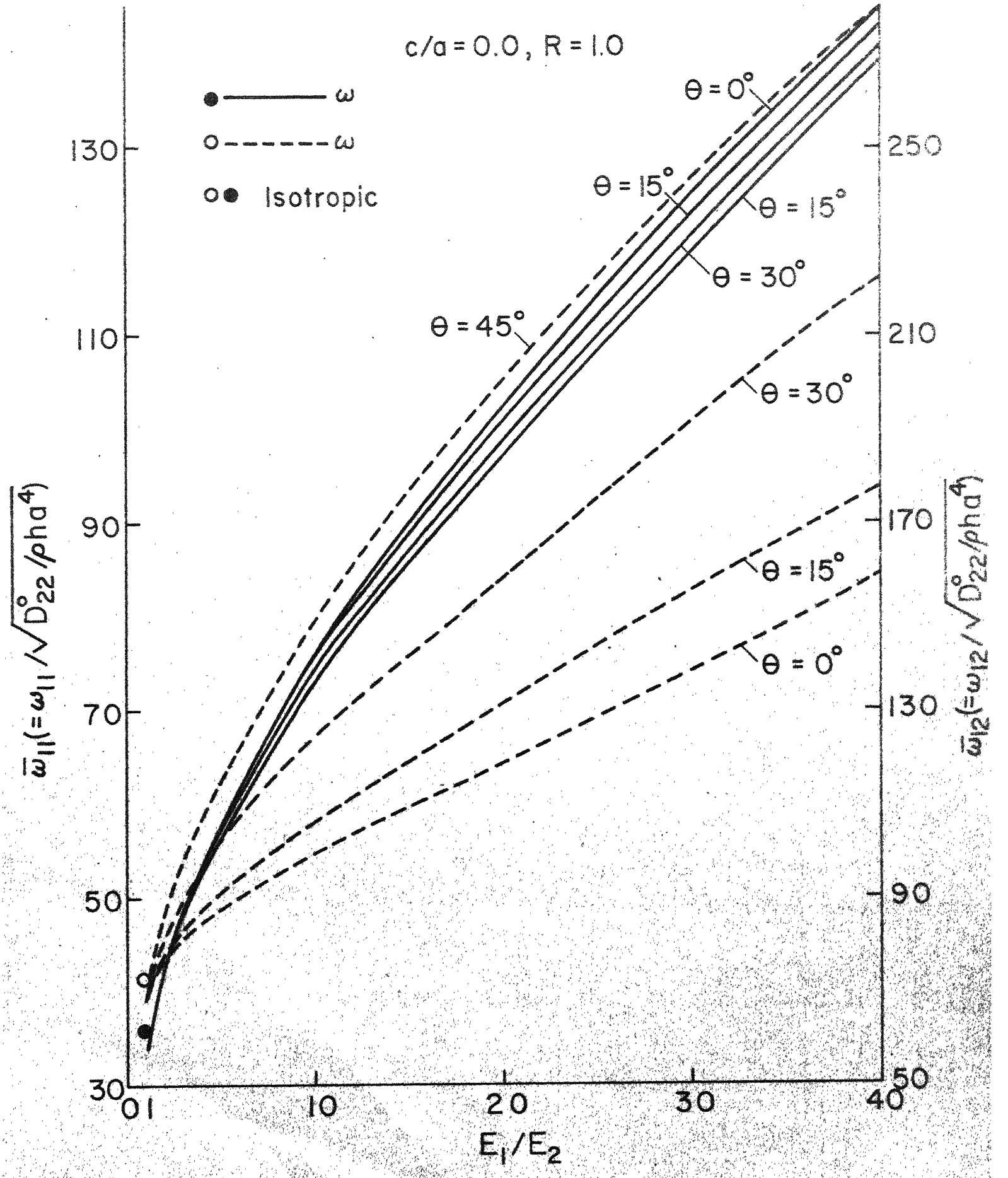

Fig. 2.37 Frequency vs modulus ratio for a clamped-clamped plate

Table 2.9

Comparison of frequency values and normalized eigenvectors for a clamped-clamped plate; $\theta = 0°$, $\bar{\omega}_{13}$.

E_1/E_2	1(Isotropic)		1(Balanced Bidirectional)		3		10		40	
c/a	0.0	0.5	0.0	0.5	0.0	0.5	0.0	0.5	0.0	0.5
A_{ij} $\bar{\omega}_{13}$	132.21	190.83	127.80	174.30	137.83	152.89	148.09	207.84	194.06	368.21
A_{11}	-0.0197	-1.3734	-0.0106	-1.0997	-0.0171	-1.3489	-0.0142	-2.4288	-0.0179	-2.8341
A_{13}	0.7040	0.7584	0.7057	0.6307	0.9990	1.4821	0.9997	1.5994	0.9997	1.2307
A_{15}	0.0038	-0.1769	0.0019	-0.1569	0.0087	-0.3928	0.0071	-0.4194	0.0093	0.0820
A_{17}	0.0009	0.0459	0.0004	0.0363	0.0021	0.1161	0.0017	0.1269	0.0023	0.1171
A_{31}	0.7040	0.7584	0.7057	0.6307	-0.0056	-0.5493	-0.0013	-0.1827	-0.0004	-0.0096
A_{33}	0.0901	0.8285	0.0609	0.8810	0.0375	-0.0368	0.0116	-0.0459	0.0040	-0.0269
A_{35}	0.0084	-0.0282	0.0044	-0.7020	-0.0019	0.1184	-0.0014	0.1180	-0.0007	0.0391
A_{37}	0.0024	0.0306	0.0011	0.0227	-0.0008	-0.0520	-0.0007	-0.0483	-0.0005	-0.0122
A_{51}	0.0038	-0.1769	0.0019	-0.1569	-0.0007	0.1445	-0.0001	0.0405	-0.0000	-0.0186
A_{53}	0.0084	-0.0282	0.0044	-0.0702	0.0063	-0.0068	0.0016	0.0185	0.0005	0.0185
A_{55}	-0.0014	0.0828	-0.0010	0.1037	-0.0008	-0.0304	-0.0003	-0.0367	-0.0001	-0.0140
A_{57}	-0.0007	-0.0351	-0.0003	-0.0381	-0.0004	0.0188	-0.0002	0.0189	-0.0001	0.0059
A_{71}	0.0009	0.0459	0.0004	0.0363	-0.0001	-0.0462	-0.0000	-0.0173	-0.0000	-0.0013
A_{73}	0.0024	0.0306	0.0011	0.0227	0.0016	0.0177	0.0003	0.0018	0.0001	-0.0017
A_{75}	-0.0007	-0.0351	-0.0004	-0.0381	-0.0003	0.0155	-0.0000	0.0063	-0.0000	0.0033
A_{77}	-0.0004	0.0158	-0.0002	0.0181	-0.0002	-0.0035	-0.0000	-0.0046	-0.0000	-0.0018

CHAPTER 3

VIBRATIONS OF COMPOSITE PLATES WITH HOLES

3.1 Introduction

A detailed study of the vibrations of plates with cut-outs was done in Chapter 2. It was noted that the theoretical results for the free vibrations of plates with cut-outs could be compared only with the available theoretical results for isotropic plates and a few experimental results available on clamped-clamped isotropic plates; practically there are no results available on vibrations of composite plates with cut-outs. The theoretical study on the vibrations of composite plates with holes has been done with a view to verify the computed results with experimental results. It is also easier to make holes in plates than to make cut-outs as the latter involve practical difficulties, especially in composite plates. In this chapter, the theoretical results are given for square, simply-supported and clamped-clamped composite plates with centrally located circular holes. No results are given here for balanced bidirectional glass-epoxy plates as it was found (in Chapter 2) that the behaviour of balanced bidirectional glass-epoxy plates is very much similar to that of an isotropic plate. A comparison of results has also been made for isotropic plates with available results and the experimental results obtained in the present study; the experimental study is discussed in detail in Chapter 4.

3.2 Method of Solution

It was seen in the vibrations of plates with cut-outs that the definite integrals necessary for the evaluation of the coefficients M_{mn}^{ij}, β_{mn}^{ij}, C_{mn}^{ij} and α_{mn}^{ij} can be found in closed form. There is no change in the expressions for M_{mn}^{ij} and C_{mn}^{ij} and they are given by equations (2.19, 2.21) and (2.30, 2.32) for a simply-supported and a clamped-clamped plate respectively. However, the integrals necessary in the computation of β_{mn}^{ij} and α_{mn}^{ij} cannot be obtained in closed form and hence a numerical integration scheme is necessary. Of the various schemes, the sixteen point Gauss quadrature formula has been found to yield sufficiently accurate results and has been used in the evaluation of β_{mn}^{ij} and α_{mn}^{ij}. The coefficients β_{mn}^{ij} and α_{mn}^{ij} are given below for simply-supported and clamped-clamped boundary conditions.

3.2.1 Simply-Supported Plates

The expressions for β_{mn}^{ij} and α_{mn}^{ij} for a simply-supported plate are,

$$\beta_{mn}^{ij} = \rho hab \; F_{H1} \tag{3.1}$$

$$\alpha_{mn}^{ij} = \frac{D_{22}ab}{a^4} \pi^4 \left[\left(\frac{D_{11}}{D_{22}} m^2 i^2 + \frac{D_{12}}{D_{22}} R^2 (i^2 n^2 + m^2 j^2) + R^4 n^2 j^2 \right) F_{H1} \right.$$
$$+ \frac{4D_{66}}{D_{22}} R^2 \, mnij \, F_{H2} - \frac{2D_{16}}{D_{22}} R \, (m^2 ij \, F_{H3} + i^2 mn \, F_{H4})$$
$$\left. - \frac{2D_{26}}{D_{22}} R^3 \, (n^2 ij \, F_{H3} + j^2 mn \, F_{H4}) \right] \tag{3.2}$$

where,

$$F_{H1} = \iint_{A_H} \sin(m\pi X) \sin(i\pi X) \sin(n\pi Y) \sin(j\pi Y)\, dX\, dY$$

$$F_{H2} = \iint_{A_H} \cos(m\pi X) \cos(i\pi X) \cos(n\pi Y) \cos(j\pi Y)\, dX\, dY$$

$$F_{H3} = \iint_{A_H} \sin(m\pi X) \cos(i\pi X) \sin(n\pi Y) \cos(j\pi Y)\, dX\, dY$$

$$F_{H4} = \iint_{A_H} \cos(m\pi X) \sin(i\pi X) \cos(n\pi Y) \sin(j\pi Y)\, dX\, dY \qquad (3.3)$$

where A_H is the area of the hole.

$$X = x/a, \qquad Y = y/b.$$

D_{ij}'s are the elements of the plate bending stiffness matrix and are related to the orthotropic elastic constants of the layer and the fibre orientation angle θ, of the layer with respect to the geometrical axis of the plate.

3.2.2 Clamped-Clamped Plates

The expressions for β_{mn}^{ij} and α_{mn}^{ij} for a clamped-clamped plate are

$$\beta_{mn}^{ij} = \rho\, hab \iint_{A_H} X_m X_i Y_n Y_j\, dX\, dY \qquad (3.4)$$

$$\alpha_{mn}^{ij} = \frac{D_{22}ab}{a^4}\left[\frac{D_{11}}{D_{22}} F_{1H} + \frac{D_{12}}{D_{22}} R^2 (F_{2H} + F_{3H}) + R^4 F_{4H} + 4R^2 \frac{D_{66}}{D_{22}} F_{5H} + 2R \frac{D_{16}}{D_{22}} (F_{6H} + F_{7H})\right] + 2R^3 \frac{D_{26}}{D_{22}} (F_{8H} + F_{9H}) \qquad (3.5)$$

where,

$$F_{1H} = \iint_{A_H} X_{m,XX} X_{i,XX} Y_n Y_j \, dX \, dY$$

$$F_{2H} = \iint_{A_H} X_m X_{i,XX} Y_{n,YY} Y_j \, dX \, dY$$

$$F_{3H} = \iint_{A_H} X_{m,XX} X_i Y_n Y_{j,YY} \, dX \, dY$$

$$F_{4H} = \iint_{A_H} X_m X_i Y_{n,YY} Y_{j,YY} \, dX \, dY$$

$$F_{5H} = \iint_{A_H} X_{m,X} X_{i,X} Y_{n,Y} Y_{j,Y} \, dX \, dY$$

$$F_{6H} = \iint_{A_H} X_{m,XX} X_{i,X} Y_n Y_{j,Y} \, dX \, dY$$

$$F_{7H} = \iint_{A_H} X_{m,X} X_{i,XX} Y_{n,Y} Y_j \, dX \, dY$$

$$F_{8H} = \iint_{A_H} X_m X_{i,X} Y_{n,YY} Y_{j,Y} \, dX \, dY$$

$$F_{9H} = \iint_{A_H} X_{m,X} X_i Y_{n,Y} Y_{j,YY} \, dX \, dY \qquad (3.6)$$

3.2.3 Evaluation of β_{mn}^{ij} and α_{mn}^{ij}

The integrals given in equations (3.3) and (3.6) for the evaluation of β_{mn}^{ij} and α_{mn}^{ij} for the simply-supported and clamped-clamped boundary conditions in the case of a cut-out have been expressed in closed form. However, for a hole there is no such simplification and a numerical integration scheme is necessary to evaluate these integrals. A sixteen-point Gauss quadrature formula has been used for this purpose. The sixteen-point formula has been compared with two nine-point Gauss quadrature formulae to evaluate a standard integral for which the exact solution is known and it was found to give more accurate results than the nine-point formulae. Table 3.1 gives the three numerical integration schemes with numerical quadrature points and corresponding weights. Table 3.2 gives the values and the computation time required on an IBM 7044 computer with these numerical integration schemes to evaluate the standard integral. The percentage error using the sixteen-point formula in the evaluation of the standard integral is found to be less than 1.2 percent and this error is considerably less than that obtained by using the nine-point formulae. Therefore, the integrals in equations (3.3) and (3.6) have been evaluated using a sixteen-point formula even though the total computation time for the evaluation of the standard integral is more than that required when nine-point formulae are used. The integrals evaluated once for a particular hole size, are stored in the memory and used whenever needed. The use of the numerical integration scheme increases the computation time required for the determination of natural frequencies and corresponding

Table 3.1

Numerical quadrature points and corresponding weights for different Gauss-quadrature formulae[87]

$$\iint_A f(x,y)\, dA = A \sum_{i=1}^{n} W_i\, f(x_i, y_i); \quad n = 9 \text{ or } 16 .$$

Gauss Quadrature Formula	i	x_i, y_i	W_i
Nine-Point (1)	1	0.0, 0.0	0.25
	2	0.92387953, 0.38268343	0.09375
	3	0.92387953, -0.38268343	0.09375
	4	-0.92387953, 0.38268343	0.09375
	5	-0.92387953, -0.38268343	0.09375
	6	0.38268343, 0.92387953	0.09375
	7	0.38268343, -0.92387953	0.09375
	8	-0.38268343, 0.92387953	0.09375
	9	-0.38268343, -0.92387953	0.09375
Nine-Point (2)	1	0.0, 0.0	0.16666667
	2	0.70710678, 0.0	0.16666667
	3	-0.70710678, 0.0	0.16666667
	4	0.0, 0.70710678	0.16666667
	5	0.0, -0.70710678	0.16666667
	6	0.70710678, 0.70710678	0.04166666
	7	0.70710678, -0.70710678	0.04166666
	8	-0.70710678, -0.70710678	0.04166666
	9	-0.70710678, -0.70710678	0.04166666
Sixteen-Point	1	0.42470820, 0.17591990	0.0625
	2	0.17591990, 0.42470820	0.0625
	3	-0.17591990, 0.42470820	0.0625
	4	-0.42470820, 0.17591990	0.0625
	5	-0.42470820, -0.17591990	0.0625
	6	-0.17591990, -0.42470820	0.0625
	7	0.17591990, -0.42470820	0.0625
	8	0.42470820, -0.17591990	0.0625
	9	0.82047322, 0.33985115	0.0625
	10	0.33985115, 0.82047322	0.0625
	11	-0.33985115, 0.82047322	0.0625
	12	-0.82047322, 0.33985115	0.0625
	13	-0.82047322, -0.33985115	0.0625
	14	-0.33985115, -0.82047322	0.0625
	15	0.33985115, -0.82047322	0.0625
	16	0.82047322, -0.33985115	0.0625

Table 3.2

Comparison of results and computation time to evaluate a standard integral using various numerical integration schemes.

$$I = \int_0^1 \int_0^1 \sqrt{x^2 + y^2}\ dx\ dy$$

Integration Scheme	Exact value of I	Computed Value of I	Percentage error	Computation time on an IBM 7044 Computer, in milliseconds
1	2.0943951	2.3561944	12.6	616
2	2.0943951	2.0045597	- 4.3	616
3	2.0943951	2.1170794	1.13	716

eigenvectors. For example, the total computation time required for the determination of four natural frequencies and corresponding eigenvectors considering only symmetric modes is approximately nine minutes for a cut-out and eighteen minutes for a hole and all fibre-orientation angles (0°, 15°, 30°, 45°) in the case of clamped-clamped plates.

3.4 Results and Discussion

Natural frequencies and corresponding eigenvectors have been computed for square, simply-supported and clamped-clamped plates with centrally located circular holes for different fibre-orientation angles in steps of 15°. Results for balanced bidirectional plates have not been given as the behaviour of natural frequencies for these plates is similar to that found in the case of an isotropic plate. Ratios of principal Young's moduli of 3,10 and 40 have been used in the computation. Results are given in terms of non.dimensional frequency $\bar{\omega}$ for fibre-orientation angles 0° and 45° only. A comparison of frequencies and corresponding eigenvectors for a particular mode is made between cut-outs and holes to study the influence of other modes. The convergence of the results has been studied and a relative comparison of the frequency values led to the decision to compute natural frequencies taking sixteen frequency equations and different combination of modes for all the cases considered. It should be noted that twenty-five frequency equations were taken in the computation of natural frequencies for plates with cut-outs. The number of equations has been reduced for plates with holes to make a compromise between the computation time and the accuracy involved. Also,

computational difficulties like non-convergence of frequency values, increase in round-off errors were encountered at larger hole sizes and therefore results could be computed for the hole size parameter varying from 0.0 to 0.5 only except in the case of fundamental frequency.

3.4.1 Simply-Supported Plates

a) Effect of Hole on the Natural Frequency

Table 3.3 gives a comparison of the non-dimensional frequencies in the case of a square, isotropic platewith a centrally located circular hole with available results. The results given by Kumai [46] in terms of frequency ratios have been converted in the non-dimensional form for comparison purposes. There is a good agreement between Kumai's results and the results computed in the present case. However, frequency values obtained by Kumai are lower than the values obtained in the present study. Kumai computed frequencies by the superposition of the solutions of circular ring plate satisfying the boundary conditions at several points along the edges of the square plate. This approximation allows some residual deflections at some portion of the outer boundary of the plate which can be assumed to make the plate less stiff and hence low frequency values can be expected. Joga Rao and Picket [48] used Rayleigh-Ritz method and modified the admissible functions to take into account the appropriate singularities within the holes. A comparison with the present theoretical and experimental results show the inaccuracy of the result obtained in Reference [48] even after making

Table 3.3

Comparison of non-dimensional frequency for a square, simply-supported isotropic plate with a central circular hole.

Source	d/a									
	0.0			0.2			0.4			0.5
	First Mode	Second Mode	Fifth Mode	First Mode	Second Mode	Fifth Mode	First Mode	Second Mode	Fifth Mode	First Mode
Kumai [46]	19.739	49.348	98.966	19.441	45.012	101.35	19.045	39.624	121.42	-
Joga Rao and Pickett [48]	-	-	-	-	-	-	-	-	-	5.615
Present										
1 Theo.	19.739	49.348	98.966	19.463	49.272	102.49	20.477	48.499	129.12	30.234
2 Expt.	21.391	52.303	100.09	20.542	49.071	100.53	23.552	45.851	127.19	28.362

corrections for the singularities in the holes and therefore, it is doubtful whether the method suggested there can give accurate results.

The variation of frequency with hole parameter, d/a for an isotropic plate is shown in Figure 3.1. The frequencies have been subscripted (11, 12,... etc.) on the basis of the largest amplitude coefficients in the corresponding normalized eigenvectors. A good agreement is obtained with the experimental results. The presence of hole in a plate gives rise to a new mode similar to the case of a plate with a cut-out. For the d/a ratios considered, there is no interchange of modes.

In Figures 3.2 and 3.3 the variation of $\bar{\omega}$ with d/a is shown for unidirectional glass-epoxy plates in the case of $\theta = 0°$ and $\theta = 45°$ respectively. For $\theta = 0°$, $\bar{\omega}_{11}$ decreases very little with the increase in d/a values and then increases as the hole size is increased. There is no decrease in $\bar{\omega}_{11}$ with d/a for $\theta = 45°$. It is seen that as the fibre-orientation angle is increased, frequency curves for $\bar{\omega}_{12}$ and $\bar{\omega}_{21}$ came closer and they coincide when $\theta = 45°$, this is also true for frequency curves $\bar{\omega}_{23}$ and $\bar{\omega}_{32}$. The modes corresponding to $\bar{\omega}_{13}$ and $\bar{\omega}_{22}$ seem to have a tendency to interchange at d/a = 0.5.

The variation of $\bar{\omega}$ with d/a is shown in Figures 3.4 and 3.5 for unidirectional boron-epoxy plates. It is seen that for $\theta = 0°$ (Figure 3.4), all frequencies except $\bar{\omega}_{13}$ decrease with increase in d/a values and at higher d/a values only $\bar{\omega}_{11}$ and $\bar{\omega}_{23}$ increase. The modes corresponding to

$\bar{\omega}_{13}$ and $\bar{\omega}_{21}$ interchange and those corresponding to $\bar{\omega}_{13}$ and $\bar{\omega}_{22}$ have a tendency to interchange. For $\theta = 45°$, there is no decrease in $\bar{\omega}_{11}$ (Figure 3.5). Modes corresponding to $\bar{\omega}_{22}$ and $\bar{\omega}_{13}$ are found to interchange at higher d/a ratios.

For unidirectionally reinforced graphite-epoxy plates, Figures 3.6 and 3.7 show the variation of $\bar{\omega}$ with d/a for $\theta = 0°$ and $\theta = 45°$. When $\theta = 0°$, $\bar{\omega}_{11}$ and $\bar{\omega}_{21}$ decrease with increasing d/a ratios and the rate of decrease is more as compared to isotropic, unidirectional glass-epoxy and unidirectional boron-epoxy plates. However, for $\theta = 45°$, $\bar{\omega}_{11}$ increases with increase in the hole size. The frequency curves for $\bar{\omega}_{12}$ and $\bar{\omega}_{21}$ come closer as the fibre-orientation angle is increased and these coincide when $\theta = 45°$. This trend was also found in unidirectional glass-epoxy and unidirectional boron-epoxy plates.

b) Effect of Fibre-Orientation Angle on the Natural Frequency

The effect of fibre-orientation angle on the frequencies $\bar{\omega}_{11}$ and $\bar{\omega}_{12}$ has been shown in Figures 3.8 - 3.10 for selected values of d/a ratios. It is seen that in all the cases $\bar{\omega}_{11}$ and $\bar{\omega}_{12}$ increase with the fibre-orientation angle for all d/a ratios. As the hole size is increased, the rate of increase of $\bar{\omega}_{11}$ increases. For unidirectional glass-epoxy plates (Figure 3.8), $\bar{\omega}_{11}$ corresponding to d/a = 0.3 is lower than that corresponding to d/a = 0.0 at $\theta = 0°$ and the curves for $\bar{\omega}_{11}$ corresponding to these two values of d/a intersect as θ is increased. In Figures 3.9 and 3.10, a similar behaviour is observed for unidirectional boron-epoxy and

graphite-epoxy plates. The frequency $\bar{\omega}_{12}$ is found to increase with θ for all hole parameters similar to $\bar{\omega}_{11}$. It is also observed from Figures 3.8 to 3.10 that for a given value of θ, the frequency $\bar{\omega}_{12}$ decreases with increase in d/a values whereas this behaviour was observed in case of $\bar{\omega}_{11}$ only for small values of θ and valuesof d/a upto 0.3.

c) The Effect of Modulus Ratio on the Natural Frequency

The influence of modulus ratio on the fundamental frequency of a plate with a hole is shown for two fibre-orientation angles - 0° and 45°. For different modulus ratios, the variation of $\bar{\omega}_{11}$ with d/a is shown in Figure 3.11 in the case of $\theta = 0°$ and $\theta = 45°$. It is observed that for isotropic plates, $\bar{\omega}_{11}$ decreases for small d/a ratios whereas for an orthotropic plate ($\theta = 0°$), the decrease in $\bar{\omega}_{11}$ occurs upto larger values of d/a. The rate of decrease increases with increasing modulus ratios. The variation of $\bar{\omega}_{11}$ with d/a for different modulus ratios is shown by a dotted line when $\theta = 45°$. The fundamental frequency is found to increase for all modulus ratios with d/a.

d) The Effect of Holes on the Mode Shape

For plates with holes also, the eigenvectors normalized with respect to the mass matrix have been obtained. A comparison of frequency values and corresponding eigenvectors has been made (Table 3.4) for the same hole and cut-out parameters for a symmetric mode. The contribution of other modes is found significant for a cut-out as well as for a hole in the plate.

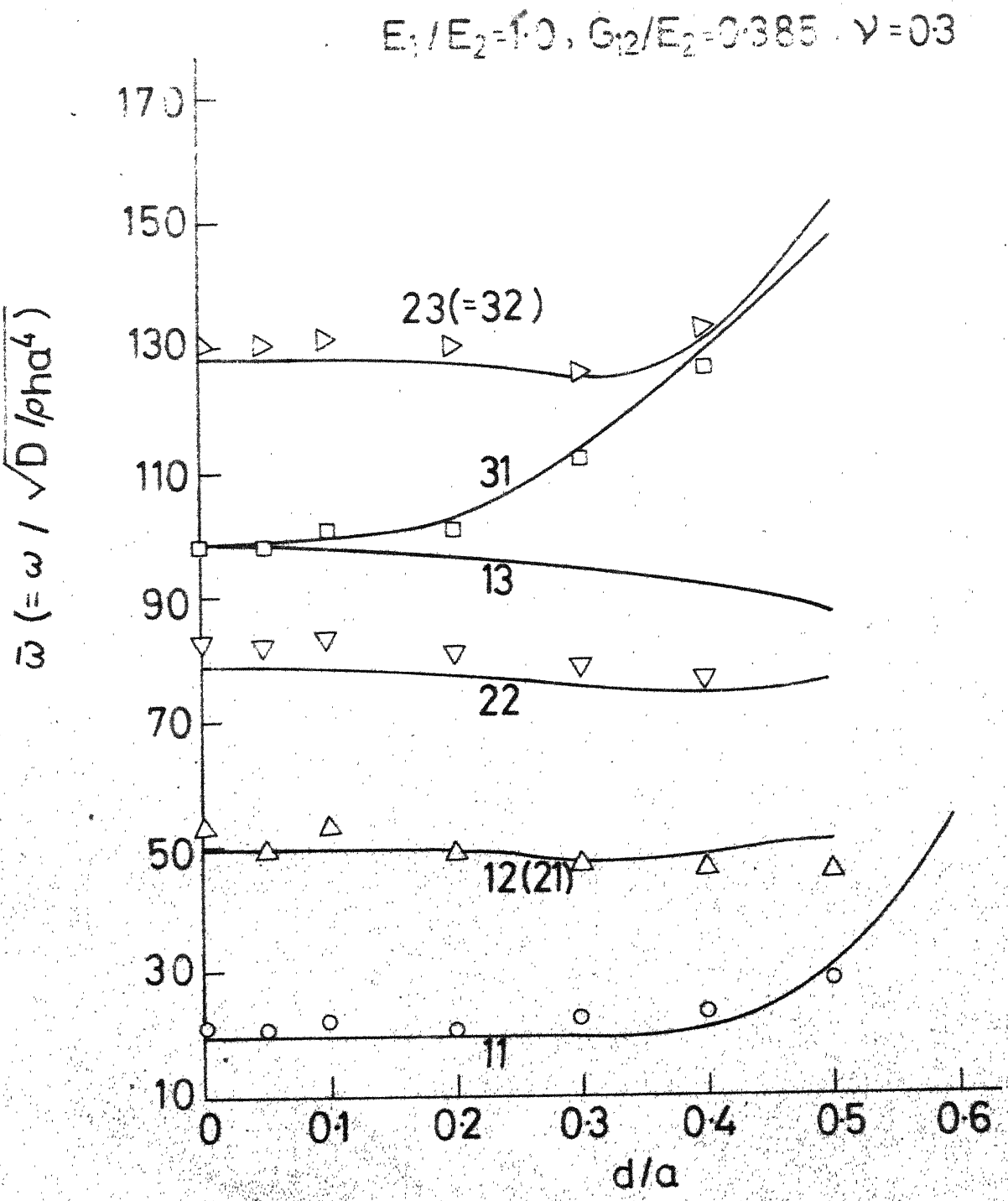

Fig. 3·1 $\bar{\omega}$ Vs d/a for a Simply-supported isotropic plate; R=1·0

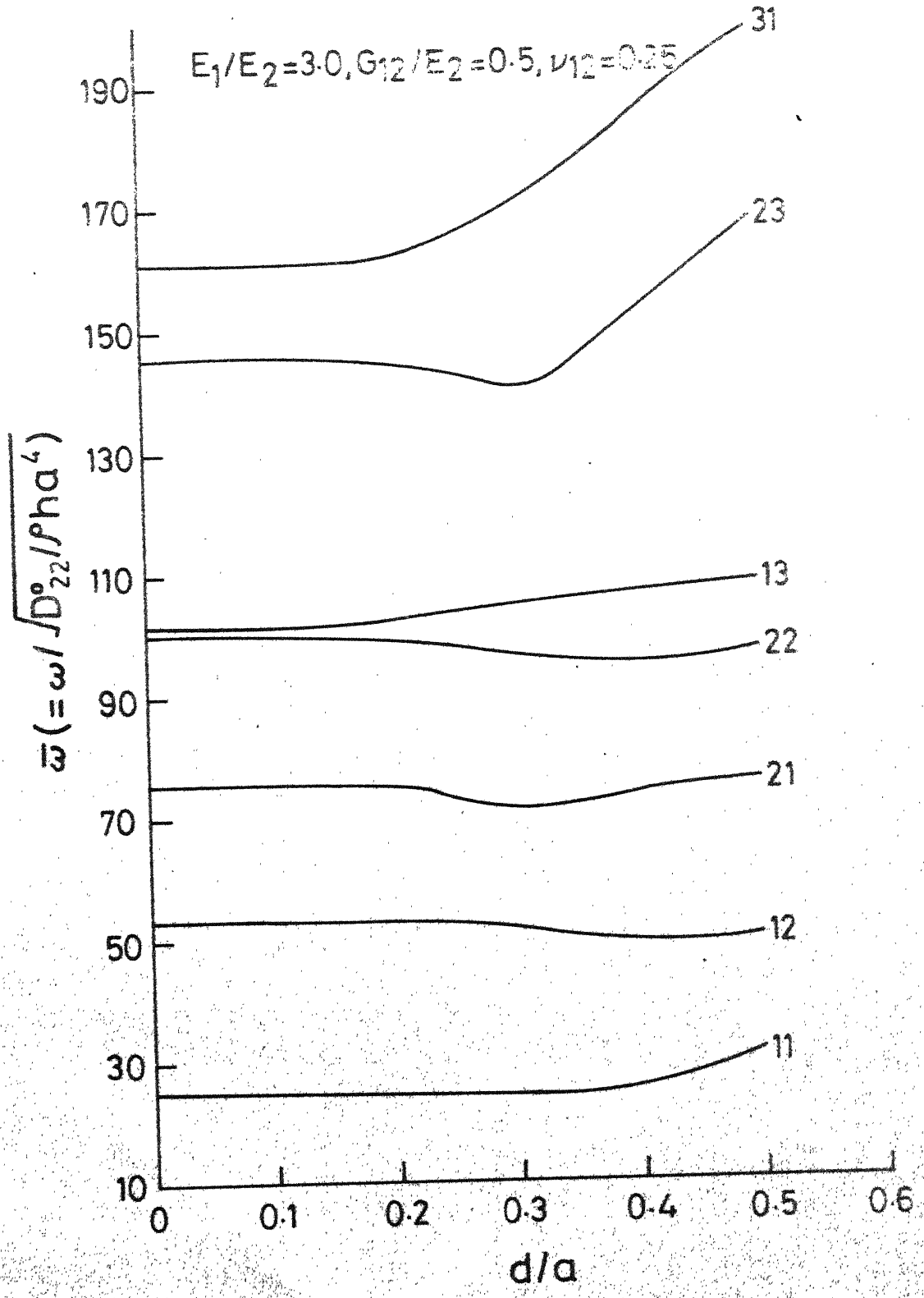

Fig. 3.2 $\bar{\omega}$ vs. d/a for a simply-supported plate; $\Theta=0°, R=1{\cdot}0$.

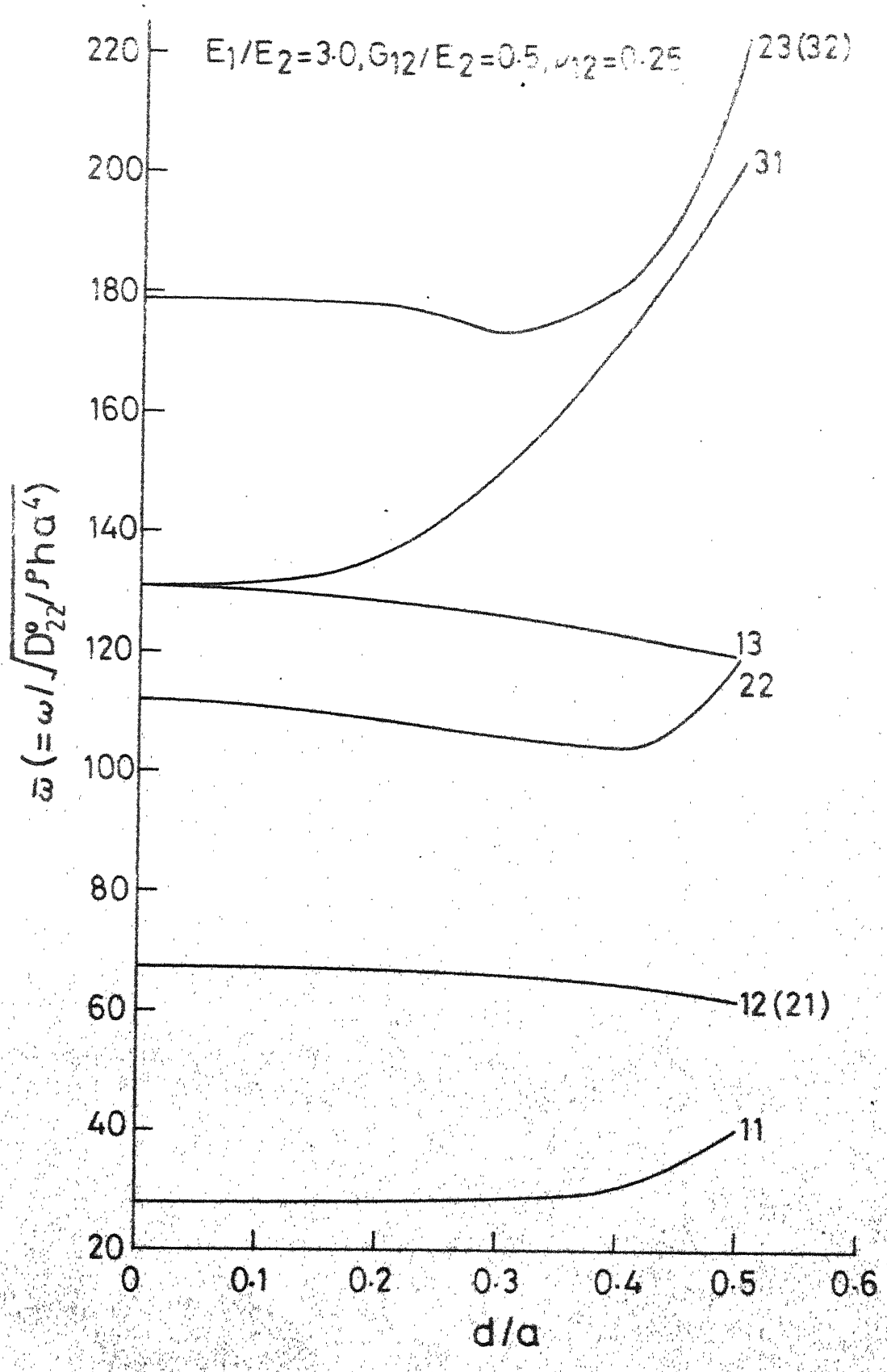

Fig. 3.3 $\bar{\omega}$ vs. d/a for a simply-supported plate; $\theta=45°$, R=1·0.

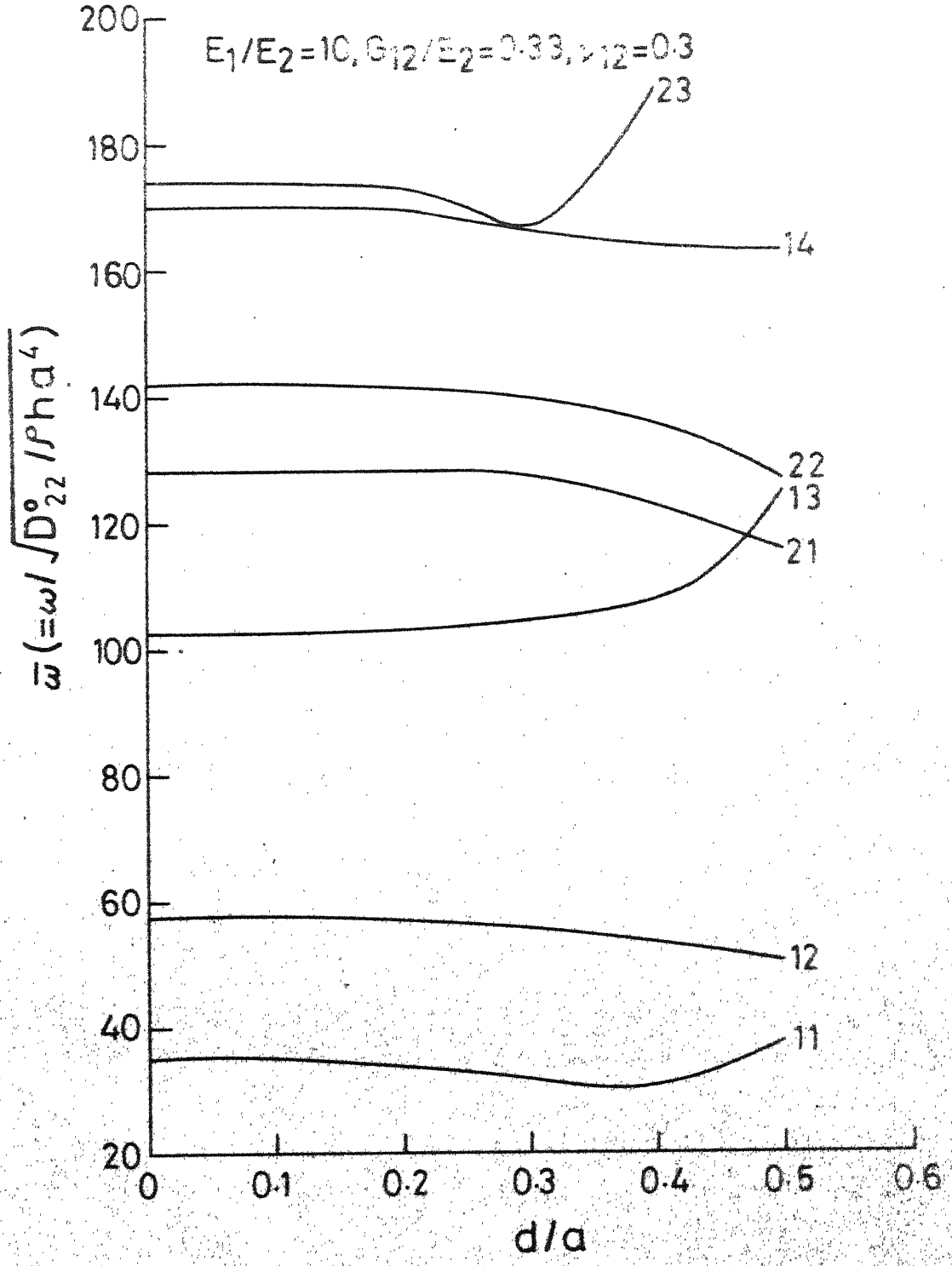

Fig. 3.4 $\bar{\omega}$ vs. d/a for a simply-supported plate; $\Theta=0°, R=1.0$.

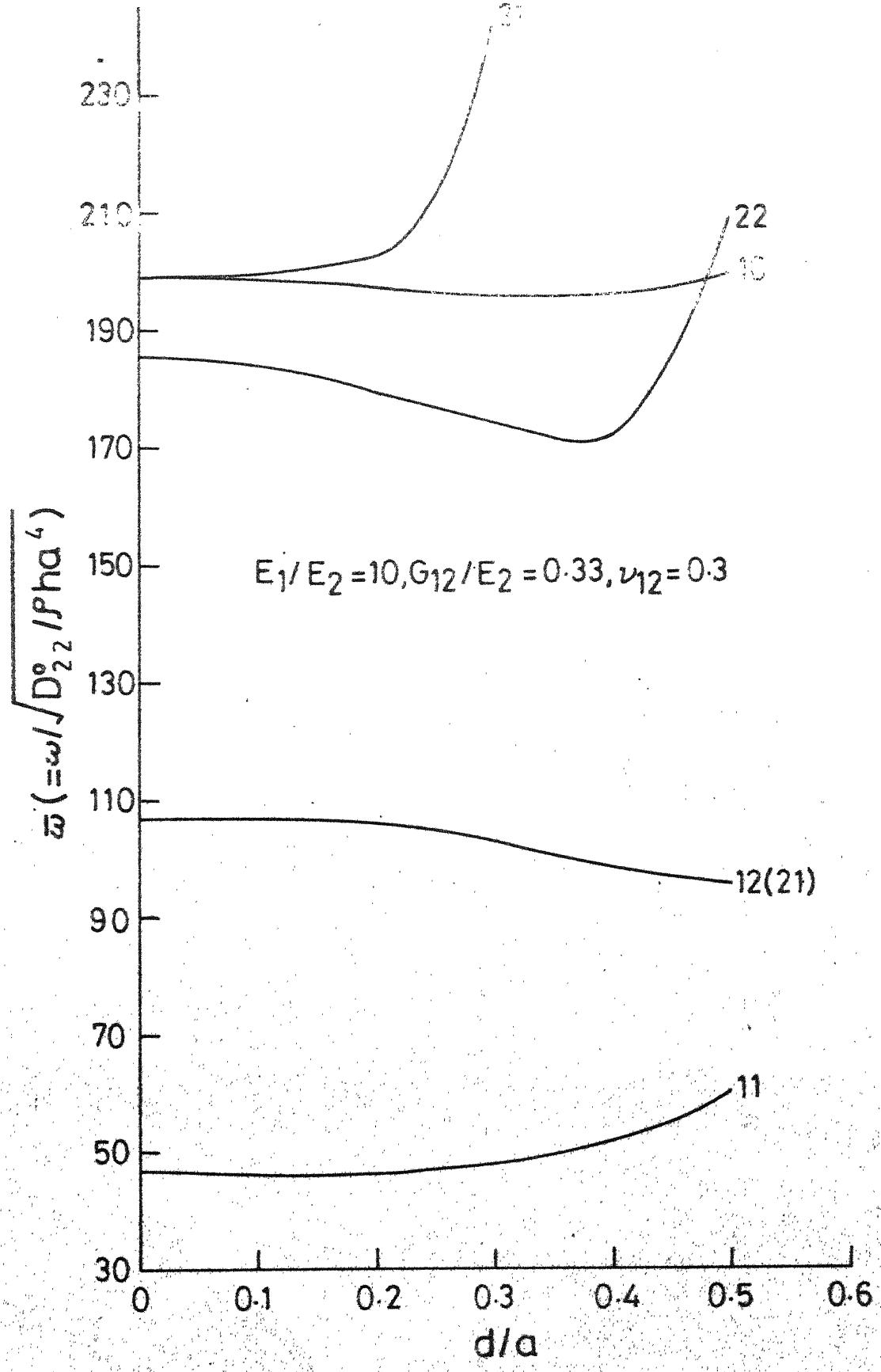

Fig. 3.5 $\bar{\omega}$ vs. d/a for a simply-supported plate; $\theta = 45°$, $R = 1{\cdot}0$.

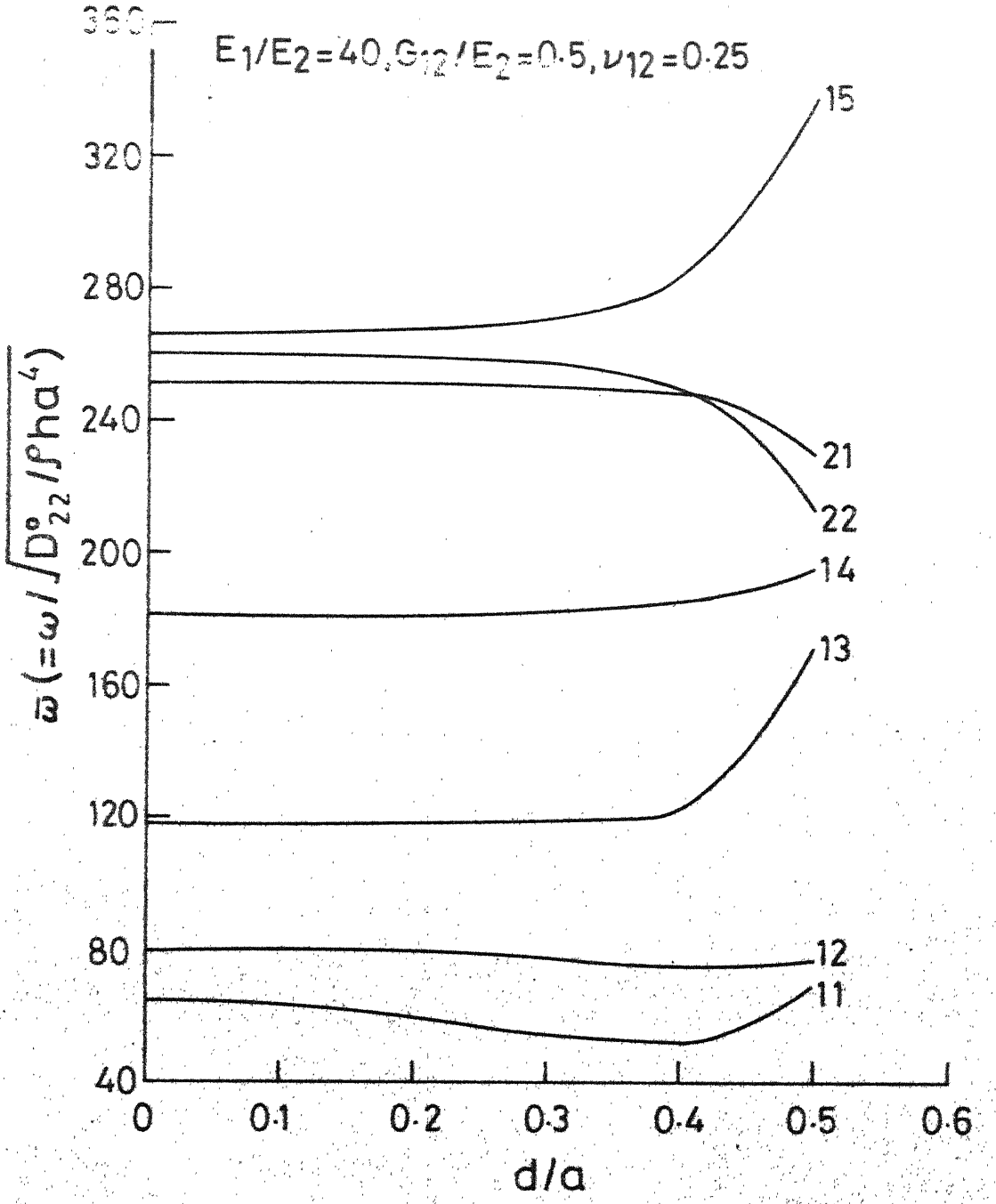

Fig. 3.6 $\bar{\omega}$ vs. d/a for a simply-supported plate; $\Theta = 0°, R = 1.0$.

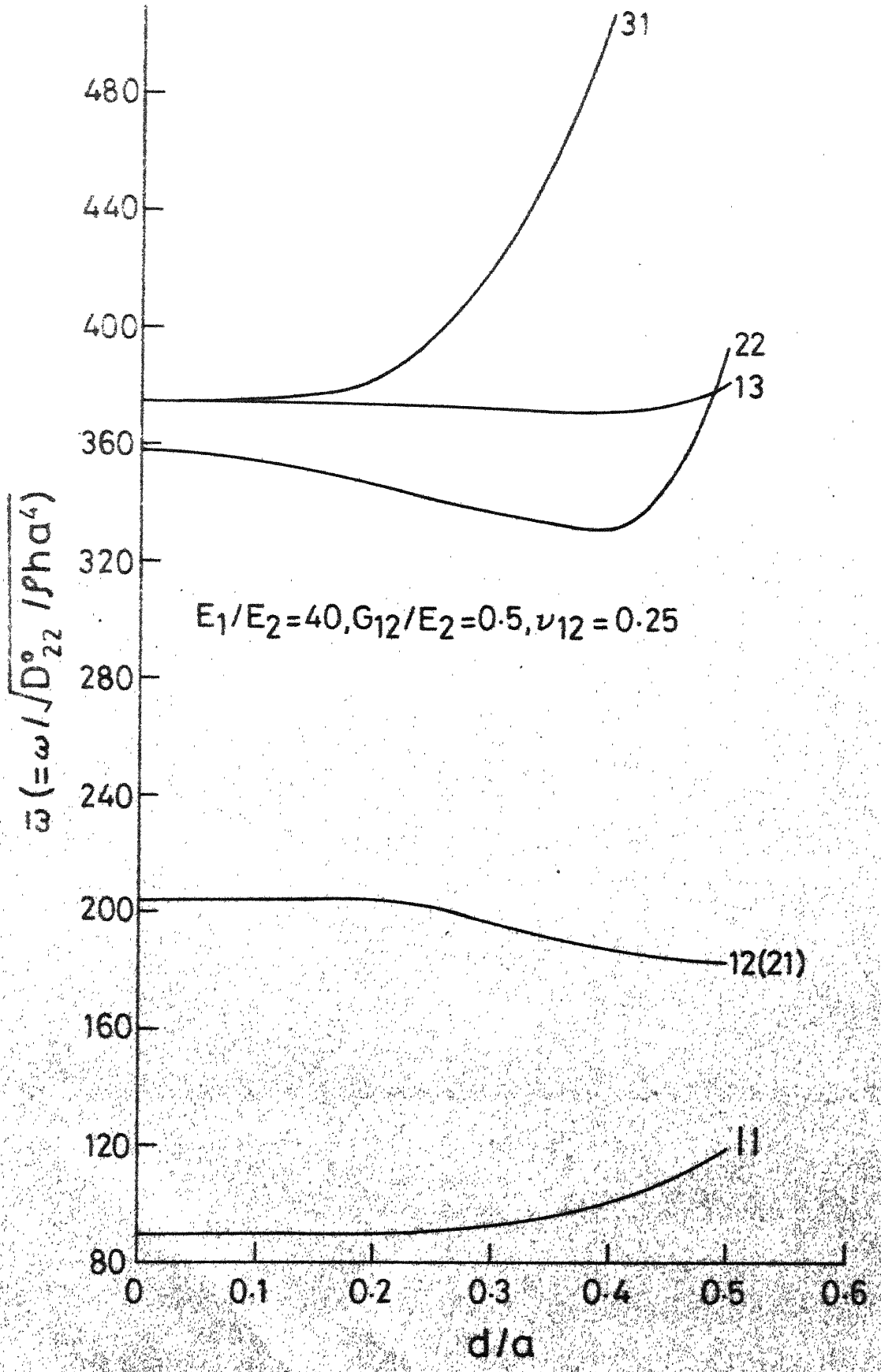

Fig.3.7 $\bar{\omega}$ vs. d/a for a simply-supported plate; $\theta = 45^\circ$, R = 1.0

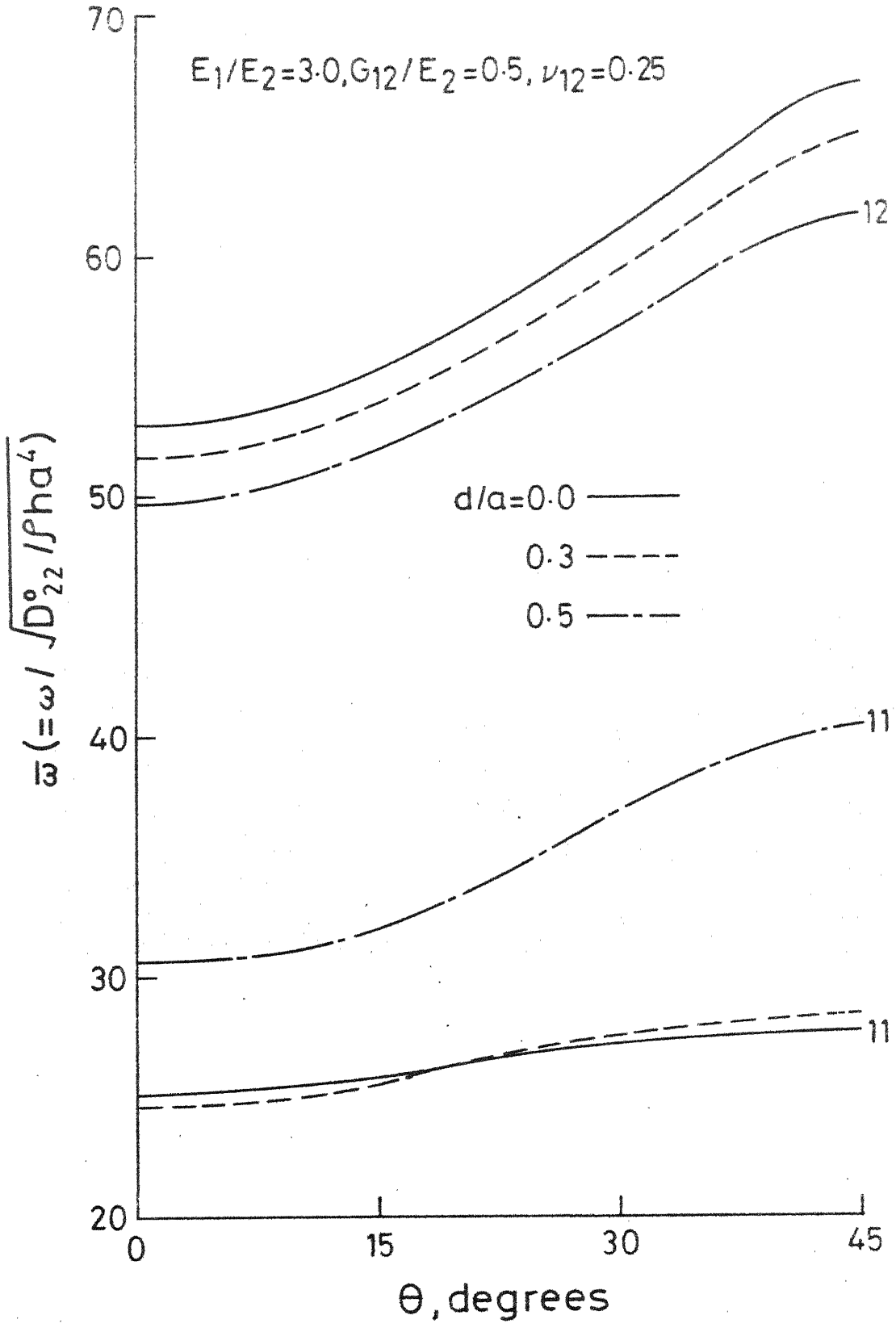

Fig.3.8 $\bar{\omega}$ vs. θ for different hole parameters for a simply-supported plate; R=1·0.

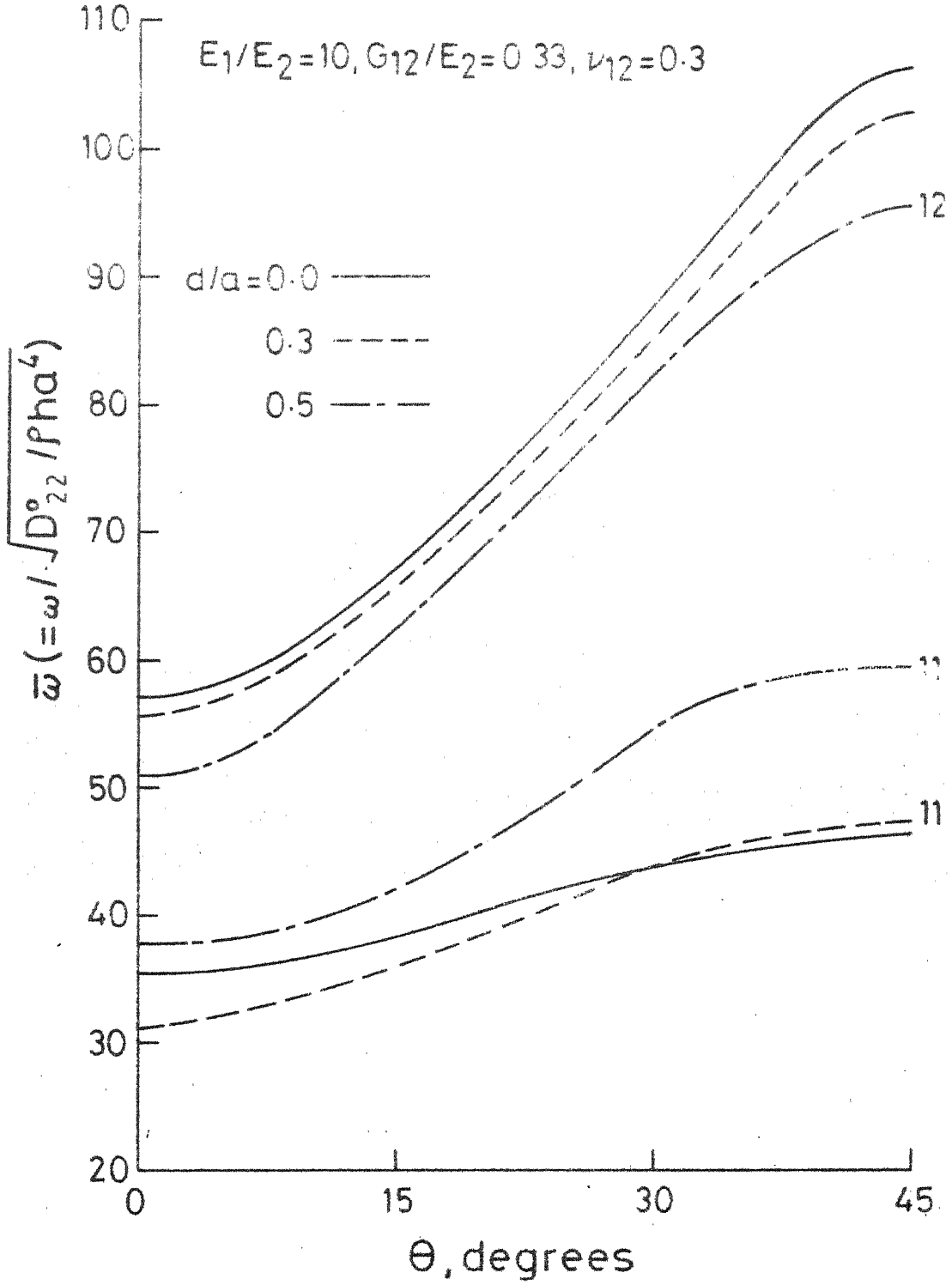

Fig.3.9 $\bar{\omega}$ vs. Θ for different hole parameters for a simply-supported plate; R=1·0.

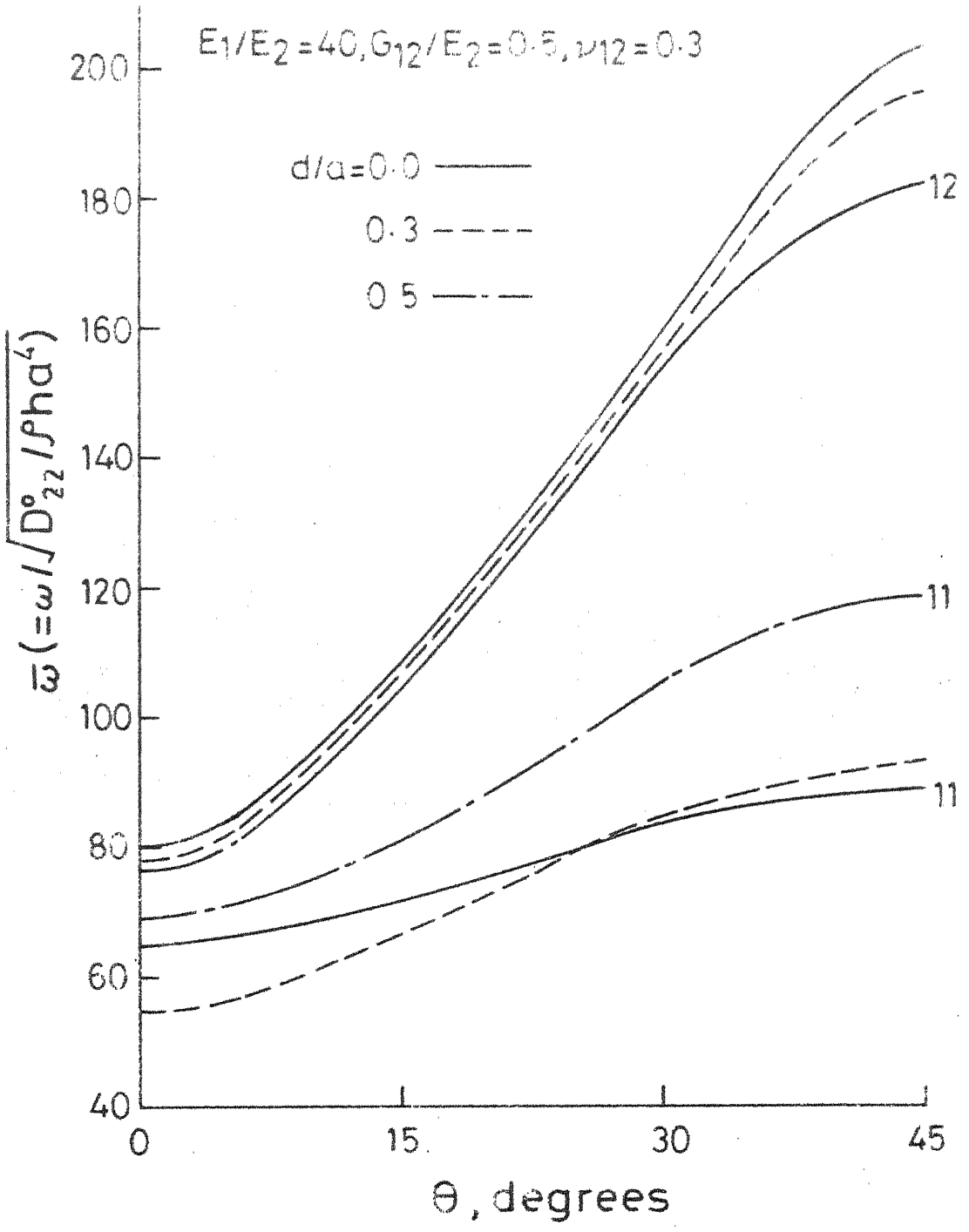

Fig. 3.10 $\bar{\omega}$ vs. θ for different hole parameters for a simply-supported plate; R = 1·0.

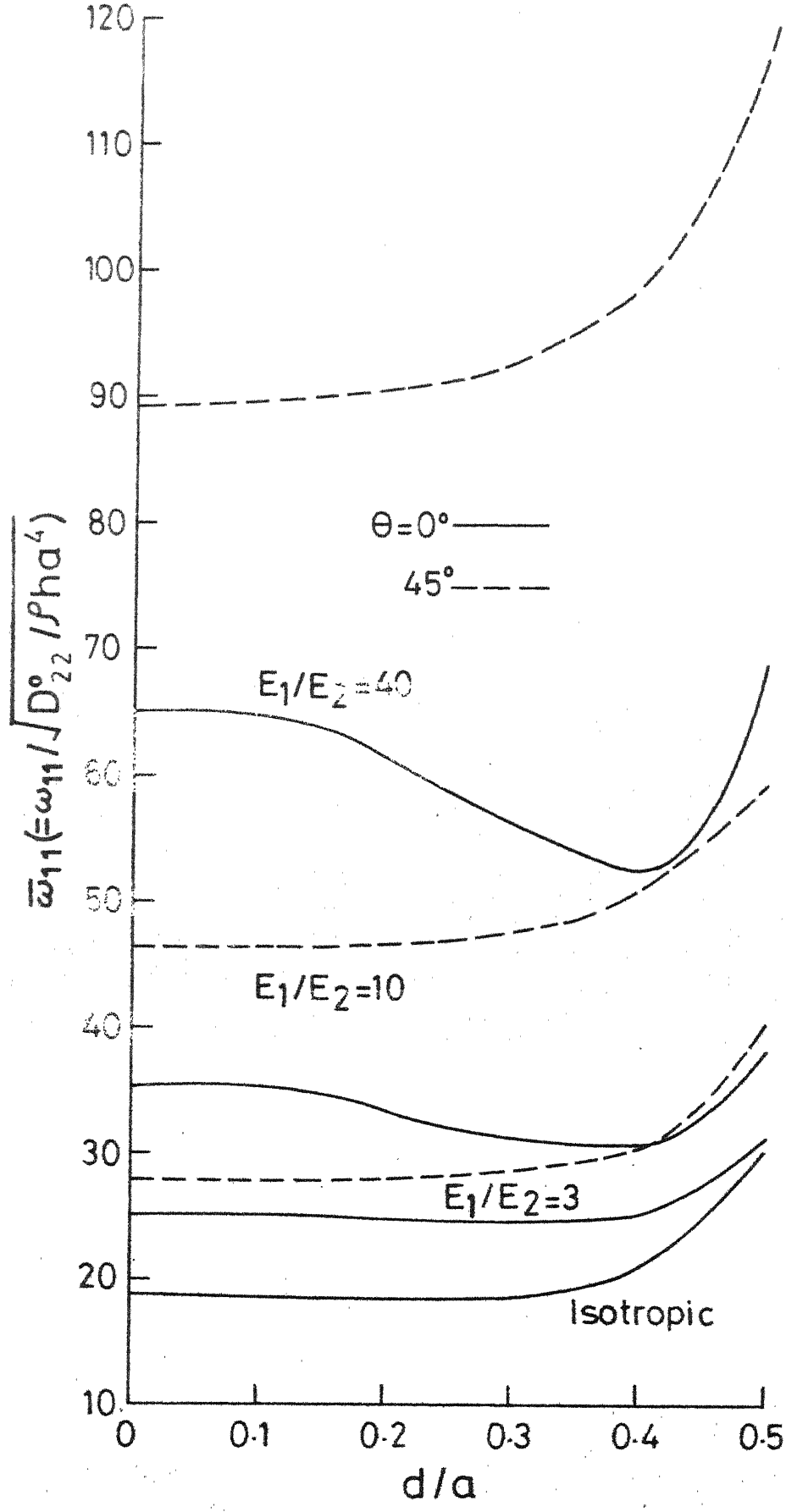

Fig. 3.11 $\bar{\omega}_{11}$ vs. d/a for different modulus ratios for a simply-supported plate; R=1·0.

Table 3.4

Comparison of frequency values and normalized eigenvectors for a simply-supported plate with a hole and a cut-out; $\theta = 0°$, $\bar{\omega}_{13}$

	E_1/E_2							
	1(Isotropic)		3		10		40	
	d/a = 0.5	c/a = 0.5	d/a = 0.5	c/a = 0.5	d/a = 0.5	c/a = 0.5	d/a = 0.5	c/a = 0.5
A_{ij} $\bar{\omega}_{13}$	147.79	146.24	108.23	98.197	158.12	100.07	169.46	117.04
A_{11}	-0.9919	-1.3171	-0.5289	-0.6458	-1.2741	-0.9512	1.0026	-0.9111
A_{13}	0.8510	1.0459	1.1176	1.3996	1.0456	1.6365	1.1300	1.6653
A_{15}	0.0140	-0.2263	-0.0190	-0.4435	1.1371	-0.5291	0.5063	-0.4732
A_{17}	0.0069	0.0913	-0.0729	0.1812	-0.8099	0.2100	-0.2311	0.1815
A_{31}	0.8510	1.0459	-0.4047	-0.4667	0.0983	-0.1513	-0.0019	-0.2099
A_{33}	0.5767	0.5021	0.0710	-0.0650	0.3197	0.0959	0.0997	-0.0963
A_{35}	-0.0101	0.0153	-0.0342	0.2066	-0.7797	0.2357	-0.1956	0.1785
A_{37}	-0.0071	-0.0118	0.0650	-0.1249	0.7890	-0.1471	0.1920	-0.1243
A_{51}	0.0140	-0.2263	0.0256	0.1945	-0.4053	0.1024	-0.0411	0.0466
A_{53}	-0.0101	0.0153	0.0003	-0.0504	0.2603	-0.0001	0.0196	0.0180
A_{55}	-0.0040	0.0654	0.0049	-0.0564	0.0240	-0.0355	0.0123	-0.0740
A_{57}	0.0106	-0.0430	-0.0216	0.0620	-0.2632	0.0305	-0.0353	0.0694
A_{71}	0.0069	0.0913	0.0467	-0.0838	0.3256	-0.0476	0.0527	-0.0248
A_{73}	-0.0071	-0.0118	-0.0395	0.0398	-0.2844	0.0089	-0.0473	-0.0021
A_{75}	0.0106	-0.0430	0.0191	0.0048	0.1672	0.0276	0.0310	0.0274
A_{77}	-0.0084	0.0390	-0.0010	-0.0199	-0.0117	-0.0323	-0.0063	-0.0288

3.4.2 Clamped-Clamped Plates

a) Effect of Hole on the Natural Frequency

A comparison of the non-dimensional frequencies for a few mode has been made in Table 3.5. The results obtained by Anderson [50] by using finite element method compare well with the present results.

The variation of $\bar{\omega}$ with d/a for a clamped-clamped isotropic plate is shown in Figure 3.12. The third and fourth modes are not found to interchange unlike in the case of clamped-clamped isotropic plates with cut-outs (Figure 2.22) whereas the 5th and 6th modes are found to interchange with each other. Results obtained by Anderson [50] compare well with the fundamental frequency whereas those obtained by Kumai [46] are lower. It was mentioned in Section 3.4.1 that the approximation of super-position of the solutions of circular ring plate allows some residual deflections at some portion of the outer boundary of plate which in fact, makes the plate less stiff. Therefore, lower frequency values are obtained by Kumai. The experimental results could not be obtained for the third and the fourth modes; however, the experimental results for other modes compare well with the theoretical results.

In Figures 3.13 and 3.14, the variation of $\bar{\omega}$ with d/a is shown for unidirectional glass-epoxy composite plates in the case of $\theta = 0°$ and $\theta = 45°$ respectively. The frequencies $\bar{\omega}_{11}$ and $\bar{\omega}_{31}$ are found to increase with d/a ratios. For $\theta = 0°$, modes corresponding to $\bar{\omega}_{22}$ and $\bar{\omega}_{13}$ interchange at a small value of d/a. As the fibre-orientation angle is

Table 3.5

Comparison of non-dimensional frequency for a square clamped-clamped isotropic plate with a central circular hole.

d/a	Present		Anderson	
	First Mode	Fourth Mode	First Mode	Fourth Mode
0.0	35.985	131.589	35.375	130.540
0.125	36.321	129.881	35.138	128.637
0.25	37.732	128.200	37.600	125.464
0.375	43.752	125.600	44.240	122.020
0.5	55.610	125.212	57.844	124.308

increased they separate from each other. Modes corresponding to $\bar{\omega}_{31}$ and $\bar{\omega}_{23}$ are found to interchange twice with each other when $\theta = 45°$ whereas they do not interchange when $\theta = 0°$. As the fibre-orientation angle is increased, the frequency curves for $\bar{\omega}_{12}$ and $\bar{\omega}_{21}$ and those for $\bar{\omega}_{23}$ and $\bar{\omega}_{32}$ come closer and coincide for $\theta = 45°$.

The variation of $\bar{\omega}$ with d/a is shown in Figures 3.15 and 3.16 for a unidirectional reinforced boron-epoxy plate in the case of $\theta = 0°$ and $\theta = 45°$ respectively. The frequencies $\bar{\omega}_{11}$, $\bar{\omega}_{31}$ and $\bar{\omega}_{15}$ increase with d/a ratios for both $\theta = 0°$ and $\theta = 45°$. The behaviour of frequency, $\bar{\omega}_{13}$ is, however, different it increases with d/a ratios when $\theta = 0°$ (Figure 3.15) whereas it is found to decrease with increasing values of d/a and then to increase at higher values of d/a when $\theta = 45°$ (Figure 3.16). The behaviour of frequencies $\bar{\omega}_{12}$, $\bar{\omega}_{21}$, $\bar{\omega}_{22}$, $\bar{\omega}_{14}$ and $\bar{\omega}_{23}$ are found similar in case of fibre-orientation angles 0° and 45°. The frequency curves for $\bar{\omega}_{12}$ and $\bar{\omega}_{21}$ and those for $\bar{\omega}_{32}$ and $\bar{\omega}_{23}$ come closer with the increase in the fibre orientation and they coincide when $\theta = 45°$.

For unidirectional graphite-epoxy plates, the variation of $\bar{\omega}$ with d/a is shown in Figure 3.17 for $\theta = 0°$. The frequencies $\bar{\omega}_{11}$, $\bar{\omega}_{13}$ and $\bar{\omega}_{15}$ corresponding to symmetric modes increase with d/a. The behaviour of frequencies $\bar{\omega}_{12}$, $\bar{\omega}_{14}$, $\bar{\omega}_{21}$ and $\bar{\omega}_{22}$ is similar to that found for unidirectional glass-epoxy and unidirectional boron-epoxy plates. It is interesting to note that there is no interchange of the modes shown when $\theta = 45°$ (Figure 3.18). Here also, as for $\theta = 0°$, $\bar{\omega}_{11}$ increases with d/a. The

frequencies $\bar{\omega}_{12}$ (= $\bar{\omega}_{21}$), $\bar{\omega}_{22}$ and $\bar{\omega}_{13}$ are found to decrease with increase in d/a values; the decrease being more in $\bar{\omega}_{22}$ compared to that in the case of $\theta = 0°$. These frequencies, however, increase with higher values of d/a.

b) The Effect of Fibre-Orientation Angle on the Natural Frequency

The influence of fibre-orientation angle has been shown on frequencies $\bar{\omega}_{11}$ and $\bar{\omega}_{12}$ for selected values of d/a ratios. (Figures 3.19 to 3.21). For a particular value of θ, $\bar{\omega}_{11}$ is found to increase with d/a ratios; this is not true for $\bar{\omega}_{12}$: the frequency curves for d/a = 0.3 always lie below the frequency curves for d/a = 0.0 and d/a = 0.5 in all the cases considered.

c) The Effect of Modulus Ratio on the Natural Frequency

In order to understand the effect of modulus ratio on the natural frequency of plates with holes, the behaviour of $\bar{\omega}_{11}$ for different modulus ratios is shown with d/a in Figure 3.22 in the case of fibre orientation angles 0° and 45°. It is found that $\bar{\omega}_{11}$ increases with d/a for all modulus ratios. The frequency curves for $\theta = 0°$ and $\theta = 45°$ for a given modulus ratio, except in the case of balanced bidirectional plates are found to intersect with each other. This behaviour was also observed in clamped-clamped plates with cut-outs.

d) The Effect of Hole on the Mode Shape

The eigenvectors normalized with respect to the mass matrix have been obtained in all the cases considered. Table 3.6 gives a comparison of the frequency values for a symmetric mode and the normalized eigenvectors for all modulus ratios for a given cut-out and hole parameters. The results are given for the fibre-orientation angle $\theta = 0°$.

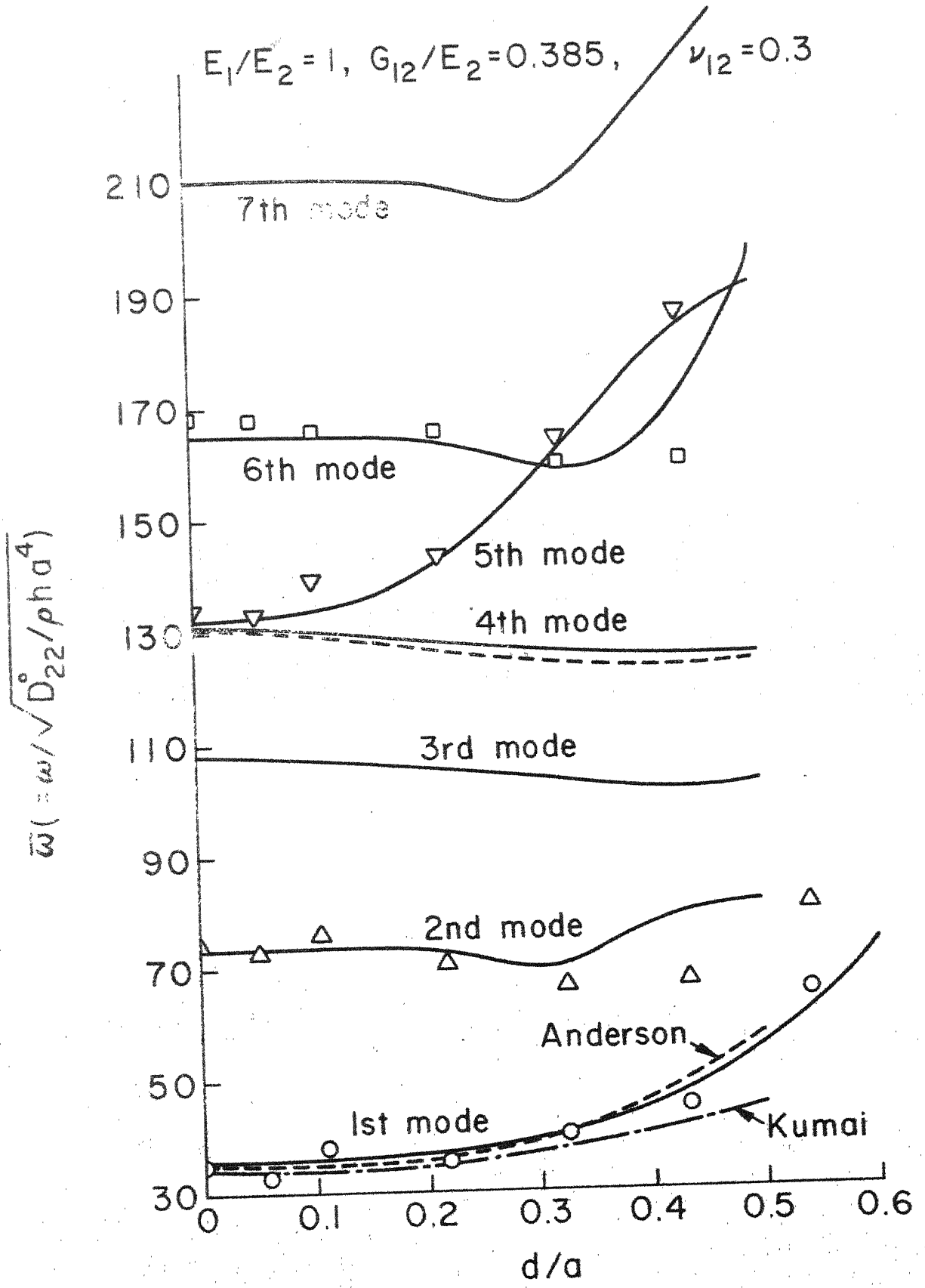

Fig.3.12 $\bar{\omega}$ vs d/a for a clamped-clamped isotropic plate; R = 1.0

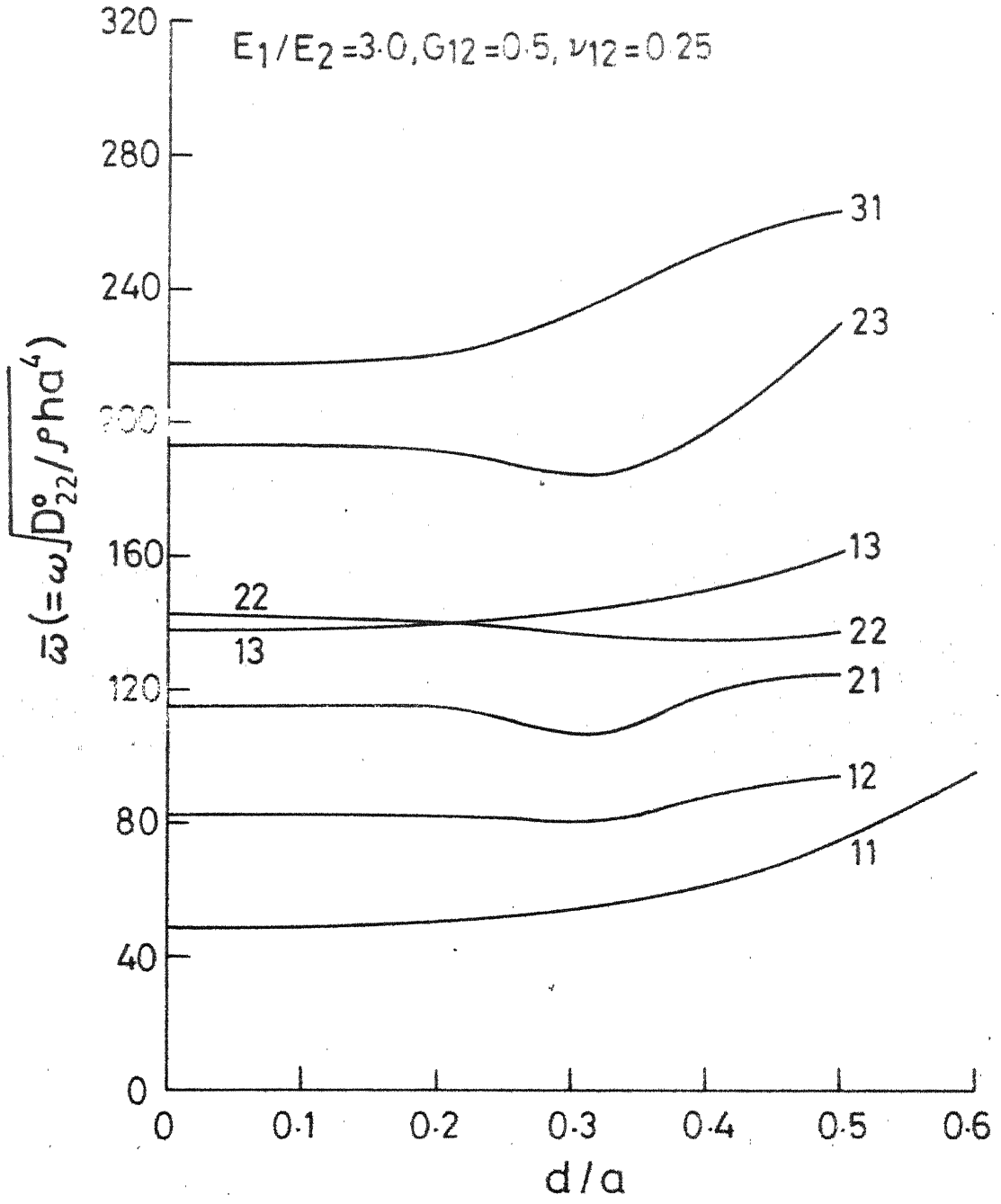

Fig.3.13 $\bar{\omega}$ vs. d/a for a clamped-clamped plate; $\Theta = 0°$, $R = 1{\cdot}0$.

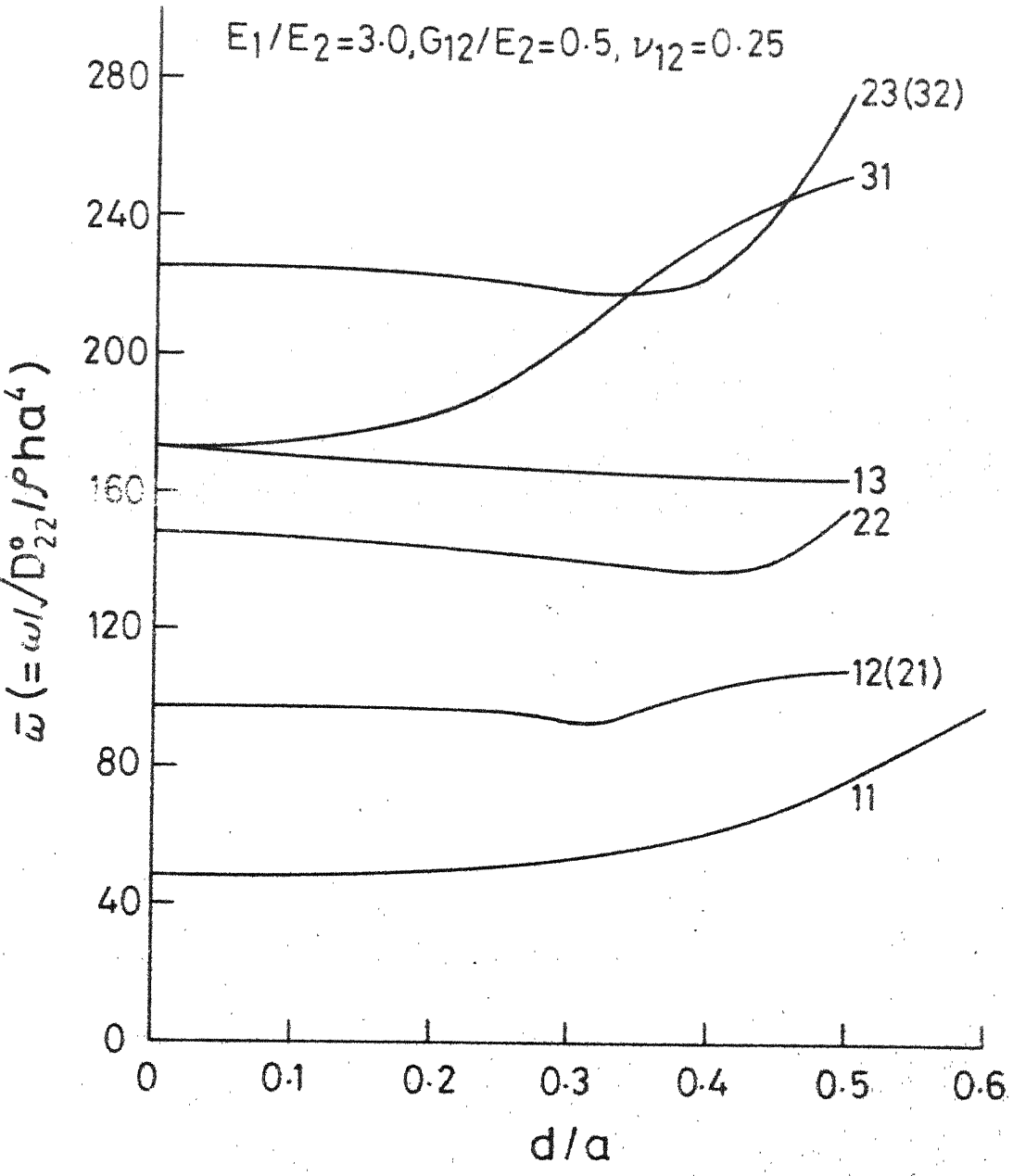

Fig.3.14 $\bar{\omega}$ vs. d/a for a clamped-clamped plate; $\theta=45°, R=1\cdot0$.

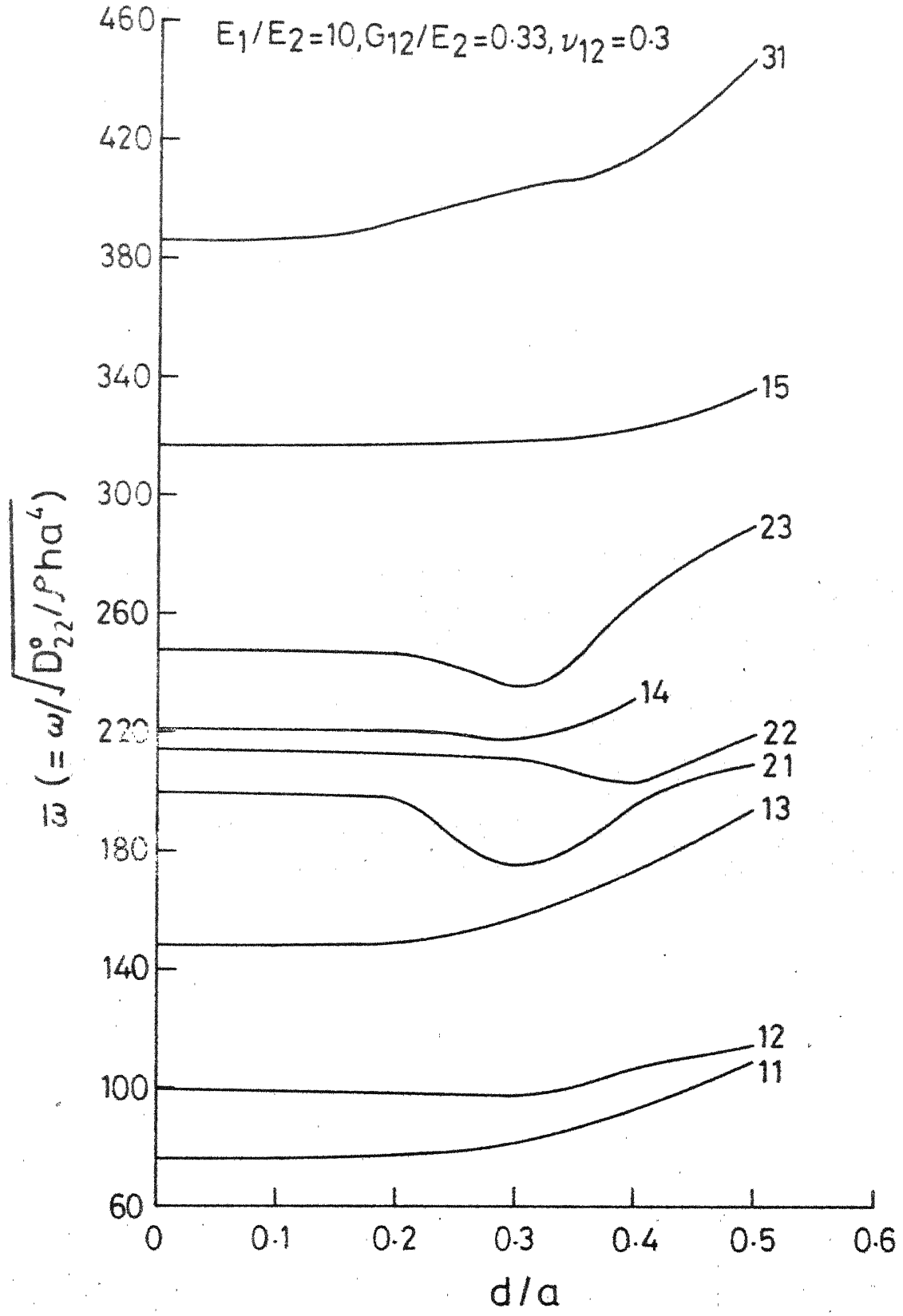

Fig.3.15 $\bar{\omega}$ vs. d/a for a clamped-clamped plate; $\theta=0°$, R=1·0.

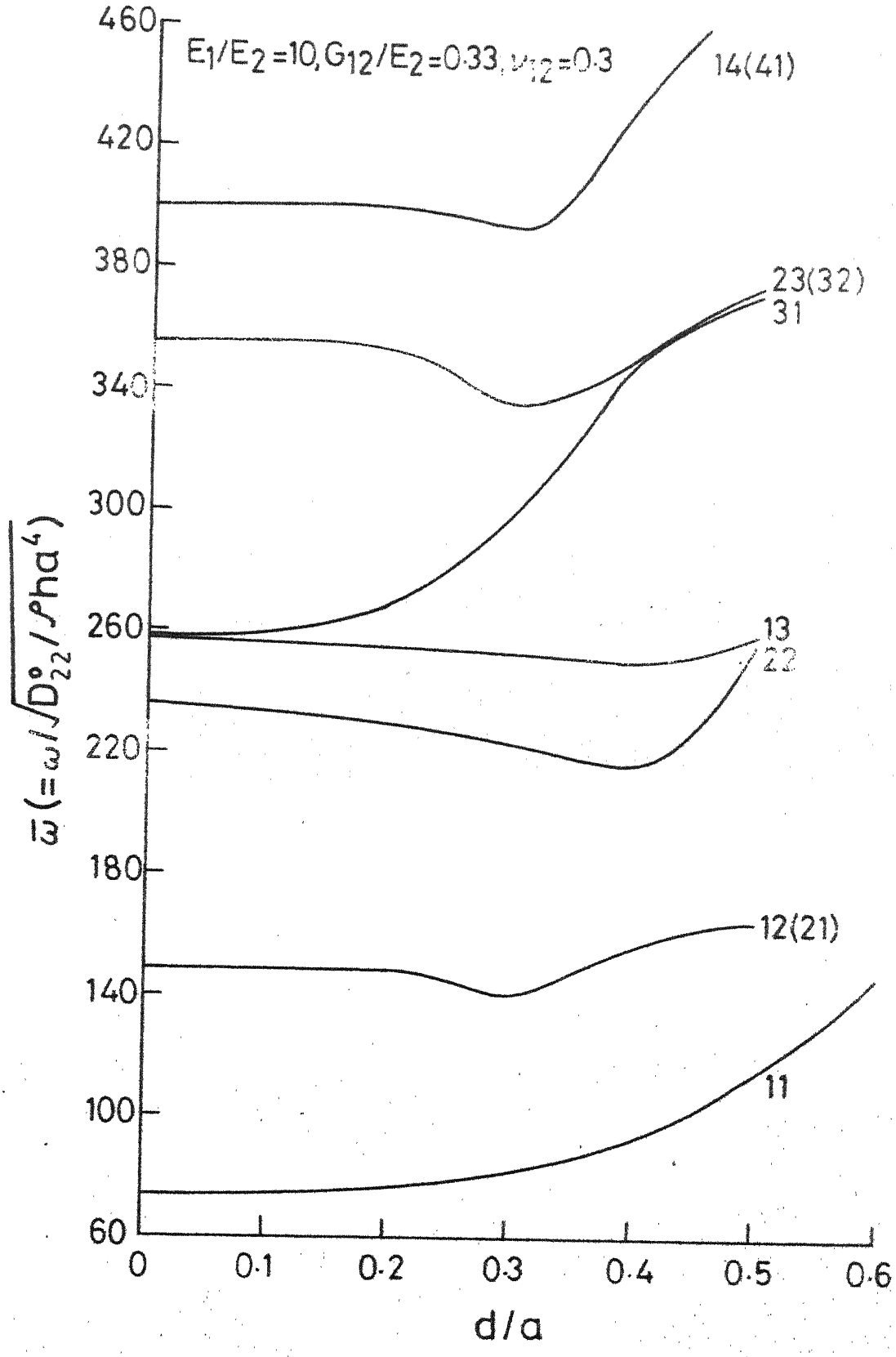

Fig.3.16 $\bar{\omega}$ vs. d/a for a clamped-clamped plate; $\theta=45^{\circ}$, R=1.0.

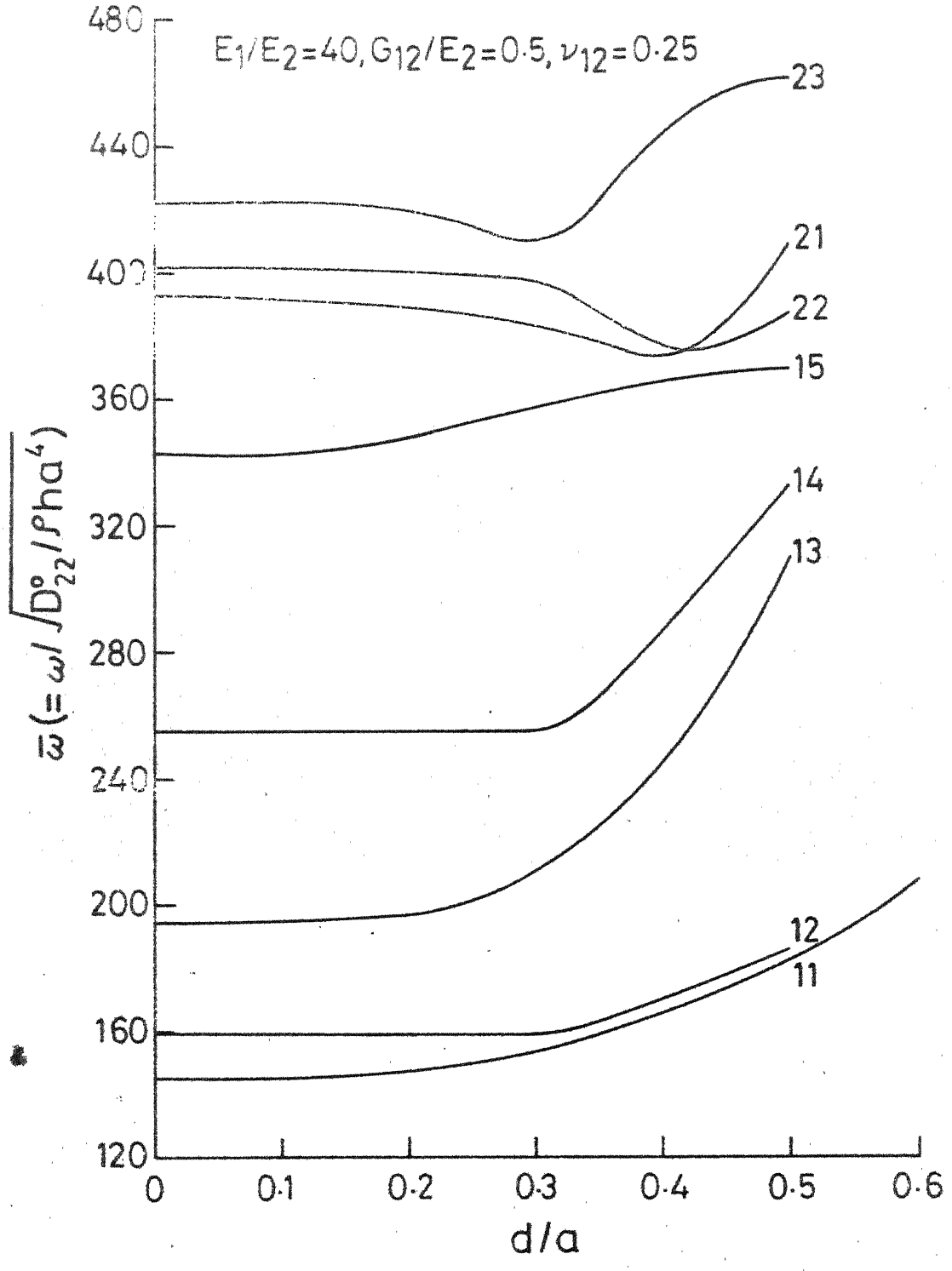

Fig.3.17 $\bar{\omega}$ vs. d/a for a clamped-clamped plate; $\Theta=0°, R=1·0$.

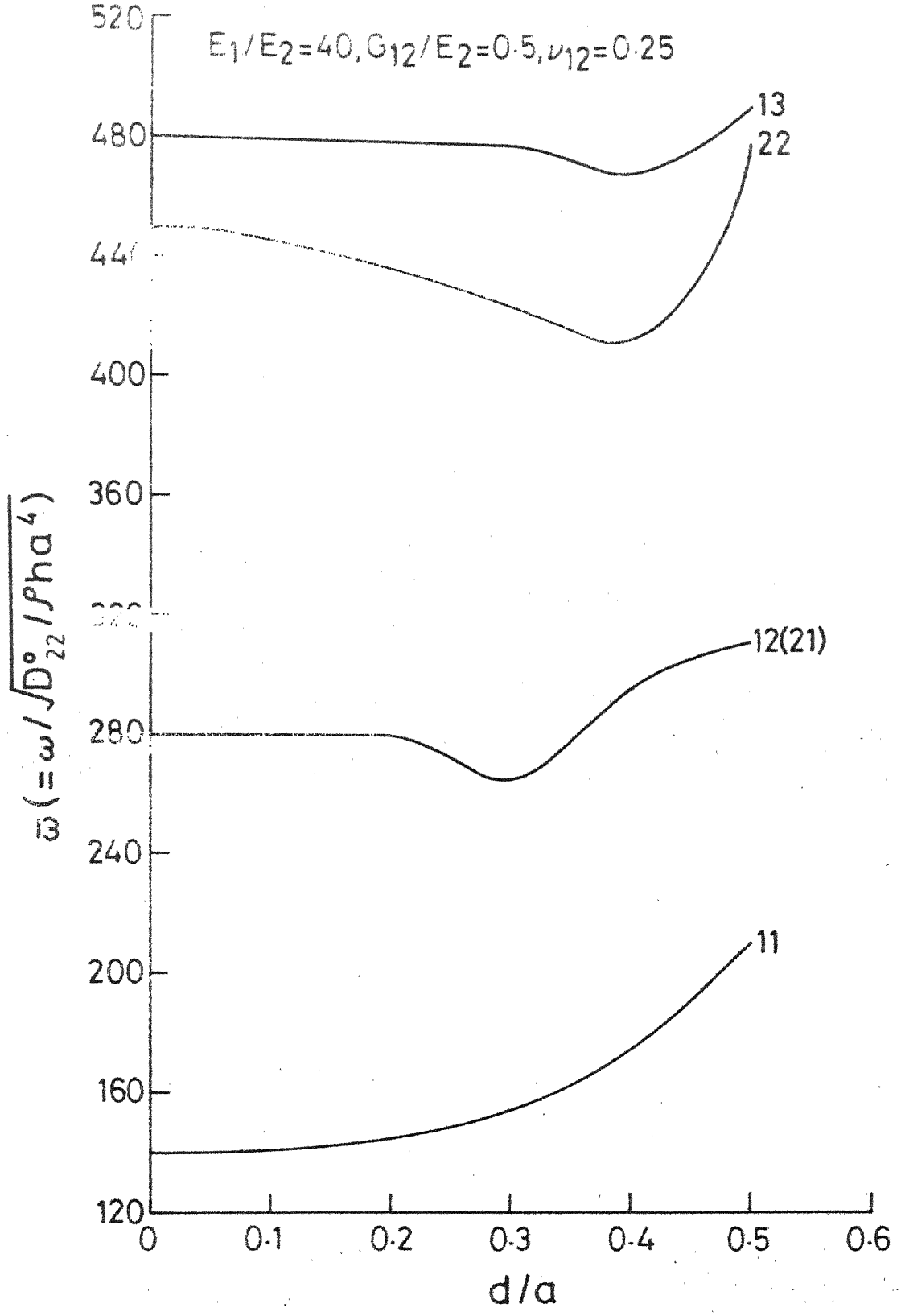

Fig. 3.18 $\bar{\omega}$ vs. d/a for a clamped-clamped plate; $\theta = 45°$, R = 1.0.

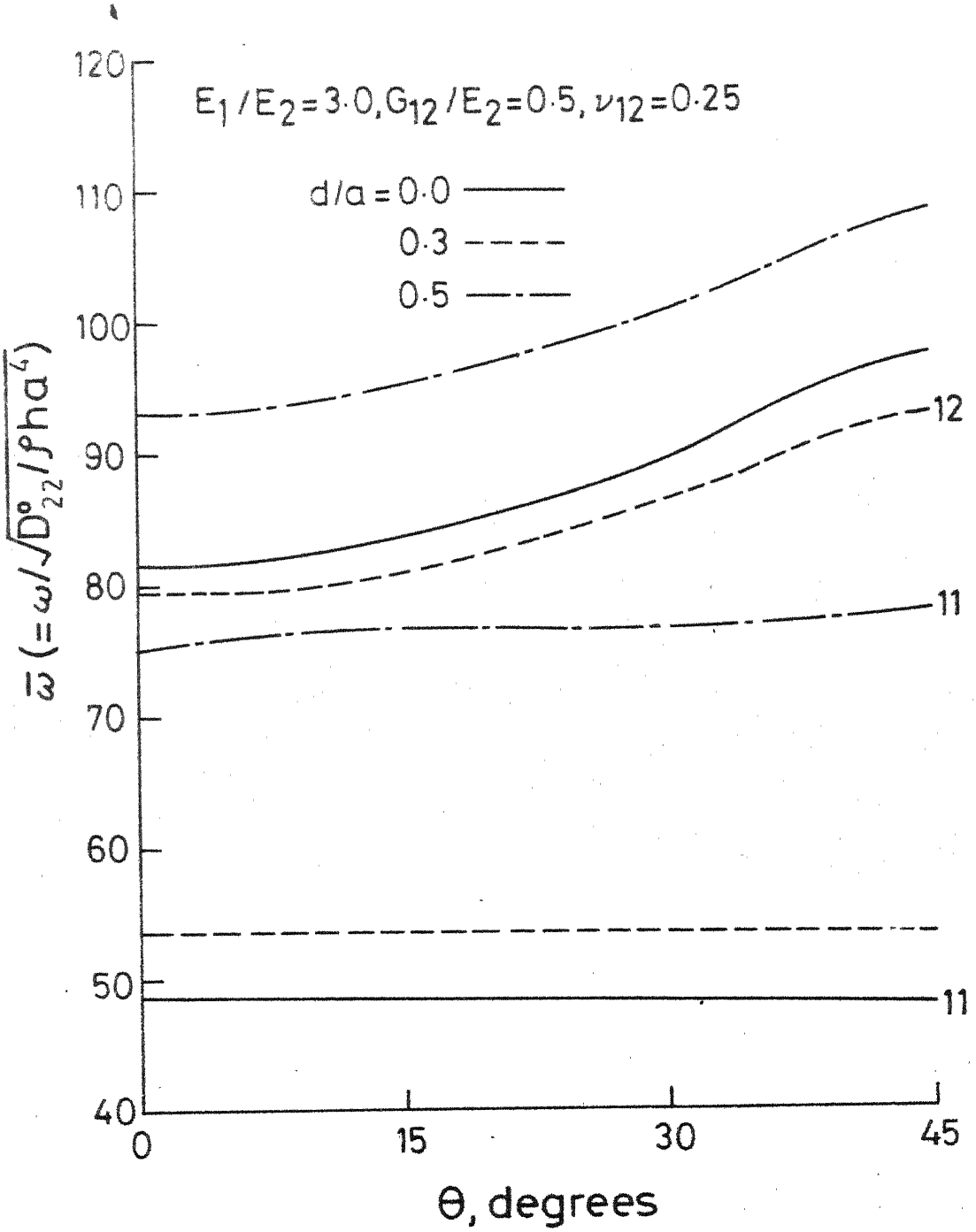

Fig. 3.19 $\bar{\omega}$ vs. θ for different hole parameters for a clamped-clamped plate; R=1.0.

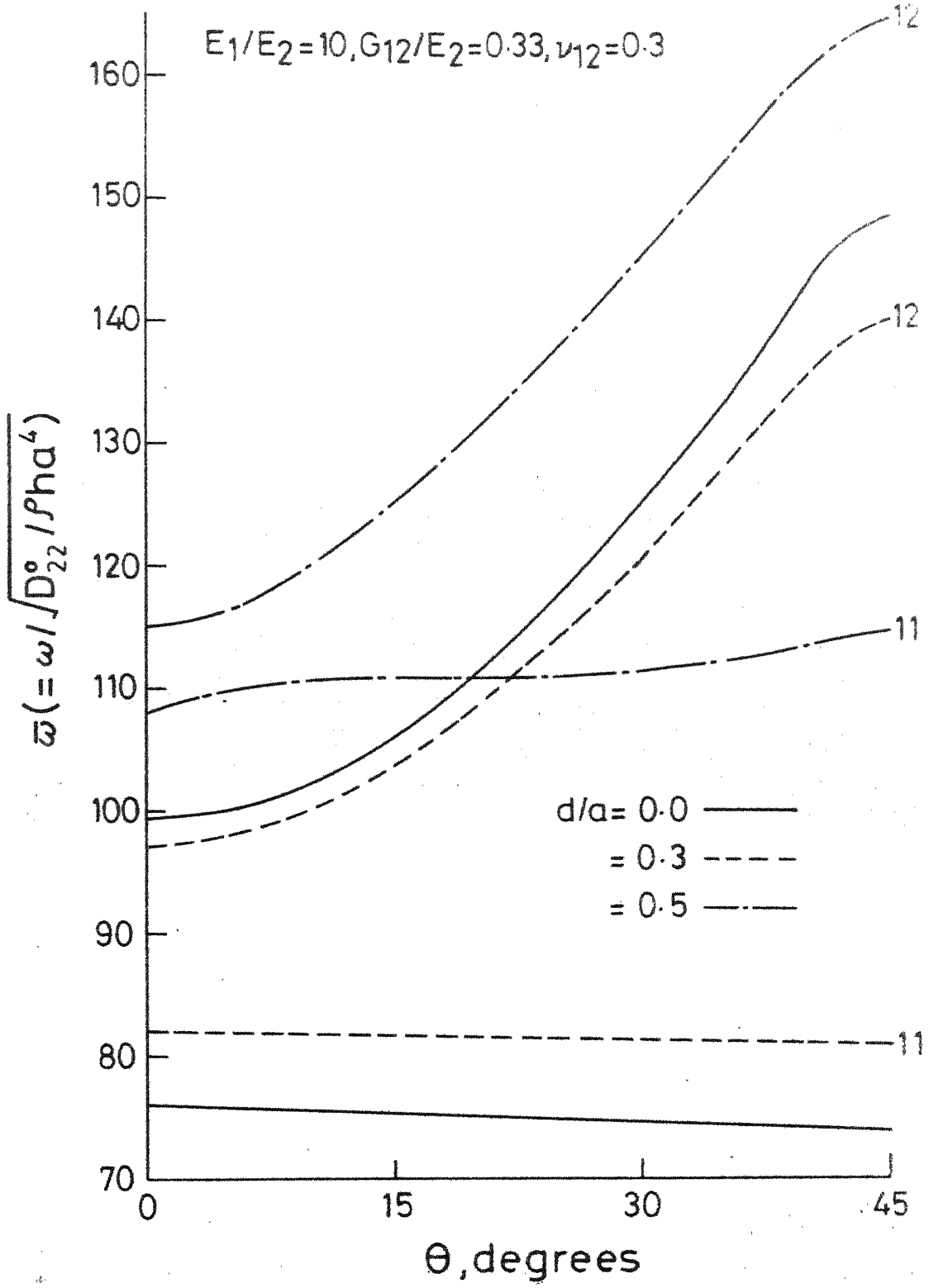

Fig. 3.20 $\bar{\omega}$ vs. θ for different hole parameters for a clamped-clamped plate; R=1·0.

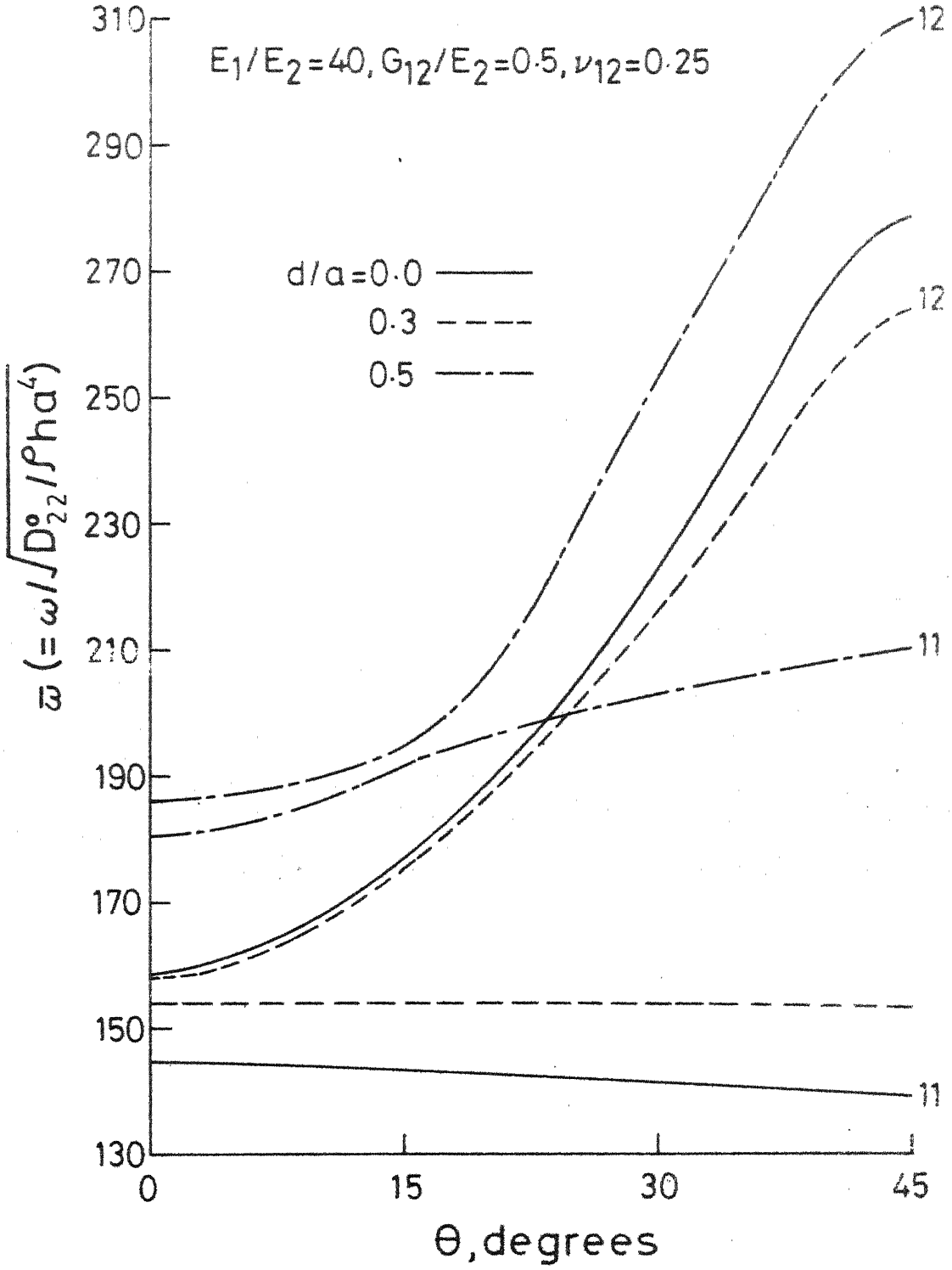

Fig.3.21 $\bar{\omega}$ vs. θ for different hole parameters for a clamped-clamped plate; R=1·0.

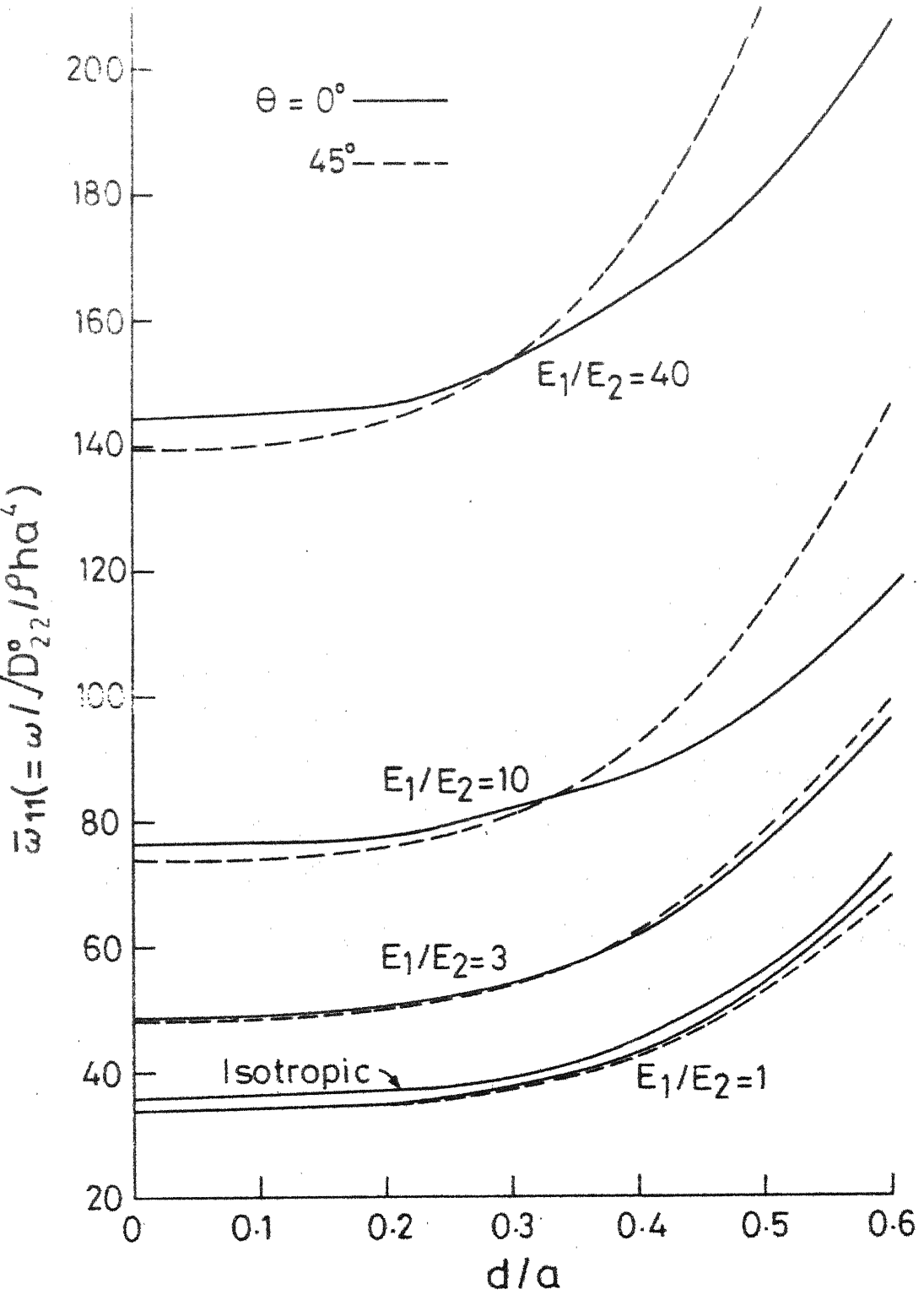

Fig.3.22 $\bar{\omega}_{11}$ vs. d/a for different modulus ratios for a clamped-clamped plate; R=1·0.

Table 5.6

Comparison of frequency values and normalized eigenvectors for a clamped-clamped plate with a hole and a cut-out; $\theta = 0°$, $\bar{\omega}_{13}$

		E_1/E_2							
		1(Isotropic)		3		10		40	
		d/a = 0.5	c/a = 0.5	d/a = 0.5	c/a = 0.5	d/a = 0.5	c/a = 0.5	d/a = 0.5	c/a = 0.5
A_{ij}	$\bar{\omega}_{13}$	176.83	190.83	159.65	152.89	206.50	207.84	298.04	368.21
A_{11}		-1.7261	-1.3734	-1.1544	-1.3489	-0.8343	-2.4288	-2.5364	-2.8341
A_{13}		0.9447	0.7584	1.3800	1.4821	-1.3418	1.5994	1.4084	1.2309
A_{15}		-0.2353	-0.1769	-0.1673	-0.3928	0.1552	-0.4194	0.1907	0.0820
A_{17}		0.0299	0.0459	0.0365	0.1161	0.0877	0.1269	0.0773	0.1171
A_{31}		0.9447	0.7584	-0.3860	-0.5493	0.3414	-0.1807	0.1658	-0.0096
A_{33}		-0.1050	0.8285	0.0033	-0.0368	0.0220	-0.0459	-0.0846	-0.0269
A_{35}		0.1382	-0.0282	0.0789	0.1184	-0.0913	0.1180	0.0097	0.0391
A_{37}		-0.0256	0.0306	-0.0385	-0.0520	0.0450	-0.0483	0.0515	-0.0122
A_{51}		-0.2353	-0.1769	0.0536	0.1445	-0.0849	0.0405	-0.0478	-0.0186
A_{53}		0.1382	-0.0282	-0.0176	-0.0068	0.0508	0.0185	0.0156	0.0185
A_{55}		-0.0562	0.0828	0.0046	-0.0304	-0.0010	-0.0367	0.0200	-0.0140
A_{57}		-0.0244	-0.0351	0.0062	0.0188	-0.0364	0.0189	-0.0456	0.0059
A_{71}		0.0299	0.0459	-0.0178	-0.0462	-0.0028	-0.0173	-0.0107	-0.0013
A_{73}		-0.0252	0.0306	0.0285	0.0177	-0.0380	0.0018	0.0128	-0.0017
A_{75}		0.0244	-0.0351	-0.0264	0.0155	0.0251	0.0063	-0.0204	0.0033
A_{77}		-0.0326	0.0158	0.0132	-0.0035	0.0071	-0.0046	0.0274	-0.0018

CHAPTER 4

EXPERIMENTAL STUDY ON VIBRATION OF PLATES WITH HOLES

4.1 Introduction

The method of analysis described in the previous chapters has been verified by comparing the results obtained with available results for isotropic plates. It was felt desirable to compare the numerical results for orthotropic plates with experimental values. For this purpose, experimental work has been carried out to study the effect of holes on the natural frequencies and mode shapes of simply-supported and clamped-clamped square plates. Cut-outs are not considered in the experimental study because of the practical difficulties in making them. The experimental set-up and procedures have been described in this chapter. The experimental study consisted in characterizing the composite material, achieving the approximate boundary conditions (simple-support and clamped-clamped) by testing solid isotropic plates for which results are known and finally testing the composite plates.

Numerical results have been computed for unidirectionally reinforced E-glass-epoxy plates by taking dynamic properties. The theoretical results for a plate with hole are compared with experimental results and are also compared with those for a plate with central square cut-outs. The theoretical mode shapes have been obtained and compared with experimental results. The effect of hole size on the normalized eigenvectors

and the effect of anisotropy for a particular hole size on the natural frequency and corresponding eigenvectors are also investigated in this chapter.*

4.2 Characterization of the Composite Material

In order to study the response of unidirectionally reinforced composite structural elements under dynamic loading conditions, it is necessary to study the dynamic behaviour of these materials. Various methods for determining dynamic stiffness and damping of composite materials have been reviewed by Bert and Clary [90]. The methods that are commonly used for determining dynamic modulus and damping coefficients are

1) free vibration technique,
2) hysteresis measurements during sinusoidal excitation,
3) forced vibration response technique,
4) pulse propagation technique.

The last two methods are the most popular methods in composite material dynamic-characterization. Forced vibration response technique, which is simpler, has been used here. In this method the modulus is determined from the resonant frequency and damping from the measurement of half-power point frequencies. The method consists essentially of exciting a thin cantilever beam (or any other specimen configuration) and using the peak amplitude as the criterion for determining the resonant frequencies. Thus the modulus and damping can be calculated at each

* A part of Chapter 4 is reported in [88, 89].

natural mode of vibration. The disadvantage of this method is that when two frequencies are closely spaced, both the modes may contribute to the amplitude of an intermediate frequency resulting in a pseudo-mode.

For thin homogeneous isotropic beams with small internal damping (loss factor less than 0.1), the Bernoulli-Euler theory of vibrations of elastic beams gives the relationship between the real part of the complex dynamic modulus and the resonant frequencies of the beam as

$$E = \frac{48\,\pi^2}{gh^2}\,\gamma l^4\,\left(\frac{\omega_{nc}}{(k_n l)^2}\right)^2 \qquad (4.1)$$

where g = gravitational constant

h = depth of the beam

γ = specific weight of the beam

l = free length of the beam

ω_{nc} = corrected resonant frequency for the n-th mode

k_n = characteristic mode constant

Bernoulli-Euler theory does not include the effects of shear deformation and rotatory inertia which are important at higher modes of vibration. Moreover, the shear deformation effects become significant even at low modes of vibration in highly anisotropic beams for which E_{11}/G_{12} ratio is greater than 25 [91]. In the present case E_{11}/G_{12} ratio is less than 25 and therefore, only at higher modes the shear deformation effects become significant.

The corrected resonant frequency, ω_{nc}, is given by

$$\omega_{nc} = \omega_n \left[1 - \frac{\pi^2}{2} \left(\frac{nr}{l}\right)^2 \left(1 + \frac{E}{KG}\right)\right]^{-1} \qquad (4.2)$$

where,

n = the mode number

r = radius of gyration

G = shear modulus

E = tensile modulus

K = shape factor constant

ω_n = measured natural frequency

ω_{nc} = corrected natural frequency

The damping ratio ζ is given by

$$\zeta = \frac{\omega_2 - \omega_1}{2\,\omega_n} \qquad (4.3)$$

where ω_1 and ω_2 are half-power point frequencies.

The composite material used to study the dynamic response of composite plates was unidirectionally reinforced E-glass epoxy material. Measurements of dynamic modulus and damping ratios were made on cantilever beams with fibre-orientations 0°, 15°, 30°, 45° and 90° with respect to the beam axis. The specimens were cut from unidirectionally reinforced sheets and machined to size on a high speed routing machine. The sheets were made by a hand lay-up technique. The dimensions of the beams were

1" wide, .094" thick and 9.1" long (The variation in width was ± .001" and that in thickness was ± .0015").

Figure 4.1 shows the vibration test set-up which used an LB model PM-50 exciter driven by an oscillator through a model 2250 LB amplifier. The beams were mounted on an electrodynamic shaker. Electrical resistance foil gauges (SR-4, AF-8) were fixed on top and bottom surfaces of the beams to record only bending strains. This was done keeping in view the fact that twisting is not pronounced in glass-fibre reinforced epoxy beams as reported by Schultz and Tsai [92]. The clamped end of the beams was given a sinusoidal harmonic motion and the output of the strain gauges was seen on an oscilloscope (Type 564B Tektronix) with a carrier amplifier plug-in-unit. The resonant frequency was determined by seeing the peaking of the strain in the oscilloscope and then carefully adjusting the exciting frequency in order to get the maximum strain. The resonant frequency was measured on an electronic counter. The beams were excited over a frequency range of 10 - 6000 cps. The dynamic modulus was determined taking into account the effect of shear correction. A few cases were found where two closely spaced resonant peaks occurred instead of the normal single peak response. These are believed to be associated with the stiffness of the clamping arrangement, and when it occurred, the data for that mode was discarded.

The modal frequency ratios ω_n/ω_1 for 0°, 15°, 30°, 45° and 90° cantilever beams are given in Table 4.1 and are compared with the theoretical value calculated on the assumption that the modulus is frequency

independent and that the beam is a uniformly homogeneous Bernoulli-Euler beam.

Figure 4.2 shows the variation of the dynamic modulus with frequency for various fibre-orientations. The effect of shear correction term is shown only for a beam with 0° fibre-orientation. The shear effect is seen to be pronounced only at higher mode frequencies. An average value of the modulus is chosen for numerical computation.

The static modulus was determined by testing tensile specimens of 0°, 45° and 90° fibre-orientations, with strain gauges mounted, on an Instron machine [93].

Table 4.2 gives the dynamic (average) and static properties of unidirectionally reinforced E-glass-epoxy composite material used in the experimental study. The static moduli are seen to be lower by 3-33 percent than the dynamic moduli.

4.3 Vibration Study

4.3.1 Test Plates

This study was concerned with the vibration of simply-supported and clamped-clamped plates with circular holes. The isotropic plates were made of aluminium, had a thickness of .048" and had dimensions of 9.5" x 9.5". Eight isotropic plates were studied. The eight plates consisted of one solid plate and seven plates with holes of 0.45", 0.90", 1.8", 2.7", 3.6", 4.5" and 5.4" diameter. The test plates used in the experimental investigation other than aluminium plates were cut from a

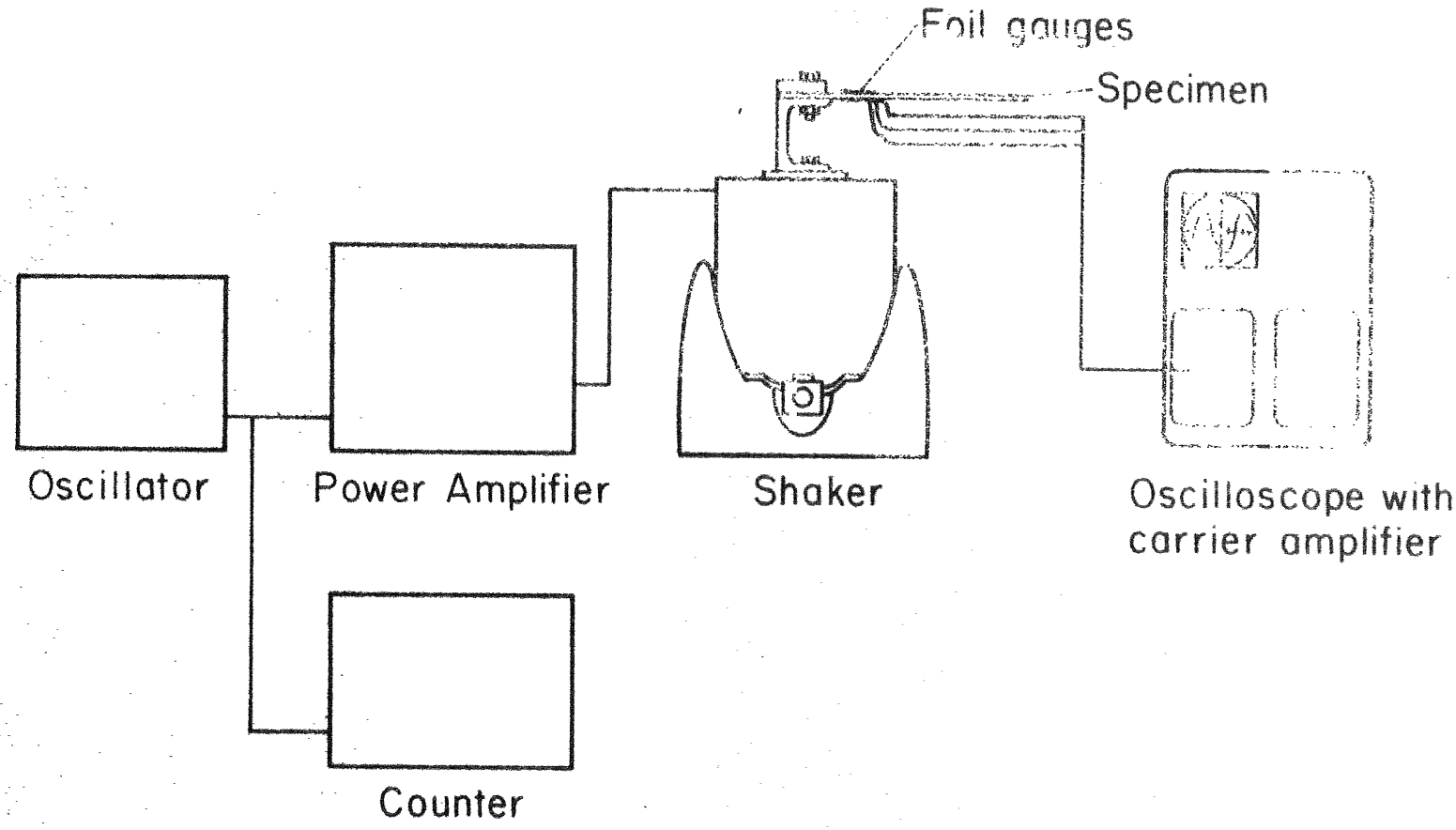

Fig. 4.1 Schematic diagram for dynamic modulus measurement

Table 4.1

Modal frequency ratios for a cantilever beam .

Mode	Isotropic (Theory)	Generally orthotropic (Measured)				
		0°	15°	30°	45°	90°
1	1	1	1	1	1	1
2	6.27	6.03	5.91	5.93	5.95	5.98
3	17.5	17.11	16.98	16.98	17.05	16.76
4	34.4	*	34.1	35.2	-	-
5	56.8	55.0	55.2	57.2	-	54.5
6	84.9	82.1	81.4	82.7	85.0	82.5
7	119	111.1	115.6	117.6	120.4	117.9
8	158	154.1	154.2	154.2	165.1	156.8
9	203	195.2			213.8	
10	253	248.4				
ω_1, Hz		23.23	20.75	16.80	14.42	14.13

* These frequencies (corresponding to blank spaces) could not be obtained because of the resonance of the clamping fixture or the presence of pseudo modes.

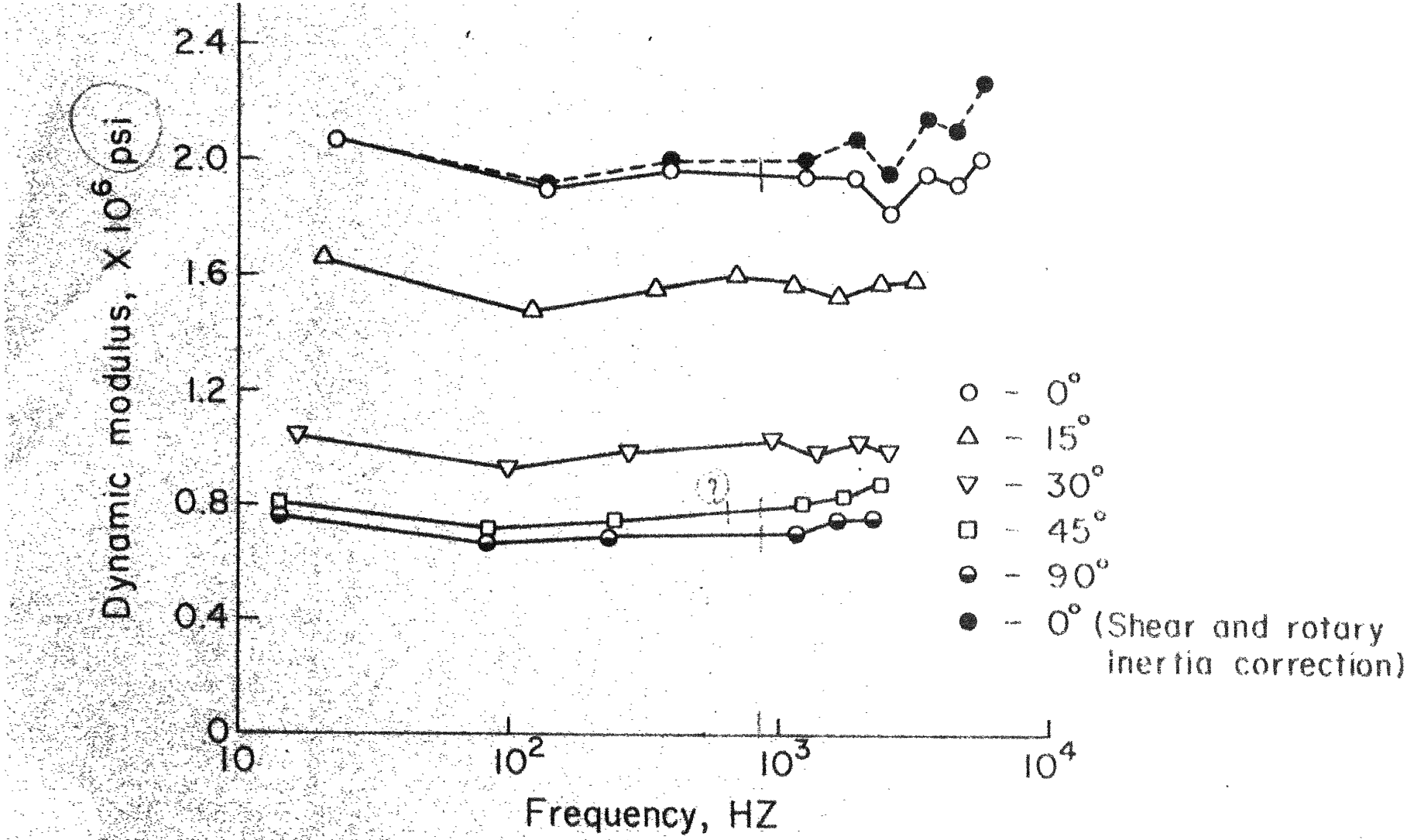

Fig.4.2 Variation of dynamic modulus with frequency

Table 4.2

A comparison of static and dynamic properties of a unidirectionally reinforced E-glass-epoxy material.

	Static	Dynamic
E_{11}	2.02×10^6 psi	2.08×10^6 psi
E_{22}	0.53×10^6 psi	0.74×10^6 psi
G_{12}	0.18×10^6 psi	0.27×10^6 psi
ν_{12}	0.35	
ρg	0.05 lb/inch^3	

unidirectionally reinforced E-glass-epoxy sheet. Square plates with 0°, 15°, 30° and 45° fibre orientations were tested. The principal elastic constants of the composite material were found by forced vibration response method and has been discussed earlier in Section 4.2. In order to study the effect of holes on the vibration characteristics of unidirectionally reinforced plates, the following steps were taken.

a) Vibration characteristics for the unidirectionally reinforced solid plates were found.

b) Small holes were drilled in the plates.

c) The holes were enlarged to size on a high speed routing machine using aluminium templates.

d) Vibration characteristics for the unidirectionally reinforced plates with holes were found.

e) The holes were increased in size by machining again and the corresponding vibration characteristics for plates were found for each predetermined hole size.

The unidirectionally reinforced plates were 9.5" x 9.5" square having a thickness of .094". The hole sizes used in the test were 0.45", 1.8" and 3.6".

4.3.2 Simple Support and Clamping Arrangements

A test fixture was designed and fabricated to study the vibrations of plates. It consisted of four vertical members bolted to the foundation and four horizontal members supported by the vertical members. On the

horizontal members a thick plate with an internal square opening was kept. The thick plate could be secured on the horizontal members. Provision was made on the thick plate to place rollers for conducting experiments on simply-supported plates. Simple supported conditions were achieved by placing test plate between two sets of rollers (Figure 4.3). The upper set of rollers were held in position on another plate with an internal square opening. The test plate was held between rollers by bolts. Tests were carried out on a solid aluminium plate and the torque on the bolts to hold the thick plates with rollers was appropriately chosen to give a good agreement between the theoretical and experimental results. The same testing conditions were maintained throughout the course of experiment.

For clamped-clamped conditions, the test plates were kept on the thick plate and clamped by means of two sets of thick mild steel flats by nuts and bolts. The effect of various torques applied for tightening the bolts was seen on the natural frequencies of an aluminium test plate without hole. With increase in the value of torque applied on bolts, the frequency was found to increase. But after a certain value of the torque there was no appreciable change in the frequency. A particular value of the torque (14 lb. ft) was chosen and maintained in testing all plates. Several tightening sequences did not produce any variation in the natural frequencies. The frequency values for the aluminium plate were checked with available results and a good agreement was found. This suggested that the desired edge conditions have been obtained. The experiments on unidirectionally reinforced E-glass-epoxy plates were conducted in identical conditions.

4.3.3 Source of Excitation

The test plates were excited acoustically by means of a loud speaker (shown in Figure 4.4). The field of the coil was driven by a d.c. supply. The signal was fed to the loud speaker from an oscillator through an amplifier and the amplitude of the signal could be controlled both from the oscillator and the amplifier. The signal frequency was accurately measured by an electronic counter. The test set-up is shown in Figure 4.5. The loud speaker was used because of the following reasons:

1) In the case of excitation by an electrodynamic shaker the whole fixture with test plate has to be mounted on the shaker which may not be always possible due to the force limitations of the shaker. Also, the test fixture resonance may create difficulty in obtaining a nodal pattern when one of the natural frequencies of a test plate happens to be near the resonant frequency of the fixture.

2) The variable frequency air jet excitation method can be used but the arrangement is quite complex as a continuous air supply is always required.

The position of the speaker did not affect the natural frequencies of the plate.

4.3.4 Measurement of Natural Frequency

A contactless vibration pick-up (type mV-200)* was used to find the natural frequencies of the vibrating aluminium plates. The pick-up generates an electrical output. The signal from the pick-up was

* Manufactured by the National Aeronautical Laboratory, Bangalore (India).

amplified and displayed on an oscilloscope. The input signal was also fed on the oscilloscope and no change in the frequency was found between the input and output signals.

The first step in obtaining the natural frequencies, which in this experiment were indicated by the maximum pick-up output, was to place the pick-up at a point above the plate. The frequency of the signal from the oscillator was slowly increased and the output of the pick-up observed on the oscilloscope. At a certain frequency the output of the pick-up is found to be maximum. The frequency is carefully adjusted at this point so as to get the maximum output displayed on the oscilloscope and is then measured on an electronic counter. Nodal patterns were also used to measure frequencies and these agreed well with those given by the contactless pick-up.

In the case of unidirectionally reinforced plates, the natural frequencies were measured when a clear modal pattern was observed on the vibrating plate.

4.3.5 Nodal Pattern Detection

When a plate is excited at a natural resonant frequency it vibrates in a particular mode shape. This shape can be visualized by sprinking dry sand or aluminium oxide granules on the surface of the plate. The particles collect on the nodal lines where there is relatively less motion. When the plate vibrates at a frequency other than the resonant frequencies there are no nodal patterns and the granules bounce forming no pattern. With the

a. Simple-support arrangement

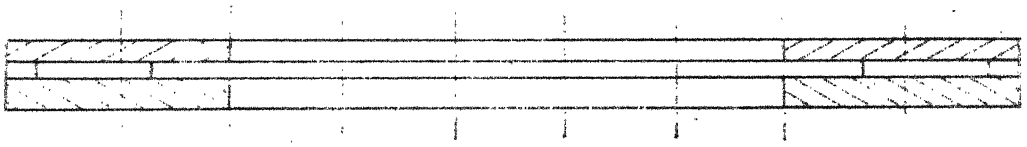

b. Clamped-clamped arrangement

Fig. 4·3 Simple-support and clamping arrangement

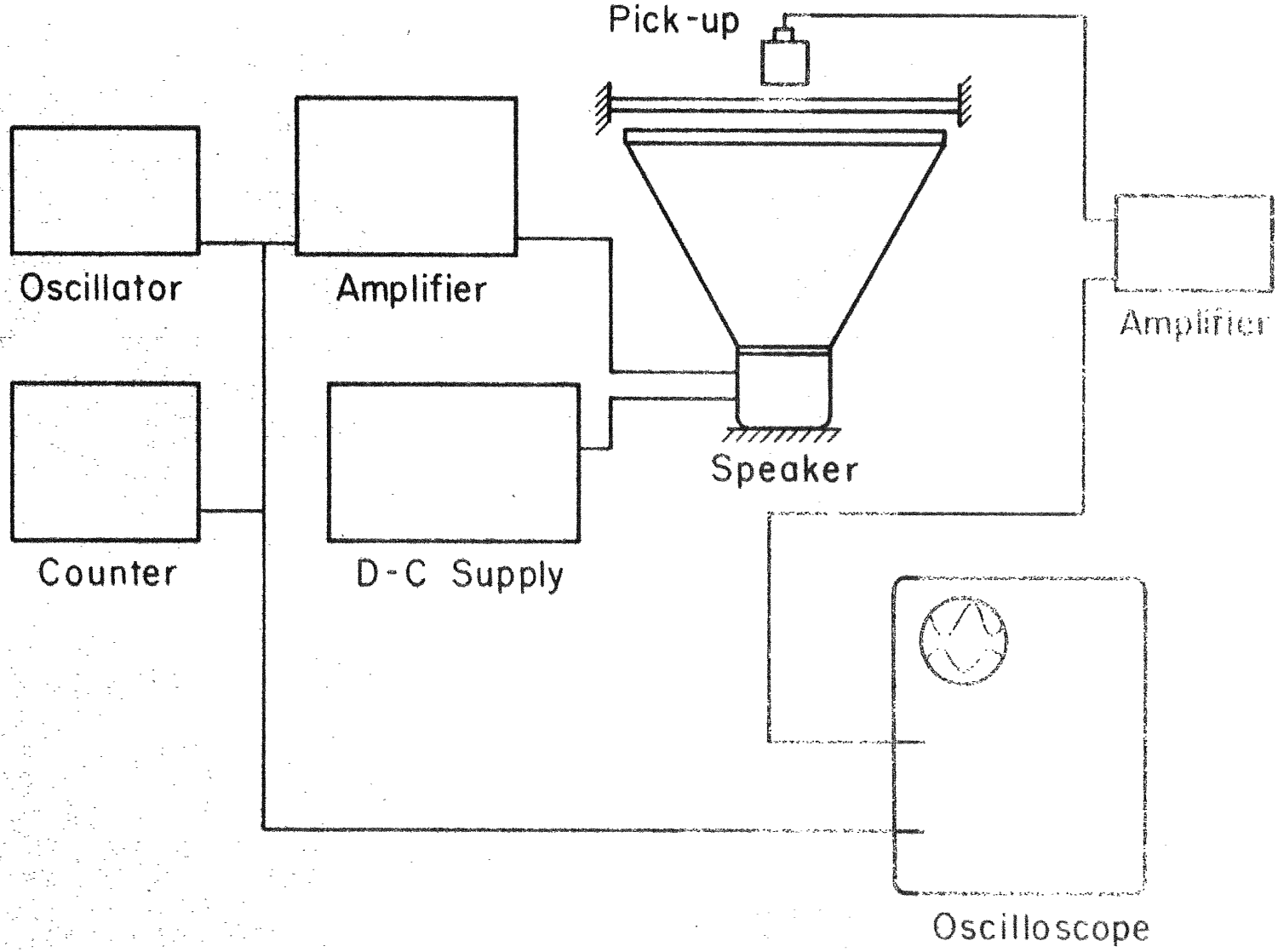

Fig.44 Schematic diagram of the vibration test set-up

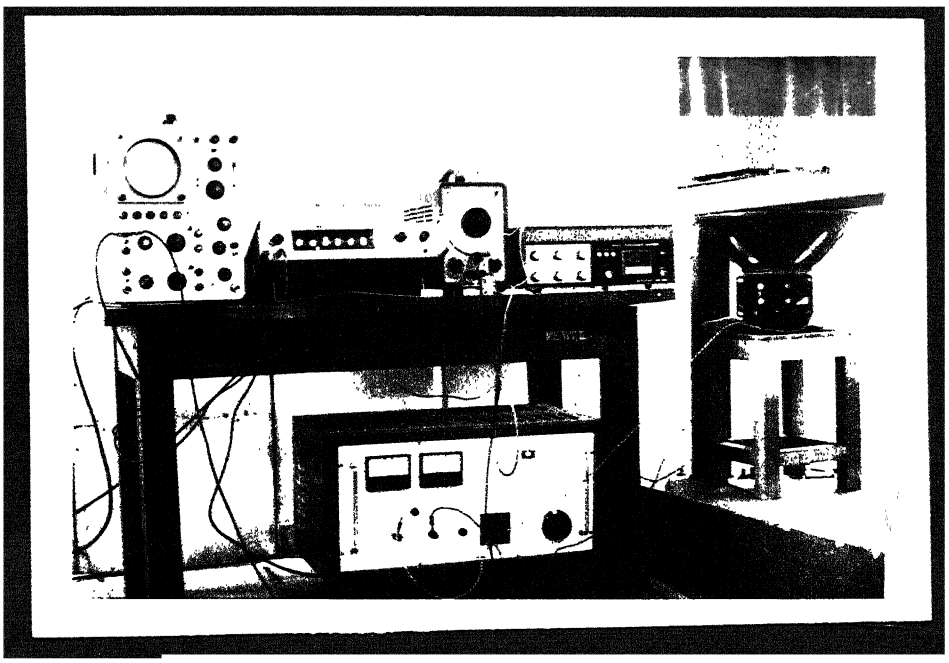

Fig. 4.5: The Test Set-up

granules on the surface of the plate, the input signal frequency was slowly increased until the motion of the aluminium oxide granules indicated a resonant condition. The frequency was then tuned to produce the most clearly defined nodal pattern. The frequency was measured on the electronic counter and the mode shape photographed. The upward frequency sweep was then continued until the next resonance was obtained, the frequency tuned in and measured and the mode shape photographed. This was continued to get higher frequencies and corresponding mode shapes.

Because of the loud speaker power limitation only the first three symmetric modes could be excited in the unidirectionally reinforced plates. However, these were considered sufficient for the verification of theoretical results.

4.4 Results and Discussion

Natural frequencies and mode shapes have been obtained for square, simply-supported and clamped-clamped unidirectional glass-epoxy plates with central circular holes for different fibre-orientation angles. A comparison between the experimental and theoretical frequencies for a simply-supported and clamped-clamped solid isotropic plate has been made to ensure that the required edge conditions have been approximated. For a comparison of experimental and theoretical frequencies the computations for unidirectionally reinforced E-glass-epoxy plates with holes were made taking the dynamic properties from Table 4.2. Results are plotted in a non-dimensional form. A comparison of experimental and theoretical mode shapes has also been made for unidirectionally reinforced glass-epoxy plates.

4.4.1 Simulation of Edge Conditions

Table 4.3 gives a comparison of the experimental and theoretical frequencies for a solid isotropic plate. The following properties have been used for the aluminium plate tested.

$E = 10.5 \times 10^6$ psi

$\rho g = 0.096$ lb/inch^3

$\nu = 0.3$

The agreement between the theoretical and experimental values is fairly good. The percentage variation in the frequency values for a simply-supported plate is maximum for the fundamental frequency but this variation is found to decrease for higher modes. In the case of clamped-clamped plates, the effect of clamping has been taken into account by considering the effective length as suggested by Laura [94]. They defined the effective length as,

$$a_{eff} = a + S/n' \qquad (4.4)$$

where a is the exposed length of the plate,

S is the clamped length, and

n' is a constant for a particular clamping.

A proper value of n' was chosen so that the theoretical frequencies compare well with the experimental values for a solid isotropic plate. The value of n', once fixed (2.34), was used for all the other experiments.

Table 4.3

A comparison of theoretical and experimental frequencies (Hz) for a solid isotropic plate .

Boundary Conditions	Simply-supported		Clamped-clamped	
Mode	Theory	Experiment	Theory	Experiment
1	117	126	249	240
2	291	308	508	509
3	465	482	749	-
4	582	589	911	-
5	756	772	915	920
6	988	-	1142	1150
7	1046	1071	1457	1419
8	1510	1476	1526	1580

It is worth mentioning here that the effect of clamping has not been considered by Ashton [31] and also by Monahan [86]. This is the reason that the theoretical frequencies obtained by them are higher than those obtained experimentally: the theoretical fundamental frequency obtained by Ashton [31] for a clamped-clamped boron-epoxy plate (0-90°) is approximately thirty percent higher than the experimental value and the error in the fundamental frequency for a rectangular isotropic clamped-clamped plate obtained by Monahan [86] is fourteen percent.

4.4.2 The Effect of Discontinuity on the Natural Frequency

The effect of cut-outs and holes on the natural frequencies of plates has been discussed at length in Chapters 2 and 3. However, all the results have been shown for fibre-orientation angles 0° and 45° only. In this section, the variation of frequency with d/a ratio is shown for fibre-orientation angles 0°, 15°, 30° and 45° for unidirectionally reinforced glass-epoxy plates. The theoretical results are compared with experimental results and are also compared with those for a plate having central square cut-outs.

A) Simply-Supported Plates

The variation of frequency with hole parameters d/a for unidirectional E-glass-epoxy plates is shown in Figures 4.6 to 4.9 for fibre-orientation angles 0°, 15°, 30° and 45°; the solid lines show the variation of the frequency with hole parameter whereas the dotted lines show that with the cut-out parameter. The results have been shown for cut-out ratio upto 0.8 whereas for plates with holes the frequency values could not be obtained

for some modes beyond d/a = 0.4 due to computational difficulties such as nonconvergence of the frequency values (and hence excess computation time involved) and large round-off errors because of the numerical integration scheme used.

The fundamental frequency is found to decrease initially with d/a ratios for fibre-orientations 0° and 15°. But as the fibre-orientation angle is increased further, the rate of decrease of $\bar{\omega}_{11}$ becomes less as shown in Figures 4.8 and 4.9 for fibre-orientations 30° and 45°. The behaviour of frequencies $\bar{\omega}_{12}$ and $\bar{\omega}_{21}$ is similar for all fibre-orientation angles. Small holes do not seem to influence these modes. However, with the increase in hole size, there is an abrupt decrease in the frequency values for these modes and they again increase as the hole size is increased. The frequencies $\bar{\omega}_{22}$ and $\bar{\omega}_{23}$ are found to decrease continuously with increase in hole size but these also increase at larger d/a ratios. For small hole sizes, the frequency $\bar{\omega}_{31}$ is constant but then increases continuously as the hole size is increased for all fibre-orientations. There is a tendency for the modes corresponding to $\bar{\omega}_{13}$ and $\bar{\omega}_{22}$ to interchange with each other for all fibre-orientation angles whereas those corresponding to $\bar{\omega}_{23}$ and $\bar{\omega}_{31}$ interchange only in case of $\theta = 30°$ and $\theta = 45°$. As the fibre-orientation angle is increased the frequency curves for $\bar{\omega}_{12}$ and $\bar{\omega}_{21}$, $\bar{\omega}_{23}$ and $\bar{\omega}_{32}$ come closer and coincide for $\theta = 45°$.

The experimental results corresponding to the first three symmetric modes ($\bar{\omega}_{11}$, $\bar{\omega}_{13}$ and $\bar{\omega}_{31}$) are compared with theoretical results for fibre-orientations 0°, 15° and 30° and those corresponding to the first and

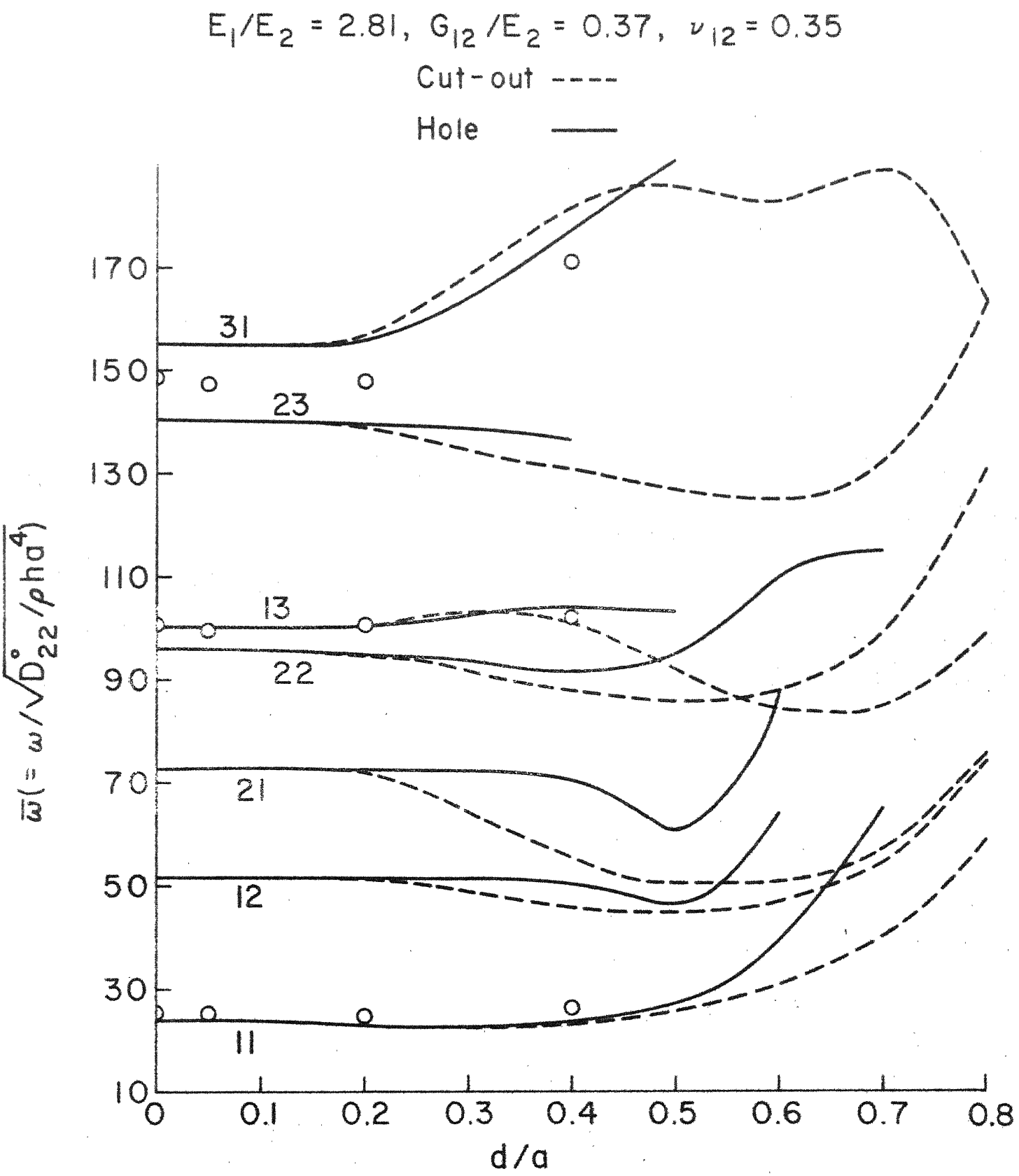

Fig.4.6 $\bar{\omega}$ vs d/a for a simply-supported plate; $\theta = 0^\circ$, R = 1.0

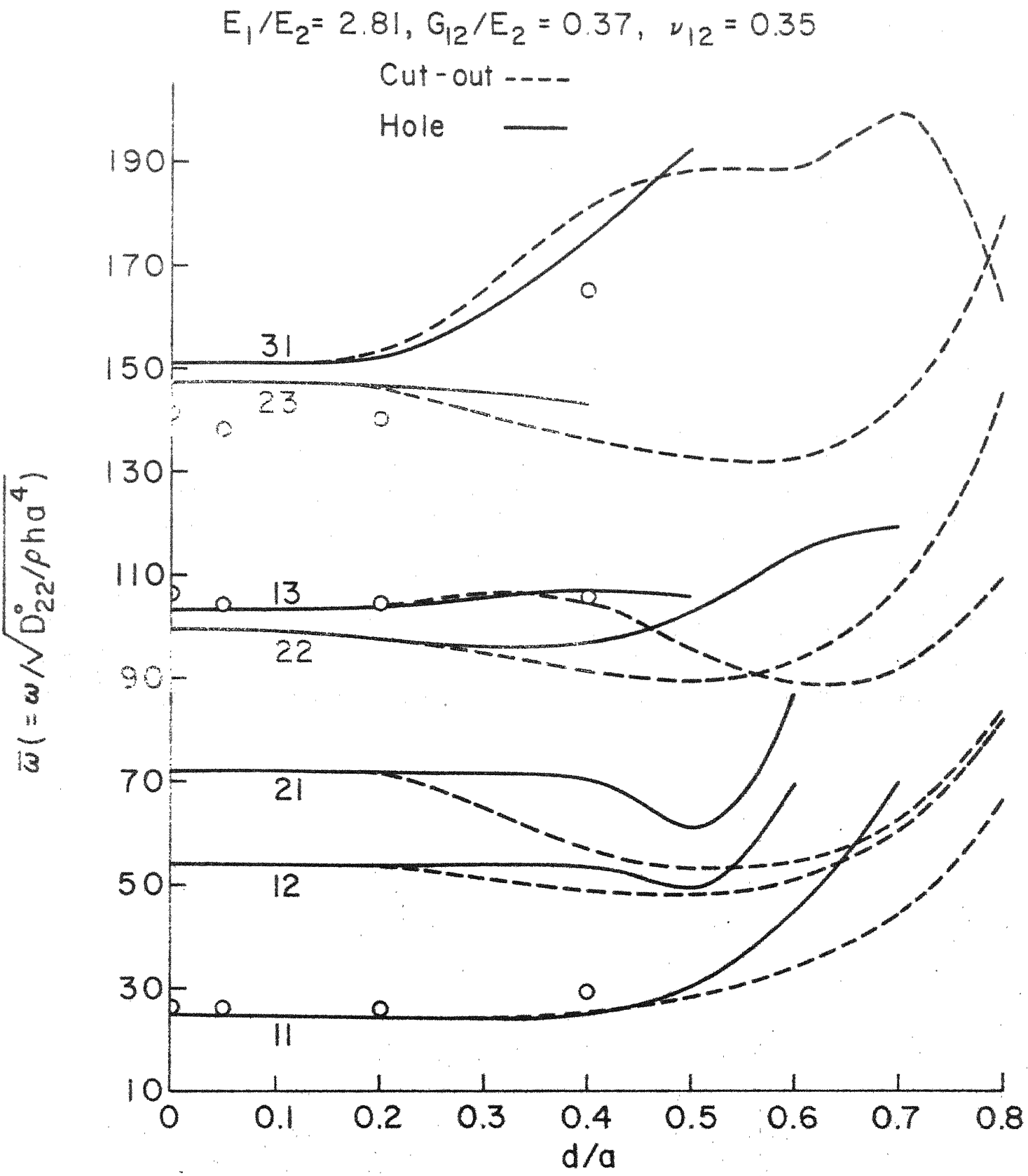

Fig.4.7 $\bar{\omega}$ vs d/a for a simply-supported plate; $\theta = 15°$, R = 1.0

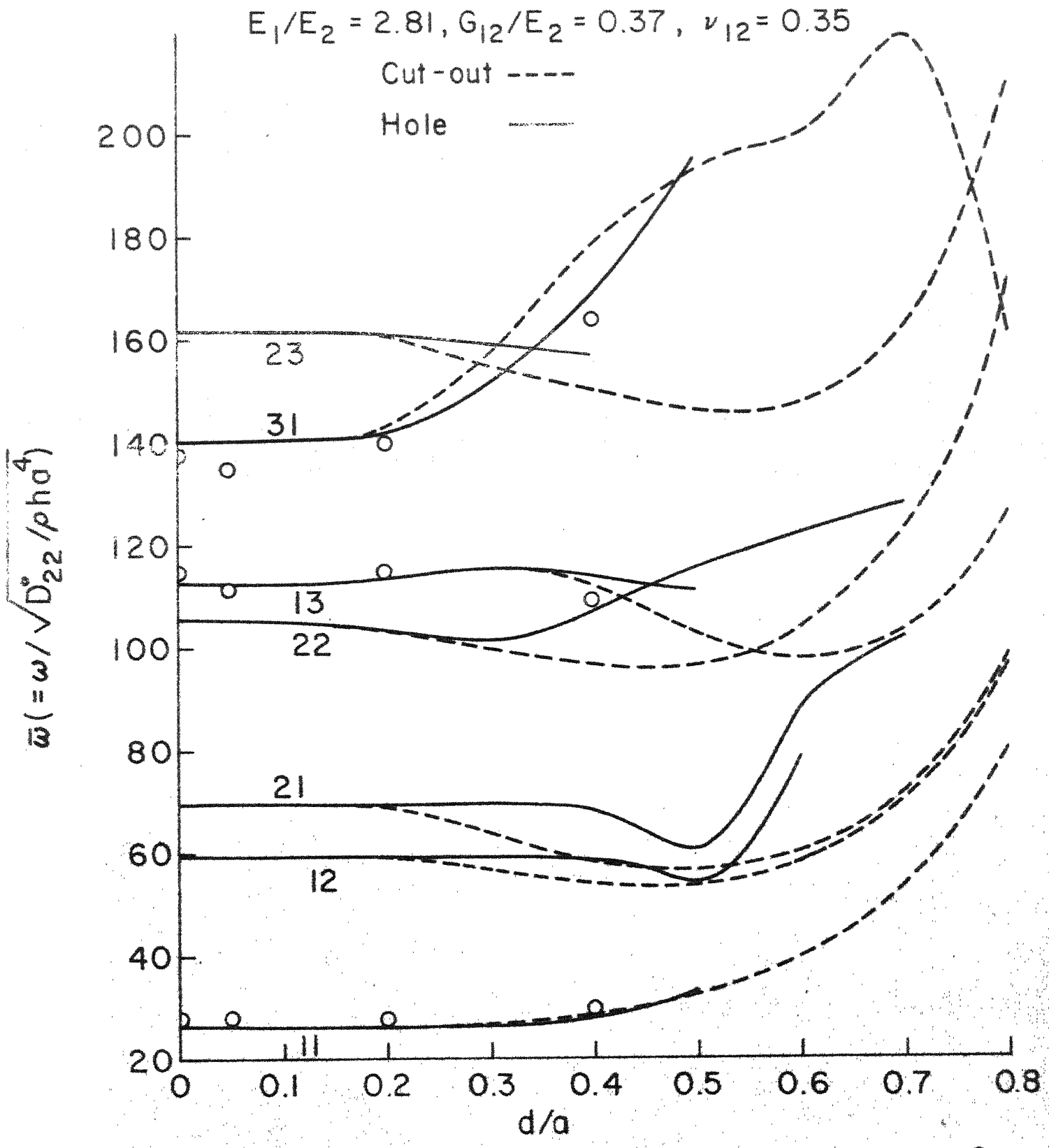

Fig.4.8 $\bar{\omega}$ vs d/a for a simply-supported plate; $\theta = 30^\circ$, R = 1.0

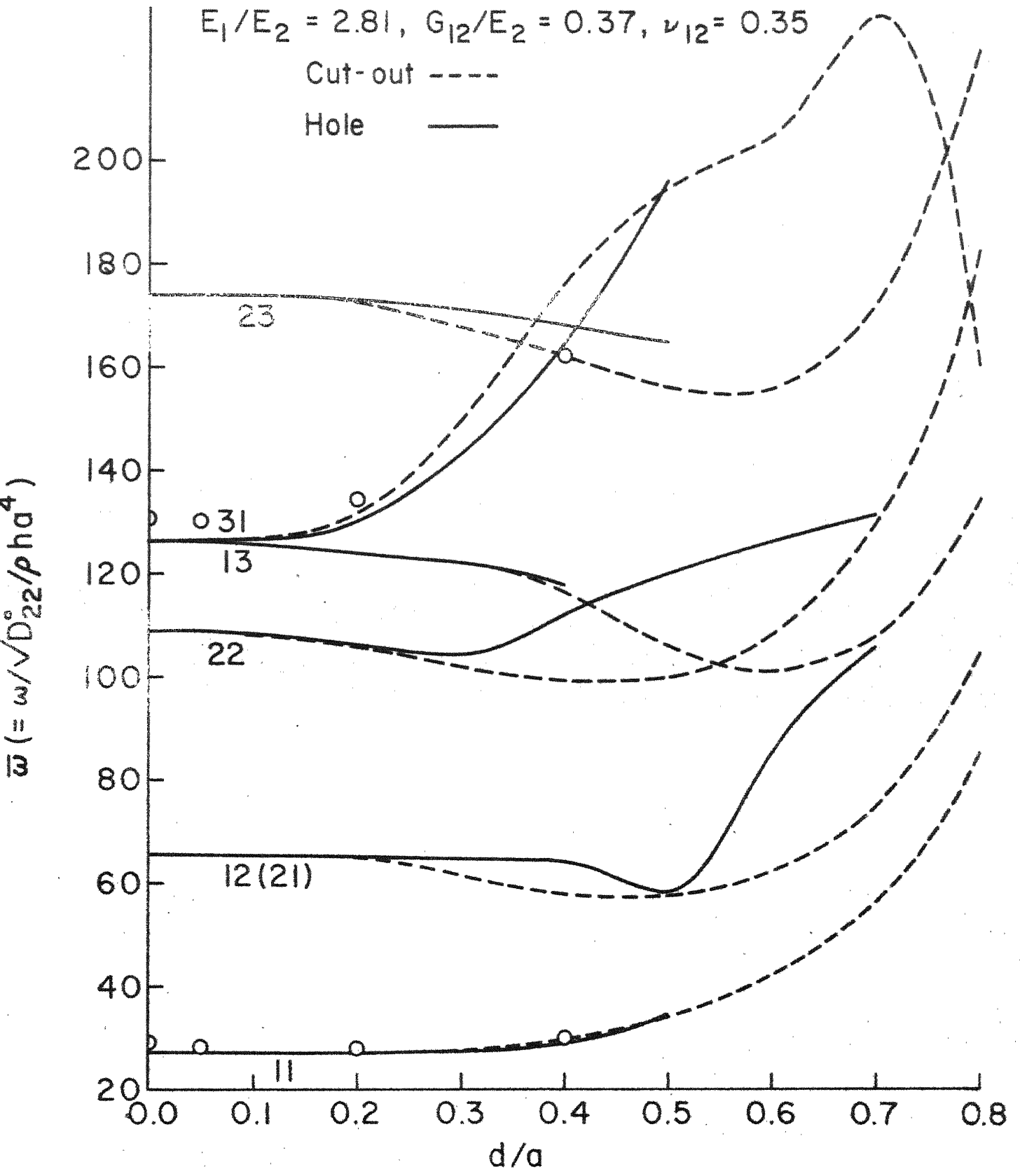

Fig.4.9 $\bar{\omega}$ vs d/a for a simply-supported plate; $\theta = 45^{\circ}$, R = 1.0

third symmetric modes for $\theta = 45°$. The agreement between the theoretical and experimental frequency values is good. Any descrepancy between the results can be attributed to the fact that it is extremely difficult to achieve perfect simple-support edge conditions experimentally. Also, there is a variation in the thickness of the plates (of the order of $\pm$ 3 percent) which may give rise to a slight change in the modulus of the plates.

A comparison of theoretical results between cut-outs and holes has also been shown in Figures 4.6 to 4.9. In general, it is seen that the variation of different frequencies for a hole and a cut-out are similar. At smaller, d/a ratios (upto 0.15 - 0.2), the frequency values for a given mode in case of a cut-out as well as for a hole are practically same. This suggests that for small d/a ratios, one can get the necessary information by computing frequencies for plates with cut-outs, the analysis for which is much simpler.

B) Clamped-Clamped Plates

The variation of frequency with d/a for unidirectional E-glass-epoxy plates is shown in Figures 4.10 to 4.13 for fibre-orientations 0°, 15°, 30° and 45°. The theoretical results are compared with those for a plate with central square cut-outs and also with experimental results. It is seen that for all fibre-orientations $\bar{\omega}_{11}$ increases with increase in d/a ratios. This is not true for frequencies $\bar{\omega}_{12}$, $\bar{\omega}_{21}$ and $\bar{\omega}_{23}$. These are constant for smaller values of d/a and decrease as d/a is increased. However, further increase in the hole size increases the frequencies. The frequency $\bar{\omega}_{22}$ behaves in a different manner; it decreases with increase in the hole size

but is found to increase with larger d/a ratios. For smaller values of d/a there is no appreciable change in $\bar{\omega}_{31}$ but it increases as the hole size is increased. For $\theta = 0°$ and $\theta = 15°$, modes corresponding to $\bar{\omega}_{22}$ and $\bar{\omega}_{13}$ are found to interchange but these do not interchange for $\theta = 30°$ and $\theta = 45°$. Modes corresponding to $\bar{\omega}_{31}$ and $\bar{\omega}_{23}$ interchange only for $\theta = 30°$ and $\theta = 45°$. It is interesting to note that frequency curves for $\bar{\omega}_{12}$ and $\bar{\omega}_{21}$ come closer and those for $\bar{\omega}_{13}$ and $\bar{\omega}_{22}$ separate from each other as the fibre-orientation angle is increased.

Experimental results for the first three symmetric modes are compared with theoretical results and the agreement is found to be good; here also, as in simply-supported plates, experimental results could be obtained only for the first and third symmetric mode when $\theta = 45°$. A good agreement between the experimental and theoretical results stress the need for considering the effect of clamping which is quite often ignored.

In Figures 4.10 to 4.13, a comparison of theoretical results between cut-outs and holes is shown. Due to computational difficulties, frequency values for some of the modes could not be obtained beyond d/a equal to 0.4 whereas results have been obtained for c/a ratios upto 0.7. It is seen from Figures 4.10 - 4.13 that the variation of different frequencies for a hole and for a cut-out are similar. At smaller d/a ratios, the frequency values for a cut-out as well as for a hole are practically same.

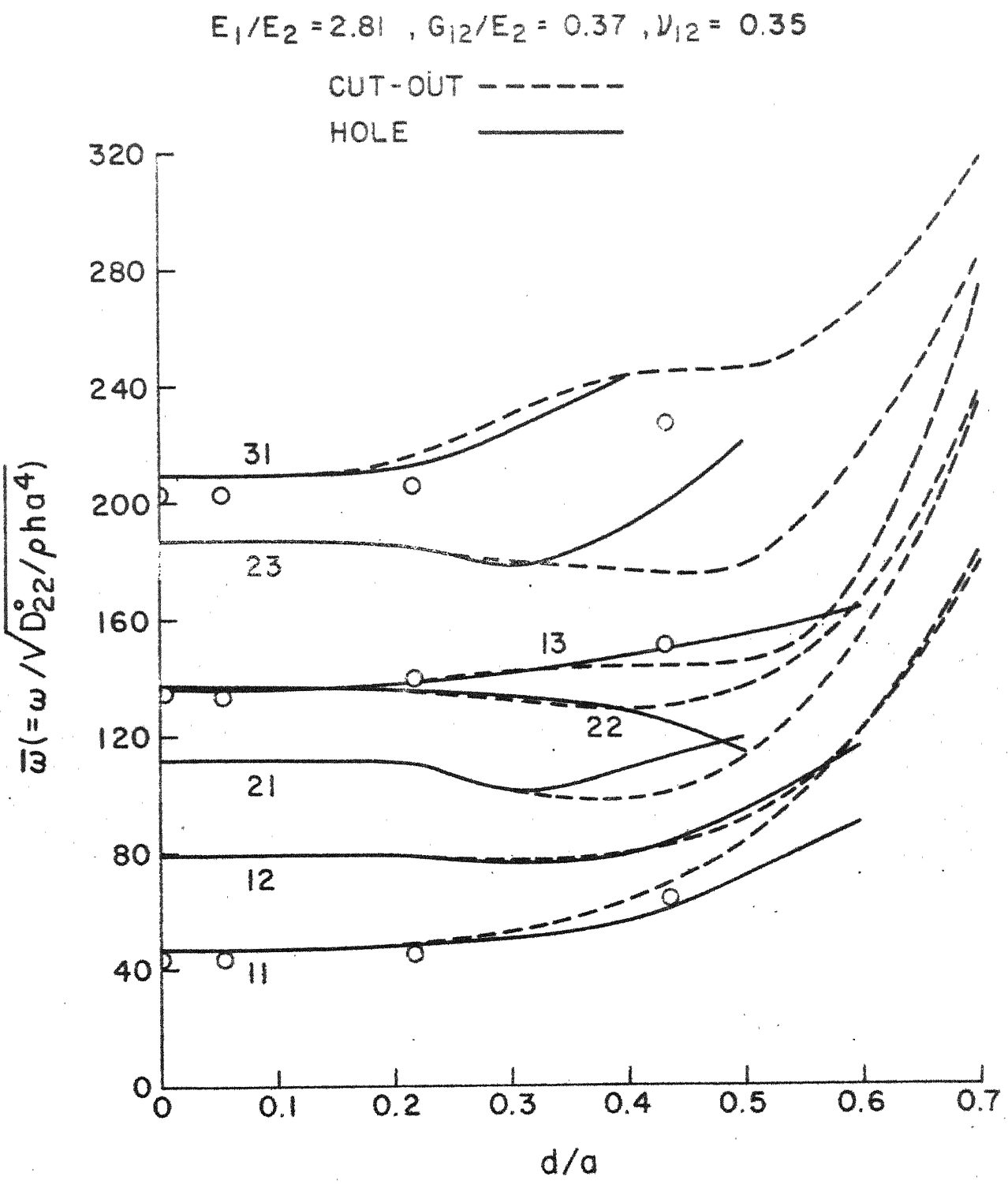

Fig.4.10 $\bar{\omega}$ vs d/a for a clamped-clamped plate; $\theta = 0^\circ$, R = 1.0

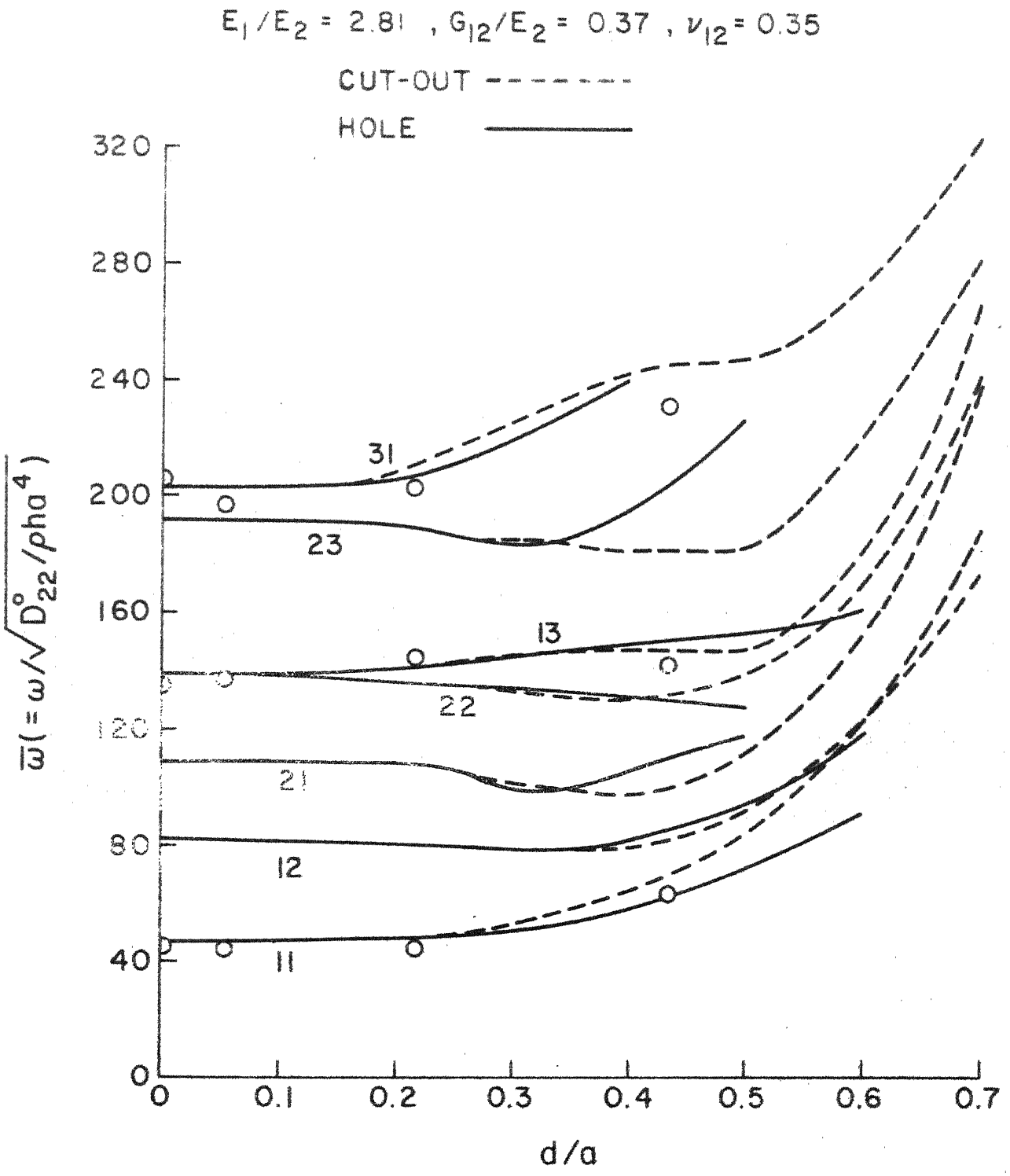

Fig.4.11 $\bar{\omega}$ vs d/a for a clamped-clamped plate; $\Theta = 15^\circ$, R = 1.0

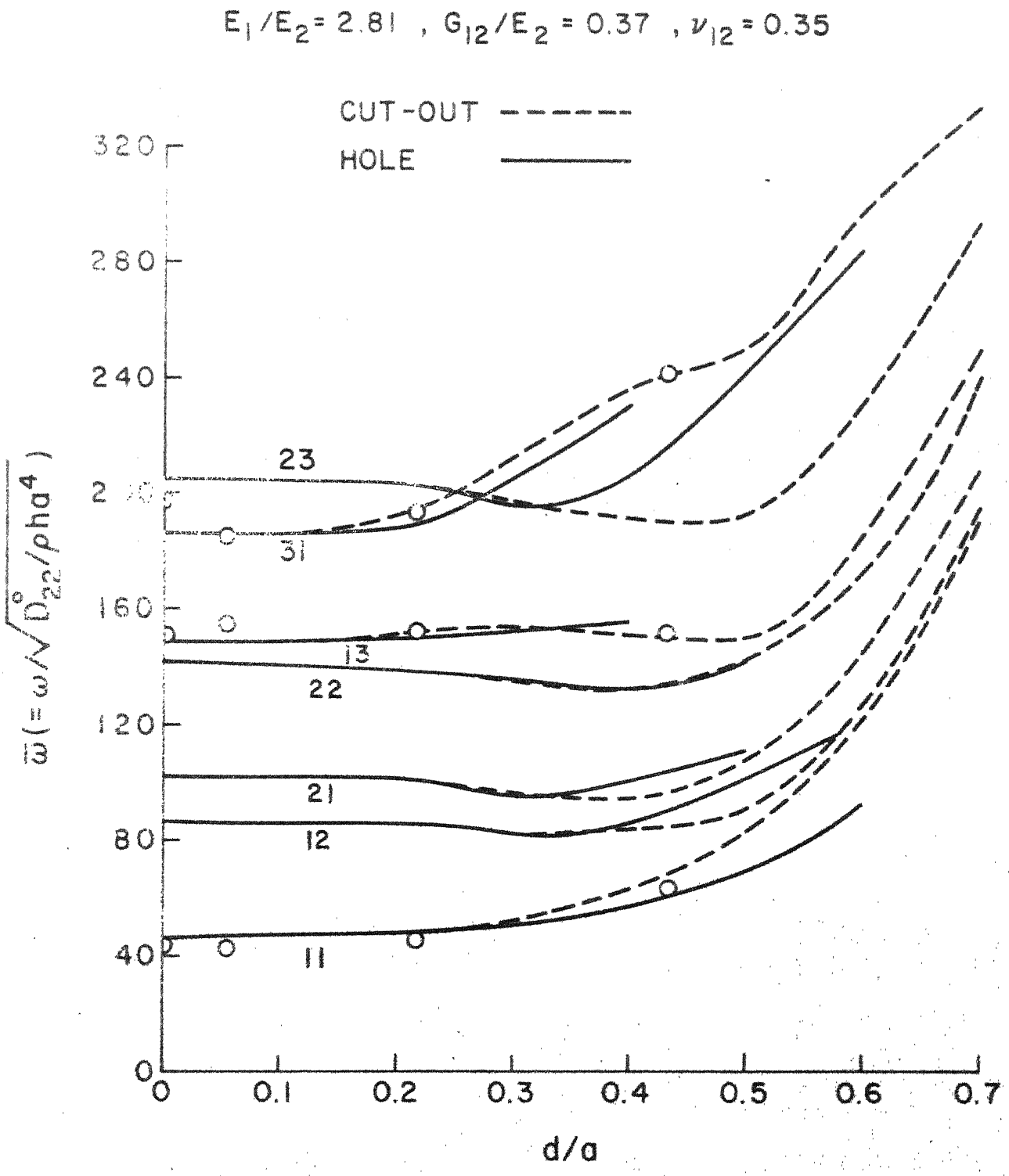

Fig.4.12 $\bar{\omega}$ vs d/a for a clamped-clamped plate; $\theta = 30^\circ$, R = 1.0

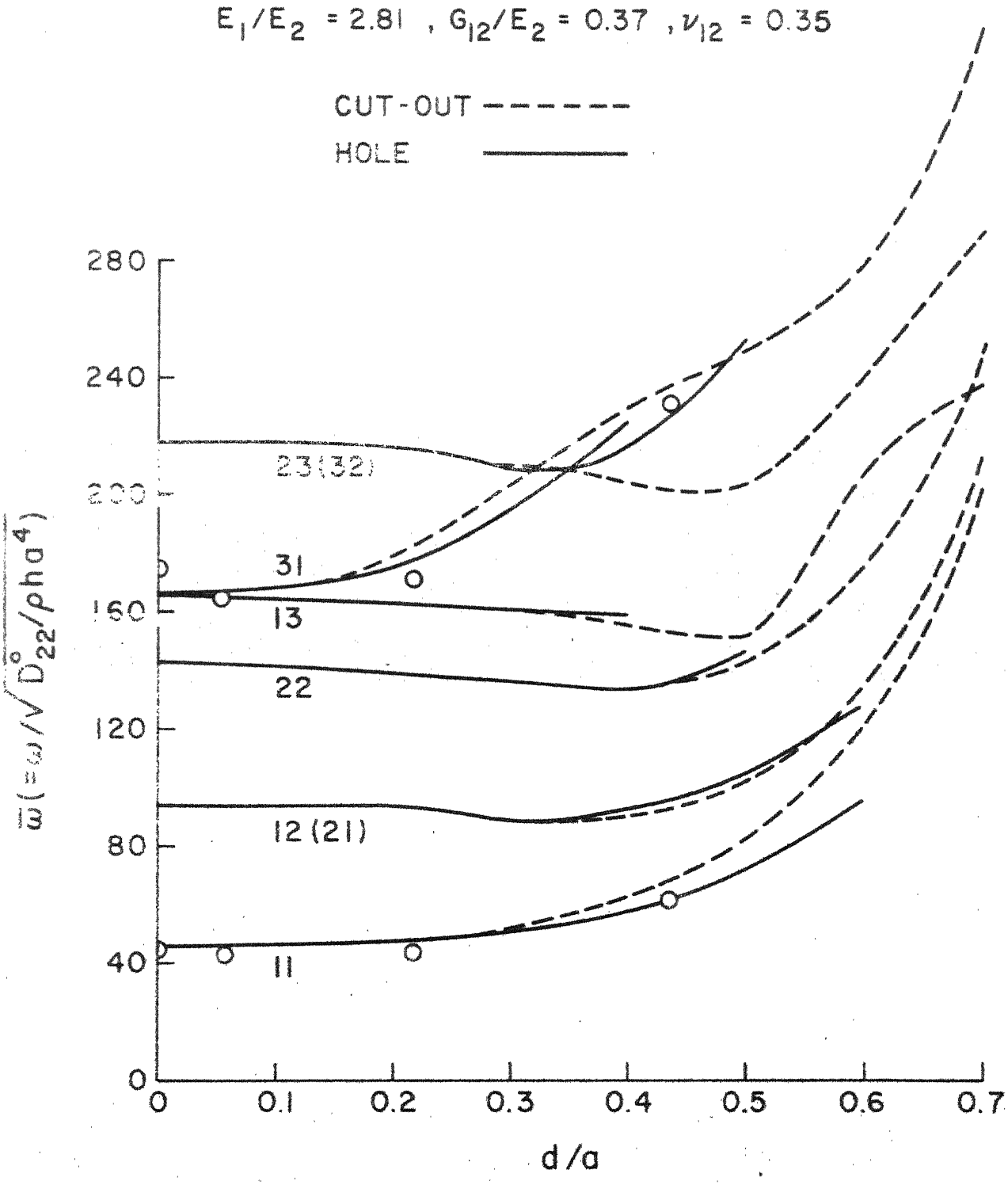

Fig.4.13 $\bar{\omega}$ vs d/a for a clamped-clamped plate; $\theta = 45^\circ$, R = 1.0

4.4.3 Mode Shapes

It becomes easier to obtain the mode shape for a particular frequency once the corresponding eigenvectors are known. The theoretical mode shapes have been obtained for both isotropic and unidirectionally reinforced glass-epoxy plates. Only the mode shapes for the composite plates are shown and these are compared with experimental mode shapes. In obtaining the mode shapes for clamped-clamped edge conditions, the computations have been carried out in double-precision arithmetic to avoid large round-off errors in function evaluation by making use of the values of coefficients given in Table 2.1. The effect of the following parameters has been considered on the mode shapes of a unidirectionally reinforced glass-epoxy plate for simple-support and clamped-clamped edge conditions.

a. Fibre-orientation angle,

b. Presence of hole,

c. Shape of the discontinuity,

d. Size of the hole.

a. Fibre-Orientation Angle

The theoretical mode shapes have been obtained for all fibre-orientation angles when d/a = 0.0 and d/a = 0.2. However, they are shown only for 0° (Figures 4.14 and 4.16) and 45° (Figures 4.15 and 4.17) fibre-orientations. This is due to the fact that the mode shapes for fibre-orientation angles 15° and 30° are similar to those for fibre-orientation angle 0°. The mode shapes shown in Figures 4.15 and 4.17 for

plates with fibre-orientation angle 45° having simple-support and clamped edges respectively are similar to those found for corresponding isotropic plates. This has also been seen [34] for a simply-supported unidirectional boron-epoxy plate having fibre-orientation angle 45° where the authors obtained mode shapes which are in fact a linear combination of modes and are similar to these obtained in the case of an isotropic plate. A good treatment for the mode shapes resulting from a linear combination of modes has been given by Hikami [30]. The experimental mode shapes (shown for all fibre-orientation angles) are given only for plates with holes in Figures 4.18 and 4.19. A comparison of theoretical and experimental mode shapes for fibre-orientation angles 0° and 45° for a plate with a hole show good agreement. The distortion in experimental mode shapes are due to 1) the edge conditions being approximate and 2) the variation in the thickness of plates (the variation was of the order of ± 3 percent).

b. Presence of Hole

The change in the mode shapes resulting from the presence of holes in plates is shown in Figures 4.14 to 4.19 for both simple-support and clamped-clamped edge conditions. It is observed that the symmetric modes get distorted due to the presence of hole in all the cases. This is due to the symmetric location of the hole with respect to the plate geometry. Asymmetric location of the hole may effect the mode shapes for antisymmetric modes. The experimental mode shapes for plates with holes are shown in Figures 4.18 and 4.19 and they compare well with theoretical results.

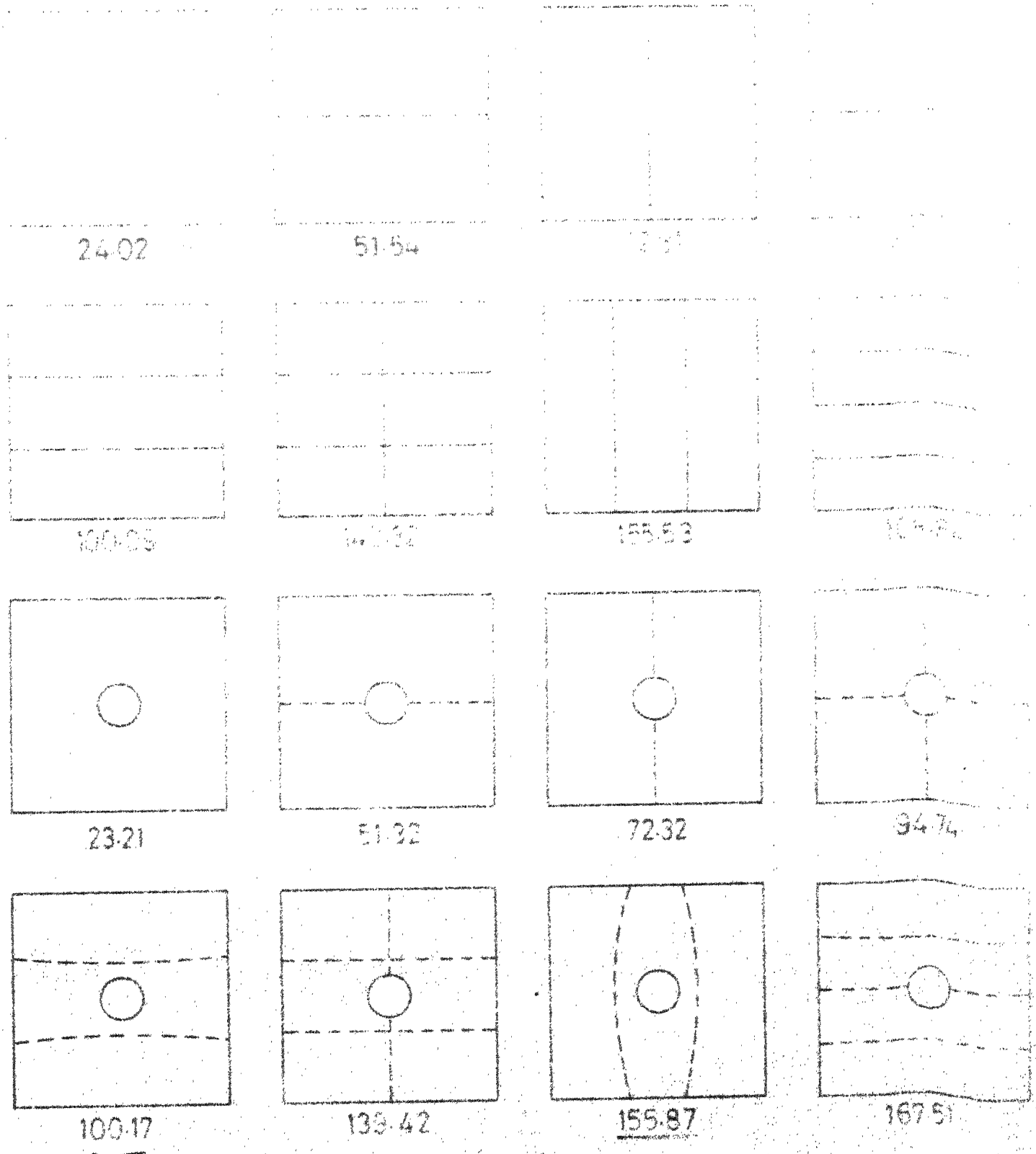

Fig.4.14 Frequencies and mode shapes for a simply-supported plate; $\theta = 0°$, $R = 1.0$; $E_1/E_2 = 2.81$, $G_{12}/E_2 = 0.37$, $\nu_{12} = 0.35$

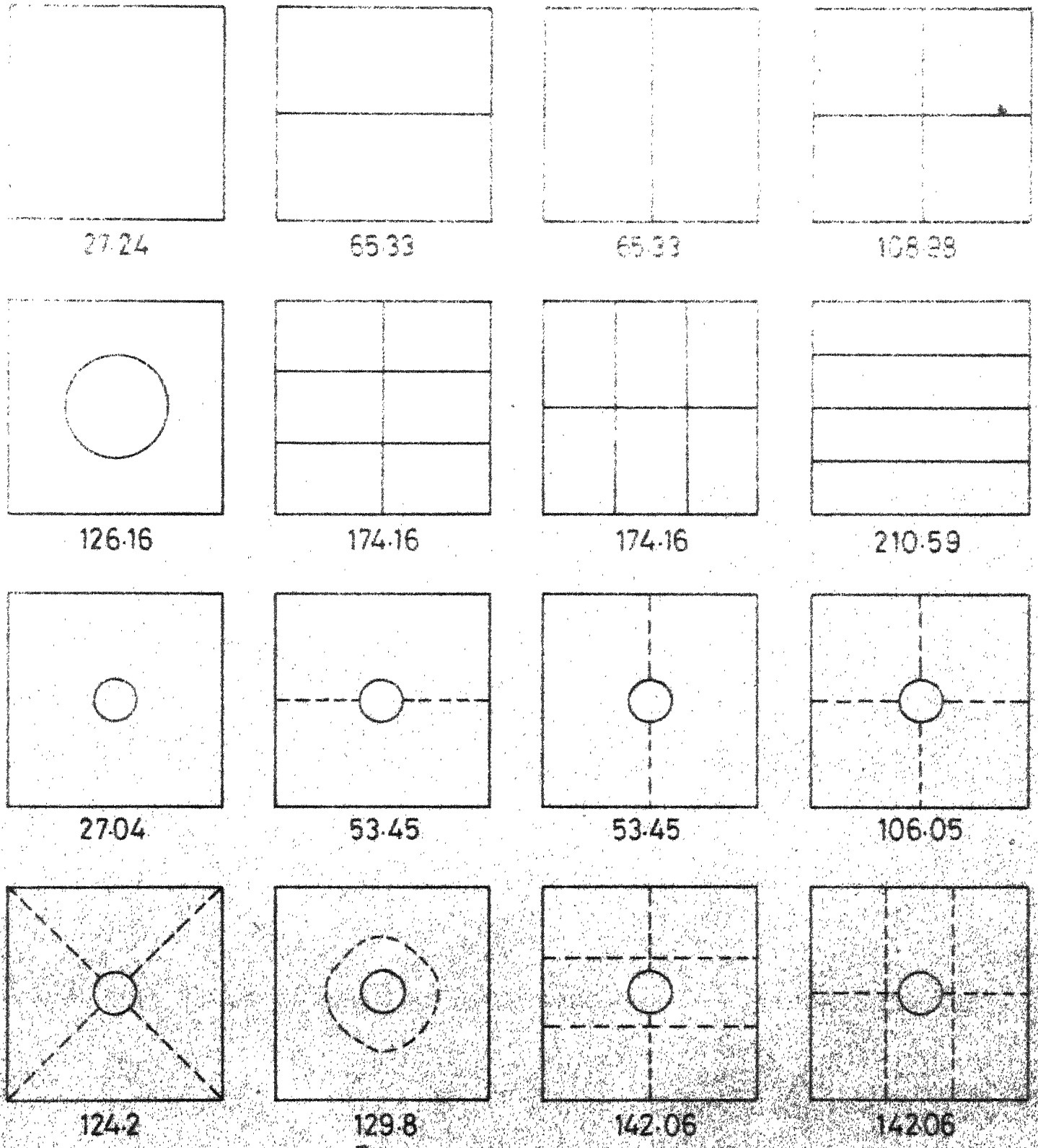

Fig.4.15 Frequencies and mode shapes for a simply-supported plate, $\theta = 45°$; $R = 1.0$; $E_1/E_2 = 2.81$, $G_{12}/E_2 = 0.37$, $\nu_{12} = 0.35$.

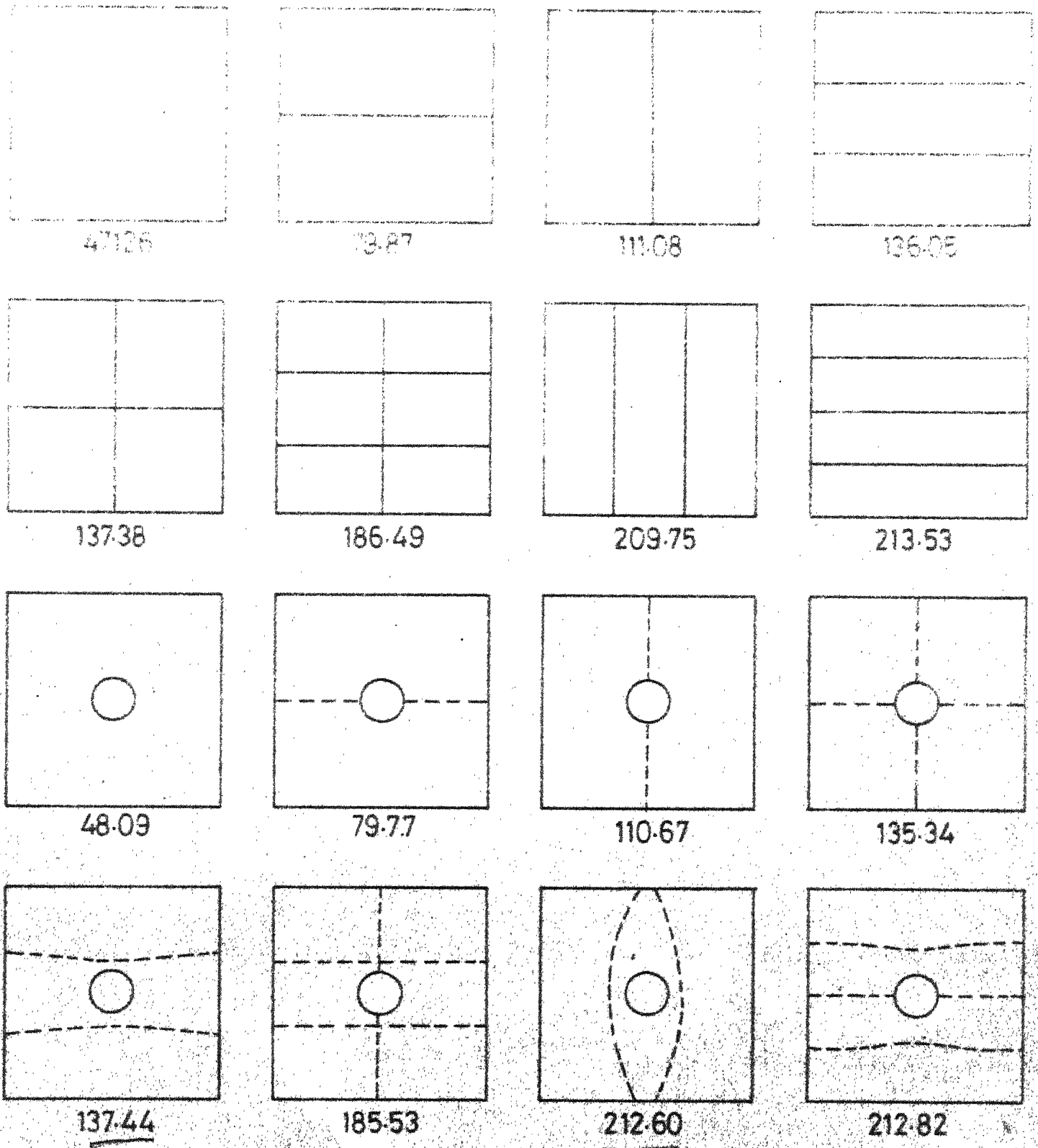

Fig.4.16 Frequencies and mode shapes for a clamped-clamped plate; $\theta = 0°$, $R = 1.0$; $E_1/E_2 = 2.81$, $G_{12}/E_2 = 0.37$, $\nu_{12} = 0.35$.

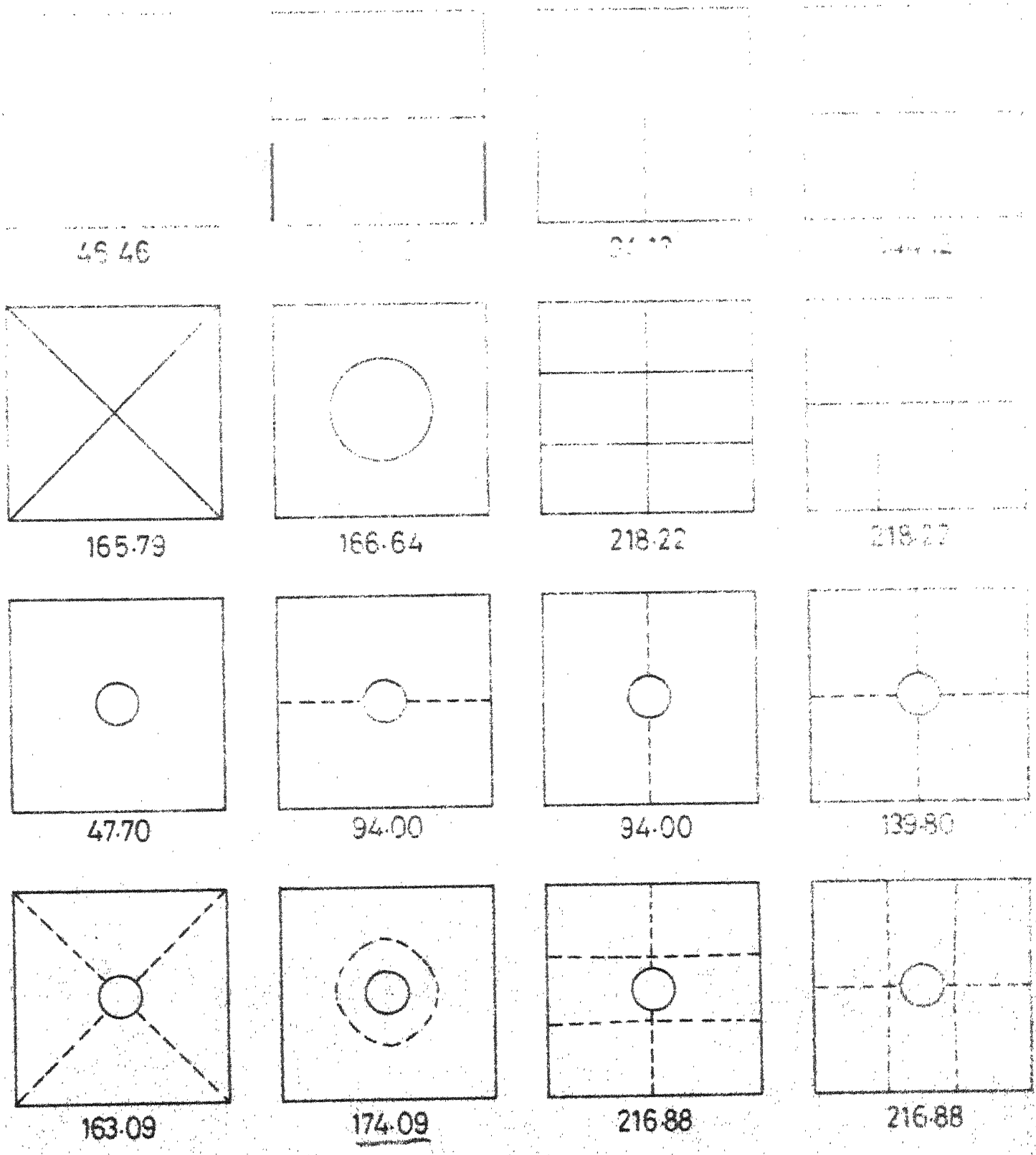

Fig.4.17 Frequencies and mode shapes for a clamped-clamped plate; $\theta = 45°$, $R = 1.0$; $E_1/E_2 = 2.81$, $G_{12}/E_2 = 0.37$, $\nu_{12} = 0.35$.

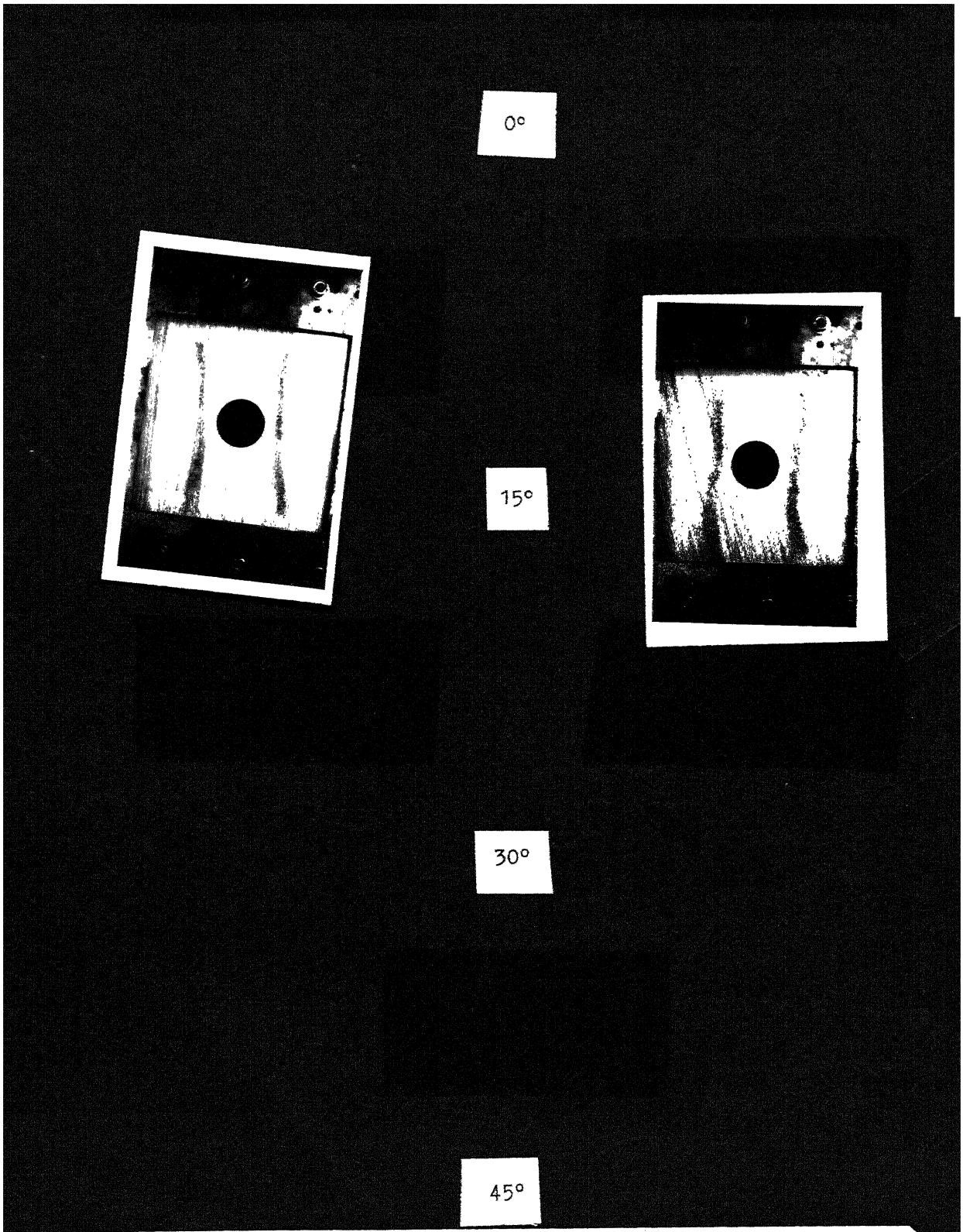

Fig. 4.18: Experimental Mode Shapes for a Simply-Supported Plate; $E_1/E_2 = 2.81$, $G_{12}/E_2 = 0.37$, $\nu_{12} = 0.35$, $R = 1.0$

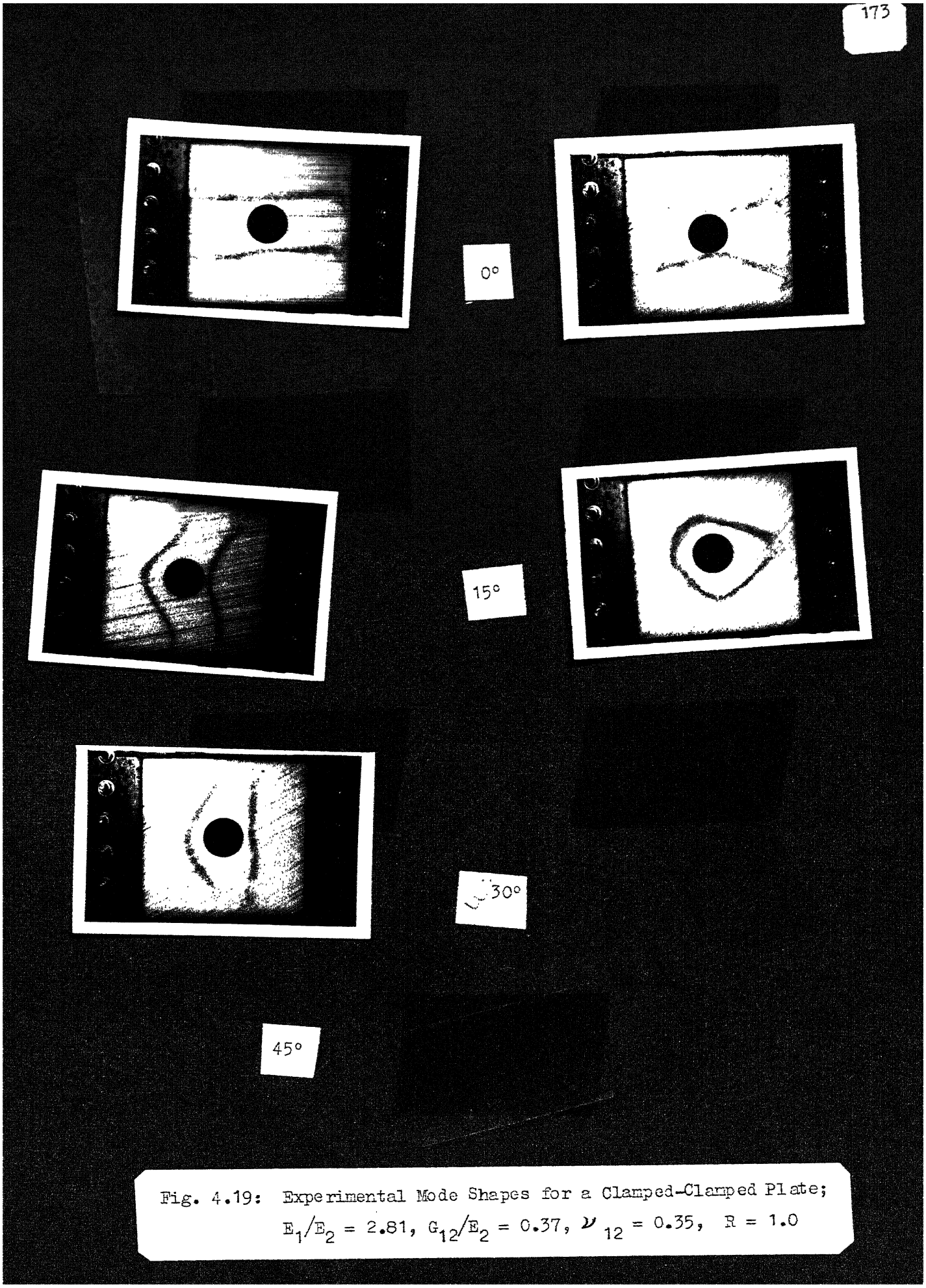

Fig. 4.19: Experimental Mode Shapes for a Clamped-Clamped Plate; $E_1/E_2 = 2.81$, $G_{12}/E_2 = 0.37$, $\nu_{12} = 0.35$, $R = 1.0$

For a simply-supported plate with fibre-orientation angle equal to 45°, the presence of hole gives rise to a new mode; this has been discussed earlier in Chapter 2. The interchange of fourth and fifth modes for a clamped-clamped plate can be seen in Figure 4.16 for fibre-orientation angle 0°.

c. Shape of the Discontinuity

A comparison of frequencies and mode shapes between a cut-out ($c/a = 0.2$) and a hole ($d/a = 0.2$) for simply-supported and clamped-clamped plates are shown respectively in Figures 4.20 and 4.21 for fibre-orientation angle 0°. The mode shapes are found to be similar. This is true for other fibre-orientation angles also.

d. Size of the Hole

It was found that the presence of holes distorted symmetric mode shapes which show the coupling of different modes. For this reason, a comparison of frequency values and normalized eigenvectors for a square, simply-supported and clamped-clamped unidirectional plate is made for different d/a ratios for a particular mode. Table 4.4 gives this comparison for fibre-orientation angle 0° and mode $\bar{\omega}_{13}$. It is observed that as the hole size is increased, the contribution of other modes becomes more.

Finally, the effect of modulus ratio on the frequency values and normalized eigenvectors for a square, simply-supported and clamped-clamped plate is shown in a tabular form (Table 4.5). The relative values of

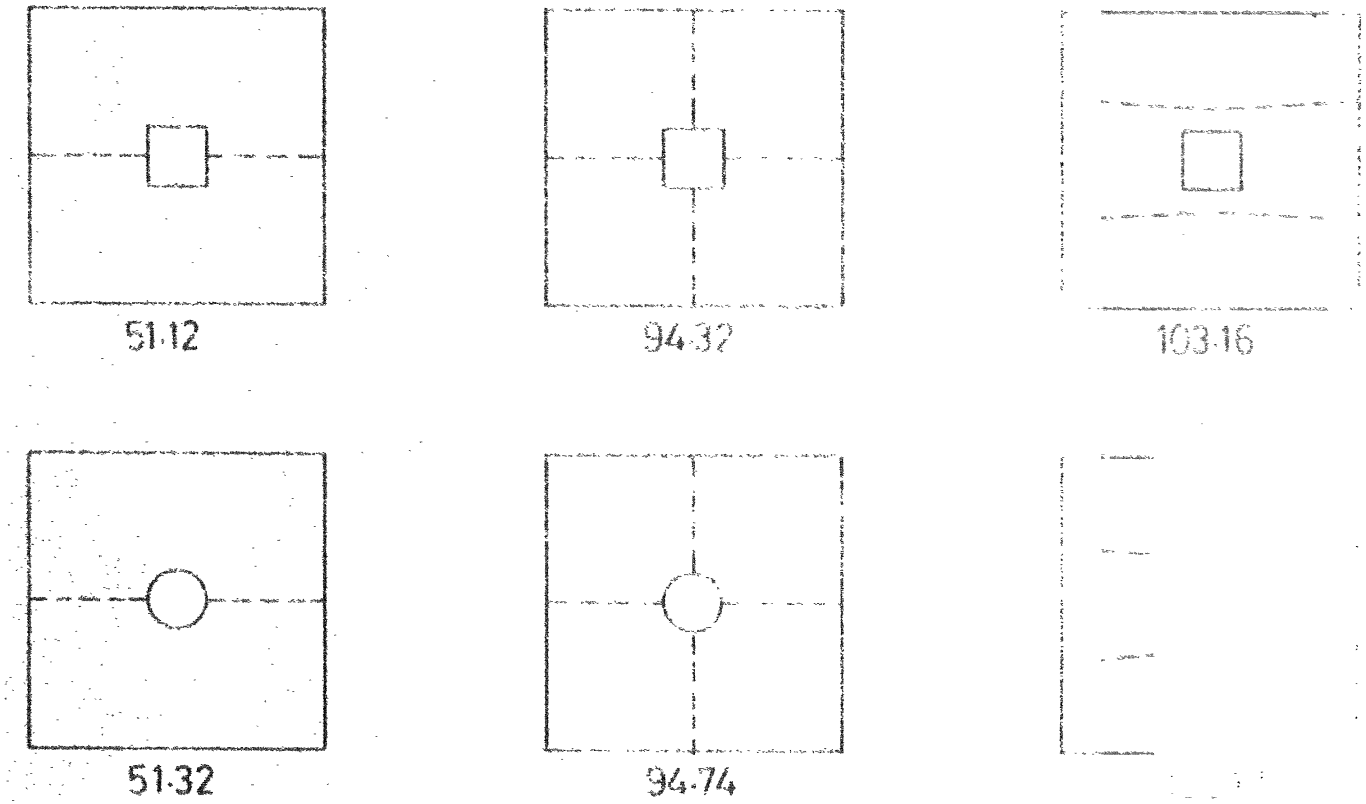

Fig.4.20 A comparison of mode shapes for a simply-supported plate; $\theta = 0°$, $R = 1{\cdot}0$; $E_1/E_2 = 2{\cdot}81$, $G_{12}/E_2 = 0{\cdot}37$, $\nu_{12} = 0{\cdot}35$.

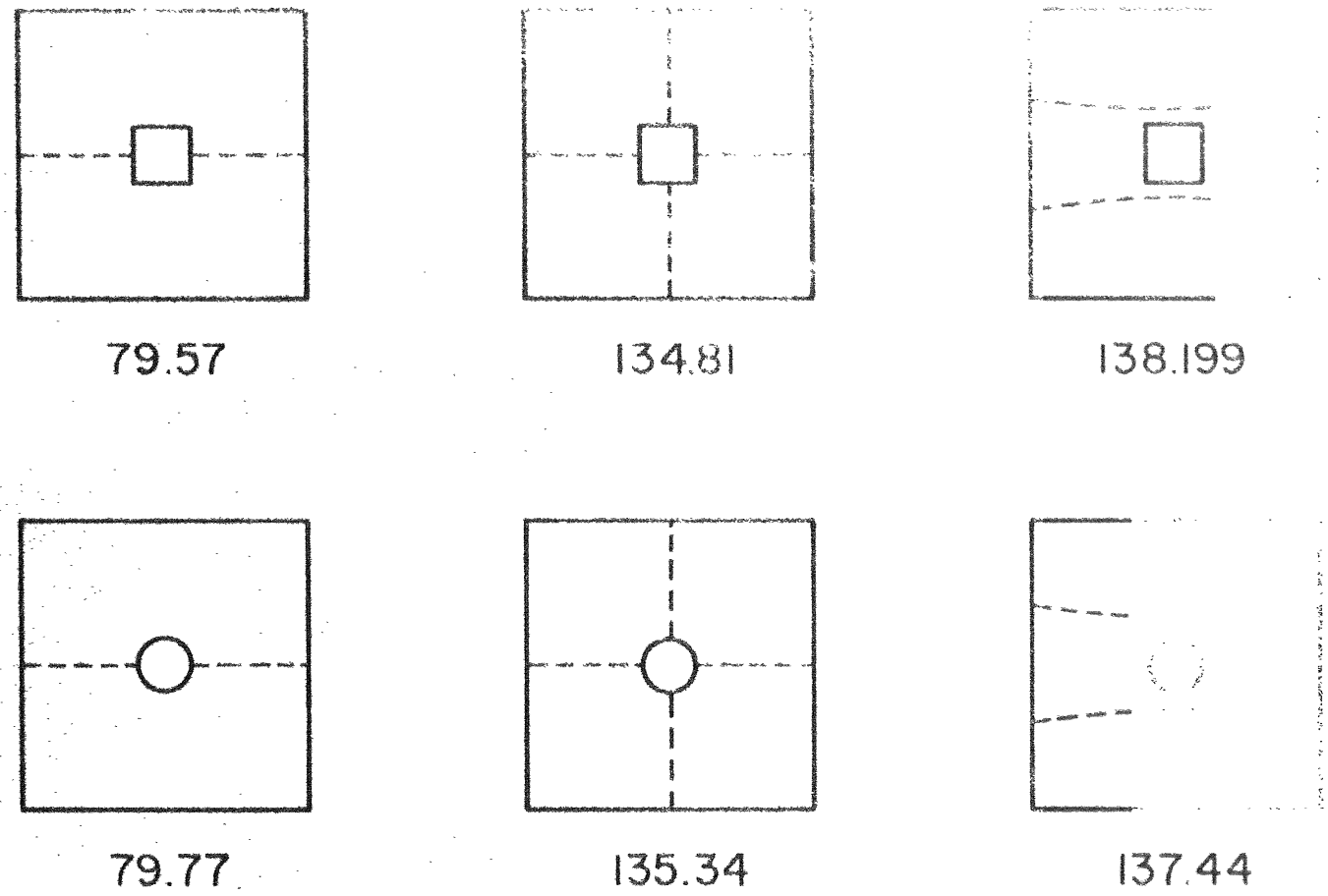

Fig.4.21 A comparison of mode shapes for a clamped-clamped plate; $\theta = 0^{\circ}$, $R = 1.0$; $E_1/E_2 = 2.81$, $G_{12}/E_2 = 0.37$ $\nu_{12} = 0.35$

Table 4.4

Comparison of normalized eigenvectors for a unidirectionally reinforced glass-epoxy plate with different hole sizes; $\theta = 0°$, $\bar{\omega}_{13}$.

A_{ij}	Boundary Conditions					
	Simply-supported			Clamped-clamped		
	d/a = 0.0	d/a = 0.2	d/a = 0.5	d/a = 0.0	d/a = 0.2	d/a = 0.5
A_{11}	0.0	-0.1222	-0.4976	-0.0151	-0.1749	-1.1198
A_{13}	1.0	1.0728	1.1274	0.9992	1.0568	1.3910
A_{15}	0.0	-0.0318	-0.0599	0.0076	-0.0220	-0.1898
A_{17}	0.0	0.0150	-0.0621	0.0019	0.0175	0.0375
A_{31}	0.0	-0.0114	-0.4327	-0.0055	-0.0395	-0.4028
A_{33}	0.0	-0.0222	0.0640	0.0354	0.0230	0.0032
A_{35}	0.0	0.0196	-0.0038	-0.0019	0.0126	0.0827
A_{37}	0.0	-0.0110	-0.0420	-0.0007	-0.0103	-0.0392
A_{51}	0.0	-0.0083	-0.0527	-0.0006	-0.0062	0.0686
A_{53}	0.0	0.0096	-0.0183	0.0059	0.0134	-0.0255
A_{55}	0.0	-0.0088	0.0036	-0.0008	-0.0075	0.0051
A_{57}	0.0	0.0060	-0.0095	-0.0004	0.0045	0.0090
A_{71}	0.0	-0.0042	0.0360	-0.0001	0.0031	-0.0022
A_{73}	0.0	-0.0042	-0.0271	0.0015	-0.0014	0.0328
A_{75}	0.0	0.0037	0.0116	-0.0003	0.0025	-0.0294
A_{77}	0.0	-0.0027	-0.0016	-0.0002	-0.0022	0.0131

Table 4.5

Comparison of non-dimensionalized frequency and amplitude coefficients for a solid plate; $\theta = 0°$, $\bar{\omega}_{13}$.

	Boundary Conditions									
	Simply-Supported					Clamped-clamped				
		$\bar{E}_1/\bar{E}_2$					$\bar{E}_1/\bar{E}_2$			
	Isotropic	1	2.81	10	40	Isotropic	1	2.81	10	40
$\bar{\omega}_{13}$	98.696	94.112	100.09	102.70	118.21	132.21	127.80	136.05	148.09	194.06
A_{ij}										
A_{11}	0.0	0.0	0.0	0.0	0.0	-0.0197	-0.0106	-0.0150	-0.0142	-0.0180
A_{13}	0.7071	0.7071	1.0	1.0	1.0	0.7039	0.7057	0.9992	0.9998	0.9998
A_{15}	0.0	0.0	0.0	0.0	0.0	0.0057	0.0019	0.0076	0.0071	0.0093
A_{17}	0.0	0.0	0.0	0.0	0.0	0.0017	0.0005	0.0019	0.0017	0.0023
A_{31}	0.7071	0.7071	0.0	0.0	0.0	0.7039	0.7057	-0.0055	-0.0001	-0.0004
A_{33}	0.0	0.0	0.0	0.0	0.0	0.0910	0.0609	0.0354	0.0117	0.0041
A_{35}	0.0	0.0	0.0	0.0	0.0	0.0085	0.0044	-0.0019	-0.0014	-0.0007
A_{37}	0.0	0.0	0.0	0.0	0.0	0.0044	0.0011	-0.0007	-0.0007	-0.0005
A_{51}	0.0	0.0	0.0	0.0	0.0	0.0057	0.0019	-0.0006	-0.0001	-0.00
A_{53}	0.0	0.0	0.0	0.0	0.0	0.0085	0.0044	0.0059	0.0016	0.0005
A_{55}	0.0	0.0	0.0	0.0	0.0	-0.0015	-0.0010	-0.0008	-0.0003	-0.0001
A_{57}	0.0	0.0	0.0	0.0	0.0	-0.0010	-0.0004	-0.0004	-0.0002	-0.0001
A_{71}	0.0	0.0	0.0	0.0	0.0	0.0017	0.0005	-0.0001	-0.0	-0.0
A_{73}	0.0	0.0	0.0	0.0	0.0	0.0044	0.0011	0.0015	0.0004	0.0001
A_{75}	0.0	0.0	0.0	0.0	0.0	-0.0010	-0.0004	-0.0003	-0.0	-0.0
A_{77}	0.0	0.0	0.0	0.0	0.0	-0.0008	-0.0002	-0.0002	-0.0	-0.0

amplitude coefficients suggest that the mode shape is not much affected by the modulus ratio for a given mode.

4.4.4 Effect of Static and Dynamic Moduli on Frequency

The computations of natural frequencies have been done by making use of dynamic properties from Table 4.2. It would be interesting to compare these frequency values with those obtained using static properties. For this purpose, a comparison between frequency values computed using static and dynamic moduli has been made. The results are given in Table 4.6 for a simply-supported unidirectional glass-epoxy solid plate for three symmetric modes and the theoretical results are also compared with experimental results. It is observed that the theoretical values obtained using static moduli are lower than those obtained by using dynamic moduli. When a comparison is made with experimental values, it is found that the error in the values of the first and third symmetric modes is comparatively less than that for the second symmetric mode; the difference in theoretical (static moduli) and experimental values for the second mode is approximately sixteen percent ($\theta = 0°$) whereas the difference in theoretical (dynamic moduli) and experimental values for the second mode is just one percent.

The above observation led to the decision to use the dynamic properties in the computation of frequencies.

Table 4.6

Comparison of frequency values for a simply-supported unidirectional glass-epoxy solid plate.

Symmetric Mode	Fibre-Orientation Angle											
	0°			15°			30°			45°		
	Theo.[a]	Theo.[b]	Expt.	Theo.[a]	Theo.[b]	Expt.	Theo.[a]	Theo.[b]	Expt.	Theo.[a]	Theo.[b]	Expt.
1	90	98	104	96	102	108	103	108	113	109	111	119
2	354	407	411	379	421	433	413	458	468	490	514	550
3	614	630	601	610	616	575	548	572	561	490	514	550

a. Theoretical values obtained using static properties.

b. Theoretical values obtained using dynamic properties.

CHAPTER 5

TRANSIENT RESPONSE OF COMPOSITE PLATES

5.1 Introduction

Dynamic analysis of the response of any structure or a structural element to shock and other transient forces is complex. Many theoretical and numerical analyses of the dynamic response of structures and structural elements have been made and these include classical normal mode solutions, lumped-parameter models, finite difference models, finite element models etc. These models are used to predict the dynamic response of structures subjected to transient loading. However, to develop a reliable dynamic analysis the following information is needed.

1) the nature of the transient loading (e.g. peak pressure, or peak force, duration of the pulse, rise time etc.),
2) the geometry and structural configuration of the element,
3) the static and dynamic material characteristics of the structure,
4) the dynamic characteristics of the structure (e.g. natural frequencies) which is dependent on the boundary conditions,
5) comparison with experimental results.

On the basis of the information needs enumerated above, theoretical and experimental studies were made on clamped-clamped rectangular isotropic and composite plates with and without holes. The theoretical study deals with the elastic response of the plates using

classical normal mode approach and the convergence of the results has been studied by taking different number of modes. In the experimental study, a shock tube has been used as the loading device. The reproducibility of the pressure and strain measurements has been checked. A comparison of the peak dynamic strains, experimental and theoretical, has been made for clamped-clamped plates. The effect of holes on the dynamic response has also been studied by comparing peak strains for plates with and without holes. A good agreement is found for strain-time histories obtained experimentally and with theory. Finally, dynamic amplification factors (defined as the ratio of the peak dynamic strain to the static strain) have been obtained and compared for isotropic and unidirectional glass-epoxy plates.

5.2 Experimental Set-up and Procedure

Experimental work has been carried out to find the effect of shock loading on the response of isotropic and unidirectional glass-epoxy plates with and without holes. The experimental set-up (shown in Figure 5.1) and procedure have been described in this section.

5.2.1 Shock Tube and Production of Shock Wave

The shock tube is a long chamber of constant cross-section which has two chambers, the high pressure and the low pressure, separated by a diaphragm. The diaphragm can be ruptured to produce a shock wave which passes down the tube. The shock tube used is of rectangular cross-section and is shown in Figure 5.2a. The high pressure chamber is 6" x 4" in

cross-section and 36" long. The low pressure side has five sections each 28" long and having 6" x 4" cross-sections. The rectangular section is made of four aluminium plates. The different sections on the low pressure side are joined by means of flanges and made air tight with rubber gaskets provided in between them. The high pressure and low pressure chambers are joined by a circular flange with provision for two O-rings. On the high pressure side, an inlet valve for filling it with compressed air and a Bourdon's pressure gauge to read the pressure are provided.

The alignment of the shock tube is checked before starting the experiment. To produce a shock wave, the diaphragm (cellophane paper has been used here) is kept between the two chambers and then both sides are joined. The high pressure chamber is pressurized by means of compressed air from a compressor (Figure 5.1). When the desired pressure as indicated by the pressure gauge is reached in the high pressure chamber, the inlet valveis is closed and the diaphragm punctured at the centre by means of a high resistance wire carrying high current. This causes the sudden rupture of the diaphragm and a shock wave is produced.

5.2.2 Measurement of Pressure

It is necessary to know the peak pressure, duration of the blast wave, rise time etc., so that comparisons can be made between experimental and computed results. For this purpose, two pressure transducers (Kistler type 623B/601A) - one mounted on the shock tube near the low pressure end to trigger the oscilloscope and the other mounted on a stiff

plate to know the exact pressure distribution on the test plate were used. The stiff plate was mounted in the same position as the test plate and one pressure transducer was mounted on the stiff plate with proper adaptors. This was done for two reasons:

a) the vibration of the plate should not affect the signal from the transducer,

b) the pressure inside the shock tube may be different at different sections and therefore, it is necessary to know the pressure-time history at the end section where the test plate is mounted.

A typical pressure-time history is shown in Figure 5.3a.

The pressure from the transducer mounted on the shock tube was also recorded and it was found that the pressure distribution and the peak value of the pressure obtained from this transducer is the same as obtained from the one mounted on the stiff plate. As the least count of the Bourdon pressure gauge was 1 psi, it was felt desirable to record the pressure from the transducer mounted on the shock tube for each test to avoid errors resulting from reading the pressure on the Bourdon gauge. For a fixed pressure on the high pressure chamber, however, the reproducibility of the shock wave was good.

It is also necessary to check the nature of the shock wave-whether the shock wave is a plane shock wave or not at the end section of the low pressure side where the test plates were mounted. For this purpose, two pressure transducers were mounted on the stiff plate at arbitrary points

and the similarity of pressure-time records (Figure 5.3b) show that the shock wave reaching the end section of the low pressure side where the test plate is mounted is a plane shock wave. If the shock wave were not a plane wave, then it is necessary to know its variation over the area of the test plate. As the pressure measurements can be made only at discrete points, it is likely that more errors are introduced in idealizing pressure distribution over the area of the plate and this may result in less accurate results obtained theoretically when the idealized pressure distribution is used for computation purposes.

The transducers used were of piezo-electrical crystal type which give a charge output proportional to pressure. The charge output is converted to voltage and amplified by means of a charge amplifier (Kistler-type 566 M3). The pressure signal from the charge amplifier is fed into a storage oscilloscope (Tektronix-type 564B). The pressure measuring device has a rise time of a few micro seconds (3 micro-seconds) and a bandwidth of several mega-cycles. Since the rise time and duration of the pulse are of the order of 0.05 milliseconds and 7-8 milliseconds respectively, the transducers were sufficient for the purpose used.

5.2.3 Measurement of Strain

The strain signals were found by means of electrical resistance foil gauges (SR4, type FAP-12-12, S6) mounted on the test plates. The position of the strain gauges on plates with and without holes is shown in Figure 5.4. As the duration of the blast load is of the order of milliseconds, these gauges were quite suitable for the measurement of

dynamic strains. The output from the strain gauges were recorded on a storage oscilloscope using a carrier amplifier plug-in-unit (type 3C66 - Tektronix); the oscilloscope being triggered by the signal from the pressure transducer mounted on the wall of the shock tube. Half-bridge circuit was used with a dummy strain gauge in the other arm. The strain gauges were calibrated with a standard calibration resistor (150 K) provided in the carrier amplifier unit before taking any measurements. The strains and corresponding pressures were recorded for all the gauges. The strains were normalized with respect to the pressure to compare the experimental results with computed results.

5.2.4 Test Plates

Aluminium and unidirectional reinforced E-glass-epoxy rectangular plates were used for blast response studies. Tests were done on plates with and without holes. Only one hole size was considered. Figure 5.4 shows the test plates and also the location of the strain gauges mounted on them.

5.2.5 Clamping Arrangement

The plates were clamped at the end of the shock tube by means of two supporting frames. One supporting frame was rigidly fixed to the shock tube. The test plate was rigidly clamped to this supporting frame with the help of another frame and bolts. Equal tightening of the bolts was achieved by means of a torque wrench.

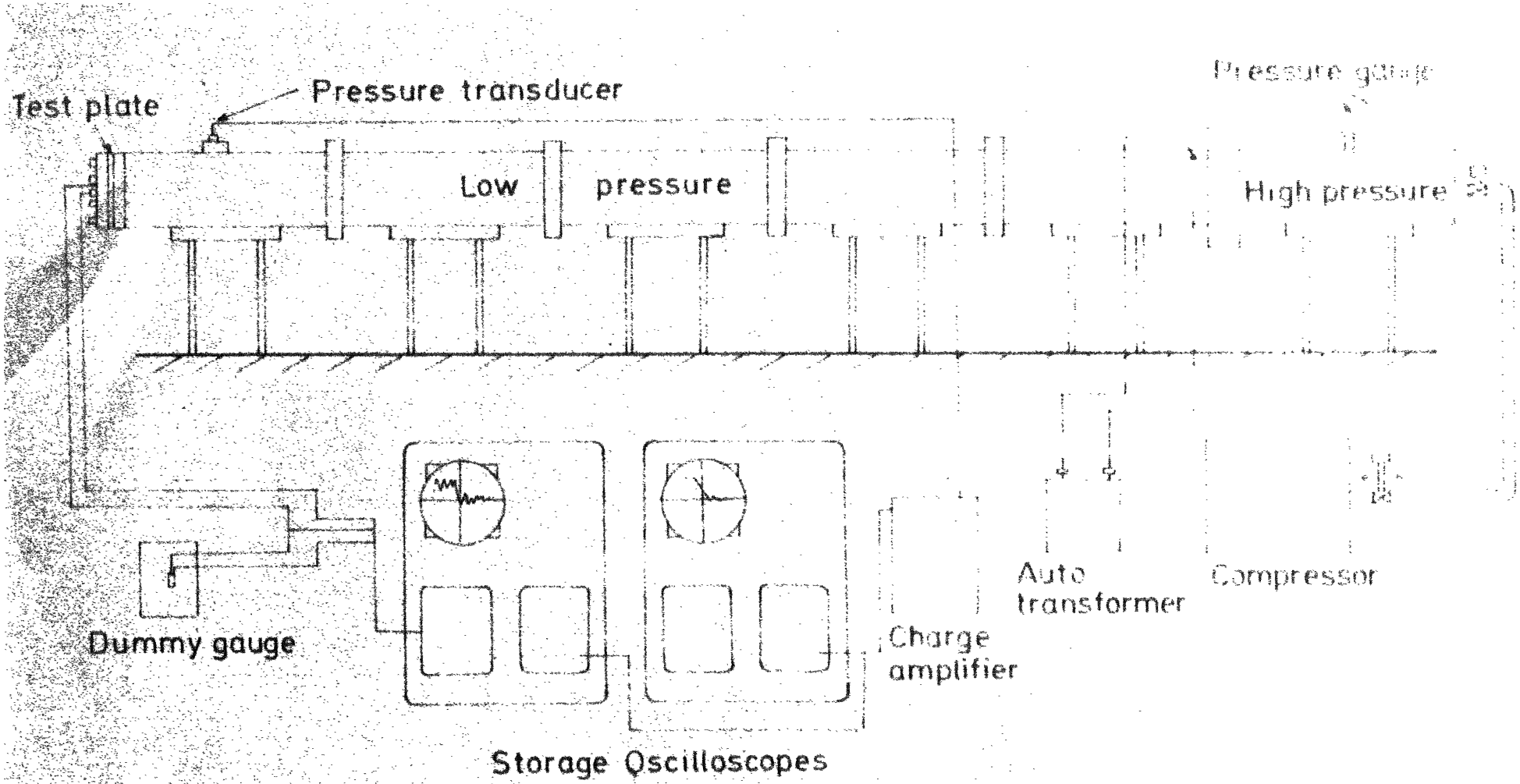

Fig. 5.1 Schematic sketch of the experimental set-up for shock studies

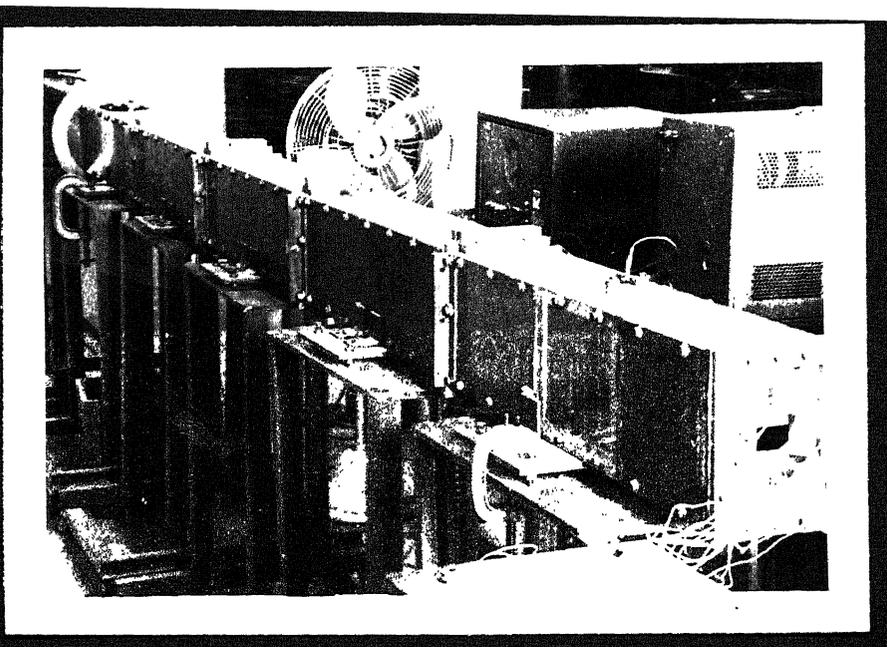

Fig. 5.2a: The Shock Tube

Fig. 5.2b: The Experimental Set-up

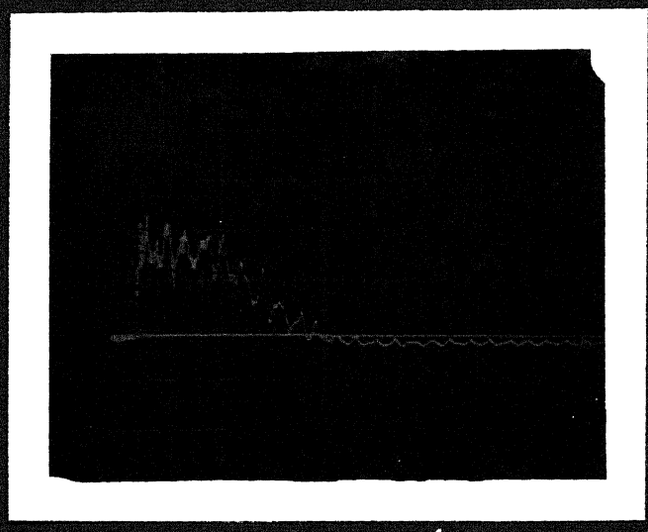

Fig. 5.3a: A Typical Pressure-Time History

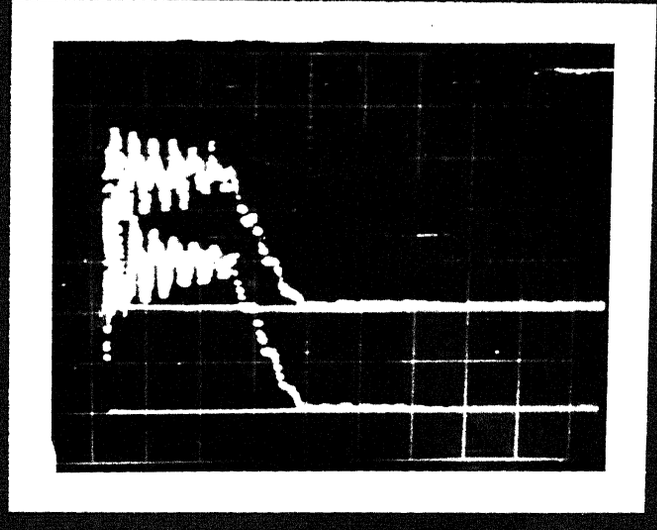

Fig. 5.3b: Pressure-Time Trace as obtained at Two Arbitrary Points of the Plate

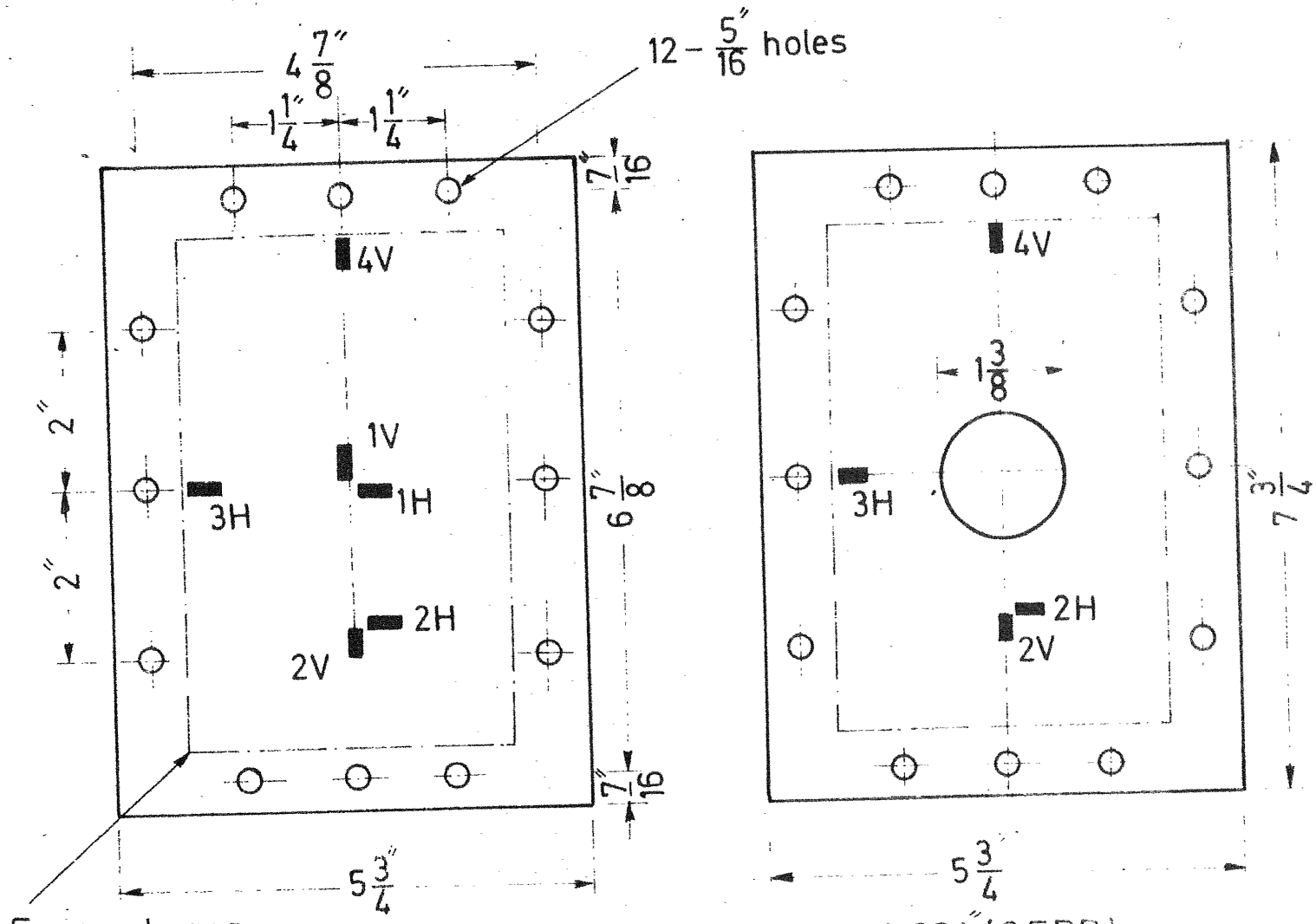

Fig. 5·4 Test plates and location of strain gauges

5.3 Method of Solution

The equations of motion for composite plates with discontinuities were derived in Chapter 2 and studies were made on the free vibration characteristics of these plates by substituting $F(x,y,t) = 0$ in equation (2.14). In the presence of an external force, the equilibrium equations given in equation (2.14) are

$$\sum_{m=1}^{R}\sum_{n=1}^{S}(M_{mn}^{ij} - \beta_{mn}^{ij})\,\ddot{q}_{mn} + \sum_{m=1}^{R}\sum_{n=1}^{S}(C_{mn}^{ij} - \alpha_{mn}^{ij})\,q_{mn} = P_{Fij} \qquad (2.14)$$

where M_{mn}^{ij}, β_{mn}^{ij}, C_{mn}^{ij}, α_{mn}^{ij} and P_{Fij} have been defined earlier in Chapter 2.

It is possible to express equation (2.14) in a matrix form as

$$[\bar{M}]\{\ddot{\bar{q}}\} + [\bar{K}]\{\bar{q}\} = \{\bar{P}\} \quad ; \qquad (5.1)$$

where,
$$\bar{M}_{pl} = M_{mn}^{ij} - \beta_{mn}^{ij} \quad ,$$

$$\bar{K}_{pl} = C_{mn}^{ij} - \alpha_{mn}^{ij} \quad ,$$

$$\bar{q}_{l} = q_{mn} \quad ,$$

$$\bar{P}_{p} = P_{Fij} \quad , \qquad (5.2)$$

and
$$p = (i - 1)\,S + j \quad ,$$

$$l = (m - 1)\,S + n \quad , \qquad (5.3)$$

S is the maximum number of terms taken in y-direction.

Mathematically, equation (5.1) represents a system of linear differential equations of second order and, in principle, the solution to these equations can be obtained by standard procedures for the solution of differential equations with constant coefficients [95, 96] . However, the procedure proposed for the solution of general system of differential equations becomes cumbersome if the order of the matrices is quite large and the equations are coupled. The procedures that are commonly used to solve equation (5.1) are divided into two methods of solution: direct integration and classical normal mode approach. These two methods of solution have been discussed in detail in [97]. The normal mode approach has been used in the present study and the effect of damping has been neglected.

5.3.1 Normal Mode Method

The mode superposition method consists in the transformation of dynamic equilibrium equations into a more effective form using the following transformation on the generalized coordinates $\bar{q}_1$

$$\{\bar{q}\} = [G]\{\eta\} \quad , \tag{5.4}$$

where $[G]$ is a square matrix and $\{\eta\}$ is a time-dependent vector of the same order as that of $\{\bar{q}\}$; the order of $\{\bar{q}\}$ is assumed to be n. The transformation is unknown and is obtained using the displacement solutions of the free vibration equilibrium equations with damping neglected (even if damping is present),

$$[\bar{M}]\{\ddot{\bar{q}}\} + [\bar{K}]\{\bar{q}\} = \{0\} \quad . \tag{5.5}$$

The solution of equation (5.5) can be assumed as,

$$\{\bar{q}\} = \{\bar{A}\}\, e^{i\omega t} \quad , \tag{5.6}$$

where $\{\bar{A}\}$ is a vector of order n. Substituting for $\{\bar{q}\}$ in equation (5.5), the general eigenvalue problem is obtained,

$$[\bar{K}]\{\bar{A}\} = \omega^2 [\bar{M}]\{\bar{A}\} \quad . \tag{5.7}$$

The solution of the eigenvalue problem in equation (5.7) yields eigenvalues $\omega_1^2, \omega_2^2, \ldots, \omega_n^2$ and corresponding eigenvectors $\{\bar{A}\}_1, \{\bar{A}\}_2, \ldots \{\bar{A}\}_n$. These eigenvectors are orthonormalized with respect to the mass matrix $[\bar{M}]$;

$$\{\bar{A}\}_i^T [\bar{M}]^T \{\bar{A}\}_j = 1 \; ; \quad i = j,$$

$$= 0 \; ; \quad i \neq j, \tag{5.8}$$

and $$0 \leq \omega_1^2 \leq \omega_2^2 \leq \omega_3^2 \ldots \leq \omega_n^2 \quad . \tag{5.9}$$

The matrix $[G]$ is defined as the modal matrix whose columns are the eigenvectors $\{\bar{A}\}_i$. We also define a matrix $[\Omega]$ which stores the eigenvalues on its diagonal. Thus,

$$[G] = [\{\bar{A}\}_1, \{\bar{A}\}_2, \ldots, \{\bar{A}\}_n] \quad ;$$

$$[\Omega] = \begin{bmatrix} \omega_1^2 & & & & \\ & \omega_2^2 & & 0 & \\ & & \cdot & & \\ & & & \cdot & \\ & 0 & & & \cdot \\ & & & & \omega_n^2 \end{bmatrix} \tag{5.10}$$

Now, the n solutions of equation (5.5) can be written as

$$[\bar{K}][G] = [\bar{M}][G][\Omega] \tag{5.11}$$

Premultiplying equation (5.11) by the transpose of $[G]$, we get

$$[G]^T[\bar{K}][G] = [G]^T[\bar{M}][G][\Omega] \tag{5.12}$$

Making use of the orthogonality relation in equation (5.8), we have

$$[G]^T[\bar{K}][G] = [\Omega] \tag{5.13}$$

The transformation on the generalized co-ordinates given in equation (5.4) leads to the following equilibrium equations in modal generalized co-ordinates,

$$\{\ddot{\eta}\} + [\Omega]\{\eta\} = \{N\} \tag{5.14}$$

where,

$$\{N\} = [G]^T\{\bar{P}\} \tag{5.15}$$

The initial conditions (i.e. at time t = 0) on $\{\eta(t)\}$ are given as

$$\begin{aligned} \{\eta(0)\} &= [G]^T[\bar{M}]\{\bar{q}(0)\} \quad , \\ \{\dot{\eta}(0)\} &= [G]^T[\bar{M}]\{\dot{\bar{q}}(0)\} \quad . \end{aligned} \tag{5.16}$$

Equation (5.14) represents a system of n uncoupled differential equations in modal generalized co-ordinates, $\{\eta(t)\}$ with the initial conditions in equation (5.16) and can be written as

$$\ddot{\eta}_r(t) + \omega_r^2 \eta_r(t) = N_r(t) \quad ; \qquad r = 1,2,\ldots, n,$$

with initial conditions as

$$\eta_r(0) = \{\bar{A}\}_r^T [\bar{M}] \{\bar{q}(0)\} \ ,$$

$$\dot{\eta}_r(0) = \{\bar{A}\}_r^T [\bar{M}] \{\dot{\bar{q}}(0)\} \ . \tag{5.17}$$

Applying Laplace transform technique, the solution of equation (5.17) is given as

$$\eta_r(t) = \eta_r(0) \cos(\omega_r t) + \dot{\eta}_r(0) \frac{\sin(\omega_r t)}{\omega_r} + \frac{1}{\omega_r} \int_0^t N_r(\tau) \sin \omega_r(t - \tau) \, d\tau \ ;$$

$$r = 1,2,\ldots, n \ . \tag{5.18}$$

If the modal generalized force $N_r(t)$ is known, equation (5.18) can be solved and $\eta_r(t)$ evaluated.

5.3.2 Evaluation of $N_r(t)$

The method outlined in Section 5.3.1 is quite general and can be applied to any structural system. In the present section, the expressions for modal generalized forces are developed for the idealized experimental pulse shape shown in Figure 5.5a.

The modal generalized force given in equation (5.15) is

$$\{N(t)\} = [G]^T \{\bar{P}\}$$

and therefore,

$$N_r(t) = [\bar{A}]_r^T \{\bar{P}\} \tag{5.19}$$

Now,

$$\bar{P}_p = P_{Fij}$$

and from equation (2.13),

$$\bar{P}_p = \iint_A F(x,y,t)\ \phi_{ij}\ dA \tag{5.20}$$

It was discussed in Section 5.2 that the shock wave reaching the plate is a plane shock wave and is therefore, uniformly distributed over the surface of the plate. The distributed load is assumed to be of unity value and its variation with time is given as

$$\begin{aligned} F(t) &= 0 && , && -\infty < t < 0 \quad \text{and} \quad t > t_2 \\ &= 1 && , && t < t_1 \\ &= 1 - \frac{t - t_1}{t_2 - t_1} && , && t_1 \leq t \leq t_2 \end{aligned} \tag{5.21}$$

Thus $N_r(t)$ can be evaluated from equations (5.21), (5.20) and (5.19).

5.3.3 Determination of Displacements and Strains

In the determination of displacements and strains, it is necessary to develop the expressions for generalized co-ordinates, q_{mn}. The generalized coordinates q_{mn} and the modal generalized coordinates are related and given in equation (5.4) as

$$\{\bar{q}\} = [G] \{\eta\} \tag{5.4}$$

and $$\bar{q}_l = q_{mn}$$

It is possible to evaluate $\eta_r(t)$ from equation (5.18) once the modal generalized forces N_r are known. The method for evaluating $N_r(t)$ has been given in Section 5.3.2. Substitution of $\eta_r(t)$ in equation (5.4) gives the generalized coordinates. The displacements and strains can be then found from the following expressions

$$w(x,y,t) = \sum_{m=1}^{R} \sum_{n=1}^{S} q_{mn}(t) \phi_{mn}(x,y) \tag{2.6}$$

$$\varepsilon_x(x,y,t) = -\frac{h}{2} \sum_{m=1}^{R} \sum_{n=1}^{S} q_{mn}(t) \frac{\partial^2 \phi_{mn}(x,y)}{\partial x^2} \tag{5.22}$$

$$\varepsilon_y(x,y,t) = -\frac{h}{2} \sum_{m=1}^{R} \sum_{n=1}^{S} q_{mn}(t) \frac{\partial^2 \phi_{mn}(x,y)}{\partial y^2} \tag{5.23}$$

5.4 Results and Discussion

The method of solution given in Section 5.3 to find the transient response of a composite structure is quite general and can be applied to any given structure if the admissible functions are properly defined for the structure. The numerical computations have been done for isotropic and composite plates in the case of simply-supported and clamped-clamped boundary conditions. As experiments were conducted on clamped-clamped rectangular isotropic and unidirectionally reinforced glass-epoxy plates ($\theta = 0^\circ$), these results have been compared with the numerical results

obtained for clamped-clamped rectangular isotropic and unidirectional glass-epoxy plates; the material properties for the glass-epoxy plate being taken from Table 4.2. The classical normal mode approach was preferred because the computer program was already developed to compute natural frequencies and normalized eigenvectors. The reliability of the theoretical results computed depends to a great extent on the accuracy in the measurement of the transient loading. This fact was observed by Baker et.al. [61] when they compared the theoretical elastic response of cantilever beams predicted from the linear elastic beam theory with measured blast response and emphasized the need for the accurate measurement of the transient loading. This fact has been kept in mind and therefore, the pressure-time history was recorded in each of the strain measurements. The theoretical strains have been computed for a unit value of the idealized blast load, shown in Figure 5.5a. The effect of the contribution of different modes as the dynamic response is studied and given in Table 5.1. for an isotropic clamped-clamped solid plate. In order to compare the theoretical and experimental strains, the latter have been normalized with respect to the pressure. The dynamic strains are also compared with static strains. The theoretical and experimental strain-time histories are shown for a particular gauge in the case of a unidirectional glass-epoxy solid plate. Finally, the influence of holes is seen on the dynamic amplification factor for an isotropic as well as a composite plate.

5.4.1 The Effect of the Number of Modes on the Dynamic Response

It is necessary to know the number of modes to be considered to get sufficiently accurate results for the dynamic response of a structure. For this purpose, deflections and strains were computed for an isotropic and a unidirectional glass-epoxy clamped-clamped plate taking different number of modes and the results are given for central deflection and strains (1H, 1V, 2H, ... etc.) in the case of a rectangular isotropic solid plate in Table 5.1. It is observed that a good estimate of the central deflection and strains 1H, 2H, etc. (strains in the x-direction) can be obtained just by considering only one mode- the fundamental mode. However, this is not true for strains 1V, 2V, etc. (strains in the y-direction). Obtaining the dynamic response by just taking the contribution of only one mode may lead to absurd results. But as the number of modes taken is increased, good convergence is obtained and therefore, the results were computed by taking nine modesxm in all the cases considered. The same observation is found to be true for unidirectional glass-epoxy plates. The contribution of higher modes becoming significant was also brought to light by Crocker [65] in a simplified analysis of the multimode response of panels, subjected to sonic booms. He mentioned that as b/a ratio is decreased (b < a), the higher mode contributions to strains in the x-direction (i.e. strain in direction parallel to the longer dimension of the plate) become larger. In the present case, a < b and therefore, it is expected that the contribution of higher modes will be important to strains in the y-direction and this has been found true. In the case of a square,

Table 5.1

Effect of the number of modes chosen on the dynamic response (at a given time) of an isotropic clamped-clamped plate for a unit distributed load, R = 0.709.

No. of Modes taken	Central Deflection, in inches	Strain, strain					
		1H	1V	2H	2V	3H	4V
1	0.024639	419.16	238.55	251.69	72.78	- 403.10	- 235.84
3	0.023281	400.07	134.92	271.93	122.82	- 380.92	- 263.85
5	0.023236	393.01	127.77	277.93	128.39	- 381.55	- 264.22
7	0.023143	380.32	129.20	268.94	127.40	- 382.84	- 263.57
9	0.023148	380.81	130.80	269.10	128.06	- 382.92	- 264.34

isotropic plate one expects that the higher mode contributions will not be significant as b = a ; however the same is not true for a square composite plate because of the orthotropy present.

5.4.2 Comparison of Theoretical and Experimental Dynamic Strains

A comparison of theoretical and experimental dynamic strains is essential to ensure the reliability and validity of the theoretical model developed [98] for the dynamic analysis of a structure. A comparison of theoretical and normalized experimental peak dynamic strains has been made for an isotropic and a unidirectional glass-epoxy composite plate and the results are given in Tables 5.2 and 5.3. The theoretical and experimental results for solid plates are also compared with those for plates having holes. The static strains have been given in all the cases.

It is found from Tables 5.2 and 5.3 that the agreement between the theoretical and experimental peak strains for solid isotropic and unidirectional glass-epoxy plates is good except in the strain 3H for a glass-epoxy solid plate where the gauge did not seem to respond properly. The same is not true for plates with holes. The agreement between the theoretical and experimental peak dynamic strains is not very good; the maximum difference being 100 percent for strain 2V in the case of an isotropic plate. This suggests that the theoretical analysis developed based on the classical normal mode approach is adequate for solid clamped-clamped plates whereas there is a need for more investigation into the transient response analysis of plates with holes.

Table 5.2

Comparison of theoretical and experimental peak strains for an isotropic clamped-clamped plate; R = 0.709.

Gauge Location	d/a = 0.0			d/a = 0.282		
	Static Strain (Theory) μ Strain	Dynamic Strain (Theory) μ Strain	Dynamic Strain (Experiment) μ Strain	Static Strain (Theory) μ Strain	Dynamic Strain (Theory) μ Strain	Dynamic Strain (Experiment) μ Strain
1H	172	380	343	-	-	-
1V	61	130	130	-	-	-
2H	123	269	214	136	334	211
2V	55	128	154	38	261	132
3H	-184	-382	-298	-190	-411	-331
4V	-107	-262	-209	-108	-182	-285

Table 5.3

Comparison of theoretical and experimental peak strains for a unidirectional glass-epoxy clamped-clamped plate ($\theta = 0°$); $\bar{R} = 0.709$.

Gauss Location	d/a = 0.0			d/a = 0.282		
	Static Strain (Theory) μ Strain	Dynamic Strain (Theory) μ Strain	Dynamic Strain (Experiment) μ Strain	Static Strain (Theory) μ Strain	Dynamic Strain (Theory) μ Strain	Dynamic Strain (Experiment) μ Strain
1H	701	1120	1033	-	-	-
1V	330	433	675	-	-	-
2H	469	830	801	525	780	712
2V	199	303	297	36	261	223
3H	-776	-1090	- 534*	-809	-916	-970
4V	-482	- 720	- 735	-497	-785	-638

* The strain gauge did not respond properly.

The theoretical and experimental strain-time histories are compared in Figure 5.5b for the strain gauge 2H in the case of a unidirectionally reinforced glass-epoxy plate. The agreement is good. The experimental peak strain, however, is less than the theoretical peak strain and there is a time lag between the experimental and theoretical strains after the application of the blast load. This may be due to the damping in the composite plates and also in the supports.

5.4.3 Comparison of Dynamic Amplification Factors

The theoretical dynamic amplification factors (defined as the ratio of the peak dynamic strain to the static strain) have been given in Table 5.4 for an isotropic and a unidirectional glass-epoxy plate. The dynamic amplification factors for a solid isotropic plate lie in between the values 2.0 to 2.5 whereas those for a solid glass-epoxy plate lie in between 1.3 to 1.8 for the strains considered. This indicates that less damage will be done to a glass-epoxy composite plate than an isotropic plate when both are subjected to similar transient loads. The dynamic amplification factors for plates with holes are approximately the same as the values for the solid plates, both in the case of isotropic and composite materials except in the case of strains 2^V where the amplification factor is very high (6 to 7) which seems unusual. An explanation, however, can be given if one compares the static strains for plates with holes and without holes. The values of static strain for 2V is considerably reduced in the presence of a hole; this is justified as 2V is normal to the hole and nearer the hole geometry. The dynamic strains,

on the other hand, are not much affected and therefore high values of dynamic amplification factors are obtained.

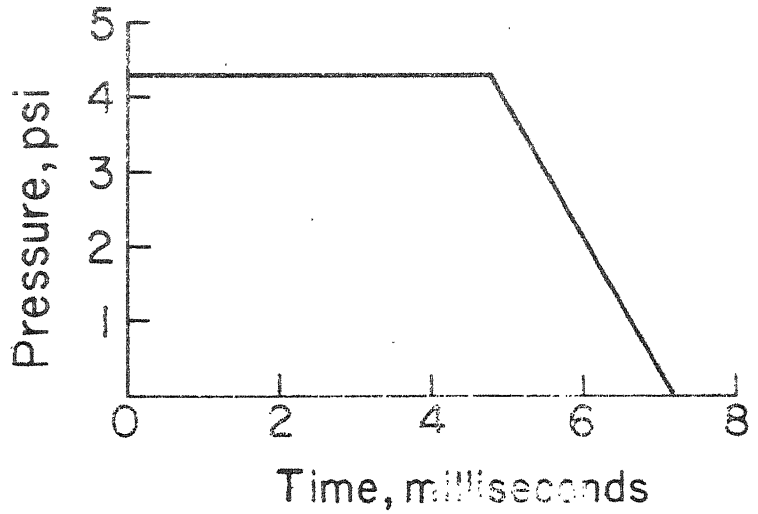

Fig.5.5a Idealized pressure time history

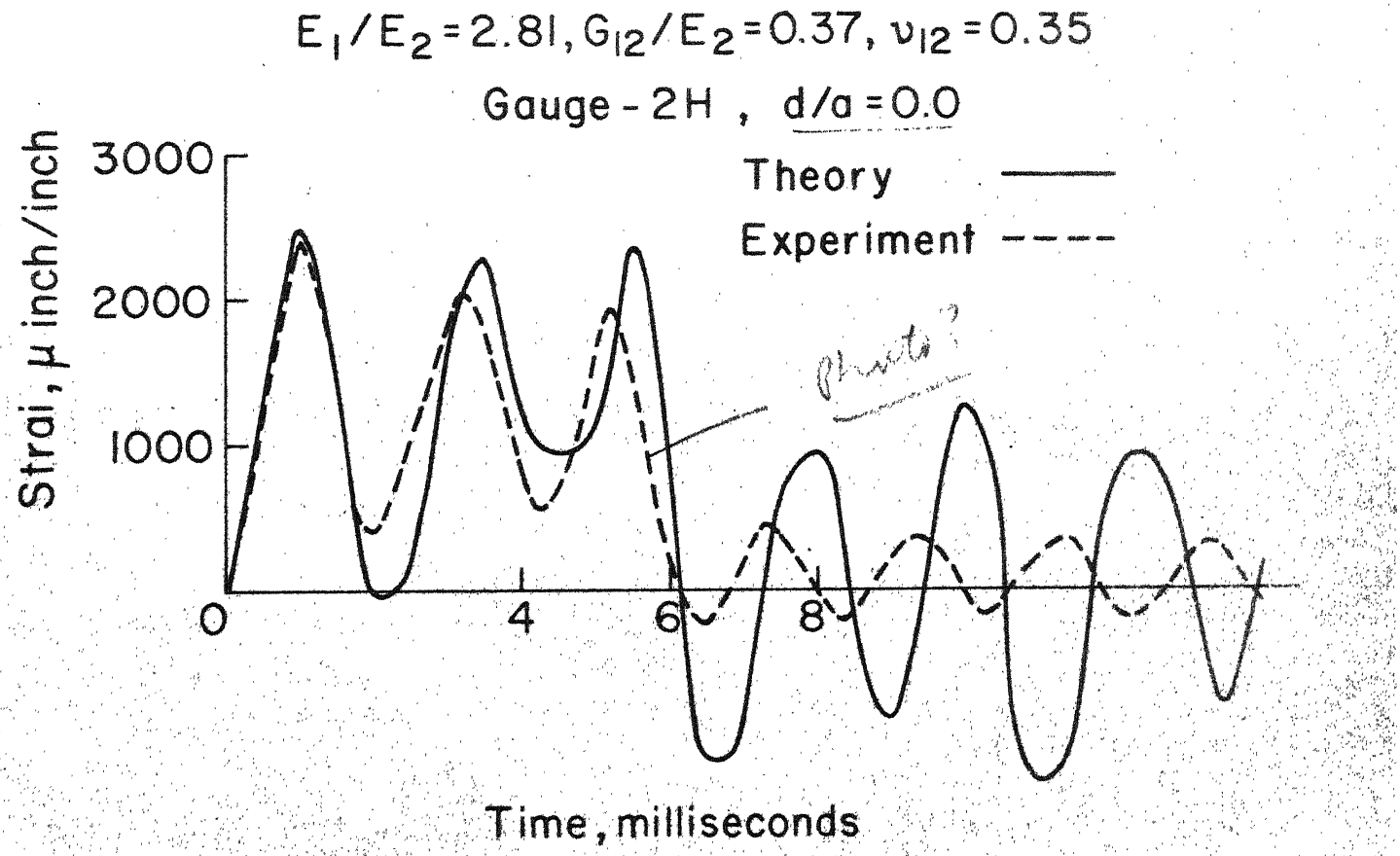

Fig.5.5b Strain-time history for a clamped-clamped plate; $\theta = 0°$, $R = 0.709$

Table 5.4

Comparison of theoretical dynamic amplification factors (peak dynamic strain/static strain) for an isotropic and a unidirectional glass-epoxy clamped-clamped plate; R = 0.709.

Gauge Location	Dynamic Amplification Factor (Theoretical)			
	Isotropic		Unidirectional glass-epoxy	
	d/a = 0.0	d/a = 0.282	d/a = 0.0	d/a = 0.282
1H	2.20	-	1.60	-
1V	2.13	-	1.31	-
2H	2.18	2.45	1.77	1.48
2V	2.32	6.88	1.53	7.25
3H	2.07	2.16	1.40	1.13
4V	2.44	1.67	1.49	1.58

CHAPTER 6

CONCLUSIONS

6.1 Conclusions

The following are the major conclusions based on the present work.

1) A method of analysis to study the free vibration characteristics and the transient response of composite plates with cut-outs (or holes) assuming the effect of cut-out (or hole) to be equivalent to a displacement-dependent loading has been developed and is found to give more accurate results compared to the other methods available.

2) The frequencies for each mode in the case of a simply-supported plate with a cut-out (or a hole) vary with cut-out parameter (or hole parameter) in different ways for all the modulus ratios and do not uniformly increase or decrease. For clamped-clamped plates also, the frequencies for each mode except the first vary with c/a (or d/a) in different ways.

3) The fundamental frequency for simply-supported orthotropic plates (fibre-orientation angle $\theta = 0^{\circ}$) decreases for medium cut-out (or hole) parameters unlike the behaviour in the case of isotropic plates where the fundamental frequency decreases for small cut-out (or hole) parameters. The rate of decrease with c/a (or d/a) increases with the increase in the

modulus ratio. In the case of clamped-clamped plates, the fundamental frequency increases with the cut-out (or hole) size for all modulus ratios and all fibre-orientation angles; this behaviour is also found for simply-supported plates when the fibre-orientation angle is 45°.

4) The fundamental frequency for simply-supported solid plates (c/a or d/a = 0.0) increases with increase in the fibre-orientation angle. The fundamental frequency, however, is found to behave in an opposite manner for a clamped-clamped solid plate; it decreases with increase in the fibre-orientation angle. This behaviour is observed for all modulus ratios considered. Thus, increase in the fibre-orientation angle make simply-supported plates more stiff whereas it decreases the stiffness of a clamped-clamped plate when there is no cut-out (or hole).

5) The behaviour of frequencies for balanced bidirectionally reinforced plates and for an isotropic plate is found similar. The fundamental frequency for a balanced bidirectional glass-epoxy, simply-supported plate is lower than the fundamental frequency for an isotropic plate when $\theta = 0°$ and is found to be higher when $\theta = 45°$. For clamped-clamped boundary conditions, the fundamental frequency for an isotropic plate is found to be always higher than that for a balanced bidirectional composite plate for all cut-out (or hole) parameters considered.

6) A similarity is observed between the behaviour of x frequencies between isotropic and the composite plates with fibre-orientation angle equal to 45°. For an isotropic plate, $\bar{\omega}_{12} = \bar{\omega}_{21}$, $\bar{\omega}_{23} = \bar{\omega}_{32}$, $\bar{\omega}_{14} = \bar{\omega}_{41}$ etc., (frequencies corresponding to a combination of symmetric and

antisymmetric modes). In composite plates, as the fibre-orientation angle is increased, frequency curves corresponding to $\bar{\omega}_{12}$ and $\bar{\omega}_{21}$, $\bar{\omega}_{23}$ and $\bar{\omega}_{32}$, etc., come closer together and coincide when $\theta = 45°$; this means $\bar{\omega}_{12} = \bar{\omega}_{21}$, $\bar{\omega}_{23} = \bar{\omega}_{32}$ etc.

7) Two interesting features have been observed due to the presence of a cut-out (or hole) in a plate: a) the existence of a new mode in the case of a simply-supported plate and b) the cross-over of frequencies. In the case of a simply-supported plate, it is observed that the fourth mode is identical with the fifth mode for a solid isotropic plate. This is also observed for frequencies corresponding to both symmetric and antisymmetric modes. The introduction of a small discontinuity seems to perturb the system for which an exact solution is known and gives rise to a new mode. In the case of a clamped-clamped isotropic plate a closed form solution is not known and the approximation in the solution can be assumed to give rise to the new mode- for example, fourth mode - even when there is no cut-out (or hole) in the plate. It is found that there is a tendency for the higher modes to interchange when there is a cut-out (or hole) in the plate. Mode shapes obtained at the cross-over and nearby points for the frequencies which cross-over show that at the cross-over frequencies the plate can have the mode shape corresponding to either of the modes which cross over.

8) The presence of holes or cut-outs influences the modes in general. The influence on the modes depends on the location of the cut-out (or hole) in the plate; symmetric location of the cut-out (or hole) is found to

influence the symmetric modes and it is expected that asymmetric location will influence the antisymmetric modes. The presence of holes, therefore, distorts the mode shapes and this has been observed when experiments were conducted an isotropic and unidirectional glass-epoxy, square plates with centrally located circular holes; the symmetric modes were influenced most as the holes were centrally located.

9) In general, the behaviour of different frequencies for a cut-out and for a hole is similar. The effect of the shape is seen only at larger cut-out (or hole) ratios.

10) An experimental study was done on the free vibration characteristics of aluminium and unidirectional glass-epoxy, square plates. The unidirectional glass-epoxy plates were made by a hand lay-up technique and the static and dynamic properties for the composite material was determined. The dynamic material properties were used in the numerical computation. A good agreement between the theoretical and experimental results has been obtained for isotropic as well as for the unidirectional glass-epoxy plates. This proves the adequacy of the present method of analysis and stresses the need a) to use dynamic properties in the numerical computation of theoretical results to get reliable results and b) to take into account the effect of clamping which is commonly ignored.

11) The mode shape for a particular frequency (identified by the largest amplitude coefficient in the corresponding eigenvector) is found to be independent of the modulus ratio for simply-supported and clamped-clamped plates.

12) An experimental study was made on the blast response of isotropic and unidirectional glass-epoxy rectangular, clamped-clamped plates using a shock tube as the loading device. The experimental results for strains have been compared with the theoretical results obtained using classical normal mode approach for the isotropic and unidirectional glass-epoxy clamped-clamped plates with and without holes. A good agreement between the experimental and theoretical results for plates without holes show that the classical normal mode approach to the solution of transient elastic response problems is satisfactory for plates without holes.

6.2 Recommendations for Future Work

Considering the direct extensions and generalizations of the present study pertaining to plates, the following problems are worth studying.

1) An extension of the present analysis can be made to include the effect of bending and stretching coupling in the composite plates.

2) The present study can be generalized to include the effect of shear deformation and rotary inertia in composite plates with discontinuities.

3) The effect of the cut-outs or holes can be studied on the dynamic response of composite shells.

4) The effect of damping which has been neglected in the present investigation can be included in the free and forced vibration response analysis of composite plates and shells with discontinuities.

5) Nonlinear vibration and nonlinear shock response studies can be made on structural elements with discontinuities.

REFERENCES

1. Pister, K.S. and Dong, S.B., 'Elastic Bending of Layered Plates', Journal of the Engineering Mechanics Division, Proceedings ASCE, Vol. 55, No. EM4, 1959, pp. 1-10.

2. Reissner, E. and Stavsky, Y., 'Bending and Stretching of Certain Types of Heterogeneous Aelotropic Elastic Plates', Journal of Applied Mechanics, Vol. 28, No. 3, 1961, pp. 402-408.

3. Dong, S.B., Pister, K.S., and Taylor, R.L., 'On the Theory of Laminated Anisotropic Shells and Plates', Journal of the Aerospace Sciences, Vol. 29, No. 8, 1962, pp. 969-975.

4. Stavsky, V., 'Bending and Stretching of Laminated Aelotropic Plates', Journal of Engineering Mechanics Division, Proceedings ASCE, Vol. 8, 1961, pp. 31-56.

5. Ashton, J.E. and Whitney, J.M., 'Theory of Laminated Plates', Technomic Publishing Company, Stamford, Connecticut, 1970.

6. Mindlin, R.D., 'Influence of Rotatory Inertia and Shear on Flexural Motions of Isotropic, Elastic Plates', Journal of Applied Mechanics, Vol. 18, 1951, pp. 31-38.

7. Yang, P.C., Norris, C.H. and Stavsky, Y., 'Elastic Wave Propagation in Heterogeneous Plates', International Journal of Solids and Structures, Vol. 2, 1966, pp. 665-683.

8. Whitney, J.M. and Pagano, N.J., 'Shear Deformation in Heterogeneous Anisotropic Plates', Journal of Applied Mechanics, Vol. 31, No. 4, 1970, pp. 1031-1036.

9. Whitney, J.M., 'The Effect of Transverse Shear Deformation on the Bending of Laminated Plates', Journal of Composite Materials, Vol. 3, 1969, pp. 534-537.

10. Sun, C.T. and Whitney, J.M., 'Theories for the Dynamic Response of Laminated Plates', AIAA Journal, Vol. 11, No. 2, 1973, pp.178-183.

11. Drumheller, O.S. and Bedford, A., 'On a Continuum Theory for a Laminated Medium', Journal of Applied Mechanics, Vol. 40, June 1973, pp. 527-532.

12. Moon, F.C., 'One Dimensional Transient Waves in Anisotropic Plates', Journal of Applied Mechanics, Vol. 40, No. 2, 1973, pp. 485-490.

13. Sun, C.T., Achenback, J.D. and Herrmann, G., 'Continuum Theory for a Laminated Medium', Journal of Applied Mechanics, Vol. 35, 1968, pp. 467-475.

14. Jones, A.T., 'Exact Natural Frequencies and Modal Functions for a Thick Off-Axis Lamina', Journal of Composite Materials, Vol. 5, 1971, pp. 504-520.

15. Jones, J.P., 'Wave Propagation in a Two-Layered Medium', Journal of Applied Mechanics, Vol. 31, No. 2, 1964, pp. 213-222.

16. Srinivas, S., Joga Rao, C.V. and Rao, A.K., 'An Exact Analysis for Vibration of Simply-Supported Homogeneous and Laminated Thick Rectangular Plates', Journal of Sound and Vibration, Vol. 2, No. 2, 1970, pp. 187-199.

17. Srinivas, S. and Rao,A.K., 'Bending, Vibration and Buckling of Simply-Supported Thick Orthotropic Rectangular Plates and Laminates', International Journal of Solids and Structures, Vol. 6, No. 11, 1970, pp. 1463-1481.

18. Bert, C.W. and Francis, P.H., 'Composite Material Mechanics: Structural Mechanics' AIAA Journal, Vol. 120, No. 9, 1974, pp.1173-1186.

19. Bert, C.W., 'Dynamics of Composite and Sandwich Panels: Part 1', The Shock and Vibration Digest, Vol. 8, No. 10, 1976, pp. 37-48.

20. Bert, C.W., 'Dynamics of Composite and Sandwich Panels: Part 2', The Shock and Vibration Digest, Vol. 8, No. 11, 1976, pp. 15-24.

21. Huffington Jr., N.J. and Hoppmann, W.H., 'On the Transverse Vibrations of Rectangular Orthotropic Plates', Journal of Applied Mechanics, Vol. 25, 1958, pp. 389-395.

22. Timoshenko, S. and Woinowsky, K.S., 'Theory of Plates and Shells', McGraw-Hill Book Company, Inc., New York, 1959.

23. Hearmon, R.F.S., 'The frequency of Flexural Vibration of Rectangular Orthotropic Plates with Clamped or Supported Edges', Journal of Applied Mechanics, Vol. 26, 1959, pp. 537-540.

24. Dickinson, S.M., 'The Flexural Vibration of Rectangular Orthotropic Plates', Journal of Applied Mechanics, Vol. 36, 1969, pp. 101-106.

25. Dill, E.H. and Pister, K.S., 'Vibration of Rectangular Plates and Plate Systems', Proceedings of the Third U.S. National Congress of Applied Mechanics, ASME, 1958, pp. 123-132.

26. Swarup, D.A. and Sundararajan, V., 'Vibration and Buckling of Generally Orthotropic Plates', Indian Journal of Technology, Vol. 10, 1972, pp. 245-248.

27. Ashton, J.E. and Waddoups, M.E., 'Analysis of Anisotropic Plates', Journal of Composite Materials, Vol. 3, No. 1, 1969, pp. 148-165.

28. Whitney, J.M. and Leissa, A.W., 'Analysis of Heterogeneous Anisotropic Plates', Journal of Applied Mechanics, Vol. 36, 1969, pp. 261-266.

29. Whitney, J.M. and Leissa, A.W., 'Analysis of a Simply-Supported Laminated Anisotropic Rectangular Plate', AIAA Journal, Vol. 8, No. 1, 1970, pp. 28-33.

30. Hikami, Y., 'Transverse Vibrations of Laminated Orthotropic Plates', Report 23, April 1969, Division of Solid Mechanics, Structures and Mechanical Design, Case Western Reserve University, Cleveland, Ohio.

31. Ashton, J.E. and Anderson, J.D., 'The Natural Modes of Vibration of Boron-Epoxy Plates', Shock and Vibration Bulletin, Vol. 39, Part 4, 1969, pp. 81-91.

32. Bert, C.W. and Mayberry, B.L., 'Free Vibrations of Unsymmetrically Laminated Anisotropic Plates with Clamped Edges', Journal of Composite Materials, Vol. 3, 1969, pp. 282-293.

33. Ashton, J.E., 'Natural Modes of Free-Free Anisotropic Plates', Shock and Vibration Bulletin 39, Part 4, 1969, pp. 93-97.

34. Mohan, D. and Kingsbury, H.B., 'Free Vibrations of Generally Orthotropic Plates', Journal of the Acoustical Society of America, Vol. 50, No. 1, 1971, pp. 266-269.

35. Whitney, J.M., 'Fourier Analysis of Clamped Anisotropic Plates', Journal of Applied Mechanics, Vol. 38, 1971, pp. 530-532.

36. Whitney, J.M., 'Free Vibration of Anisotropic Rectangular Plates', Journal of Acoustical Society of America, Vol. 52, No. 1, 1972, pp. 448-449.

37. Green, A.E., 'Double Fourier Series and Boundary Value Problems', Cambridge Philosophical Society Proceedings, Vol. 40, 1944.

38. Decapua, N.J. and Sun, B.C., 'Transverse Vibration of a Class of Orthotropic Plates', Journal of Applied Mechanics, Vol. 39, No. 2, 1972, pp. 613-615.

39. Maurizi, M.J. and Laura, P.A., 'Vibration Analysis of Clamped, Rectangular Plates of Generalized Orthotropy', Journal of Sound and Vibration, Vol. 26, No. 3, 1973, pp. 299-305.

40. Clary, R.R. and Cooper, P.A., 'Vibration Characteristics of Aluminium Plates Reinforced with Boron-Epoxy Composite Material', Journal of Composite Materials, Vol. 7, 1973, pp. 348-365.

41. Thornton, E.A. and Clary, R.R., 'A Correlation Study of Finite-Element Modeling for Vibrations of Composite Material Panels', Composite Materials: Testing and Design (3rd Conference), ASTM, STP 546, 1974, pp. 111-129.

42. Rosettos, J.N. and Tong, P., 'Finite Element Analysis of Vibration and Flutter of Cantilever Anisotropic Plates', Journal of Applied Mechanics, Vol. 41, No. 4, 1974, pp. 1075-1080.

43. Jones, R.M., 'Buckling and Vibration of Unsymmetrically Laminated Cross-Ply Rectangular Plates', AIAA Journal, Vol. 11, No. 12, 1973, pp. 1626-1632.

44. Elishakoff, I.B., 'Vibration Analysis of Clamped Square Orthotropic Plates', AIAA Journal, Vol. 12, No. 7, 1974, pp. 921-924.

45. Lin, C.C. and King, W.W., 'Free Transverse Vibrations of Rectangular Unsymmetrically Laminated Plates', Journal of Sound and Vibration, Vol. 36, No. 1, 1976, pp. 91-103.

46. Kumai, T., 'Flexural Vibrations of the Square Plate with a Central Circular Hole', Proceedings of the Second Japan National Congress for Applied Mechanics, 1952, pp. 339-342.

47. Takahashi, S., 'Vibration of Rectangular Plates with Circular Holes', Bulletin of Japan Society of Mechanical Engineers, Vol. 1, No. 4, 1958, pp. 380-385.

48. Joga Rao, C.V. and Pickett, G., 'Vibrations of Plates of Irregular Shapes and Plates with Holes', Journal of the Aeronautical Society of India, Vol. 13, No. 3, 1961, pp. 83-88.

49. Brogan, F., Forsberg, K. and Smith, S., 'Dynamic Behaviour of a Cylinder with a Cut-out', AIAA Journal, Vol. 7, No. 5, 1969, pp.903-911.

50. Anderson, R.G., Irons, B.M. and Zienkiewicz, O.C., 'Vibration and Stability of Plates Using Finite Elements', International Journal of Solids and Structures, Vol. 4, 1968, pp. 1031-1055.

51. Kristiansen, V. and Soedel, W., 'Fundamental Frequencies of Cut-Out Square Plates with Clamped Edges', Journal of Engineering for Industry, ASME, February 1971, pp. 343-345.

52. Paramsivam, P., 'Free Vibration of Square Plates with Square Openings', Journal of Sound and Vibration, Vol. 30, No. 2, 1973, pp. 173-178.

53. Basdekas, N.L. and Chi, M., 'Dynamic Response of Plates with Cut-Outs', The Shock and Vibration Bulletin, Vol. 41, 1970, pp. 29-35.

54. Basdekas, N.L. and Chi, M., 'Response of Oddly-Stiffened Circular Cylindrical Shells', Journal of Sound and Vibration, Vol. 17, 1971, pp. 187-206.

55. Basdekas, N.L. and Chi, M., 'Non-Linear Forced Vibration of a Non-Prismatic Beam Due to Combined Flexure and Stretching', Journal of Sound and Vibration, Vol. 15, 1971, pp. 447-454.

56. Aksu, G. and Ali, R., 'Prediction of Dynamic Characteristics of Orthotropic Plates by a Finite Difference Unequal Interval Formulation', Journal of Sound and Vibration, Vol. 35, 1974, pp. 119-128.

57. Aksu, G. and Ali, R., 'Determination of Dynamic Characteristics of Rectangular Plates with Cut-Outs Using a Finite Difference Formulation', Journal of Sound and Vibration, Vol. 44, 1976, pp. 147-158.

58. Mahabaliraja, Boyd, D.E. and Brugh, R.L., 'Vibrations of Stiffened Cylinders with Cut-Outs', Journal of Sound and Vibration, Vol. 52, 1977, pp. 65-78.

59. Ramamurti, V. and Pattabiraman, J., 'Dynamic Behaviour of a Cylindrical Shell With a Cut-Out', Journal of Sound and Vibration, 52, 1977, pp. 193-200.

60. Toda, S. and Komatsu, K., 'Vibrations of Circular Cylindrical Shells with Cut-Outs', Journal of Sound and Vibration, Vol. 52, 1977, pp. 497-510.

61. Baker, W.E., Ewing Jr., W.O., Hanna, J.W., and Bunnewith, G.E., ' The Elastic and Plastic Response of Cantilevers to Air Blast Loading', Proceedings of the 4th U.S. National Congress of Applied Mechanics, 1962, pp. 853-866.

62. Cheng, D.H. and Benveniste, J.E., 'Response of Structural Elements to Travelling Pressure Waves of Arbitrary Shape', International Journal of Mechanical Sciences, Vol. 8, 1966, pp. 607-618.

63. Cheng, D.H. and Benveniste, J.E., 'Dynamic Response of Structural Elements Exposed to Sonic Booms', NASA, CR-1281, March 1969.

64. Banerjee, S.K., 'Dynamic Response of Beams to Blast Load', M.Tech. Thesis, Indian Institute of Technology, Kanpur, 1971.

65. Crocker, M.J., 'Multimode Response of Panels to Normal and to Travelling Sonic Booms', Journal of Acoustical Society of America, Vol. 42, No. 5, 1967, pp. 1070-1079.

66. Crocker, M.J. and Hudson, P.R., 'Structural Response to Sonic Booms', Journal of Sound and Vibration, Vol. 9, 1969, pp. 454-469.

67. Rajamani, A. and Sundararajan, V., 'Blast Response of Plates', Journal of Sound and Vibration, Vol. 39, 1975, pp. 401-408.

68. Symonds, P.S., 'Survey of Methods for Plastic Deformation of Structures Under Dynamic Loads', Brown University Report, BU/NSRDC/1-67, 1967.

69. Jones, N., 'A Literature Review of the Dynamic Plastic Response of Structures', Shock and Vibration Digest, Vol. 7, No. 8, 1975, pp. 89-105.

70. Jones, N., Dumas, J.W., Giannotti, J.G. and Grassit,K.E., 'The Dynamic Plastic Behaviour of Shells' in Dynamic Response of Structures, Edited by G.Herrmann and N.Perrone, Pergamon Press, 1972, pp. 1-30.

71. Moon, F.C., 'One-Dimensional Transient Waves in Anisotropic Plates', Journal of Applied Mechanics, Vol. 40, No. 2, 1973, pp.485-490.

72. Chow, T.S., 'On the Propagation of Flexural Waves in an Orthotropic Laminated Plate and its Response to an Impulsive Load', Journal of Composite Materials, Vol. 5, 1971, pp. 306-319.

73. Sun, C.T. and Whitney, J.M., 'Forced Vibrations of Laminated Composite Plates in Cylindrical Bending', Journal of Acoustical Society of America, Vol. 55, No. 5, 1974, pp. 1003-1008.

74. Sun, C.T. and Whitney, J.M., 'Dynamic Response of Laminated Composite Plates under Initial Stress', AIAA Journal, Vol. 14, No.2, 1976, pp. 268-270.

75. Sun, C.T., Whitney, J.M. and Whitford, L., 'Dynamic Response of Laminated Composite Plates', AIAA Journal, Vol. 13, No. 10, 1975, pp. 1259-1260.

76. Siu, C.C. and Bert, C.W., 'Sinusoidal Response of Composite-Material Plates with Material Damping', Journal of Engineering for Industry, ASME, Vol. 96 B, No. 2, 1974, pp. 603-610.

77. Sun, C.T. and Chattopadhyay, S., 'Dynamic Response of Anisotropic Laminated Plates Under Initial Stress to Impact of a Mass', Journal of Applied Mechanics, Vol. 42, No. 3, 1975, pp. 693-698.

78. Kubo, J.T. and Nelson, R.B., 'Modal Analysis for Impact of Layered Plates', Journal of Engineering Mechanics Division, ASCE, Vol. 101, No. EM 1, 1975, pp. 45-56.

79. Rajamani, A. and Prabhakaran, R., 'Dynamic Response of Composite Plates with Cut-Outs, Part 1: Simply-Supported Plates', Journal of Sound and Vibration, Vol. 54, No. 4, 1977, pp. 549-564.

80. Rajamani, A. and Prabhakaran, R., 'Dynamic Response of Composite Plates with Cut-Outs, Part 2: Clamped-Clamped Plates', Journal of Sound and Vibration, Vol. 54, No. 4, 1977, pp. 565-576.

81. Ashton, J.E., Halpin, J.C. and Petit, P.H., 'Primer on Composite Materials: Analysis, Technomic Publication, Stanford, 1969.

82. Felgar, R.P., 'Formulas for Integrals Containing Characteristic Functions of a Vibrating Beam', The University of Texas, Circular No. 14, Bureau of Engineering Research, 1950.

83. Young, D., 'Vibrations of Rectangular Plates by Ritz Method', Journal of Applied Mechanics, Vol. 17, 1950, pp. 448-453.

84. Leissa, A.W., 'Vibrations of Plates', NASA SP-160, 1969.

85. Agarwal, S.C., 'Vibration of Plates with Cut-Outs', M.Tech Thesis, Indian Institute of Technology, Kanpur, 1973.

86. Lt. Monahan, J., Nemergut, P.J. and Maddux, G.E., Natural Frequencies and Mode Shapes of Plates with Interior Cut-Outs', The Shock and Vibration Bulletin, Vol. 41, 1970, pp. 37-49.

87. Stroud, A.H., 'Approximate Evaluation of Multiple Integrals', Prentice Hall Inc., 1971.

88. Prabhakaran, R. and Rajamani, A., 'Free Vibration Characteristics of Simply-Supported Composite Plates with Circular Holes and Square Cut-Outs', Accepted for Presentation at the 11th Congress of International Council of the Aeronautical Sciences, 1978.

89. Prabhakaran, R. and Rajamani, A., 'Free Vibration Characteristics of Clamped-Clamped Composite Plates with Circular Holes and Square Cut-Outs', To be Presented at the Second International Congress on Composite Materials, Toronto, 1978.

90. Bert, C.W. and Clary, R.R., 'Evaluation of Experimental Methods for Determining Dynamic Stiffness and Damping of Composite Materials', Composite Materials: Testing and Design (Third Conference), ASTM STP 546, 1974, pp. 250-265.

91. Dudek, T.J., 'Young's and Shear Moduli of Unidirectional Composites by a Resonant Beam Method', Journal of Composite Materials, Vol. 4, 1970, pp. 232-241.

92. Schultz, A.B. and Tsai, S.W., 'Dynamic Moduli and Damping Ratios in Fiber-Reinforced Composites', Journal of Composite Materials, Vol.2, 1968, pp. 368-379.

93. Greszczuk, L.B., 'Experimental Determination of Shear Moduli of Fiber-Reinforced Anisotropic Laminates', Presented at the Society for Experimental Stress Analysis Spring Meeting, 1967.

94. Smith, G.A., Laura, P.A. and Matis, M., 'Experimental and Analytical Study of Vibrating Stiffened Rectangular Plates Subjected to Inplane Loading', Journal of Acoustical Society of America, Vol. 48, No. 3, 1970, pp. 707-713.

95. Collatz, L., 'The Numerical Treatment of Differential Equations', Springer-Verlag, New York, 1966, p. 116.

96. Froberg, C.E., 'Introduction to Numerical Analysis', Addison-Wesley Publishing Company, Inc., Reading, Mass. 1969.

97. Bathe, K.S., and Wilson,E.L., 'Numerical Methods in Finite Element Analysis', Prentice Hall, Inc. Englewood Cliffs, New Jersey, 1976, Chapters 8 and 9.

98. Baker, W.E., 'Validity of Mathematical Models of Dynamic Response of Structures to Transient Loads', The Shock and Vibration Bulletin, Vol. 41, Part 7, 1970, pp. 19-28.

APPENDIX A

INTEGRATION CONSTANTS FOR CLAMPED-CLAMPED PLATES

The admissible function $\phi_{mn}(x, y)$ in the mn mode for a clamped-clamped plate is given by,

$$\phi_{mn}(x, y) = X_m(x)\, Y_n(y) \tag{A.1}$$

where,

$$X_m(x) = \cosh \frac{\alpha_m x}{a} - \cos \frac{\alpha_m x}{a} - A_m \left(\sinh \frac{\alpha_m x}{a} - \sin \frac{\alpha_m x}{a}\right)$$

$$Y_n(y) = \cosh \frac{\alpha_n y}{b} - \cos \frac{\alpha_n y}{b} - A_n \left(\sinh \frac{\alpha_n y}{b} - \sin \frac{\alpha_n y}{b}\right) \tag{A.2}$$

Defining $X = x/a$, $Y = y/b$, we have,

$$X_m(x) = X_m(X)$$

$$\frac{dX_m}{dx} = \frac{1}{a}\frac{dX_m}{dX}$$

$$\frac{d^2X_m}{dx^2} = \frac{1}{a^2}\frac{d^2X_m}{dX^2}$$

$$\frac{d^3X_m}{dx^3} = \frac{1}{a^3}\frac{d^3X_m}{dX^3} \tag{A.3}$$

Similar expressions are given for Y_n, $\frac{dY_n}{dy}$, $\frac{d^2Y_n}{dy^2}$, $\frac{d^3Y_n}{dy^3}$.

$$F_1(m, n) = \int_0^1 X_m X_n \, dX$$

$$= 1 \qquad \text{for } m = n$$

$$= 0 \qquad \text{for } m \neq n \tag{A.4}$$

$$F_2(m, n) = \int_0^1 X_{m,X} X_{n,X} \, dX$$

$$= \frac{4 \alpha_m^2 \alpha_n^2 \left(A_m \alpha_m - A_n \alpha_n\right)}{\left(\alpha_n^4 - \alpha_m^4\right)} \left[1 + (-1)^{m+n}\right] \tag{A.5a}$$

$$F_2(m, n) = A_m \alpha_m \left(A_m \alpha_m - 2\right) \tag{A.5b}$$

$$F_3(m, n) = \int_0^1 X_{m,XX} X_{n,XX} \, dX$$

$$= \alpha_m^4 \qquad \text{for } m = n,$$

$$= 0 \qquad \text{for } m \neq n. \tag{A.6}$$

$$F_4(m, n) = \int_0^1 X_{m,X} X_n \, dX$$

$$= \frac{4 \alpha_n^2 \alpha_m^2}{\alpha_n^4 - \alpha_m^4} \left[1 - (-1)^{m+n}\right] \qquad \text{for } m \neq n,$$

$$= 0 \qquad \text{for } m = n. \tag{A.7}$$

$$F_5(m, n) = \int_0^1 X_{m,XX}\, X_n\, dX$$

$$= \frac{4\alpha_m^2\, \alpha_n^2\, (A_n\, \alpha_n - A_m\, \alpha_m)}{(\alpha_n^4 - \alpha_m^4)} \left[1 + (-1)^{m+n}\right] \qquad \text{(A.8a)}$$

$$F_5(m,m) = A_m\, \alpha_m\, (2 - A_m\, \alpha_m) \qquad \text{(A.8b)}$$

$$F_6(m, n) = \int_0^1 X_{m,XX}\, X_{n,X}\, dX$$

$$= \frac{4\alpha_m^3\, \alpha_n^3\, A_m\, A_n}{(\alpha_n^4 - \alpha_m^4)} \left[1 - (-1)^{m+n}\right] \qquad \text{for } m \neq n,$$

$$= 0 \qquad \text{for } m = n. \qquad \text{(A.9)}$$

$$F_{1c}(m, n) = \int_{X_A}^{X_B} X_m\, X_n\, dX$$

$$= \frac{1}{\alpha_n^4 - \alpha_m^4} \left[X_m \frac{d^3X_n}{dX^3} - X_n \frac{d^3X_m}{dX^3} - \frac{dX_m}{dX}\frac{d^2X_n}{dX^2} + \frac{dX_n}{dX}\frac{d^2X_n}{dX^2}\right]_{X_A}^{X_B} \qquad \text{(A.10a)}$$

$$F_{1c}(m, m) = \frac{1}{4\alpha_m^4} \left[3X_m \frac{d^3X_m}{dX^3} + X\alpha_m^4 X_m^2 - 2X \frac{dX_m}{dX}\frac{d^3X_m}{dX^3} - \frac{dX_m}{dX}\frac{d^2X_m}{dX^2} + X\left(\frac{d^2X_m}{dX^2}\right)^2\right]_{X_A}^{X_B} \qquad \text{(A.10b)}$$

$$F_{2c}(m, n) = \int_{X_A}^{X_B} X_{m,X}\, X_{n,X}\, dX$$

$$= \frac{1}{(\alpha_n^4 - \alpha_m^4)} \left[\alpha_n^4 X_n \frac{dX_n}{dX} - \alpha_m^4 X_m \frac{dX_n}{dX} - \frac{d^2X_m}{dX^2} \frac{d^3X_n}{dX^3} + \frac{d^2X_n}{dX^2} \frac{d^3X_m}{dX^3} \right]_{X_A}^{X_B} \qquad \text{(A.11a)}$$

$$F_{2c}(m, m) = \frac{1}{4} \left[3X_m \frac{dX_m}{dX} + X \left(\frac{dX_m}{dX}\right)^2 - 2X\, X_m \frac{d^2X_m}{dX^2} - \frac{1}{\alpha_m^4} \frac{d^2X_m}{dX^2} \frac{d^3X_m}{dX^3} + \frac{X}{\alpha_m^4} \left(\frac{d^3X_m}{dX^3}\right)^2 \right]_{X_A}^{X_B} \qquad \text{(A.11b)}$$

$$F_{3c}(m, n) = \int_{X_A}^{X_B} X_{m,XX}\, X_{n,XX}\, dX$$

$$= \frac{1}{(\alpha_n^4 - \alpha_m^4)} \left[\alpha_n^4 \frac{dX_n}{dX} \frac{d^2X_m}{dX^2} - \alpha_m^4 \frac{dX_m}{dX} \frac{d^2X_n}{dX^2} - \alpha_n^4 X_n \frac{d^3X_m}{dX^3} + \alpha_m^4 X_m \frac{d^3X_n}{dX^3} \right]_{X_A}^{X_B} \qquad \text{(A.12a)}$$

$$F_{3c}(m, m) = \frac{1}{4} \left[3 \frac{d^2X_m}{dX^2} \frac{dX_m}{dX} + X \left(\frac{d^2X_m}{dX^2}\right)^2 - 2X \left(\frac{dX_m}{dX}\right) \left(\frac{d^3X_m}{dX^3}\right) - X_m \frac{d^3X_m}{dX^3} + X\, \alpha_m^4\, X_m^2 \right]_{X_A}^{X_B} \qquad \text{(A.12b)}$$

$$F_{4c}(m, n) = \int_{X_A}^{X_B} X_{m,X}\, X_n\, dX$$

$$= \frac{1}{(\alpha_m^4 - \alpha_n^4)} \left[\alpha_m^4\, X_n\, X_m - \frac{dX_n}{dX}\,\frac{d^3X_m}{dX^3} + \frac{d^2X_n}{dX^2}\,\frac{d^2X_m}{dX^2} - \frac{dX_m}{dX}\,\frac{d^3X_n}{dX^3}\right]_{X_A}^{X_B} \qquad (A.13a)$$

$$F_{4c}(m, m) = \frac{1}{2}\left[X_m^2\right]_{X_A}^{X_B} \qquad (A.13b)$$

$$F_{5c}(m, n) = \int_{X_A}^{X_B} X_{m,XX}\, X_n\, dX$$

$$= \frac{1}{(\alpha_n^4 - \alpha_m^4)} \left[\alpha_m^4 \left(X_m \frac{dX_n}{dX} - X_n \frac{dX_m}{dX}\right) - \frac{d^2X_n}{dX^2}\,\frac{d^3X_m}{dX^3} + \frac{d^2X_m}{dX^2}\,\frac{d^3X_n}{dX^3}\right]_{X_A}^{X_B} \qquad (A.14a)$$

$$F_{5c}(m, m) = \frac{1}{4}\left[X_m \frac{dX_m}{dX} - X\left(\frac{dX_m}{dX}\right)^2 + 2X\, X_m \frac{d^2X_m}{dX^2} + \frac{1}{\alpha_n^4}\,\frac{d^2X_m}{dX^2}\,\frac{d^3X_m}{dY^3} - \frac{X}{\alpha_n^4}\left(\frac{d^3X_m}{dX^3}\right)^2\right]_{X_A}^{X_B} \qquad (A.14b)$$

$$F_{6c}(m, n) = \int_{X_A}^{X_B} X_{m,XX}\, X_{n,X}\, dX$$

$$= \frac{\alpha_m^4}{(\alpha_n^4 - \alpha_m^4)} \left[X_m \frac{d^2X_n}{dX^2} - \frac{dX_m}{dX}\frac{dX_n}{dX} \right.$$

$$\left. + \frac{\alpha_n^4}{\alpha_m^4} X_n \frac{d^2X_m}{dX^2} - \frac{1}{\alpha_m^4} \frac{d^3X_m}{dX^3} \frac{d^3X_n}{dX^3} \right]_{X_A}^{X_B} \qquad \text{(A.15a)}$$

$$F_{6c}(m, m) = \frac{1}{2} \left[\left(\frac{dX_m}{dX}\right)^2 \right]_{X_A}^{X_B} \qquad \text{(A.15b)}$$